THE UNIVERSITY
of EDINBURGH

“A computational approach to magnocellular oxytocin neuron dynamics.”

Jorge Maícas Royo

PhD

The University of Edinburgh

2019

Declaration

I declare that the thesis has been composed by myself and that the work has not be submitted for any other degree or professional qualification. I confirm that the work submitted is my own, except where work which has formed part of jointly-authored publications has been included. My contribution and those of the other authors to this work have been explicitly indicated below. I confirm that appropriate credit has been given within this thesis where reference has been made to the work of others.

The work presented in Chapter 3 was previously published in Journal of Neuroendocrinology as *Oxytocin Neurones: Intrinsic Mechanisms Governing the Regularity of Spiking Activity*, by J. Maícas Royo, C. H. Brown, G. Leng and D. J. MacGregor. I, J. Maícas Royo, was the first author, my supervisors D.J. MacGregor and G. Leng were co-authors, and C.H. Brown provided us with some recordings of oxytocin neurones. Trystan Leng also carried some statistical analysis. This study was conceived by all of the authors. I carried out the experiments and participated in the writing.

The work presented in Chapter 4 was previously published in Endocrinology as *A Predictive, Quantitative Model of Spiking Activity and Stimulus-Secretion Coupling in Oxytocin Neurons*, by J. Maícas Royo, G. Leng and D. J. MacGregor, being I, J. Maícas Royo, the first author and my supervisors D.J. MacGregor and G. Leng co-authors. This study was conceived by all of the authors. I carried out the experiments and the writing.

The work presented in Chapter 5 has been published in The Journal of Physiology as *The spiking and secretory activity of oxytocin neurones in response to osmotic stimulation: a computational model,* by J. Maícas Royo, G. Leng and D. J. MacGregor, being me, J. Maícas Royo, the first author*,* and my supervisors D.J. MacGregor and G. Leng co-authors. This study was conceived by all of the authors. I carried out the experiments and the writing.

Jorge Maícas Royo, June 2019

Acknowledgements

-Too often you say more than you need. A hundred words to praise a woman. Too many.
-So when I meet a woman, I should simply say: *You are beautiful*?
-No. You would say simply *beautiful*, and let the woman decide the rest of what you mean
-Isn't that vague, unspecific? Doesn't that lead to confusion?
-It leads to thoughtfulness. It is delicate.

Patrick Rothfuss. TWMF

List of abbreviations.

(E)(I)PSP	(Excitatory) (Inhibitory) Post Synaptic Potential
AHP	After Hyperpolarizing Potential
ANP	Atrial Natriuretic Peptide
BK	Big K^+
CCK	Cholecystokinin
cGMP	cyclic Guanosine Monophosphate
DAP	Depolarising Afterpotential
EVF	Extra Vascular Fluid
GABA	Gamma-Aminobutyric Acid
HAP	hyperpolarising after potential
i.p.	Intraperitoneal
i.v.	Intravenous
ID	Index of Dispersion
IK	Intermediate K^+
ISI	Inter Spike Interval
ICF	Intra Cellular Fluid
LIF	Leaky Integrate and Fire
LT	Lamina Terminalis
min	Minute(s)
MnPO	Median Pre-Optic nucleus
NO	Nitric Oxide
NTS	Nucleus of the Solitary Tract
OVLT	Organum Vasculosum of the Lamina Terminalis
PEG	Polyethylene Glycol
PVN	Paraventricular Nucleus

s	Second(s)
SD	Standard Deviation
SEM	Standard Error of the Mean
SFO	Subfornical *O*rgan
SK	Small K^+
SON	Supra Optic Nucleus

Lay Summary of thesis

Without us noticing it, our bodies regulate themselves through a series of homeostatic processes. These processes involve the control mechanisms of body temperature, fluid and energy balance, the maintenance of blood pH and the arterial pressure. Also, the body tries to maintain adequate blood levels of glucose, iron, oxygen, calcium, potassium, copper and sodium, all necessary for the correct functioning of the brain. Many of the mechanisms are governed by the neuroendocrine system, which includes different organs in the body connecting the kidneys, liver, heart and gut, to the brain in bidirectional and intricate pathways. The body sends information to the brain through nerves whose terminal receptors detect the changes of hormones, ions, pressure or temperature. That information arrives to the hypothalamus, which integrates inputs from various parts of the body and the brain itself, producing a response in the shape of different hormones. Those hormones will be secreted to the blood stream, through which they will reach the whole body, being detected by the organs participating in each homeostatic process.

Magnocellular oxytocin neurones, found mainly in the supraoptic nucleus and in the paraventricular nucleus of the hypothalamus, project their axons to the posterior pituitary, from where they secrete oxytocin into the bloodstream. Oxytocin is well known for its essential role in breastfeeding and for facilitating labour. However, in the last decades oxytocin has also been recognised to have roles in social bonding, energy balance and osmotic pressure balance.

These five processes, breastfeeding, labour, social bonding, and energy and osmotic pressure balance are associated with different behaviours of the oxytocin neurons. During breastfeeding and labour, the spiking activity of oxytocin neurones alternates between long periods of slow basal activity and a few seconds of bursting, when oxytocin neurones fire synchronously at up to 100 spikes per second. Social bonding is associated with dendritic oxytocin secretion, through which oxytocin will reach other neurones in the brain. Finally, energy and osmotic

pressure balance are associated with small to medium linear alterations of the basal spike activity of oxytocin neurons.

Spikes are a sudden positive change of the difference in the voltage potential between the inner and the external side of the neuron membrane. Usually in equilibrium, each oxytocin neuron is affected by neurotransmitters able to change, negatively or positively, that equilibrium. When the resultant contribution of all of them is positive and make the voltage difference reach a certain level, a spike is produced, reacting the oxytocin neuron membrane immediately after with several currents to recover the equilibrium. However, spikes are not the final neuronal product. Spikes, transported along the neuron axon, are the mechanism that neurones use to trigger release of messenger chemicals at their dendrites and axon terminals.

The computational model shown here simulates the spiking activity of oxytocin neurones described in the literature. That spiking activity has been simulated during basal activity, in response to cholecystokinin (CCK), a gut peptide involved in energy balance, and in response to osmotic pressure. However, the final product of oxytocin neurones is the secreted oxytocin and its plasma concentration. Thus, it was developed a secretion model matched to experimental data in the literature, coupled it with the spiking model, and added a model for oxytocin clearance from plasma. That allowed simulating the plasma oxytocin response to CCK and to changes in the osmotic pressure. In addition, the model offered important insights, by helping to understand the importance of particular properties of the neurons for generating biologically appropriate signals.

Abstract of thesis

Magnocellular oxytocin neurones, found mainly in the supraoptic nucleus and in the paraventricular nucleus of the hypothalamus, project their axons to the posterior pituitary, from where they secrete oxytocin into the bloodstream. Oxytocin is well known for its essential role in breastfeeding and for facilitating labour. However, in the last decades oxytocin has also been recognised to have roles in energy balance and osmotic pressure balance.

During breastfeeding and labour, the spiking activity of oxytocin neurones alternates between long periods of slow basal activity and a few seconds of bursting, when oxytocin neurones fire synchronously at up to 100 spikes per second. Energy and osmotic pressure balance are associated with small to medium linear alterations of the basal activity of oxytocin neurons.

A computational model was developed to simulate the spiking activity of oxytocin neurones described in the literature. The simulations mimicked their basal activity, their response to cholecystokinin (CCK), a gut peptide involved in energy balance, and their spiking response to osmotic pressure. However, the final product of oxytocin neurones is the secreted oxytocin and its plasma concentration. Thus, it was developed a secretion model matched to experimental data in the literature, coupled it with the spiking model, and added a model for oxytocin clearance from plasma. That allowed simulating the plasma oxytocin response to CCK and to changes in the osmotic pressure. In addition, the model offered important insights. It supports the necessity of a depolarization after potential (DAP) in some oxytocin neuron membranes, the essential role of inhibitory inputs during the oxytocin osmotic response, a new mechanism for partially explaining oxytocin response to hypovolemia, and explains the role of the after hyperpolarizing (AHP) current as a filter of synaptic inputs to oxytocin neurones.

Contents

Chapter 1.

General introduction

"What a child can do today with assistance, she will be able to do by herself tomorrow".

-Lev S. Vygotsky (1980)

2500 years ago, pythagorics and other Greek philosophers believed that nothing but a perfect sphere could fit with how they imagined our planet's shape (Dicks, 1970; Burkert, 1972). A hundred years later, their hypothesis had spread all over ancient Greece, making other mathematicians, philosophers and astronomers wonder how big that ball could be. That led to clever ways of figuring it out, to the point that Eratosthenes (276BC-195BC) could give a number just 15% larger than the real circumference (Goldstein, 1984; Engels, 1985), 17 centuries before the Earth was first circumnavigated by Juan Sebastian Elcano (de Navarrete, 1837; Pigafetta, 1986). Although Elcano's journey was not pleasant (it took three years and only 17 Spaniards and one of the five departing ships returned), it gave the world the final proof of its own sphericity. The promise of extraordinary wealth to the ones controlling the new territories and the enormous, strange and terrible new oceans connecting them, made kings, queens, merchants and popes in the old continent devote more and more resources to mathematics and engineering, leading for the first time in history to a rapid improvement of those studies across many different countries (Arnold, 2013). The same story has been only repeated since, in the conquest of the air, space or, more recently, the global economy and human wellbeing. In these, mathematics has shown its ability to formulate theories, model scenarios and predict outcomes, sometimes quite ahead of their time, saving huge amounts of effort, resources and lives.

Among the applications of mathematics, there is one that, being always present nowadays, might not be given all its phenomenal relevance. Not so long ago, devices that could make certain calculations or repeat certain movements over and over, were usually not more than toys for the wealthy or dreams in visionary minds (Koetsier, 2001). Then George Boole, a XIXth century mathematician, developed a family of algebraic rules to solve logic operations, where inputs and results could only take two values, true or false, 1 or 0 (Boole, 1854). Soon, people realized that two values could be used to represent all the elements of much larger families (see

Table 1); this led to Boolean algebra, potentially able to calculate anything imaginable.

Table 1. Binary representation of the numbers 0 to 7.

000	→	0	100	→	4
001	→	1	101	→	5
010	→	2	110	→	6
011	→	3	111	→	7

As with the pythagorics' idea, it took time for the dream to become true. At the beginning of the XXth century, electricity started allowing a continuous source of energy to unsupervised automated devices (Bennett, 1993) and the first implementations of arithmetic operations with 0's and 1's were possible thanks to vacuum tubes. For instance, with 28 vacuum tubes, a classic automatic accumulator could be implemented (Panda *et al.*, 2009). In 1945, the ENIAC, a supercomputer with 17,468 vacuum tubes that weighed 2.5 tons and occupied 167 m^2, could calculate in 30 s a projectile trajectory that would take 20 h for a human with a desk calculator (McCartney, 1999). Conceptually, things have not changed much since. Logic gates fed by 1's and 0's are still the pillars of our supercomputers. However, our supercomputers could not have been possible without extreme miniaturization. The Nobel-awarded invention of the transistor (Bardeen & Brattain, 1948), a tiny substitute for the vacuum tube, made it possible. Sixty years later, the latest mobile phones can integrate several thousand billion of those transistors in their small processors.

Maths and computers are used in more and more tasks every day. Biomedical sciences are not an exception, and in this thesis I will try to show how I worked with computers to make a mathematical model of the oxytocin neurone; how I programmed it in a computer language; how the model can simulate experimental data, accurately predicting other results; and how it can help to understand and generate hypotheses for further experiments.

Oxytocin. A historical introduction

Somehow, this thesis' story also begins in the humid valleys of Mesopotamia. The dawn of agriculture brought, among other things, the spread of the ergot fungi among the cultivated fields. When cereals infected with ergot are consumed

repeatedly, they can become poisonous. Several historical epidemics with thousands of people suffering from seizures, burning sensation and gangrene, taught us that ergot provokes convulsive and vasoconstriction symptoms (Schiff, 2006). In small doses, though, the convulsive and vasoconstriction effects facilitate childbirth, causing uterine contractions and reducing postpartum haemorrhage. Thus, for at least three thousand years and particularly during the XIXth century, but also in the XXth century, ergot was used as an oxytocic agent (Ringrose, 1962; Schiff, 2006). Still, the recording of cases of women and children dying during birth after the use of ergot aroused caution among obstetricians (Smith, 1892), propelling research on either ergot's safe component and dosage or an alternative to it.

Interested in the properties of acetylcholine, Sir Henry Dale made an extensive comparative study of ergot and other chemicals or extracts capable of triggering excitatory symptoms in different mammals (Dale, 1906). As part of that extensive work, he tested the response of the cat's uterine muscles to an extract of cattle pituitary. He found that the extract, apart from its already known vasoconstriction effects (Oliver & Schäfer, 1895), provoked uterine contractions when injected, marking the start of a revolution in obstetric medicine. Later studies localized the active component in the posterior pituitary, and different versions of the extract were used for years without knowing exactly what was triggering the uterine contractions (Kosmak, 1918). What was discovered was that the posterior pituitary contained two main substances, one, responsible for vasopressor effects and another, responsible for the oxytocic effects; these were finally dissociated in 1928 (Kamm *et al.*). However, only when the oxytocic component's formula was discovered and the component synthesized (du Vigneaud *et al.*, 1954) did it become possible to study its dynamics in plasma. The oxytocic component was given the name *oxytocin*, from the Greek *swift* or *quick birth*, and it is still the first line treatment to prevent postpartum haemorrhage, the main cause of maternal mortality in the world (Anyakora *et al.*, 2018).

By 1954, the most prominent roles of oxytocin, related to high concentrations of the hormone in plasma, were already known. Just four years after Dale published its actions on the uterus, the posterior pituitary extract also showed effects in breastfeeding (Ott & Scott, 1910). A role of the extract in water balance was proposed shortly after as well (Buckley, 1924), but that effect was initially only

associated with vasopressin, the antidiuretic hormone (Ginsburg, 1954; Fong *et al.*, 1960).

Once oxytocin and vasopressin were synthesized, many assays were designed to measure them, not without some difficulties. The first problem solved was of specificity, so that vasopressin and oxytocin could be measured independently. After that, sensitivity was improved, producing assays able to measure the low concentrations of oxytocin and vasopressin present at basal levels in plasma. After some promising first results that elucidated the fate of oxytocin after large i.v. injections or infusions (Ginsburg & Smith, 1959; Fabian *et al.*, 1969*b*, 1969*a*), it started to be hinted that different assays could be giving different absolute values (Forsling, 1986). Something that it is still happening to this day (Leng & Sabatier, 2016).

Oxytocin, though, was already being studied from other points of view. Before the discovery of its formula, it was known that neurones innervating the posterior pituitary were located in the supraoptic nucleus (SON) and the paraventricular nucleus (PVN) (Harris, 1951). Thus, after the oxytocin and vasopressin formulae were discovered, researchers looked for them in the SON and PVN (Cross & Green, 1959), discovering that each hormone was produced and secreted by a dedicated group of neurones (Sokol & Valtin, 1967). Some years later it was also shown that, every neuron in the SON and PVN that projects to the posterior pituitary was secreting either vasopressin or oxytocin (Rhodes *et al.*, 1981).

That answered the questions of where in the brain oxytocin is produced and which neurones are responsible for oxytocin secretion into the blood. However, that only led to new questions as how oxytocin neurones *know* how much oxytocin they have to secrete and how that secretion is triggered.

Neuronal electrical activity

Curiously enough, the study of the mechanisms that neurones use to communicate with each other has an important person in common with the discovery of oxytocin. After his work with the posterior pituitary extract, Sir Henry Dale resumed his interest in acetylcholine, for which work he was co-awarded the Nobel Prize in 1937 (Tansey, 2006). In those works, he studied the synaptic communication between neurones, describing how chemical neurotransmitters alter the electrical balance near the membrane of neurones.

A neurotransmitter is a molecule released at a synapse that can bind to receptors on the surface of a neurone. If that happens, neurotransmitters can alter the *electrical resting state* of that neurone (Levitan & Kaczmarek, 2015). The resting state is a negative voltage inside the neurone, maintained by actively pumping more Na^+ out than letting K^+ in. That mechanism creates and maintains an electrochemical gradient of around -60 mV across the membrane, a fragile equilibrium that can change rapidly in relevant circumstances.

When a neurotransmitter binds to its receptor, it can trigger the opening of ion channels in the postsynaptic neurone, producing either a depolarization of the postsynaptic cell or a hyperpolarization. A sufficient depolarization can activate voltage-gated Na^+ and Ca^{2+} channels, resulting in the generation of an action potential (a spike).

Neurones react to a spike by activating two voltage-dependent mechanisms which restore the resting state. The first mechanism involves closing voltage-gated Na^+ and Ca^{2+} channels, which prevents further depolarisation; the second involves opening voltage-gated K^+ channels, which allows K^+ to flow out of the neuron, following the voltage gradient. As a result, the action potential created in a certain location, usually at the axon initial segment (Bender & Trussell, 2012), will propagate along the axon. The action potential is regenerated every time it encounters new membrane channels, and is followed by a refractory period (Debanne *et al.*, 2011). When the action potential reaches the axon terminal and dendrites, it can potentially trigger exocytosis through opening voltage-dependent Ca^{2+} channels

This description of how spikes are produced and travel inside the neuron closely relates with the movement of electrons, the most elemental negatively charged particles, which are responsible for the transmission of electricity in any circuit. Hodgkin and Huxley exploited that similarity, adapting the mathematical principles that described electricity to study spike propagation in the particularly large giant axon of the squid (Hodgkin & Huxley, 1952). They represented the squid's axon membrane as an electrical circuit, modelling the bilayer membrane of the neuron as a capacitance, the ion channels as conductances, the gradients that drive passively those ions as batteries and the ones that drive them actively as generators. Their equations are to this day the most exact representation of the currents and dynamics involved in action potential propagation in neurones (Izhikevich, 2004).

The spiking activity of oxytocin neurones

Of the around 200 million neurones of the rat's brain (Herculano-Houzel & Lent, 2005), "only" 300 thousand are in the hypothalamus (Hsu & Peng, 1978), a group of nuclei that occupy a small space at the bottom of the brain, where signals from the brain and the body are integrated, and which send processed information to both brain and body. The latter happens, in part, through the pituitary gland, a tiny oval protrusion that seems to hang from the bottom of the brain, just below the hypothalamus. The pituitary gland is densely vascularised by a network of fine capillaries, which convey hormones secreted by hypothalamic neurones to control hormone secretion from the anterior pituitary (Leng, 2018*a*).

The magnocellular neurones innervate the posterior pituitary gland. They produce either oxytocin or vasopressin in their huge somas, from which a long axon is projected to the posterior pituitary, where they secrete their products into the blood. In total, Rhodes *et al.* (1981) estimated that there are around ten thousand of these neurones in the rat, two thirds of them located either in the PVN or in the SON.

Bursting activity

As noted earlier, oxytocin was first known for its participation in parturition and breastfeeding. At those times, the plasma concentration of oxytocin reaches its highest levels, whilst vasopressin neurones do not change their spiking activity. That made the use of lactating rats the traditional way to distinguish oxytocin neurones from vasopressin neurones *in vivo*. During lactation or parturition, oxytocin neurones alternate intervals of around 300s of basal spike activity with bursts, during which oxytocin neurones can fire up to 100 spikes during 2-3 s, reaching a maximum of 100 spikes/s over 200-300 ms (Wakerley & Lincoln, 1973; Belin & Moos, 1986). Looking at it closely, during the 300 s of non-bursting activity, oxytocin neurones produce around 300 spikes too. However, the coupling between spike activity and secretion is highly non-linear (Bicknell *et al.*, 1984). 300 spikes over 300 s would trigger the secretion of 15 times less oxytocin than 150 spikes occurring during just 3 s. That sudden increment of oxytocin in plasma, produced by those short bursts, is the necessary pulsatile ingredient in both uterine contractions and milk ejection.

Normal activity

However, oxytocin neurones also play a role in male rats and in female rats that are neither pregnant nor lactating. Oxytocin neurones are involved in two major

homeostatic processes in the rat. During those processes, oxytocin neuronal behaviours contrast with the lactating or parturition patterns, and are defined by firing that typically does not surpasses 13 spikes/s and is often in a range of 0 to 8 spikes/s (Maícas-Royo *et al.*, 2018). During lactation or parturition, oxytocin neurones synchronize and respond abruptly and all together to the same input. However, during homeostatic processes, oxytocin neurones respond smoothly and without synchronizing with each other. For instance, systemic injection of cholecystokinin (CCK) (a peptide produced in the gut after food intake) steadily increases the firing rate of oxytocin neurones (Leng *et al.*, 1991). This activity will then slowly decrease over 10-15 min until it has returned to the previous state (Velmurugan *et al.*, 2010). Another example is the response of oxytocin neurones to osmotic pressure. Osmolality is maintained in equilibrium through the whole body, including plasma, extravascular fluid and intracellular fluid. Thus, changes in osmolality tend to be slow, and oxytocin neurones respond to them linearly (Brimble & Dyball, 1977), maintaining the response if the osmotic pressure does not decrease (Leng *et al.*, 2001).

Channels and currents involved in the spiking activity

In all cases, activity in oxytocin neurones is initiated when they receive synaptic inputs. The inputs can be excitatory (EPSPs) and inhibitory (IPSPs), and how their membranes react has been extensively studied both *in vivo* (Richard *et al.*, 1997; Leng *et al.*, 1999; Hatton & Wang, 2008; Brown *et al.*, 2013) and *in vitro* (Hatton & Li, 1999; Pittman *et al.*, 1999; Armstrong *et al.*, 2010; Brown *et al.*, 2013).

Hodgkin & Huxley (1952) were the first to describe voltage-gated Na^+ channels, the main channels responsible for initiating spikes in neurones. They proposed that those channels can be in three different states. Initially, when the membrane is ready to produce a spike, the Na^+ channels are deactivated. Secondly, if the voltage reaches a threshold due to a recent positive balance between EPSPs and IPSPs, the channels open, allowing Na^+ to enter, producing a fast depolarisation. Finally, the Na^+ channels inactivates, and will not respond again to voltage until enough Na^+ is actively transported out of the neurone. Although these three states accurately describe the membrane dynamics during the initial steps of an action potential, when the voltage reaches intermediate or high levels, it triggers the opening of other channels that will let Ca^{2+} enter the membrane (Katz & Miledi, 1970). Together, the entry of Na^+ and Ca^{2+} shape the rising form of the spike.

In magnocellular neurones, the membrane reacts to an action potential with three different currents. The first one, the hyperpolarising after potential (HAP), is actually the combination of at least three dynamics (Roper *et al.*, 2003). The transient outward current, I_A, is the first hyperpolarizing current to appear when the membrane depolarizes. It inactivates quickly, giving the membrane voltage a characteristic *A* shape if the depolarization does not produce a spike.

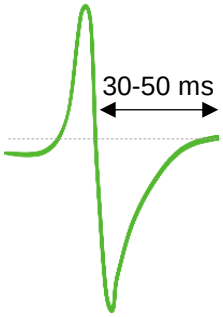

Figure 1. After a spike is produced, the hyperpolarising potential (HAP) prevents the oxytocin neurone to produce another spike for about 30-50 ms.

If the voltage keeps rising, the delayed rectifier current, I_K appears. Both, I_A and I_K, have also a role in the spike shape, which broadens when they are blocked. Finally, the big potassium (BK) voltage-gated channels, allow a big quantity of K^+ cross the membrane. They are only activated under a strong depolarization, deactivating quickly, with a time constant of just 1 ms if the neurone repolarizes. The resultant HAP will be enough to suppress the neuron's ability to fire again for 30 - 50 ms (Figure 1). That hyperpolarization will translate into two scenarios. If PSPs only occasionally exceed the threshold for triggering a spike, a spike will be produced every time that that happens. Then, the neurone will follow its inputs with high temporal accuracy. However, if PSPs often exceed that threshold, the HAP will regularise the neuronal activity, allowing spike production only at intervals of 30-60 ms. As a result, the spike activity will not accurately follow the activity of the inputs. Mathematically speaking, it could be said that the HAP reduces the variability of spike production, filtering the input noise.

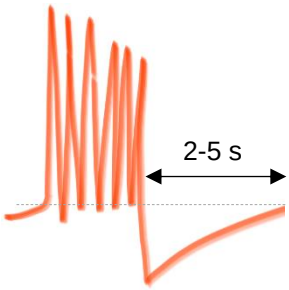

Figure 2. When several spikes are produced close together, the accumulative effect of the after hyperpolarizing potential (AHP) can prevent further spiking activity for few seconds

In magnocellular neurones, other channels produce a long (for up to 5 s) *after hyperpolarizing potential* (AHP) (Roper *et al.*, 2003) (Figure 2). The AHP has at least two components, a medium AHP due to small K^+ channels (SK) that can be blocked by the toxin apamin, and a slow AHP, with intermediate K^+ channels (IK), which can be inhibited by muscarine (Table 2). The

fact that channels can be blocked by certain chemicals makes it possible, among other things, to isolate the contribution of each channel to the spiking activity of oxytocin neurones.

The AHP channels are activated by an increment of Ca^{2+} inside the membrane, letting K^{+} cross more slowly than the BK channels. However, they take longer to become inactivated. Because of their long-lasting effect, they are more relevant in the second scenario that has been introduced for the HAP. When the neurone is stimulated strongly, the SK and IK channels are continuously open and as a result, the maximum firing rate is lowered, hence the firing rate is less variable, producing a smoother response and filtering noisy inputs.

Finally, a third type of current can slowly depolarize the membrane after a spike – the *depolarising afterpotential* (DAP) (Figure 3). As a result, the neuron has more chances to produce another spike. Those channels, also activated by Ca^{2+}, play an important role in the phasic activity of vasopressin neurones (Ghamari-Langroudi & Bourque, 1998). However, in oxytocin neurones, the DAP is usually masked by a larger AHP. The AHP and the DAP have similar time courses and opposite sign. Because of this, only about 20% of oxytocin neurones show DAP activity: in many cases, a DAP is only noticeable after blocking the AHP channels (Maícas-Royo *et al.*, 2016).

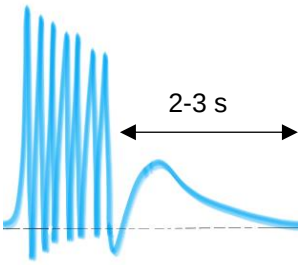

Figure 3. When a depolarising afterpotential (DAP) is present, several spikes firing close together can make the oxytocin neurone more responsive to produce further spikes during two or three seconds.

This summary does not include many other factors that affect the membrane dynamics, such as the location of the channels, that can vary from neuron to neuron, or that oxytocin neurones dendrites can also trigger action potentials.

However, as seen in Table 2, even if only the most relevant membrane dynamics are used, the way to calculate spike activity can be quite complex. The first models trying to mimic the membrane dynamics followed Hodgkin-Huxley equations. That required modelling voltage-dependent activation and inactivation.

Table 2. Currents, channels and channels' blockage in magnocellular neurones (Ghamari-Langroudi & Bourque, 1998, 2004; Roper *et al.*, 2003).

Name	Components	Current	Mechanism	Effect	Blockage
HAP	BK	Ca^{2+} and voltage-dependent K^+	Large conductance (BK) channel	Membrane inexcitability for 30-50ms	charybodotoxin
	Delayed rectifier	voltage-sensitive K^+ currents	Cubic activation and non-inactivating	Continues rectification. Shape spike broadening	Tetraethyla-monium
	Transient outward current		Quartic activation & linear inactivation	A-type Starts rectification. Shape spike broadening	4-aminopyridine
AHP	Medium AHP	Ca^{2+} - activated K^+	Small conductance (SK) channel	Membrane inexcitability for 300-500 ms	apamin
	Slow AHP		Intermediate conductance (IK) channel	Membrane inexcitability for 2-5 s	muscarine
DAP	Fast DAP	Ca2+ activated	Non-specific cation channel	Membrane excitability for 300-500 ms	Caesium (Cs+)
	Slow DAP	Ca^{2+} activated	Non-specific cation channel	Membrane excitability for 2-3 s	
		Ca^{2+} activated	Switch off of hyperpolarising K^+ leak		

Thus, complex equations were needed for every channel involved in depolarization, hyperpolarization and maintenance of the resting potential. Computationally speaking, Hodgkin-Huxley equations are very demanding and soon other simplified models were used. To some extent, computational resources are not a problem anymore. Current computational power makes it possible to simulate small populations of neurones with Hodgkin-Huxley equations (Borges et al., 2016; Yao et al., 2017; Xu et al., 2018). However, dozens of ion channels per neurone and several parameters per current, generate such an amount of data that makes difficult to analyse the influence of each individual parameter (Burkitt, 2006).

The Leaky Integrate and Fire model

Other solutions, less accurate but much faster to compute that the Hodgkin-Huxley model have been proposed. Among these is the *Integrate and Fire model*, first proposed as a very simple circuit that included a capacitor and a resistor in parallel

(Lapicque, 1907). Slowly charged by a battery, when the capacitor was full ('when the membrane had reached the spike threshold'), it liberated the voltage stored as potential spike. After that, the membrane returned abruptly to the initial state. The model lacked three important elements. It did not consider any inputs that could mimic EPSPs and IPSPs; it lacked any mechanism through which the membrane could become refractory after a spike; finally, it did not have the capacity to recover a resting state without passing first through potential spike. Those elements were slowly added to the Integrate and Fire model (Burkitt, 2006). Inputs are now commonly simulated by a Poisson distribution; hyperpolarization has been added to mimic different contributions in different cells; and the ability to permanently recover the resting state is commonly modelled by a leak current. With that final contribution, the model became known as the *Leaky Integrate and Fire (LIF) model*.

The LIF model also reduces the Hodgkin & Huxley model's complexity by simplifying the spike occurrences, which shape is not calculated at all. The LIF model focuses on the membrane's dynamics before a spike is triggered, and on what happens after that spike. For these, the LIF model is a good approximation to the Hodgkin-Huxley model (Burkitt, 2006), and is also much faster (Izhikevich, 2004). With that in mind, my supervisors proposed a LIF model with three sets of equations to model the membrane response to every spike: a HAP, an AHP and a DAP (MacGregor *et al.*, 2009). In that model, the three HAP components present in magnocellular neurones are mimicked by a single equation. The two AHP components are also simulated by a single equation, with an intermediate time constant. Finally, two DAP components are present in the vasopressin spiking model (MacGregor & Leng, 2012), but generally it is not necessary to include a DAP in the oxytocin spiking LIF model (Maícas-Royo *et al.*, 2016), either because the DAP has a similar time course than the AHP and the DAP is masked by the AHP, or because the DAP is not present in some oxytocin neurones.

Despite all that, the LIF model matches the Hodgkin- Huxley model for magnocellular neurones remarkably well (Leng *et al.*, 2017), and it will be shown in this thesis how robustly this LIF model can mimic the action potential production of oxytocin neurones under different circumstances.

Oxytocin secretion

Spike activity allows the neuron to integrate information and filter certain kinds of noise. However, spikes are not the final product of oxytocin neurones: oxytocin secretion is.

The spiking activity of oxytocin neurones triggers secretion in two different ways. Oxytocin is secreted peripherally, from the axon terminals, but it is secreted centrally too, in a semi-independent way from the dendrites (Ludwig, 1998). Both types of secretion can be studied independently because oxytocin does not trespass the blood-brain barrier (Mens *et al.*, 1983; Lee *et al.*, 2018). Classically, dendrites were thought to just receive inputs from other neurones and initiate action potentials. In the case of oxytocin neurones, central oxytocin's origin was thought to be exclusively parvocellular. However, magnocellular neurone's dendrites are active as well, and magnocellular neurones have the largest stores of the oxytocin in the brain (Ludwig & Leng, 2006). When secreted centrally, oxytocin behaves as a neuropeptide (Leng, 2018*b*), reaching concentrations 100-1000 fold higher than in blood. Central oxytocin autoregulates oxytocin neurones, directly promoting oxytocin secretion, but it has also two opposite indirect effects. It increases the production of endocannabinoids which inhibit glutamatergic afferents to oxytocin neurones. At the same time, oxytocin attenuates GABA inputs with the resulting increment of spiking activity. All that seems to be related with the role oxytocin has in synchronizing oxytocin neurones, increasing their activity during bursting periods (Ludwig *et al.*, 2002).

Diffused central oxytocin also plays an important role. During the last years it has been shown that central oxytocin is involved in the regulation of maternal bonding and social interaction (Donaldson & Young, 2008) or in food choice or food reward (Sabatier *et al.*, 2013; Olszewski *et al.*, 2016).

Although oxytocin and vasopressin can be secreted from dendrites, the focus was put here in axonal secretion, through which oxytocin reaches the whole body. For both vasopressin and oxytocin neurones, when spikes arrive at the axon terminal, they open voltage-gated Ca^{2+} channels. This produces three main effects. First, the entrance of Ca^{2+} maintains the depolarization provoked by the spike, broadening in time the depolarizing effect (Bourque, 1990; Muschol & Salzberg, 2000). Second, while the depolarization is maintained, oxytocin vesicles fuse with the axonal membrane, releasing the hormone into the blood (Mansvelder & Kits, 2000). Finally,

if the [Ca^{2+}] becomes too high, it produces a negative feedback, opening Ca^{2+}-dependent K^+ channels that hyperpolarize the membrane (Jackson *et al.*, 1991). The three mechanisms are present in both vasopressin and oxytocin neurones but with differences. The negative feedback is more rapid in vasopressin neurones, producing fatigue after just 18 s when spikes arrive at rates of 13 Hz or more. However, oxytocin neurones do not show symptoms of fatigue at 13 Hz even if the stimulation lasts many minutes (Bicknell *et al.*, 1984; Bicknell, 1988).

Thus, vasopressin and oxytocin secretion have several things in common but other things that differentiate them. The similarities made us think that it would be possible to adapt a vasopressin mathematical model developed by my supervisors (MacGregor & Leng, 2013) to simulate secretion from oxytocin neurones. The differences led the adaptation made in the vasopressin model to obtain a secretion model for oxytocin neurones.

Synergy between spiking and secretion activities

Those differences in secretion closely relate to differences in spiking activity. A large DAP in vasopressin neurones makes many of them stay depolarized after a spike, making them able to produce bursting activity, which they alternate with periods of silence. During bursts, vasopressin neurones fire at between 10 to 14 spikes/s, which maximizes the secretion per spike, due to the non-linear coupling between spike activity and secretion (Bicknell, 1988). However, if they are active at that rate for more than 30 s, vasopressin secretion shows *fatigue* (Bicknell *et al.*, 1984). That makes the phasic activity a perfect complement to their secretory characteristics. Alternating periods of activity at 13 spikes/s with silences maximizes the efficiency of secretion.

Unlike vasopressin neurones, oxytocin neurones fire spikes continuously, not producing bursts except during lactation or parturition. That bursting activity presents itself at a much higher frequency than the bursts in vasopressin neurones, reaching frequencies of 30-100 spikes/s.

However, during normal, regular activity, oxytocin neurones do not present large excursions in firing rate, which would lead to even larger excursions in secretion. They rarely fire above 13 spikes/s and their average spiking activity changes smoothly, even under acute challenges. Thus, preventing large excursions in

secretion combines with the ability of oxytocin neurones to maintain spike activity at around 13 spikes/s for minutes. (Bicknell *et al.*, 1984; Leng *et al.*, 2001).

Interestingly, and despite all the differences between each other, the concentrations of oxytocin and vasopressin in plasma follow similar patterns under hypovolemic and osmotic challenges (Stricker & Verbalis, 1986; Stricker *et al.*, 1987). This is because vasopressin neurones do not synchronize their activity. Thus, the phasic firing some vasopressin neurones present, do not affect the average response of the whole population (MacGregor & Leng, 2013).

The AHP and its role in secretion.

The synergy between spiking and secretion dynamics in both vasopressin and oxytocin suggests that they evolved together to produce a co-operative response. In the case of vasopressin, if an elevated spiking activity is maintained for 18 seconds, fatigue will appear in the secretion, smoothing vasopressin secretion down. Even more, if vasopressin neurones would fire above 13 spikes/s, their secretion rate per spike will be reduced (Bicknell, 1988).

Oxytocin neurones present a similar mechanism of Ca^{2+} related fatigue to that in vasopressin neurones but at much higher spikes rates. Whilst secretion rate per spike peaks in vasopressin neurones at 13 spikes/s, in oxytocin neurones it peaks at 50 spikes/s. In fact, oxytocin neurones can maintain a firing activity of 13 spikes/s for minutes. Above that level, secretion fatigue also appears in oxytocin secretion. However, if oxytocin neurones would fire steadily above 13 spikes/s they would also deplete their hormone stores (Leng *et al.*, 1994).

The main candidate to prevent the depletion is the AHP, which produces small, cumulative hyperpolarisations. In fact, because of the non-linearity of the coupling between spike activity and secretion, the AHP role has even bigger consequences for secretion (Figure 34Figure 35Figure 36).

The oxytocin computational model

As mentioned earlier, when I began my PhD, my supervisors had already shown that a mathematical model with a HAP and an AHP could mimic the basal dynamics of a single oxytocin neuron (MacGregor *et al.*, 2009).

The rest of this introduction is dedicated to summarizing how the model was expanded to mimic several dynamics of the spiking activity in response to different

challenges associated with energy homeostasis, osmotic pressure and hypovolemia, coupling it with an oxytocin secretion model and an oxytocin clearance model, all based on published experimental data.

The spiking model

When oxytocin is secreted from the axon terminals in the posterior pituitary, oxytocin behaves as a hormone, helping in the energy homeostasis by reducing food intake and meal duration, and in osmotic homeostasis by inducing natriuresis (sodium excretion in the urine). After food intake, the spiking activity and production of plasma oxytocin increases (Hume *et al.*, 2017). This is part of the satiety mechanism that limits the size of the meals we eat: oxytocin released in the brain is anorexigenic – it inhibits food intake (Sabatier *et al.*, 2013; Morton *et al.*, 2014). One excitatory signal that contributes to the activation of oxytocin neurones during food intake is the one provoked by CCK, a peptide secreted from the duodenum in response to food ingestion. CCK acts at CCK1 receptors on the nerve endings of gastric vagal nerves. These vagal neurones project to the nucleus tractus solitarius (NTS) in the caudal brainstem, from which noradrenergic neurones of the A2 cell group project directly to the SON and the PVN (Sabatier *et al.*, 2013; Morton *et al.*, 2014).

Systemic injections of CCK increase the firing rate of oxytocin neurones, whilst they supress or do not affect vasopressin neurones (Leng *et al.*, 1991). During the last two and a half decades, this has made CCK a great tool for differentiating oxytocin neurones from vasopressin neurones, being still used in electrophysiological (Paiva *et al.*, 2017) or *c-fos* experiments (Katoh *et al.*, 2014).

The first thing to develop the model was to mimic the response to CCK in an LIF model with just an AHP and a HAP. The response looks simple when averaged in bin widths of several seconds. It basically consists of a linear increase in spiking activity during the injection and an exponential decrease after it (Velmurugan *et al.*, 2010). The model mimicked that response closely (Figure 29) but, more importantly, was able to differentiate the contributions of the HAP and the AHP (Figure 26).

Taking advantage of that, the model was used to further elucidate the role of the AHP, as the AHP is a key component modulating excitability in many types of neurones (Sah, 1996). First, it was done for the spiking model (Maícas-Royo *et al.*, 2016). In that paper it is used the *index of dispersion*, a statistic calculated as the

quotient between the variance and the mean of a variable. The index of dispersion gives a measure of the variability of a variable. When the variable is the spike rate of oxytocin neurones, it was seen that its index of dispersion was smaller than expected when calculated for bins longer than 4s (Figure 23). This happened for most oxytocin neurones, but not for all of them. So, it could be hypothesised that the ones where the index of dispersion was reduced at longer bins had a more dominant AHP, while the ones where that was not happening had a more dominant DAP. As mentioned, a component of the AHP can be blocked by apamin. Thus, data from oxytocin neurones exposed to apamin was compared with the data produced by the model when mimicking those spiking behaviours, simulating the effect of apamin by making AHP equal to 0 (Figure 27). Those experiments helped to elucidate the role of the AHP in the spike activity of oxytocin neurones but also helped to confirm the presence of a DAP in some oxytocin neurones, usually masked by a stronger AHP.

The secretion model

This success motivated me to pursue further horizons in relation to the role of the AHP. In particular, the question about how the presence of an AHP affected oxytocin secretion and plasma concentrations of oxytocin arose. To do that, it was necessary to build a secretion model, and I adapted a model that had been developed by my supervisors to simulate vasopressin secretion (MacGregor & Leng, 2013). There are substantial differences between oxytocin and vasopressin secretion, but the vasopressin model should also have many things in common, biologically and mathematically, with the oxytocin secretion model that had to be implemented.

When vasopressin neurones fire faster than 13 spikes/s, the incremented $[Ca^{2+}]$ in the axon terminal starts to negatively affect the secretion. As a result, vasopressin neurones secrete less at 26 spikes/s than at 13 spikes/s. In the model for oxytocin secretion, it was necessary to shift that behaviour up to at least 52 spikes/s (Bicknell *et al.*, 1984; Bicknell, 1988) (Figure 30). Thus, in the oxytocin secretion model, as in the vasopressin one, there is a negative feedback and a fatigue effect, and both are still provoked by the Ca^{2+} accumulated after arrival of spikes at a high rate. However, the $[Ca^{2+}]$ starts triggering negative feedback in the oxytocin secretion model, leading to fatigue, only when the spiking model fires above 13 spikes/s. (Maícas-Royo *et al.*, 2018).

From a single oxytocin neuron to oxytocin concentrations in plasma

Having simulated the secretion of the whole population of magnocellular oxytocin neurones to mimic the available experimental data, it was necessary to make a conceptual jump. The spiking model was a single neuron model. However, there is no data in the literature linking the spiking activity of single oxytocin neurones to their secretion. What there was in the literature were data linking the *total* oxytocin secretion from the posterior pituitary in response to electrical stimulation at different frequencies to (Bicknell *et al.*, 1984; Carolyn A. Bondy, 1987; Bicknell, 1988). That electrical stimulation was assumed to trigger secretion by first triggering spikes in the axons of the magnocellular neurones from the SON and the PVN. Thus, the goal was to develop a secretion model simulating that electrical activity as spikes from our spiking model.

While secretion is the final product of oxytocin neurones, what the body sees is the oxytocin concentration in plasma. Accordingly, a secretion model would not be complete without also simulating the fate of oxytocin in plasma. Fortunately, there are classic experiments (Ginsburg & Smith, 1959; Fabian *et al.*, 1969*a*) giving the necessary data to develop a model of oxytocin clearance from plasma (Figure 33A,B).

From that point, with a complete predictive model for oxytocin neurones, it could be used, as shown in chapter 3, to predict the data of several papers which had connected the spiking activity of oxytocin neurones with the plasma concentration of oxytocin (Figure 33C-D).

Heterogeneity

Like any other group of neurones, oxytocin neurones are heterogeneous. Each oxytocin neurone differs from every other in the precise composition of receptors that it expresses and in the precise complement of afferent inputs that it receives. Each neurone receives several thousand afferent nerve endings from many hundreds of other neurones. Most of these inputs are GABAergic or glutamatergic, but oxytocin neurones express many other receptors (Leng *et al.*, 1999). They have, for example, noradrenaline receptors, which transduce the excitatory inputs from the NTS neurones (Randle *et al.*, 1986; Onaka *et al.*, 1995). They also express dopamine receptors, associated with penile erection (Baskerville *et al.*, 2009) and acetylcholine receptors (Shioda *et al.*, 1997). Finally, the spiking activity of oxytocin

neurones is modulated by a vast diversity of peptides. Among these, oxytocin neurones have receptors for oxytocin (Freund-Mercier *et al.*, 1994), CCK (Day *et al.*, 1989) and opioids (Brown *et al.*, 2000).

Oxytocin neurones are also heterogeneous in their membrane characteristics. One of the clearest examples is that some of them express a DAP (Stern & Armstrong, 1996), probably related with different densities of high voltage Ca^{2+} currents (Teruyama & Armstrong, 2005). That characteristic affects, for instance, the response to histamine, which through the presence of the histamine receptor, can enhance, inhibit or let unaffected different oxytocin neurones (Smith & Armstrong, 1993). Furthermore, channel properties are not fixed (Teruyama & Armstrong, 2005) and oxytocin neurones can modify their response over time (Sannino *et al.*, 2017).

The heterogeneity in the inputs and membrane's properties make oxytocin spike responses heterogeneous as well. If it is added to that the fact that oxytocin neurons can fire in two different ways: regular sustained spiking activity or bursting activity (Armstrong *et al.*, 2002), it might be expected that oxytocin neurones will produce a wide range of spiking responses depending on the situation.

Heterogeneity also affects oxytocin secretion. Every oxytocin neurone contains several hundred thousands of vesicles, each with ~85,000 molecules of oxytocin (Nordmann & Morris, 1984). Exocytosis from the axon terminals depends, again, on various factors such as the number of Ca^{2+} channels, that are unique to each oxytocin neurone (Fisher & Bourque, 2001).

Knowing that those levels of heterogeneity exist, the model has tools to simulate it, varying different parameter values amongst neurones and looking at the final secretory average. Ideally, the model could introduce that heterogeneity in every aspect of the spiking model or the secretion model, where the neurones are still treated individually before their products accumulate into a global one in the diffusion model. Following the literature and our own electrophysiological library of oxytocin neurone recordings, the model was tested with two factors where huge variability was found (Figure 37). The first factor was the basal spike rate. Analysing 23 oxytocin neurones that responded to CCK, it was found they had a mean basal firing rate of 2.5 spikes/s but with a range of 0.02 to 7.9 spikes/s. Similarly, the mean response to injecting 20 µg/kg of CCK was an increment of 1.5 spikes/s. However, this varied between 0.57 and 3.6 spikes/s (Maícas-Royo *et al.*, 2018).

Finally, it was necessary to balance the level of heterogeneity the model should have. In the simulations, it will be seen that sometimes the average response of the whole population of oxytocin neurones can be mimicked without heterogeneity, or even with a single neuron response. In other occasions, particularly to mimic the *in vivo* variability in the response, in both the spiking and secretory response, it was required to simulate a population with a certain level of heterogeneity.

Oxytocin and osmotic pressure

Vasopressin, also called the antidiuretic hormone, was placed soon in a privileged position, among the hypothalamic hormones, in the control of osmotic pressure. However, oxytocin participation in the fluid homeostasis was also suspected after hypertonic saline injection was shown to induce milk ejection in goats (Andersson, 1951) and to affect uterine activity in the dog (Abrahams & Pickford, 1954). Today, it is known that oxytocin has a role in electrolyte homeostasis in many species (Antunes-Rodrigues *et al.*, 2004; Bourque, 2008; Zimmerman *et al.*, 2017). In particular, oxytocin promotes natriuresis (Verbalis *et al.*, 1991; Huang *et al.*, 1996) after a hypertonic saline injection in rats (Huang *et al.*, 1995), but not in humans (Rasmussen *et al.*, 2003). In the kidneys, Na^+ is excreted when cGMP, an intracellular second messenger, is produced. Oxytocin promotes its production in two different ways. First, when oxytocin binds to NOergic cells in the kidneys, it activates nitric oxide synthase, which releases NO. The presence of NO leads to an increment in cGMP that closes Na^+ channels, preventing the reabsorption of sodium. At high concentration levels, oxytocin also promotes the production of the atrial natriuretic peptide (ANP) which also promotes the production of cGMP, reducing the Na^+ reabsorption and producing natriuresis (Antunes-Rodrigues *et al.*, 2004).

Oxytocin released in the brain also participates in the regulation of sodium appetite in rats (Blackburn *et al.*, 1995). Conversely, hypoosmolality inhibits oxytocin secretion (Brimble & Dyball, 1977), which can lead to a reduction in natriuresis and salt appetite.

Osmoreceptors

Oxytocin neurones change their activity in response to changes in osmolality in two different ways. First, they behave as osmoreceptors (Oliet & Bourque, 1992), which it is a term given to the cells that can change their electrical activity depending on

their extracellular osmolality. Hyperosmolality activates capsaicin-insensitive cation channels in magnocellular neurones. Those channels present receptor which detect mechanic changes. Due to a layer of actin filaments and a network of microtubules, they can detect if the neurone shrinks (Prager-Khoutorsky & Bourque, 2015). In addition, oxytocin neurones receive synaptic inputs from other osmoreceptors in the circumventricular organs (Bourque, 2008), areas that do not possess a proper brain barrier (McKinley *et al.*, 2003). Among these areas there are two that contain a great quantity of osmoreceptors: the subfornical organ (SFO) and the organum vasculosum of the Lamina Terminalis (OVLT). Osmoreceptors from those areas can detect changes in the osmolality of the ventricles or from the plasma, due to the vascular innervation in the walls of the ventricles, close to the SFO and the OVLT. The osmoreceptors in those areas detect mainly the change of $[Na^+]$, ignoring other solutes like urea or glucose. A couple of exceptions are mannitol and sucrose, which also make osmoreceptors respond, but those sugars are usually not in plasma (Verbalis, 2007; Bourque, 2008). Osmoreceptors from the OVLT and the SFO translate any osmotic change into a change in electrical activity, which will modify the synaptic release of either glutamate or GABA. Both the SFO and the OVLT project to the nucleus medianus (MnPO), which integrates all kinds of information related to thirst, fluid volume and osmotic pressure, coming from other centres of the brain (Zimmerman *et al.*, 2017).

Of these three nuclei, the SFO is the most extensively studied. It contains populations of both glutamatergic and GABAergic neurones. Both populations of neurones communicate bidirectionally with the OVLT and the MnPO. Glutamatergic pathways from the SFO also reach the SON, where they activate magnocellular neurones.

The OVLT and the MnPO also contain glutamatergic and GABAergic neurones but it has been more difficult to differentiate their functions and projections (Zimmerman *et al.*, 2017). Entangled excitatory innervations from the OVLT and the MnPO have been traced to the SON. However, although there are GABA neurones in the OVLT and the MnPO, there is no literature showing where those neurones, or other GABA neurones from the SFO, could project or what the function of those projections is.

Because neurones receive a mix of inputs, from different locations, produced by different neurotransmitters that alter the membrane in different ways, neuroscientists use blockers to try to separate the different influences (Table 3). For instance,

GABA receptors can be blocked, usually with bicuculline, and see if the response of neurones is affected. That strategy was used to show that the OVLT projects inhibitory pathways to the SON (Yang *et al.*, 1994). However, Richard & Bourque (1995) found that, in a hypothalamic explant preparation, although changes in the osmolality in the OVLT changed the activity of oxytocin neurones in the SON, none of those changes were produced by inhibitory inputs. Some years later, Leng *et al.* (2001) showed that during an hypertonic saline i.v. infusion, oxytocin neurones respond more if bicuculline had been injected previously. That contradictory result was attributed by Leng *et al*. to the fact that the explant preparation used by Richard & Bourque did not contain the MnPO.

Table 3. Neurotransmitter blockers (Yang et al., 1994).

Blockers	**Receptor**
Mecamylamine, hexamethonium hydrochloride	Nicotinic acetylcholine
Kynurenic acid	Excitatory amino acids
APV (Aminophosphonovaleric acid)	NMDA receptors
Bicuculline methiodide	$GABA_A$
2-hydroxysaclofen	$GABA_B$
Losartan	Angiotensin-II AT_1
Proglumide	CCK
CNQX (6-cyano-7-nitroquinoxaline-2,3-dione)	Non NMDA receptors
CNQX	Block fast EPSP
APV	Slow EPSP (partially)

Apart from showing the necessity of IPSPs for the response of oxytocin neurones to osmotic challenges, Leng *et al*. established the oxytocin spiking and secretory response to i.v. infusions of hypertonic NaCl. They found a linear relationship between the NaCl infused and the increment in firing rate of the neurones in the SON.

The osmotic model

Those two results, the necessity of IPSPs, and the linear response of oxytocin neurones to the NaCl infusion, made us think of a new way of testing the model.

To do it, a model was made to simulate the distribution of $[Na^+]$ in the rat's body after a NaCl i.v. infusion (Figure 38). From this, it was estimated the $[Na^+]$ detected by the circumventricular organs and created a new input to our oxytocin spiking

model as a linear function of that [Na^+]. A model was also developed to recreate the [Na^+] dynamics after an i.p. NaCl injection, testing the model with results obtained in experimental data (Brimble & Dyball, 1977). The same data allowed us also to test the oxytocin spiking model for stable osmotic pressures. Finally, it was simulated the oxytocin response after an i.v. NaCl injection (Higuchi *et al.,* 1985) (Figure 39).

Our oxytocin model mimicked very well the results obtained experimentally, for both the spiking and the plasma oxytocin dynamics (Figure 41). That gave evidence of its robustness and also supported the hypothesis that IPSPs from the lamina terminalis are necessary for the oxytocin response to osmotic changes in the body (Figure 42).

To complete the study on oxytocin neurones responding to osmotic challenges, it was also explored the interaction of osmolality with hypovolemia. Initially, it was expected that the oxytocin model would simply simulate the response to hypovolemia. However, the model gave much more.

Oxytocin and hypovolemia

In mammals, blood loss leads to a cascade of mechanisms that the body uses to maintain or recover blood pressure. During the first stage of blood loss, blood pressure is maintained by an increment in heart rate and vasoconstriction (Schadt & Ludbrook, 1991). This response is mediated by baroreceptors and the atrial natriuretic peptide (ANP).

Baroreceptors are stretch sensors located in the blood vessels which decrease their activity under hypovolemia and increase it under hypervolemia or a rise in heart beat (Heesch, 1999). In the brain, the NTS, area postrema and nucleus ambiguous, receive information from the baroreceptors situated in the left atrium, aortic arch and carotid sinus through the aortic and vagus nerves. An increased activity of the baroreceptors inhibits vasopressin secretion, though to different degrees depending on the species. In the dog and sheep, vasopressin is released after small hypovolemia whilst in the rat, a much higher volume reduction is needed (Share, 1988).

Atrial natriuretic peptide (ANP) is a hormone produced firstly in the heart, as a mechanism to quickly reduce blood pressure, but also in the hypothalamus (Curry, 2005). The hypothalamic production of ANP is mediated by the baroreceptors' afferent signals to the brain (Antunes-Rodrigues et al., 1992). Circulating ANP increments under blood pressure and decreases under hypovolemia and its

changes are detected by atrial receptors, which send the information to the NTS. From there, GABAergic projections reach vasopressin neurones in the PVN, modulating an excitatory vasopressin projection to spinal renal neurones (Haselton & Vari, 1998). In parallel, excitatory projections from the NTS project to oxytocin neurones in the PVN, which project to spinal cardiac nerves, incrementing their activity (Coote, 2005).

Lastly, the renin-angiotensin hormonal system is also involved in hypovolemia. Under a reduction of renal blood flow, renin is synthesised in the kidneys. Circulatory renin transforms angiotensinogen, produced by the liver, into angiotensin, which is rapidly converted into angiotensin II. Angiotensin II is a vasoconstrictor by itself but it also triggers the secretion of aldosterone, which produces the reabsorption of water and sodium from the liver (Carey & Siragy, 2003).

If blood loss is maintained and becomes moderately high (~30% in rats), the excitatory effect of angiotensin II in vasopressin and oxytocin neurones becomes more important. Also, baroreceptors stop firing if the blood pressure decreases massively, affecting as well the ANP production. In that scenario, vasopressin and oxytocin increment quickly their concentration in plasma. From that point, the arterial pressure falls (Schadt & Ludbrook, 1991) and the circulating vasopressin and oxytocin become main actors in the regulation of the water retention and cardiac activity.

Experiments have shown that circulating angiotensin II stimulates vasopressin secretion whilst ANP reduces it. And even more, that both chemicals modulate each other effect (Matsukawa & Miyamoto, 2010). However, angiotensin II affects magnocellular neurones following a different pathway.

Apart from presenting osmoreceptors, some OVLT and SFO neurones also express receptors for angiotensin II (McKinley et al., 2004; Zimmerman et al., 2017). Vasopressin neurones respond strongly to high levels of angiotensin II, produced by large volume or blood pressure changes. Due to it, a vasopressin plasma increment would help to the hypovolemia or low blood pressure promoting water retention (Phillips, 1987). However, not only vasopressin is secreted in response to volume or pressure changes. In the rat, hypovolemia increases the plasma concentration of oxytocin in a very similar way (Stricker et al., 1987).

Thus, magnocellular neurones in the rat are strongly connected with the body response to hypovolemia and blood pressure, and, as has been discussed, they also respond to osmotic pressure. Nevertheless, the resultant increment of vasopressin or oxytocin is generally difficult to associate exclusively with hypovolemia. For instance, if an animal is dehydrated it becomes hypovolemic, but its osmolality increases as well.

A simple way to test hypovolemia without changing osmolality is by using controlled haemorrhages. As mentioned before, uterine contractions are produced during labour due to the pulsatile secretion of oxytocin. That secretion also prevents post-partum haemorrhage in the third stage of labour (Arrowsmith & Wray, 2014). On the other hand, it is also known that haemorrhage enhances the production of oxytocin in the rat (Fabian et al., 1969a) and in larger animals (Weitzman et al., 1978) .

However, experiments including haemorrhage present different problems. The blood volume changes restrict the number of samples that can be taken. In addition, taking samples from a rat that have already lost a 10-40% of its blood in an haemorrhage would presumably alter the physiology in a 300 g animal, which only have around 10 ml of plasma. Apart from being dangerous for the animal, the extravascular fluid and the intracellular fluid will rapidly shift part of their volumes to restore the plasma volume. Thus, during haemorrhage and until the body fluids recover balance, the body will suffer many quick changes in blood pressure, haematocrit concentration, osmolality and fluids volume.

In particular, and independently of the volume shift, during haemorrhage there will be a reduction in blood pressure. Hypotension and hypovolemia are entangled. However, they also independently trigger oxytocin secretion, using different pathways (Smith & Day, 2003).

Polyethylene glycol (PEG) has been used to produce a more controlled hypovolemia (Dunn et al., 1973). PEG produces an edema in the EVF. The fluid for that edema comes from the plasma, producing hypovolemia without altering blood pressure or osmolality, but increasing the haematocrit concentration in plasma. In addition, the change in the plasma volume last for hours (Stricker & Verbalis, 1986). That helps in the experimentation with rats, allowing more samples, usually replaced by the same amount of saline, and more time to recover.

Using PEG to produce hypovolemia, it was reported that oxytocin neurones were responding in the same way as during haemorrhage, i.e. the plasma concentration of oxytocin increased. In addition, because PEG does not alter the osmolality in plasma, the osmosensitive inputs coming from the circumventricular organs should not be altered (Smith & Day, 1995, 2003). That opened the door to experiment if osmotic pressure and hypovolemia, that independently increased the oxytocin in plasma, would increase it more, summing their contributions or working synergistically to obtain an even bigger oxytocin response (Stricker & Verbalis, 1986; Stricker et al., 1987; Windle et al., 1993).

The oxytocin model response to hypovolemia

That kind of complex experiment would imply first, a way for oxytocin to control the volume of plasma and extravascular fluid. Second, a way to increment the response of oxytocin neurones under hypovolemia. And finally, an independent way of modifying the osmotic pressure. Those three sets of changes can be implemented in our computational model. The model can simulate the PEG effect of shifting part of the plasma into the extravascular volume. It can, independently, raise the osmotic pressure. Finally, the model can, independently as well, modify the PSPs arriving due to the hypovolemia. For this last point, there are two hypotheses. The first one says that hypovolemia triggers an increment of EPSPs arriving to oxytocin neurones (Smith & Day, 2003). The second says that that the increment in oxytocin secretion might also come from a reduction in IPSPs, as happens for vasopressin (Yamaguchi & Hama, 2011).

The model, however, showed another result. It suggested that part of the increase in the plasma oxytocin rise produced by PEG could not be assigned either to an increment on EPSPs or to a reduction on IPSPs (Figure 43). In other words, part of the rise of oxytocin concentration in plasma was not due to an increment of oxytocin secretion of any kind. An answer usually masked by the intricate fluid dynamics, arose from the simulations: the increment in plasma oxytocin was partially provoked by the shift of already existing oxytocin between the plasma and the EVF. That diffusion and the nature of the clearance, which only happens from the plasma volume, can explain an increment in the plasma concentration without an increment in the oxytocin neurones activity.

A thesis of three parts

This thesis includes three papers. The first paper describes the spiking model of oxytocin neurones, the role of the AHP and how the AHP can mask the presence of a necessary DAP in some oxytocin neurones. The second paper presents three models in one: the spiking, secretion and clearance models. They show the importance of the AHP as a noise filter also in secretion; the oxytocin neurones' response to CCK; and the relevance of heterogeneity. The third paper tests the three-part model under three new scenarios involving osmotic pressure: osmotic pressure generated by i.p. or i.v. injections or infusions, the presence of bicuculline and the response to hypovolemia. Apart from the three papers, the thesis contains another three chapters. The first one is this introduction. The second, a chapter of methods, explains in detail the fundamentals of the mathematical tools used in the papers. Finally, there is a short conclusions chapter.

Funding

Both homeostatic processes where oxytocin is involved, eating and osmotic pressure homeostasis, were relevant to Nudge-it, the European Commission project funding my PhD:

> "The project engages internationally leading experts in the neurobiology of motivational behaviour, reward and regulation of appetite, experimental psychology, functional brain imaging, behavioural economics and computational modelling. The overall aim is to better understand decision-making in food choice and to build predictive models to contribute to improving public health policy".

Chapter 2.

Methodologies for computationally modelling oxytocin neurones

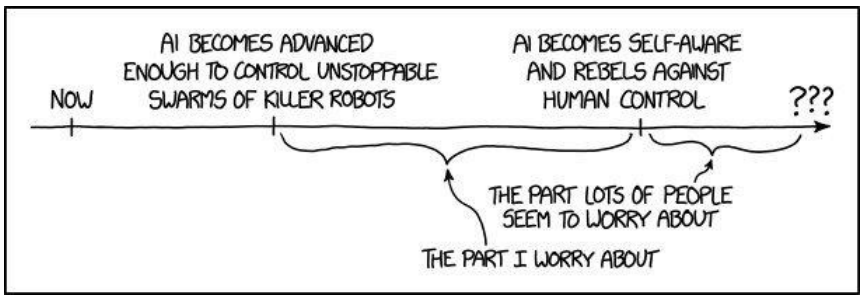

xkcd.com

As shown in the introduction, computers work with 1's and 0's, storing information as combinations of them and making mathematical operations following the rules of Boolean algebra. In the 1950's, the first computers were programmed by instructions consisting of those two numbers. For years, programmers needed to know the architecture of the computer to use the correct inputs in the correct place. With time, interfaces were developed to the point that, nowadays, most users do not need to know anything about the computer architecture to interact with devices millions of times more complex and powerful than those first ones. Programming languages, a set of syntactic rules closer to normal languages, allow programmers to create complex algorithms that can be understood and modified by other users who know the same language. Some of those languages, well known in the neuroscience field, are Matlab, Python, R and, in our case, C++. The translation between the language that the programmer uses and the 1's and 0's that computers work with is made by compilers and assemblers (Figure 4), programs written to do just that, with the particularity that the programmers do not need to know how compilers or assemblers work to use them.

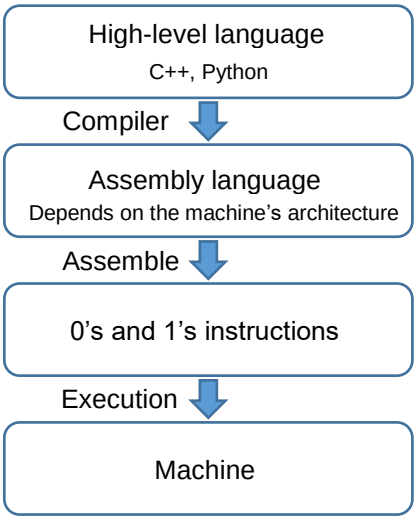

Figure 4. Layers between the written code and the machine.

C++, which has been used to develop most of the software in this thesis, is a language that allows control of the way the computer works in a deeper level than the other ones mentioned. That, in general, makes it more complex to understand and work with but also

between faster and much faster if properly used (Aruoba & Fernández-Villaverde, 2015; Borag & Fernández-Villaverde, 2018) .

In addition, the differences in resources and time consumed tend to be accumulative. Thus, when the coded tasks grow in complexity, C++ become an increasingly more efficient solution.

To model neurones, it is necessary to simulate fast behaviours, such as the arrival of post synaptic potentials or the opening and closing of Na^+, K^+ or Ca^{2+} membrane channels in response. The time constants to properly simulate those activities are on the order of a millisecond. At the other extreme, on certain occasions, simulations need to mimic data that lasts for more than an hour. Thus, the computer would need to run all the equations 216,000,000 times, to simulate 60 min of all the necessary behaviours happening every millisecond. The complexity increases when equations are added to simulate the secretion and clearance activity, and again, when the dynamics of the $[Na^+]$ in plasma (that ultimately affect the spiking activity) are incorporated. However, that would be only to simulate the spiking activity of one neuron and its consequences. The resources and time necessary would increase, at least, arithmetically, to simulate a population of neurones.

Computers, in contrast with the brain, have traditionally worked sequentially. They could not execute more than one task at a time, in contrast with the highly parallelized behaviour of the brain, where every neuron tends to have between 100 and 100,000 connections with other neurones. However, the last decade has brought personal computers with several cores, capable of running tasks in parallel. To run a population model, parallelization, also called threading, is a good solution. Threads, in computational science, are algorithms that allow a computational program to use multiple cores of a single CPU and/or multiple CPUs at the same time for different tasks.

In the studies detailed in this thesis, I set out to mimic neural dynamics of oxytocin neurons and groups of oxytocin neurons responding to different challenges. To do it, a model was first made of the spiking activity of a single oxytocin neuron based on the kind of inputs, channels or currents that these neurones are known to have. When the model showed reliability, the spiking model was integrated with a secretion model, challenging it again with different inputs, trying to mimic the resultant experimental data and using multithreading to simulate populations of

neurones The same process was repeated to integrate into the model the ability to predict the oxytocin levels in plasma and the response to osmotic pressure.

The spiking model. Converting mathematical equations to code.

From the first megalithic year calendars to the particle accelerators, mathematics has helped to predict or recreate all kinds of natural processes. First applied in evolutionary dynamics during the XIXth century, mathematical models have become commonplace in biological sciences with the advent of increasingly powerful computers, to the point that a new term, *in silico*, has appeared to describe computational models in biology.

In neuroscience, mathematics took a bit longer to show its capacity. However, when it was finally incorporated to the field, it did it in style. In the late 40's and early 50's, Hodgkin and Huxley developed equations to simulate how action potentials are propagated in the squid giant axon (Hodgkin & Huxley, 1952). They considered the axon as a circuit with currents, voltages, conductances and capacitances, and modelled the neuron dynamics with the same differential equations that describe the temporal dynamics of those electrical circuits.

The results accurately simulated the experimental data, but Hodgkin-Huxley's equations are extremely demanding computationally speaking. Thus, different simplified models have been proposed since then. Some of them lose the ability to mimic accurately certain behaviours but require fewer calculations and still produce statistically similar results. Others give a clearer idea of the different components involved, allowing the researcher to manipulate them in an independent fashion. Others look for both accuracy and low computational demands, but lack the ability to distinguish between the independent contributions of the different components of the "circuit" (Izhikevich, 2004).

To simulate the spiking activity of oxytocin neurones I used the *Leaky Integrate and Fire* model (LIF). The LIF model simulates the *integration* of neural inputs that changes the membrane's voltage until it crosses a threshold and *fires*, producing a spike. The addition of *leaks* to the *integrate* and *fire* simulates the ability of the neural membrane to recover a certain resting state, due to the ion flux through different channels. The LIF model is one of the computationally most efficient models (Izhikevich, 2004). In addition, it can be analysed by changing parameters

biologically meaningful to the inputs or the ion channels responsible for the membrane changes (Burkitt, 2006; MacGregor *et al.*, 2009).

To test the mathematical model and the matching with the real neuronal behaviour, different methods have been used. A vast platform to rapidly visualize the accuracy of the matches was already created by my supervisor Duncan MacGregor. It included the possibility to change parameter values and visualize the results in graph panels, changing the bin widths for many tools so the analysis could be made, for instance in 1, 5 or 10 s bins. Part of the task has then been to adapt my code and any new tools to work with his framework, trying to not do again something that he already had implemented. Thus, the framework was maintained, using the same programming language, C++ running it in the Microsoft Visual Studio 2010 Professional with the GUI library WxWidgets. I added, however multiple Microsoft Excel templates to store and analyse data, programming sometimes small macros to handle certain types of more complex or repetitive analysis or to develop small parts of the main C++ program, something I have done occasionally with Python as well.

Across my student and professional career, Microsoft Excel has been omnipresent, yet only recently did I realise that Excel is a perfect tool to build interdisciplinary bridges. As commented before, I programmed different scripts to analyse data with it, but I did much more than that. I used it often as intermediate way to explain data or even code in meetings. And, with time, I used it to store huge amounts of data accompanied by text, graphs, small algorithms and links. I followed a pattern in the files and sheet names, tracking the history and the visualization of my research's progress. I do not know what will happen with all those files in the future, but if anybody is interested on them, Excel will probably be a bridge between us.

Working with equations

One of the tasks for the biomathematician consists of translating biological processes into mathematical equations. In the simplest scenario, a single dependent variable *Y* will have a linear relationship with the only independent variable, X.

If the results are plotted in Excel, or any similar software, it will even tell us that our results can be approximated by a linear equation:

$$Y = a \cdot X + b \tag{1}$$

Where *a* will indicate the slope of the relationship and *b* the offset.

The linear relationship between two variables is simple, common in biology, easily translated into computational code and cheap in computer resources consumed. Many times it will be preferred to other solutions equally or even more accurate but more complex in one of those characteristics.

Exponential equations

With an element in their formulas in the form of e^x, exponential equations are very useful to model different biological systems.

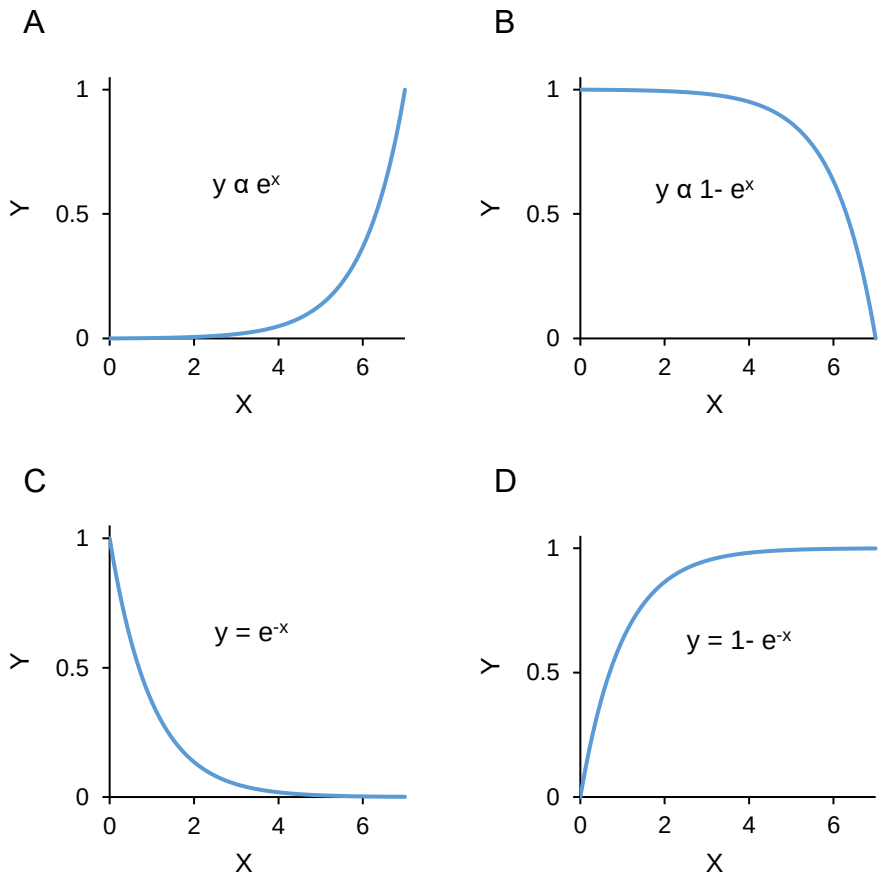

Figure 5. Typical exponential equations used in biological models. Curves A and B are normalised to have maxima of 1 on the domain shown. Notice how B shows the result of 1 minus what happens in A. The same happens between the figures D and C.

A bacterial growth in a petri dish would follow an exponential curve like the one in Figure 5.A, while the space in that petri dish still not colonized by the bacteria could be modelled by Figure 5.B. The recovery of resting state is usually modelled by an exponential like the one in Figure 5.C and saturation processes can be simulated by the shape Figure 5.D shows.

With linear and exponential equations, it is possible to model many biological behaviours. However, relationships between variables can be highly complex and there will be situations where it is tempting to try to model them with time dependent equations that mimic behaviour without modelling the underlying dynamics. For example, the plasma oxytocin levels obtained in a set of experiments after a CCK injection follow what could be considered as a sequence of two equations (Figure 6).

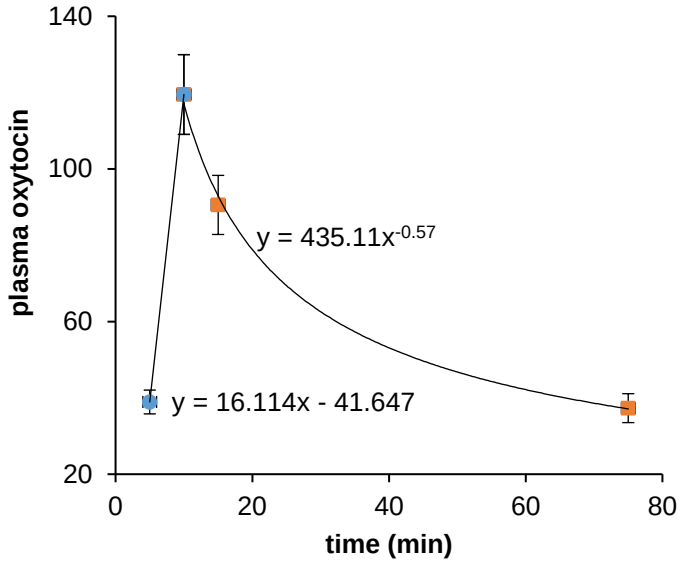

Figure 6. Incorrect use of mathematical equations to fit biological measurements. The plasma oxytocin levels response to an injection of 20µg/kg of CCK can be fitted in this experiment by two equations with the formulas shown in the figure. However, the formulas do not give information of the inner mechanisms producing that response and they are highly vulnerable to changes in the CCK values. In addition, the exponential decay should start when CCK is injected, not after the injection has finished.

The first one would simulate the time until the injection finishes and the second one the recovery and that would be a good approximation to the experimental data (Velmurugan *et al.*, 2010). However, that mathematical model does not tell us anything about what is happening in the secretion, or in the spiking activity of the oxytocin neurones. It is not predictive so, if anything changes in the biological model, the simulation will fail to follow it.

An equation should have biological sense. Equations should give us both information and the ability to model changeable dynamics using biological data. Each equation used tries to model a dynamic that has been measured in the literature. And the complex dynamic related with time will be replicated by integrating the simpler relationships between variables.

Translating the neuronal inputs into code. A not so simple example.

The first step is to know the purpose of the model in detail. I want to model the neural inputs, always with the same magnitude. They can be excitatory (EPSPs) or inhibitory (IPSPs) post synaptic potentials and I want to make them arrive randomly. To do the latter, I will make their arrival follow a Poisson distribution.

Second, the process has to follow a fixed set of steps, or algorithm:

1. In every unit of time or step of 1ms, a random arrival time, e_{pspt}, it is produced with a rate r_e, for the next EPSP.
2. The number of EPSPs in that unit of time, n_{epsp}, is incremented by 1.
3. If the sum of that arrival time plus the time the previous EPSP arrived is smaller than 1 ms, then (1) is repeated.
4. If not, do the (1), (2) and (3) steps for the IPSPs.
5. If both (3) and (4) have finished, go to (6).
6. Once the number of EPSPs and IPSPs that occurred in a unit of time are obtained, their influence, *input*, is calculated by summing both, applying a negative sign to the IPSPs.
7. I incorporate the input into the membrane voltage, making the membrane voltage recover a certain voltage, V_{rest} = -56 mV, with a time constant, *gamma*. I assume that the membrane tries to recover to V_{rest} all the time. If the afferent signals are positive, the recovery will have a negative sign, and vice versa.

Finally, the algorithm has to be translated into C++ code (Figure 7), assigning initial values to the variables. Different codes and variables' values will end in different results, the goal being getting a good match to the process being simulated.

```
// hstep = unit of time; epspt = time used for the arriving epsps

// Excitatory signals.
while(epspt < hstep) {  // Will do the same while there is remaining space in the unit of time
        nepsp = nepsp + 1;   //the number of epsps in an unit of time is incremented by 1.
        epspt = -log(1 - mrand01())/re + epspt;  // calculates when the next epsp will arrive.
}
//  when epspt is bigger than hstep, we will start the next iteration from the remaining epspt
epspt = epspt - hstep;

// Same process for inhibitory signals.
while(ipspt < hstep) {
        nipsp = nipsp + 1;
        ipspt = -log(1 - mrand01()) /ri + ipspt;
}
ipspt = ipspt - hstep;

// The total amount is the sum of excitatory minus inhibitory pulses
input = epsph * nepsp - ipsph * nipsp;

// Input voltage follows an equation decaying exponentially with "gamma" half-life
vsyn = vsyn - (vsyn - vrest) * gamma * hstep + input;
```

Figure 7. C++ code that simulates a neuron's random inputs. Comments and explanations, not processed by the computer, are in green and preceded by //.

Differential equations

The different mathematical models, heirs of the Hodgkin Huxley model, including the LIF used here, are based on differential equations in the time domain, which means that the value of a function in a certain infinitesimal time is related to the values of the same function in past infinitesimal time(s).

In the way they are used here, differential equations help to see the relationship between a function and its own changes. These equations are called *differential* because the evaluation of those changes is made in tiny fractions of the function. The sequence of all those changes, in all the fractions, is called the derivative of the function.

For instance, the differential change of the membrane voltage of a single neuron, dV/dt, can be expressed as a function of the same membrane voltage during the previous moment, V, affected by two constants, a, and b.

$$\frac{dV}{dt} = V \cdot a + b \tag{2}$$

The solution function *V* of Eq. (2) is, in fact, an exponential function similar to the one in Figure 5.C. In this particular case, it can be said that *V* is a *solution* of Eq. (2). However, there are several reasons to do not use either the differential equation, Eq. (2), or the solution function, *V.* To see them, let's rewrite the differential equation as an Euler approximation:

$$\frac{V_{t1} - V_{t0}}{(t_1 - t_0)} = V_{t0} \cdot a + b \tag{3}$$

Where V_{t1} is the membrane voltage in the instant t_1 *and* V_{t0} the voltage one unit of time before. ($t_1 - t_0$) gives the interval size, or unit of time, where the changes are measured, being set to 1 millisecond in our simulations.

From Eq.(3), V_{t1} can be calculated in a way easily translated to most programming languages (Eq (4)).

$$V_{t1} = (V_{t0} \cdot a + b)(t_1 - t_0) + V_{t0} \tag{4}$$

Written as a combination of sums, subtractions and multiplications, the Euler approximation offer some advantages:

- Computationally, it requires much less resources to calculate the sums and multiplications of Eq. (4) than to calculate an exponential function.
- Working with the approximation, the new value of a function can be related with the previous one, having the possibility of adding other terms at particular times.
- When a term has been added, it is incorporated to the value of the function for the next unit of time.

Once it is known how to codify an approximation to the differential equation, the next step is to decide which behaviours are going to be modelled. A good example can be found in the last line of the piece of code given in Figure 7.

```
// Input voltage follows a equation decaying exponentially with "gamma" half-life
vsyn = vsyn - (vsyn - vrest) * gamma * hstep + input;
```

Figure 8. Code of a differential equation written in C++.

Due to this codification as an Euler approximation (Figure 8), an equation that would calculate an exponential function over time can be modified to incorporate, every unit of time, the value called *input*, calculated in the previous lines (Figure 7).

The LIF model mimics changes in excitability but not the spike.

Once the inputs that alter the membrane voltage are known, it is necessary to define when a spike is going to happen, and which dynamics will be triggered because of it. In a typical neuron, when the sum of the excitatory and inhibitory inputs surpasses a certain voltage, V_{thresh}, the membrane dynamics change abruptly, rapidly depolarizing the membrane potential, then making it hyperpolarise quickly , even preventing the membrane to produce another spike for a while (refractory period). However, the LIF model used here simulates the spike times but not in its shape. To shape the equations needed to do that, depolarization and repolarization are reduced to the task of storing the moment when the spike occurred (Figure 9).

The spike times and their statistics are what the model really mimics when comparing its results with the real data. Thus, the model, based on a previous one developed by my supervisors (MacGregor *et al.*, 2009), does simulate the refractory period, because it is necessary to know when the membrane can produce a spike again.

Membrane response to a spike and time constants.

The main things responsible for the membrane dynamics that react to a spike are two currents, a hyperpolarising afterpotential (HAP) and an after-hyperpolarisation potential (AHP). They will help us to explain the use of time constants in the differential equations used through different parts of the thesis.

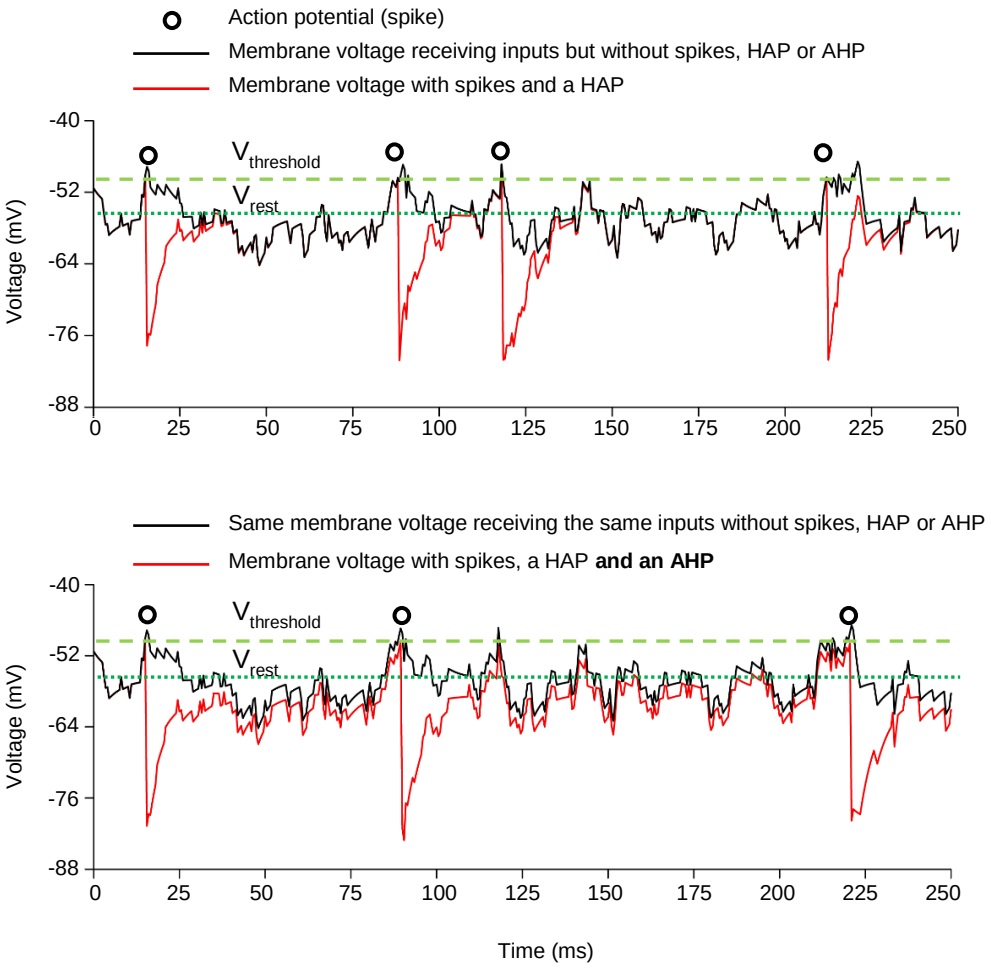

Figure 9 Upper. In black, modelled membrane potential without a $V_{threshold}$, AHP or HAP – i.e. this shows the response to randomly arriving PSPs. In red, the same membrane potential repolarising following a HAP when it reaches a $V_{threshold}$ = -50mV (in green). **Bottom**. In this case, the reactive membrane -in red- has a V_{th} and HAP but also accumulates hyperpolarization due to an AHP. Notice how, with the same synaptic input, a spike (black circles) is not produced at 120 ms when the AHP is present and the time when spikes are triggered is changed as well. Also, notice how the LIF model does not simulate the depolarization, just the repolarization after potential. Notice how the model does not simulate the depolarization above the $V_{threshold}$.

When a spike is produced in an oxytocin neuron the membrane depolarizes, and immediately after this, the HAP makes the membrane unable to fire again for around 30-50 ms (Figure 9.Upper). The AHP prevents the membrane from producing a spike as well, but its influence is slower and more noticeable when a sequence of spikes arrives in rapid sequence. In that case, the AHP can prevent firing for longer periods, up to half a second or more (Figure 9.bottom).

The behaviour of the voltage at the membrane is defined as:

$$V = V_{rest} + V_{syn} - HAP - AHP \tag{5}$$

Where V_{syn} is the voltage due to the PSPs, as it was shown in Figure 7, and γ the membrane time constant to recover the resting state, which has half-life of 3.5 ms:

$$\frac{dV_{syn}}{dt} = -(V_{syn} - V_{rest}) * \gamma + input \tag{6}$$

In Eq.(5), the voltage of the membrane is initially at a resting potential, V_{rest}. When V_{syn}, the resultant contribution of EPSPs and IPSPs, becomes different from 0, V_{syn} is added to V_{rest}. Both HAP and AHP can be modelled by exponential equations with time constants for recovery τ_{HAP} and τ_{AHP}. However, HAP and AHP can be modified if (V_{rest} + V_{syn}) gets greater than the threshold potential, V_{thresh}. At that moment, the model will produce a spike, changing δ from 0 to 1 during just that millisecond. During that small amount of time two hyperpolarising voltages, k_{HAP} and k_{AHP}, will be added to the HAP and AHP currents.

$$\frac{dHAP}{dt} = -\frac{HAP}{\tau_{HAP}} + k_{HAP} \cdot \delta \tag{7}$$

$$\frac{dAHP}{dt} = -\frac{AHP}{\tau_{AHP}} + k_{AHP} \cdot \delta \tag{8}$$

Several things about equations (7) and (8) should be noticed:

a) They are differential equations. When $\delta = 0$, which is most of the time, equations (6)(7) have the shape of Figure 5C, meaning that the AHP and the HAP contributions exponentially decrease with time constants τ_{AHP} and τ_{HAP}. Every new infinitesimal change of the HAP or the AHP depends on the previous value of HAP or AHP. Both equations can be translated into code as seen in Eq. (4).

b) The model simulates the spike contribution by making $\delta = 1$ during 1 ms. That suddenly changes the value of AHP and HAP by k_{AHP} or k_{HAP}, incrementing in those factors their contribution to the hyperpolarisation of the voltage membrane.

c) The presence of the time constants τ, which are an inverse function of the so-called half-life, λ,

$$\tau = \frac{ln2}{\lambda} \tag{9}$$

The time constant, or the half-life, represents how quickly the influence of the HAP or AHP triggered by previous spikes vanishes (Figure 10). The larger the half-life, or the smaller the time constant, the longer the influence. The HAP's half-life, λ_{HAP}, is short. That makes the membrane not usually affected by previous spikes. However, the AHP half-life is much larger and that would increase the influence of the past on this kind of current. The AHP has a strong, accumulative effect when several spikes are produced consecutively making the membrane much less likely to produce another spike for a while (Figure 9).

d) Working with differential equations makes it possible to modify those equations at any time increment. That is done with the amplitudes of the currents, k_{AHP} or k_{HAP}, which are added only when a spike occurs ($\delta = 1$). During that small space of time, 1 ms in our model, the membrane potential depolarizes and repolarises in no time in our simulations, producing a hyperpolarization which will probably make the modelled membrane enter a refractory period.

Together, equations (6) and (7) show that the membrane needs time to be able to produce a spike again. Moreover, that time will depend on the amplitude of those

currents, on the past occurrence of spikes and on the half-life of the current, the time the membrane needs to recover the V_{rest}. Without new spikes, both the AHP and the HAP will tend to 0 at some point but the AHP will take longer to get to that resting state.

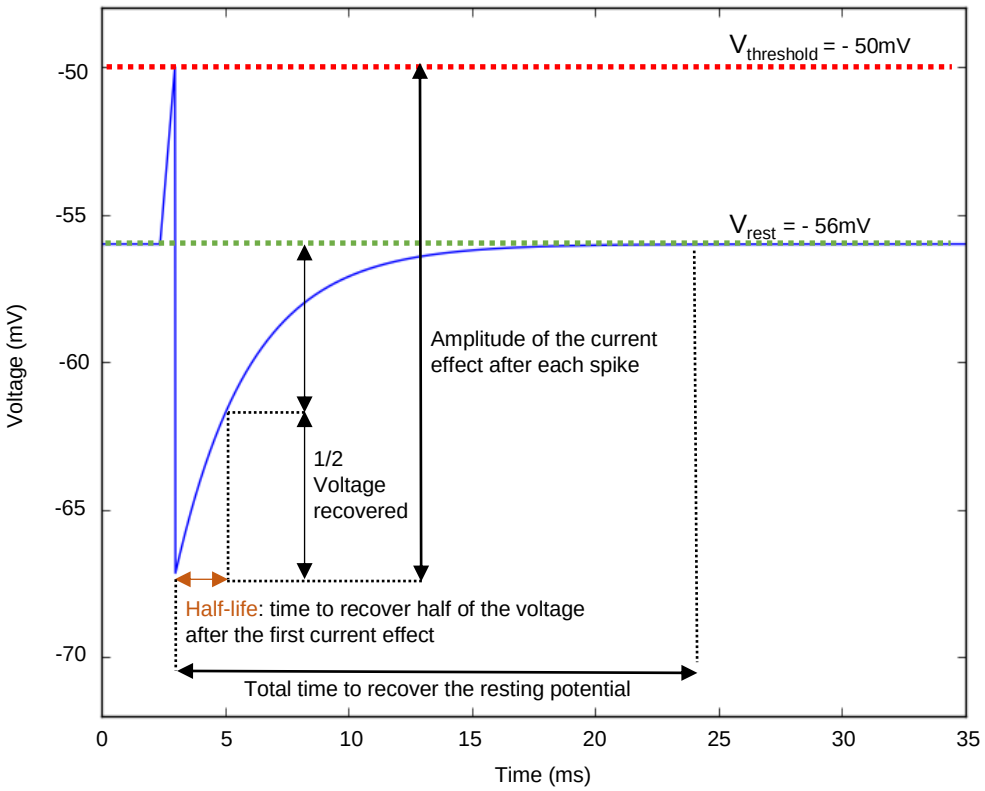

Figure 10. Parameters of a membrane current and how they affect the membrane voltage. The half-life is the time the voltage takes to recover half of the voltage until V_{rest} is reached.

Using similar equations for other models.

To this point, I explained different mathematical options I used to simulate the spiking activity. Linear, exponential and differential equations are among the simplest options to describe biology dynamics. It will be shown that, although the biology of the oxytocin neurons spiking, secretion, clearance from plasma and $[Na^+]$ in the body have not much in common, their dynamics have. Thus, what has been explained here about the spiking mathematical modelling, will serve as a common background for the rest of the models in this thesis.

Statistical measurements.

I have to say it. I find exciting using statistics. The fact that, what looks like a random set of data, can suddenly appear in front of my eyes as something meaningful makes it really rewarding. And it happens with all the statistical tools I used during the PhD. From the average and the standard deviation to the more complex tools, and specific to my research, as I will explain below.

Firing Rate

Regarding the spiking model, as noted earlier, I only want our LIF model to mimic different statistical measurements of the recorded spike times.

The firing rate is defined as the ratio between the number of spikes and the unit of time chosen. Usually I use it as “number of spikes per second” dividing the total number of spikes of an interval by the total amount of seconds in that interval (Figure 11). Other typical ratios could be “spikes per minute” or, in general, “spikes per X seconds”. This is a very simple measurement but, at the same time, it is essential. I need to always mimic the firing rate as a first step of our matching tests.

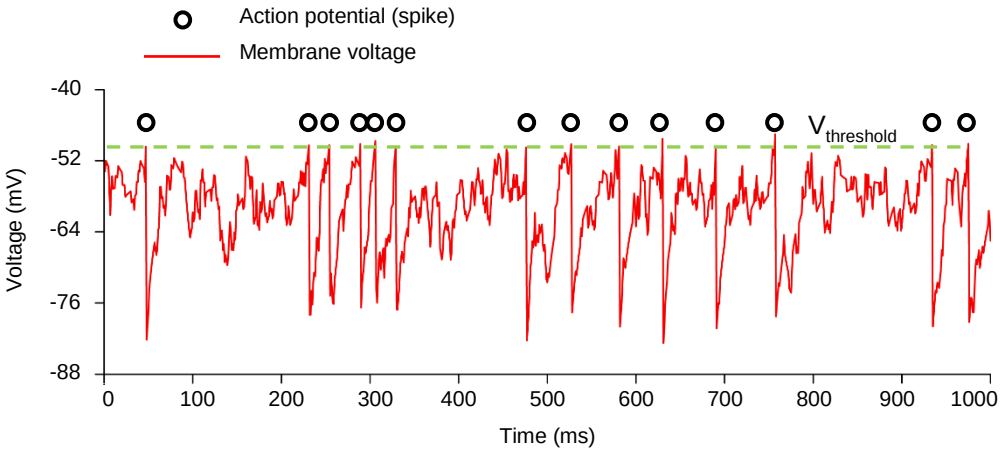

Figure 11. Calculating the spike rate. The model has produced 14 spikes in 1s (distinguishable by their abrupt hyperpolarization of ~30 mV). Thus, the firing rate in that interval (a second) is 14 spikes/s.

Once I know how to calculate the spike rate in an interval, it is often useful to know how it changes over time (Figure 12).

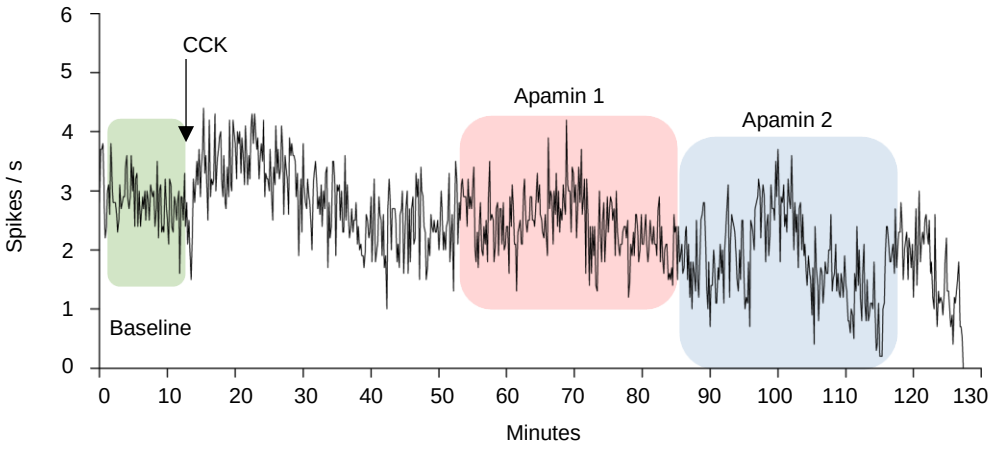

Figure 12. Spike rate calculated over a 130-min recording of an oxytocin neurone exposed to a systemic CCK injection and two different doses of 30 min infusions of apamin (Bull *et al.*, 2011).When calculating changes in the firing rate, I compare the response to different chemicals with the firing rate before applying any, in the baseline (in green).

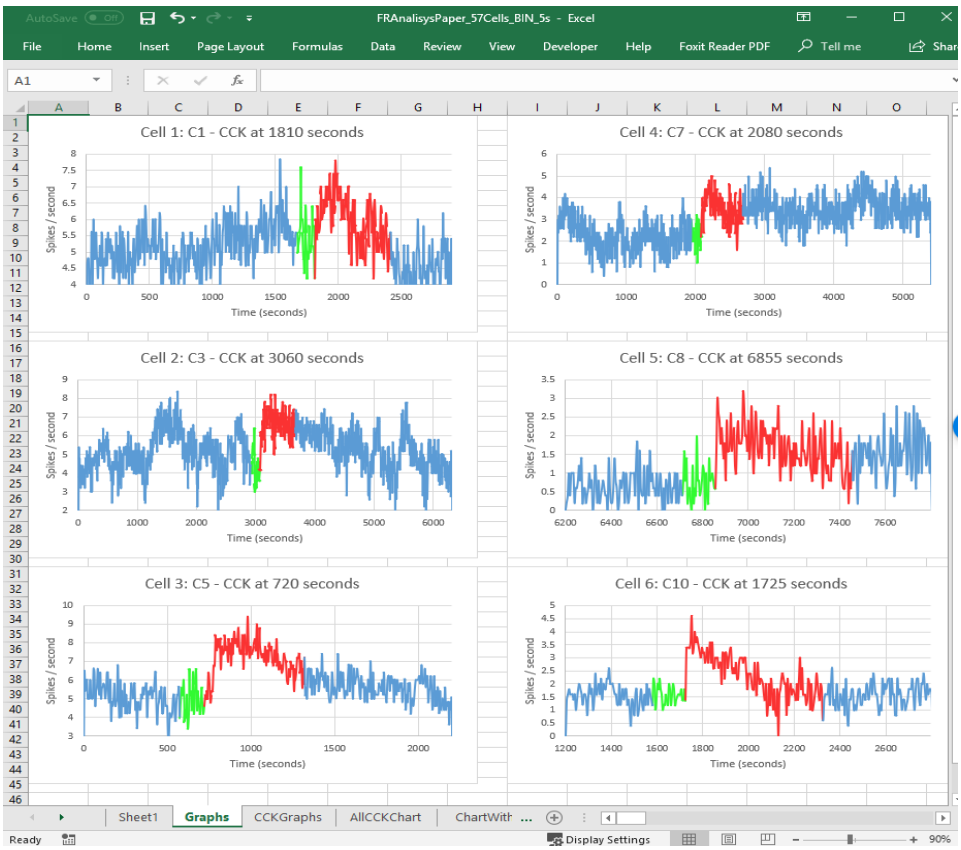

Figure 13. Screenshot of an Excel file created with Visual Basic Advance. Firing rates of six recorded oxytocin cells, out of a total of 57, exposed to CCK. The algorithm detects when CCK was injected and with preassigned times, colours in green the baseline (150 s), in red the response (500s) and in blue the rest of the time for each cell. It also automatically labels the charts with the cell number and name and the injection time.

Interspike interval distribution

The interspike interval (ISI) distribution is a measurement of the incidence of the different intervals between spikes that occur in a recording or in a modelled test.

In Figure 14 it can be seen a typical oxytocin neuron ISI distribution. From that figure it can be obtained relevant information:

- Spikes do not occur until at least 15-20 ms have passed since the previous one.
- Spikes occur more often with a interval to the previous one of ~50 ms (largest incidence).
- After that peak, the incidence is reduced following an exponential decay.

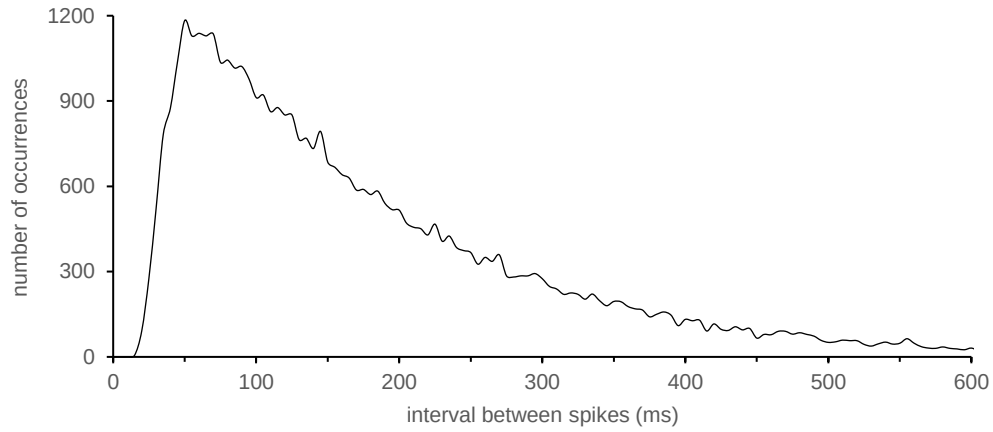

Figure 14. Interspike interval distribution of a model of a typical oxytocin neurone simulated during 8000s with a k_{HAP} = 0.15 mV, no DAP and firing rate of 5.5 spikes/s. Notice how there are not spikes separated for less than 15 ms.

Once familiarized with it, the ISI distribution also shows which kind of currents had more importance during the recording of a neuron. That is very important to change the model's parameters values in the correct direction and achieve a good match.

For example, there are several things that will "shift" the ISI distribution to the left, making more probable smaller intervals between spikes (Figure 15):

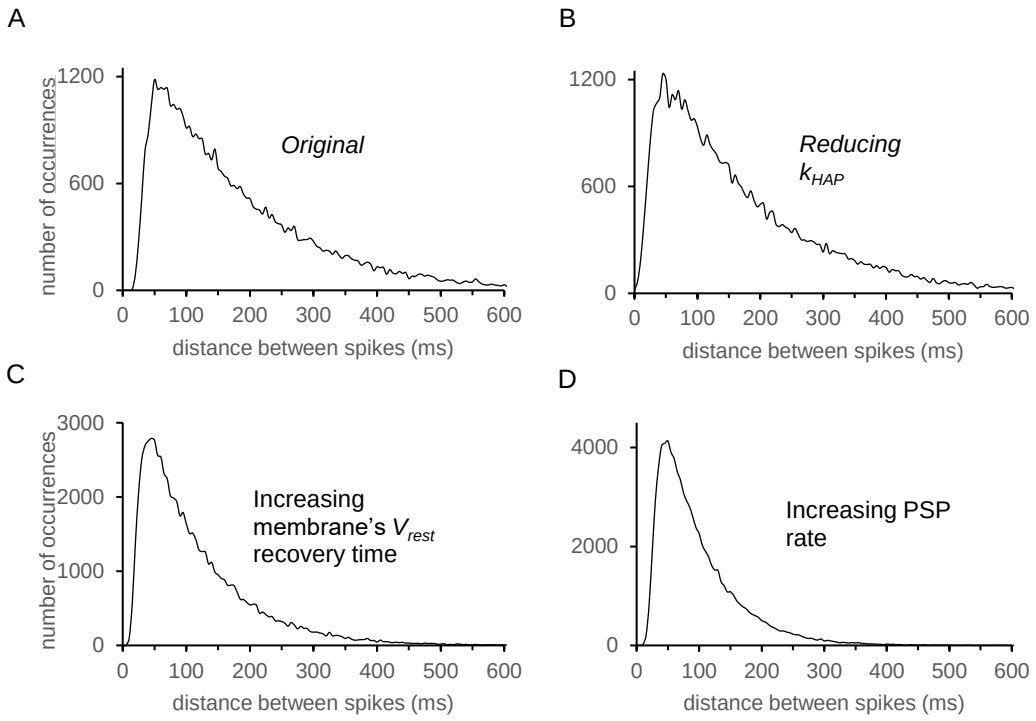

Figure 15. Shifting the interspike interval distribution to the left. A) Shows the original histogram in Figure 14. **B)** The ISI distribution is shifted to the left by reducing k_{HAP} from 30mV to 10mV. **C)** Shifted by increasing the membrane half life to recover V_{rest} from 3.5 ms to 7.5 ms. Notice how the number of occurrences is much higher. **D)** Shifted by increasing the rate of input afferences from 350PSP/s to 600 PSP/s.

- Larger or more frequent EPSPs , or smaller or less frequent IPSPs
- Longer half lives of the EPSPs or shorter half lives of the IPSPs
- Smaller HAP or AHP amplitudes or half lives.

Accordingly, changing those parameter values in the opposite direction I will have an ISI distribution "shifted" to the right, having less probability to find shorter intervals between spikes (Figure 16):

- Shorter EPSPs
- Shorter half-lives of the input afferences
- Bigger HAP or AHP amplitudes or half-lives.

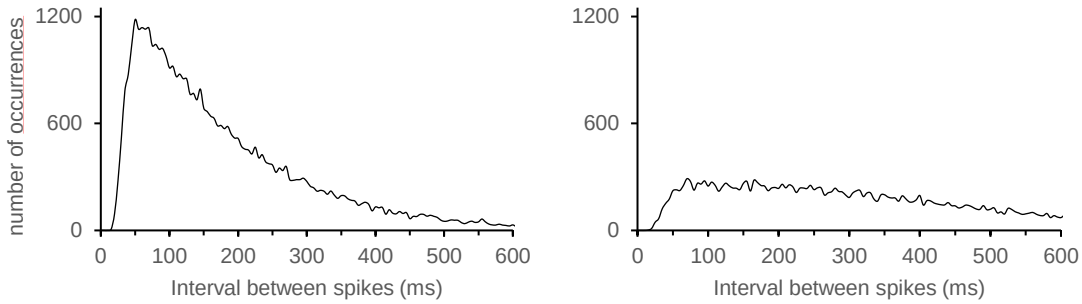

Figure 16. Shifting the interspike interval (ISI) distribution to the right. **Left.** Original ISI distribution from Figure 15.A. **Right.** Shifted when I increase the AHP amplitude from k_{AHP} = 0.15 mV to k_{AHP} = 1mV.The increment in the AHP also flattens the ISI distribution.

Hazard

Once the ISI distribution is calculated, the Hazard allows us to go a step further. The hazard gives us the probability of occurrence of a spike taking place versus the time elapsed since the previous one.

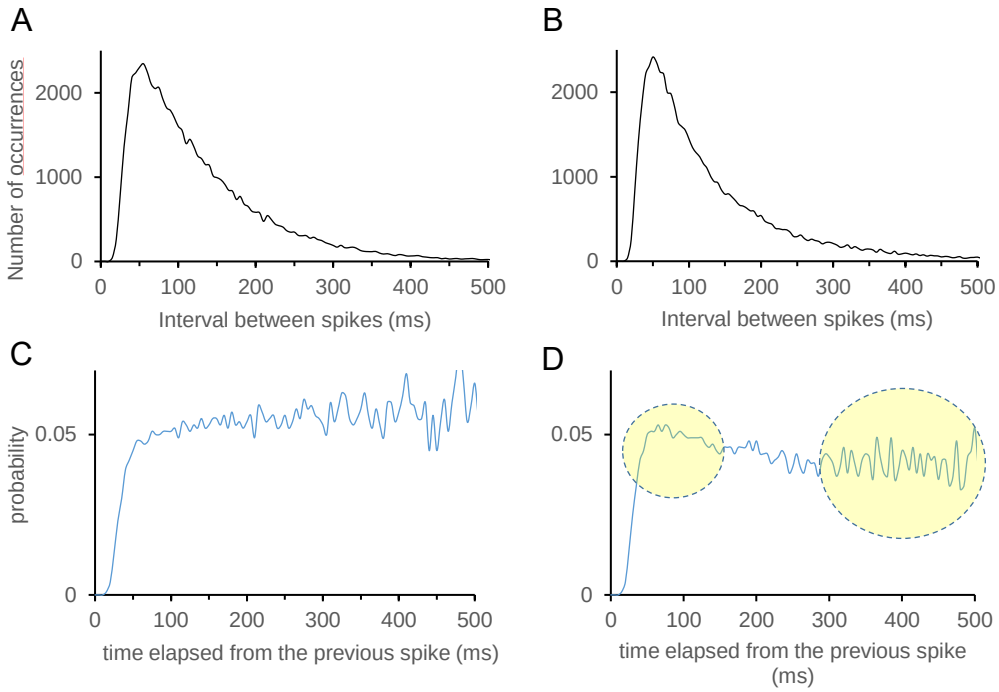

Figure 17. Hazard distribution. When the ISI distributions of the spikes rates of two different neurones do not show clear differences, the hazard distribution may give additional information. **A)** The ISI distribution in Figure 15.D, obtained from Figure 15.A by increasing the input rate, is similar to the ISI distribution in **B)** where the change in the ISI distribution was obtained by adding a new current. **C)** The hazard calculated from A) shows the probability that a spike has to happen after some time has passed from the previous spike. **D)** The hazard calculated from the ISI distribution in B) shows how the new current (a DAP)

makes more probable having a spike after a small amount of time and less probable to have spikes after intervals larger than 350 ms. (A-D) are calculated with 5ms bins.

As the hazard is calculated from the ISI distribution data, they share tendencies and the kind of information that can be obtained from them. However, the hazard is sometimes a better tool to detect masked influences of a membrane current (Figure 17).

Index of dispersion

The index of dispersion (ID) is the quotient of the two most common statistical measurements, the variance and the mean:

$$ID = \frac{\sigma^2}{\mu}$$

As the average and the variance, the ID can be calculated in different bin widths (Figure 18). If the average and the variance of a signal in bin of 4s is calculated, the resultant quotient between that variance and that average will be the ID in 4 s bins.

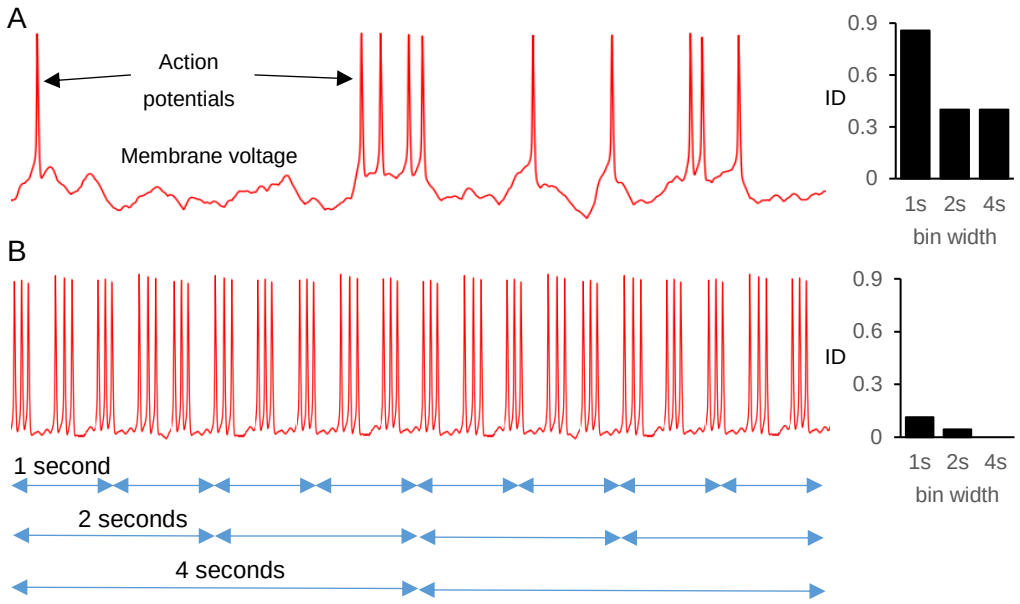

Figure 18. Index of dispersion of the firing rate in different bin widths. **A)** (left) An erratic spiking activity (in red) produces a high variability and a low average in the firing rate when looking at it in bin widths from 1s to 4s. The result is a considerable index of dispersion for every bin width (right). **B)** A regular spiking activity (left) reduces the variability of the firing rate for every bin width. On the other hand, the average firing rate is higher than in A for every bin width. Therefore, the index of dispersion for every bin width is small.

The ID gives us a tool to find the variability in our data with independence to its mean, being particularly relevant when a series of numbers generated following a Poisson distribution is analysed. In that case, the ID is equal to 1 for every interval taken (bin width), indicating purely random. That is precisely the case of the PSPs our oxytocin model generates. In addition, combining the ID of the spike activity and the ISI distribution, it is possible to spot details that could be more difficult to detect using them alone. If a membrane that recovers immediately from PSPs and that does not react to spikes (no HAP, AHP, DAP) is simulated, the index of dispersion of the spikes generated will be around 1 (Figure 19.A). Because the membrane do not react in any way to PSPs or spikes, the ISI distribution has the particularity that a spike can follow the previous one without any waiting time (or refractory period) (Figure 19.A).

However, the membrane needs time to recover after every PSP (it does it in our model with a half-life of 3.5ms). In that case, still without any HAP, AHP or DAP, the ISI distribution shows that the neuron would be producing spikes continuously. In those circumstances, the index of dispersion is increased for all the bin widths, which gives a hint that the model has lost a bit of regularity (Figure 19.B). When a HAP is added, the regularity is recovered, an even improved from the one given by a Poisson distribution. It happens for every bin width because the time constant of the HAP (λ_{HAP} = 30ms) is much smaller than the smallest bin width used when a HAP is added. In addition, the HAP also prevents spikes being triggered with less than 30 ms between them (Figure 19.C).

When an AHP is added, it will also reduce the ID of dispersion for every one of our bin widths, but it will do it more to larger bin width, as its time constant is larger (λ_{AHP} = 350ms), and it can accumulate the hyperpolarising effects of several spikes for a couple of seconds (Figure 19.D).

When a DAP is added, but not an AHP, the effect on the ID is the opposite to the one founded when an AHP is present (Figure 19.E). If both, an AHP and DAP, are added, the ID is governed by the effect of the AHP, masking the DAP. The ISI distribution gives, on the other hand, a hint that something different from having just an AHP might be happening (Figure 19.F).

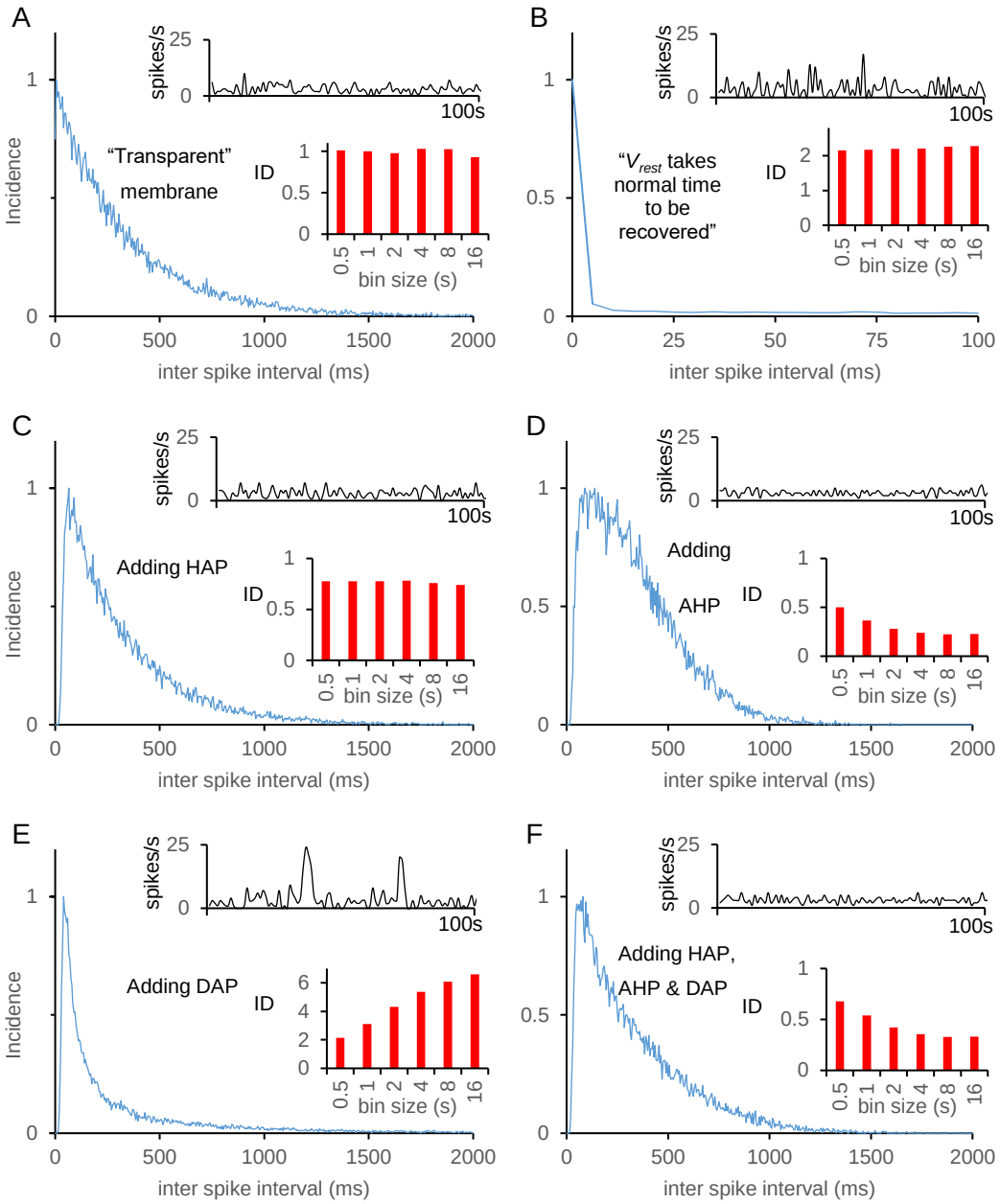

Figure 19. The index of dispersion. Single neuron simulations of 8000 s at 3 spikes/s. Indexes of dispersion (ID) and interspike interval (ISI) distributions are calculated from the 8000s activity. ISI distributions are normalized to 1 and only 100s of the firing rate is shown in each case. **A)** The simulated membrane does not have HAP, AHP or DAP and it recovers its resting state immediately after every PSP arrival. As the PSP arrival times follow a Poisson distribution, in this case the ISI distribution is right skewed, and the ID follows also the theoretical value of 1 for random numbers following a Poisson distribution. **B)** If I add to the model the physiological time the membrane needs to recover from PSPs, the neuron will produce consecutive spikes much more often, the ISI distribution will be much more positively skewed, –notice that the time axis only shows 100ms- and the ID will raise for every bin width, as a result of the increment of variability in the spike production. **C)** If a HAP is added, the variability is reduced below 1, being the spike production less variable than the arrival of PSPs. Also, the ISI distribution shows that the membrane has acquired a refractory

period. **D)** If I add an AHP, the ISI distribution is skewed to the left. The refractory period increases and, more importantly, the ID decreases, more for bins widths of 4s or more. **E)** With a HAP and a DAP but without an AHP, the effect is the opposite than in D. Now consecutive spikes are more probable, and the variability increases for longer bin widths. **F)** In a typical oxytocin neurone, with a HAP, AHP and DAP, I obtain a similar ISI to that in C, but the variability is dominated by the presence of the AHP and the DAP effect is difficult to spot.

Secretion and clearance analysis.

The goal of the secretion model was to connect the spiking activity of an oxytocin neuron, which is measured with a timescale of milliseconds, with the oxytocin concentration in plasma, which is often measured experimentally in intervals of 5 min or more.

Because of that, the secretion model needed firstly to work in a timescale of milliseconds, receiving as an input the spike activity of one or more neurons. And second, it needed to simulate the total amount of oxytocin secreted into the blood stream as a result of the spike activity. To do that, I matched experimental data of the secretion measured after the pulsatile stimulation of the posterior pituitary gland, responsible for the whole oxytocin secretion to plasma.

Thus, the secretion model will always simulate the populational secretion of the ~9000 oxytocin neurones in the SON and PVN. However, the secretion model can be connected either to a spiking model of a single neuron, in which case it will be assumed that that spiking activity is the average of the whole population, or to the spiking activity of several neurons, summing their different secreting responses to obtain the global one.

On many occasions, I will modify the PSP rate to match the experimental basal levels of the oxytocin neurone. However, the secretion model behaviour will only depend on the arrival times of the spikes generated by the spiking model. Also, when the model simulates a heterogeneous population of neurones, the variability between each neuron secretion depends on its spiking activity, generating from identical sequences of spikes the same secretion.

Mathematically speaking, the secretion model is more intricate than the spiking one. The secretion model simulates different feedback pathways, recreating biological processes affected by the arrival of a spike to the axon terminal and the axon terminal Ca^{2+} dynamics. However, most of the equations used are linear or

exponential equations written as differential equations. The only exception are two inverted Hill equations that emulate the inhibition produced in the submembrane and cytosolic Ca^{2+} currents due to the presence of Ca^{2+}.

Hill equations

Hill equations are used because of their sigmoid behaviour, which is very useful to represent the change of state, from open to closed, in the Ca+ channels of the axon terminal. However, I use them in a simpler way, to modulate the amount of spike triggered Ca^{2+} entry due to reduced spike propagation, i.e. producing fewer or smaller amplitude spikes at the axon terminal (Figure 20). When the $[Ca^{2+}]$ in the cytosol, c, and in the submembrane, e, is low enough, the Ca^{2+} channels are open, being $c_{inhib} = e_{inhib} = 1$. The channels start closing when the $[Ca^{2+}]$ is near a threshold, $c_\theta = 0.14$, $e_\theta = 12$. The quickness of those changes is defined by the gradients $c_n = e_n = 5$:

$$c_{inhib} = 1 - \frac{c^{c_n}}{c^{c_n} + c_\theta{}^{c_n}} \qquad (10)$$

$$e_{inhib} = 1 - \frac{e^{e_n}}{e^{e_n} + e_\theta{}^{e_n}} \qquad (11)$$

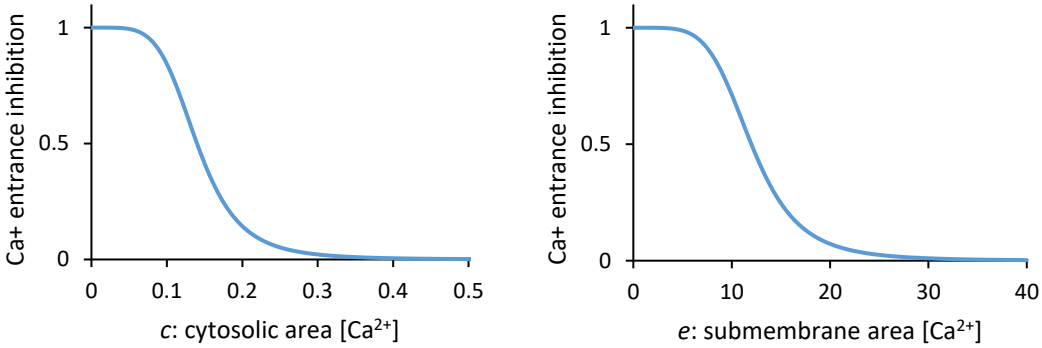

Figure 20. Hill functions. Left: In the model, the Ca^{2+} channels openness in the cytosolic area depends on the $[Ca^{2+}]$ in the same area. The bigger the $[Ca^{2+}]$ the larger is the inhibition (it tends to 0). The threshold is set at $c_\theta = 0.14$. **Right**: The same happens for the submembrane of the axon terminal but for the submembrane the threshold is $e_\theta = 12$. Thus, the inhibition needs a much bigger $[Ca^{2+}]$ to start being significant.

Statistical tools and other tools

As noted earlier, the time scale of experimental data of plasma oxytocin is in seconds, many times in minutes, being the sets of data relatively small, due to the difficulty that taking blood samples has in the rat.

Because of that, the way of matching the experiments is frequently limited to the comparison of average and the standard deviation of the mean and error, which are the typical measures given in the literature. Nevertheless, that does not limit the way the modelling data can be analysed or makes the secretion and clearance models less valid. Both models are built combining mathematical equations that simulate the most relevant biological processes associated with their dynamics. In addition, the computational analysis allows to simulate the secretion and plasma oxytocin dynamics in much more detail than the experiments can give. That allows us to infer what is happening between the measurements taken in the experiments, once those experimental values are mimicked.

Another strength of the model is its modularity. The spiking, secretion and clearance models can work independently and together. One interesting way of taking advantage of the modularity of the model is to run it substituting the spiking model with real spike recordings or both the spiking and secretion model for real secretion data, calculating the resultant oxytocin in plasma. Replacing the model by real data can be done in the spiking model in two different ways. The first one is by using recorded spike times. In that case (Figure 21), the model will calculate the firing rate and simulate the secretion and oxytocin in plasma. It is also possible to introduce the firing rate itself, using the model to simulate spike times at an experimental measured rate This can be useful in the occasions where I do not have the spiking times, but I have the firing rate, either of a single cell or the average of several ones.

Another way is to infer the spiking activity of the oxytocin neurones once I know the plasma oxytocin.

Lastly, as will be shown in Chapter 4, the clearance model helped us to infer a hidden role of the volume exchange in hypovolemic rats.

Issues about mimicking oxytocin secretion and plasma oxytocin

The way of measuring oxytocin secretion and plasma oxytocin is different but coincidental in the final step. The secretion tends to be obtained by measuring the

oxytocin in the animal glands after stimulating the neural lobe with electrical pulses (Bicknell *et al.*, 1984) or with injection of different solutions (Leng *et al.*, 1994). The glands are then surgically separated killing the animal immediately after the procedure.

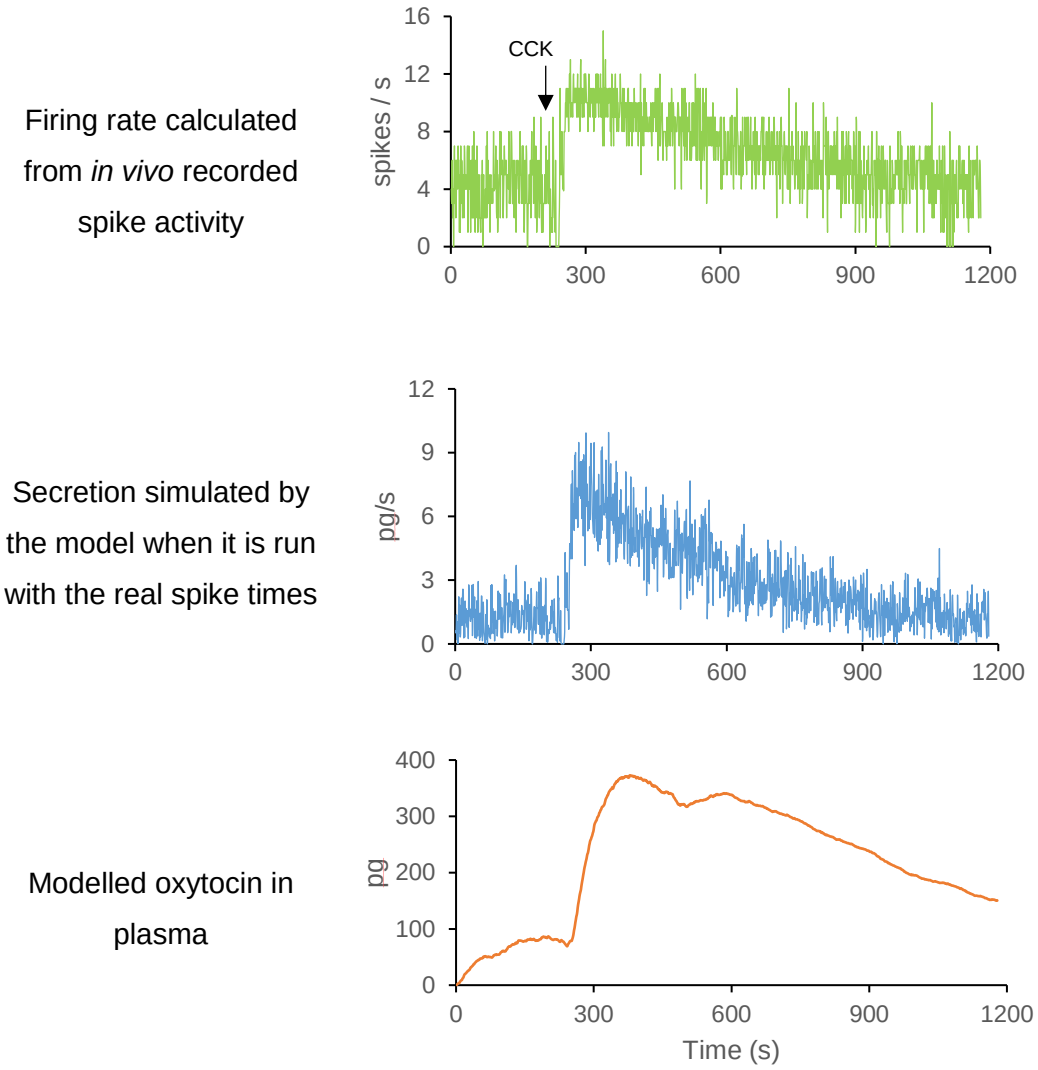

Figure 21. After *in vivo* recording how an oxytocin neurone responds electrophysiologically to a systemic CCK injection, I can calculate its firing rate (**top**) and feed the computational model with the spiking times from the real recording. The model simulates the predicted secretion (**centre**) and plasma oxytocin (**bottom**).

On the other hand, the level of plasma oxytocin does not require to kill the animal. However, it usually requires collecting samples, which is problematic in small animals due to the small quantity of plasma they have. Thus, experiments with many

samples are not possible and long intervals between samples or samples taken from different animals tend to be usually seen in experiments. However, the secretion and the plasma oxytocin need an assay to obtain the oxytocin.

There are multiple issues relative to the assessment of oxytocin levels in secretion or in plasma (Leng & Sabatier, 2016). To develop a mathematical model to simulate those levels of oxytocin I needed to choose to which immunoassay I wanted to get tied to. However, the fact that different experiments give values of plasma oxytocin hugely different in magnitude does not mean that the temporal pattern in the response was also different. Absolute values vary hugely when different immunoassays use different antibodies but, if the calibration is good, response times to different challenges should be similar. Thus, I have considered the measured times through the literature as a consistent data to mimic, whereas I have only used the data measured with the Higuchi immunoassay (Higuchi *et al.*, 1985) when trying to match absolute values.

Chapter 3 (paper):

Oxytocin neurones: intrinsic mechanisms governing the regularity of spiking activity

Introduction to the First Paper

Maícas-Royo J, Brown CH, Leng G & MacGregor DJ (2016). Oxytocin Neurones: Intrinsic Mechanisms Governing the Regularity of Spiking Activity. *J Neuroendocrinol* **28.**

The first part of my PhD consisted of reading a lot and learning how to use the computational framework my supervisor Duncan MacGregor had developed. The software consisted of many thousand lines of code with a high level of interconnectivity and abstraction. When I had barely managed to deal with it and I had also started to understand the basics of neuroendocrinology, Gareth Leng asked me if I could use the model to check an idea that had occurred to him.

The spike rate in oxytocin neurones looks quite noisy if it is seen in bin widths of 1 s or less. However, when the bin width is increased, let's say to 16 s, the spike rate looks quite regular. Most people would say that is normal. That is what happens when you average a set of data in a timeline. However, that smoothing effect was stronger than expected. In the transitions of making averages with bin widths from 2 s to 8 s, the firing rates seemed to get smoother than in the transitions from averages with smaller bin widths (from 0.5s to 2s) or larger ones (from 8s to 32s). To check that his intuition was correct, he used the index of dispersion and found that his intuition was accurate. However, when Gareth applied the index of dispersion to the firing rate of more oxytocin recordings, he found that not all of them behaved in the same way. Sometimes, the index of dispersion did not change for longer bin widths. Other times, the index of dispersion increased with the bin width. He did all those tests working in an excel file full of the spike times of different oxytocin neurones, with columns for the different statistics.

Then he asked me if I could develop a model with a HAP, and AHP to check how the index of dispersion, and the rest of statistics, were changing depending on the presence of the different currents.

The model with a HAP and an AHP could mimic the firing rate and the interspike interval distribution of the different neurones. However, when I tried to match as well the index of dispersion, I realized that for some neuron recordings, it was impossible to match at the same time the three statistics. Knowing that some oxytocin neurones also present a DAP and that the DAP could potentially increase the

variability of the firing rate in bin widths of 4s or more, I added one to the model and started working with it.

Abstract

Oxytocin neurones of the rat supraoptic nucleus are osmoresponsive, and, other things being equal, they fire at a mean rate that is proportional to the plasma sodium concentration. However, individual spike times are governed by highly stochastic events – the random occurrences of excitatory synaptic inputs, the probability of which are increased by increasing extracellular osmotic pressure, and, accordingly, interspike intervals (ISIs) are very irregular. However, we show here by statistical analyses of firing patterns in oxytocin neurones that the mean firing rate as measured in bins of a few seconds is more regular than expected from the variability of ISIs. This is consistent with an intrinsic activity-dependent negative feedback mechanism. To test this, we compared observed neuronal firing patterns with firing patterns generated by a leaky integrate-and-fire model neurone, modified to exhibit activity-dependent mechanisms known to be present in oxytocin neurones. The presence of a prolonged afterhyperpolarisation (AHP) was critical for the ability to mimic the observed regularisation of mean firing rate, but we also had to add a depolarising afterpotential (DAP; sometimes called an afterdepolarisation) to the model to also match the observed ISI distributions. We tested this model by comparing its behaviour to the behaviour of oxytocin neurones exposed to apamin, a blocker of the medium AHP. Good fits indicate that the medium AHP actively contributes to the firing patterns of oxytocin neurones at rest, and that oxytocin neurones generally express a DAP, even though it is usually masked by superposition of a larger AHP.

Introduction

Neurones code information as patterns of action potential (spike) activity, patterns that reflect an interaction between the afferent input activity and their intrinsic membrane properties. Spike activity influences these intrinsic membrane properties, and hence can alter how a neuron responds to its inputs. In addition, the inputs may be modulated by the neurone's activity, both as a result of retrograde modulation of afferent activity, and as a consequence of recurrent neuronal circuits. Such changes occur over different time scales and by different mechanisms, and, as a result, different neuronal types process information differently (Leng & MacGregor, 2008).

The rat supraoptic nucleus contains only magnocellular neurosecretory neurones; all of these neurones project to the posterior pituitary gland where they secrete the hormones vasopressin and oxytocin, into the systemic circulation. The homogeneity of this nucleus, and the ability to relate neuronal behaviour to physiological function has made this an important “model system” in neuroscience, and these neurones have been studied very extensively by electrophysiological approaches *in vivo* and *in vitro* (Bourque, 2008; Armstrong *et al.*, 2010; Brown *et al.*, 2013; Leng *et al.*, 2015).

Oxytocin neurones in the rat supraoptic nucleus discharge under the influence of randomly arriving excitatory and inhibitory post-synaptic potentials (EPSPs and IPSPs) (Armstrong, 1995; Li *et al.*, 2007; Armstrong *et al.*, 2010). Each spike is followed by a hyperpolarising afterpotential (HAP; sometimes called a fast afterhyperpolarisation). It appears that the major contributor to the HAP is activation of I_C (Roper *et al.*, 2003), a Ca^{2+}- and voltage-dependent K^+ current carried by a large conductance (BK) channel that can be blocked by charybodotoxin. The HAP makes the neurone relatively inexcitable for 30-50 ms after a spike, and its effects on spike timing can be mimicked in a modified leaky integrate-and-fire model of a neurone by assuming that a spike instantaneously raises the spike threshold, and that this change decays exponentially (Leng *et al.*, 2001). This simple model can match, very accurately, the distribution of interspike intervals (ISIs) observed in magnocellular oxytocin neurones *in vivo.*

However, the ISI distribution holds no information about spike patterning that results from serial interdependence of ISIs. For oxytocin neurones, any given ISI is virtually independent of the length of the preceding ISI, but this is not true for longer trains: there is an inverse relationship between the length of a train of 6-10 ISIs and the length of the next ISI, and this relationship cannot be explained by the HAP, which only lasts for ~50 ms (MacGregor *et al.*, 2009). However, the HAP is not the only activity-dependent conductance change that affects neurone excitability. When strongly activated to fire repeated spikes, oxytocin neurones display a deep and prolonged hyperpolarisation called the afterhyperpolarisation (AHP). This is the result of the summation of small, prolonged hyperpolarisations that accompany each spike (Bourque *et al.*, 1985; Bourque & Brown, 1987; Greffrath *et al.*, 1998, 2004; Teruyama & Armstrong, 2005) that result from activation of Ca^{2+}-activated K^+ currents. The AHP has at least two components that differ in their duration: a

“medium AHP” carried by small conductance (SK) channels which can be blocked by apamin, and a “slow AHP”, carried by intermediate conductance (IK) channels which can be blocked by muscarine (Ghamari-Langroudi & Bourque, 2004).

There is also an activity-dependent depolarising afterpotential (DAP) that has at least two components: a “fast DAP” carried by Ca^{2+} activated non-specific cation channels (Teruyama & Armstrong, 2007), and a “slow DAP”. Two different Ca^{2+} activated mechanisms have been proposed for the slow DAP: an additional non-specific cation channel (Ghamari-Langroudi & Bourque, 2002), and the switching off of a hyperpolarising K^+ leak current (Li & Hatton, 1997). The DAP, by raising post-spike excitability, encourages bursting, and is mostly associated with vasopressin neurones, but is also found in at least some oxytocin neurones (Stern & Armstrong, 1996; Teruyama & Armstrong, 2007). The fast DAP and the medium AHP have similar time courses and tend to mask one another in recorded membrane potential. They can be more easily detected when the other is blocked pharmacologically (Teruyama & Armstrong, 2007).

With spike interval analysis and model fitting, we infer the presence of afterpotentials from activity-dependent changes in excitability. We use “generalised” AHPs or DAPs with parameters determined by the detected excitability effects, rather than being derived from a specific ionic current. The detected and fitted AHP or DAP may correspond to a specific current, or may represent the compound action of multiple ionic currents. For example, every spike is followed by a relative refractory period that lasts about 50 ms; this we call the HAP, but the HAP has been proposed to have at least two components - a BK channel, and an A-type K^+ channel (Roper *et al.*, 2003).

The AHP is thought to be important for “shaping” the intense bursts of spike activity that oxytocin neurones display during the milk-ejection reflex. The milk-ejection reflex is a dramatic and exceptional event. An oxytocin neurone firing typically at just a few spikes/s will suddenly discharge up to more than 100 spikes in 2-3 s, with a peak discharge rate of up to 100 spikes/s achieved within about 100 ms of the burst onset (Rossoni *et al.*, 2008). These bursts are followed by a longer period of relative quiescence. This post-burst quiescence is too long to be accounted for by the AHP alone, and we have proposed that it reflects a suppression of afferent input induced by burst-evoked release of endocannabinoids (Rossoni *et al.*, 2008). The AHP itself seems likely to be responsible for the ‘shape’ of the milk-ejection burst – the manner

in which it slows down after the peak of excitation (Rossoni *et al.*, 2008). An AHP also plays a role in shaping the prolonged bursts in phasic firing vasopressin neurones (MacGregor & Leng, 2012). In the bursts an initial peak of rapid spiking drops to a sustained plateau, determined by the competing actions of a slow DAP which sustains the burst and the AHP.

However, here we focus on the more subtle effect of the AHP during the more common non-bursting activity observed in oxytocin neurones. We have previously shown that by adding an AHP to the model we can account fully for the serial dependence of ISIs in spontaneous activity (MacGregor *et al.*, 2009). From this we can infer that the AHP restrains the firing rate of oxytocin neurones even at low firing rates, but what other consequences there are for the information processing properties of oxytocin neurones is unexplored. In addition, at least some oxytocin neurones (~20%) display a fast DAP with a time course intermediate between the HAP and the AHP (Teruyama & Armstrong, 2007), and the physiological significance of this is also largely unexplored. Here, we show that, when averaged over intervals of 5 s or longer, the spontaneous firing activity of oxytocin neurones in the rat is surprisingly stable - the spike counts are much more regular than expected from the irregularity of firing observed in short intervals, suggesting that the intrinsic membrane properties of oxytocin neurones preserve a memory of past activity by which activity is “smoothed out”. Here we explored whether the AHP accounts for this behaviour, using statistical analyses and computational modelling, and with the aid of data from experimental studies in which the medium AHP was blocked pharmacologically using apamin (Bull *et al.*, 2011). We go on to discuss the possible physiological significance of a mechanism that stabilises the firing rate on a timescale of 5 s and longer.

Methods

We analysed extracellular recordings of the spike activity of single neurones in the supraoptic nucleus of adult virgin female rats, using a large library of recordings made over many years. The selected recordings were from adult rats anaesthetised with urethane (ethyl carbamate, 1.3 g/kg body weight i.p.) in which the supraoptic nucleus and neural stalk were exposed by ventral surgery, and a femoral vein was cannulated for i.v injection of cholecystokinin (CCK) (Brunton *et al.*, 2006; Velmurugan *et al.*, 2010, 2013; Leng & Sabatier, 2014). All of the selected neurones had been antidromically identified as projecting to the neural stalk to identify them as magnocellular neurosecretory neurones, and had been further identified as oxytocin neurones by their excitatory response to i.v. injections of CCK. Full details of experimental procedures have been published previously (Leng & Sabatier, 2014). Further data on the effects of apamin on the firing patterns of supraoptic neurones were from published studies in female rats under urethane anesthesia, in which apamin was delivered by retrodialysis to the supraoptic nucleus during recordings from single, identified oxytocin neurones (Bull *et al.*, 2011).

If spikes were generated independently of the previous incidence of spikes, then the spike trains would constitute “Poisson” processes and exhibit certain well-established statistical features. Spikes are not independent of past activity for any neurone – most obviously, oxytocin neurones possess a prominent HAP that imposes a long relative refractory period after spikes. Nevertheless, we state here what is expected of a Poisson process, in order to judge how far and in what way, the statistics of spike trains deviate from randomness.

1. *Inter-event distributions.* For a Poisson process, the probability of an event occurring at any particular time is independent of the time of the preceding event. This implies that the inter-event histogram (the ISI distribution) can be described by a single negative exponential, and that the calculated hazard function (described below) is constant over time since the last spike.

2. Data that arise as a random process should show invariant statistical characteristics when these data are shuffled randomly.

3. *Index of dispersion.* The *variance* of the event frequency (σ^2) is equal to the *mean* of the event frequency (μ). If spike timings are purely random, the “index of dispersion”, σ^2/μ, should therefore equal 1, should be independent

of μ in a sample of data where μ varies, and should be independent of bin-width.

4. *Coefficient of variation (CV).* The mean of the inter-event interval (μ) is equal to the standard deviation (σ), so the "coefficient of variation", σ/μ , should equal 1 if spike timings are random.

After excluding neurones from our library with a spontaneous firing rate too low to meaningfully calculate measures of variability, and neurones without at least 400 s of stationary activity, we selected stationary periods of activity recorded from 76 oxytocin neurones. By 'stationary activity' we mean not wholly regular activity, because fluctuations in activity such as periodic bursting are features of activity that are often themselves generated in an activity-dependent way. Instead, we mean activity that, in the period concerned, shows no clear progressive trend (in the first few minutes of a recording, neurones may either speed up or slow down before reaching a steady firing rate) and no singular abrupt changes (as sometimes occur, for example, in conjunction with a change in spike amplitude that indicates a movement of the neurone relative to the electrode). We imported event data (spike timings resolved to 0.1 ms) from Spike2 (Anon, n.d. p.2) files into Excel worksheets, and from these calculated firing rate in different bin widths (from 0.5 s to 20 s) and calculated the mean index of dispersion as the variance/mean rate for a given bin width. We converted the sequences of spike times into sequences of ISIs, randomly shuffled these using Excel, and converted them to a new sequence of event timings, from which we calculated the values for index of dispersion for shuffled data. We constructed ISI distributions (in 5-ms bins), and calculated the coefficient of variation of ISIs as the standard deviation/mean. We constructed hazard functions from the ISI data in 5-ms bins as previously described (Sabatier *et al.*, 2004) according to the formula (hazard in bin [t, t+ 5]) = (number of ISIs in bin [t, t+ 5]) / (number of ISIs of length > t). A hazard function plots how the excitability of a neurone evolves after a spike has fired and it reflects the superimposed effects of Ca^{2+}- and voltage-dependent currents that are triggered by a spike, and the perturbations of afferent input that result from that spike. To measure log interval entropy, we used the Interlab software generated by Bhumbra and Dyball (Bhumbra & Dyball, 2004; Bhumbra *et al.*, 2004, 2005).

Model neurones

To model the behaviour of the oxytocin neurones we used an integrate-and-fire based spiking model described in (MacGregor *et al.*, 2009) and further refined in (MacGregor & Leng, 2012) to model vasopressin neurones. The model uses a 1-ms step size and is implemented using modelling software developed in C++ with the open source wxWidgets graphical interface library (Anon, n.d.). Simulations were run for 1000–100,000 s of simulated activity. Briefly, the model simulates the firing response to Poisson randomly timed, exponentially decaying, inputs, representing excitatory and inhibitory post-synaptic potentials (EPSPs and IPSPs) at mean rates I_{re} and I_{ri}. I_{ri} is defined as a proportion of I_{re} given by I_{ratio} and all of the results here use I_{ratio} = 1 so that input rate is controlled using just I_{re}. We assumed that EPSPs and IPSPs have equal and opposite magnitude (fixed at 2 mV) and a half-life (λ_{syn}) fixed at 3.5 ms. The model variable V_{syn} represents the summed EPSPs and IPSPs. The other model variables represent a set of spike triggered influences on membrane excitability, here the HAP, the DAP, and the AHP. Following a spike the HAP, DAP, and AHP variables are incremented by fixed values k_{HAP}, k_{DAP} and k_{AHP}, and decay exponentially with half-lives λ_{HAP}, λ_{DAP}, and λ_{AHP}. In contrast to the classic integrate-and-fire model, there is no post-spike reset of the variables, allowing the DAP and AHP in particular, with their longer half-lives, to accumulate across multiple spike intervals.

All the model variables are summed with the resting potential (V_{rest}, fixed at -56mV) to generate the membrane potential V:

$$V = V_{rest} + V_{syn} - HAP - AHP + DAP$$

When V exceeds the spike threshold (V_{thresh}, fixed at -50mV), the neurone fires a spike and the ISI is recorded. The large magnitude fast decaying HAP simulates the post-spike refractory period. The DAP and AHP have more subtle but longer lasting effects which are more activity dependent. The DAP is new to the oxytocin model, but follows the form of the fast DAP used in the vasopressin spiking model (MacGregor & Leng, 2012).

Parameter Fitting

The model was fitted to recorded data by generating a matching number of spike intervals and adjusting parameters to match the firing rate, ISI distribution, and index of dispersion. Initially spikes were generated using the default parameters in Table 4, and parameters I_{re} and λ_{HAP} were adjusted by trial and error to match the firing rate and ISI distribution. The AHP parameters were then adjusted to match the index of dispersion range while maintaining the match to the ISI distribution and firing rate. A similar process was used when adding the DAP. The parameter sensitivity of the AHP and DAP half-lives was tested by attempting to fit with smaller and larger values (λ_{AHP} = 50, 1000 and λ_{DAP} = 50, 600), compensated by adjusting the respective AHP and DAP magnitude parameters. These tests confirmed that values in the range presented in the Table 5 and Table 6 are necessary to produce good fits to the data.

Table 4. Default parameters used for oxytocin neurone model. Adapted from MacGregor & Leng (2013).

Name	Description	Value	Units
I_{re}	excitatory input rate	300	Hz
I_{ratio}	inhibitory input ratio	1	-
e_h	EPSP amplitude	2	mV
i_h	IPSP amplitude	-2	mV
λ_{syn}	PSP half-life	3.5	ms
k_{HAP}	HAP amplitude per spike	30	mV
λ_{HAP}	HAP half life	7.5	ms
k_{DAP}	DAP amplitude per spike	0	mV
λ_{DAP}	DAP half life	150	ms
k_{AHP}	AHP amplitude per spike	0.2	mV
λ_{AHP}	AHP half life	350	ms
V_{rest}	resting potential	-56	mV
V_{thresh}	spike threshold potential	-50	mV

Results

In initial exploratory analyses we analysed three long recordings (Figure 22.A) made in urethane-anaesthetised male rats in which activity had been slowly increased by i.v. infusions of hypertonic saline (1 or 2M NaCl at 26–52 µl/min for 30–80 min) (Leng *et al.*, 2001). As previously described for oxytocin neurones from male rats (Sabatier *et al.*, 2004), these neurones displayed ISI distributions that were skewed with very few ISIs shorter than the mode, a long tail that was well fit by a single negative exponential (Figure 22.B), and a hazard function that rose monotonically over 30-80 ms to a plateau level of excitability (Figure 22.C). We have previously shown that these ISI distributions matched closely those produced by a leaky integrate-and-fire neurone model that incorporates an exponentially decaying post-spike refractoriness,

corresponding to a HAP (Leng *et al.*, 2001). Successive ISIs were relatively independent, although relatively long ISIs (>150 ms) tended to be followed by ISIs that were shorter than average (Figure 22.D). However, there was a strong inverse linear relationship between the length of an ISI and the sum of the preceding 10 ISIs (Figure 22.E). These are typical features of oxytocin neurones that we have previously attributed to the effects of the AHP (MacGregor *et al.*, 2009).

We examined the regularity of spike activity by looking at the spike rate distribution during periods of stationary activity. For each of the three neurones, the distribution of spike counts in 10-s bins was symmetrical around the mean, and narrower than the distribution of spike counts for the same set of ISIs after random shuffling to eliminate any order effects (Figure 22.F): this discrepancy indicates that that the counts in 10-s bins are more regular than would be expected from the variability of ISIs. We explored this further by calculating the index of dispersion in 0.5-s bins and in 10-s bins every 50-s during the infusion of hypertonic saline that increased the firing rate linearly (Figure 23.A): at all firing rates, the index of dispersion in 10-s bins was much lower than in 0.5-s bins indicating timescale dependent regularity. By contrast, after randomly shuffling ISIs, the index of dispersion of reconstructed spike counts was higher than in the original data, and was independent of bin width (Figure 23.B).

We studied the relationship between index of dispersion and two other measures of ISI variability: the coefficient of variation, and the log interval entropy. For the neurone shown in Figure 23, the log interval entropy was strongly linearly correlated with firing rate (Figure 23.C), and with the CV (Figure 23.D). The CV was also strongly correlated with the index of dispersion as measured in 0.5-s bins (Figure 23.E), but relatively weakly correlated with the index of dispersion measured in larger bins (not shown).

These relationships held for oxytocin neurones generally; in a sample of 26 oxytocin neurones, log interval entropy was inversely correlated with mean firing rate (r^2=0.46; best fit y = -0.06x + 7.6), and positively correlated with the CV (r^2=0.84; best fit y = 1.8x + 5.9). From this we concluded that, for oxytocin neurones, the CV and log interval entropy are equivalent measures of interval variability.

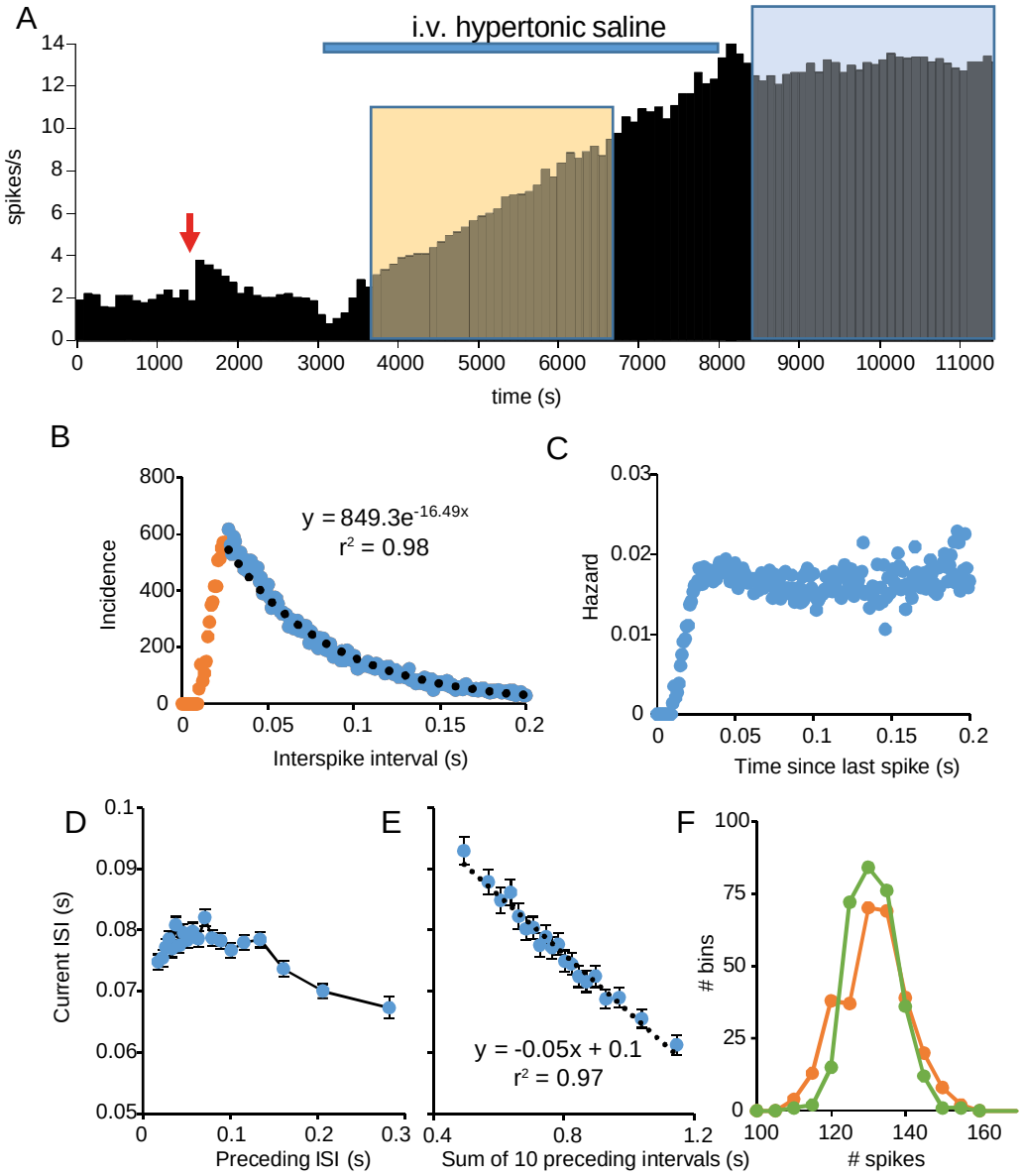

Figure 22. A) shows the mean firing rate of an oxytocin neurone (in 100-s bins) recorded from the supraoptic nucleus of a urethane-anesthetised rat (see (Leng & Sabatier, 2014)). The neurone was antidromically identified as projecting to the posterior pituitary and identified as an oxytocin neurone by the transient excitation in response to i.v. injection of CCK (red arrow). The neurone was then recorded throughout an i.v infusion of hypertonic saline (blue bar) which increased its firing rate linearly from an initial rate of 2.9 spikes/s to 12.9 spikes/s in this period. **B)** shows the ISI distribution of this neurone for the 3000-s period of stable high frequency activity (38,798 ISIs) indicated by the blue shaded area in A). The distribution is typical of oxytocin neurones, displaying a mode at ~ 30 ms and relatively few ISIs shorter than this mode, reflecting a strong post spike relative refractoriness characteristic of a prolonged HAP. The ISI distribution after the mode (blue symbols) is well fit by a negative exponential (black dotted line, equation of best fit given). This suggests that after the HAP, spikes arrive apparently randomly. **C)** shows the corresponding hazard function, confirming that the hazard of a spike occurring is independent of the time since the last spike after the end of the period of relative refractoriness. **D)** shows the relationship between each ISI and the preceding ISI, calculated from the same data. Each point plotted is the average of 2000 ISIs, sorted by the length of the preceding ISI. This shows that the length of an ISI is essentially

independent of the length of the previous ISI unless the preceding ISI is relatively long (>150 ms), when there is a weak inverse relationship. By contrast, **E)** shows the strong linear relationship between each ISI and the sum of the preceding 10 ISIs. Bars are SEM (n=2000). **F)** Shows the distribution of spike counts in 10-s intervals for original data (green symbols) and for randomly shuffled data (orange symbols). The distribution is narrower for the raw data than for the shuffled data.

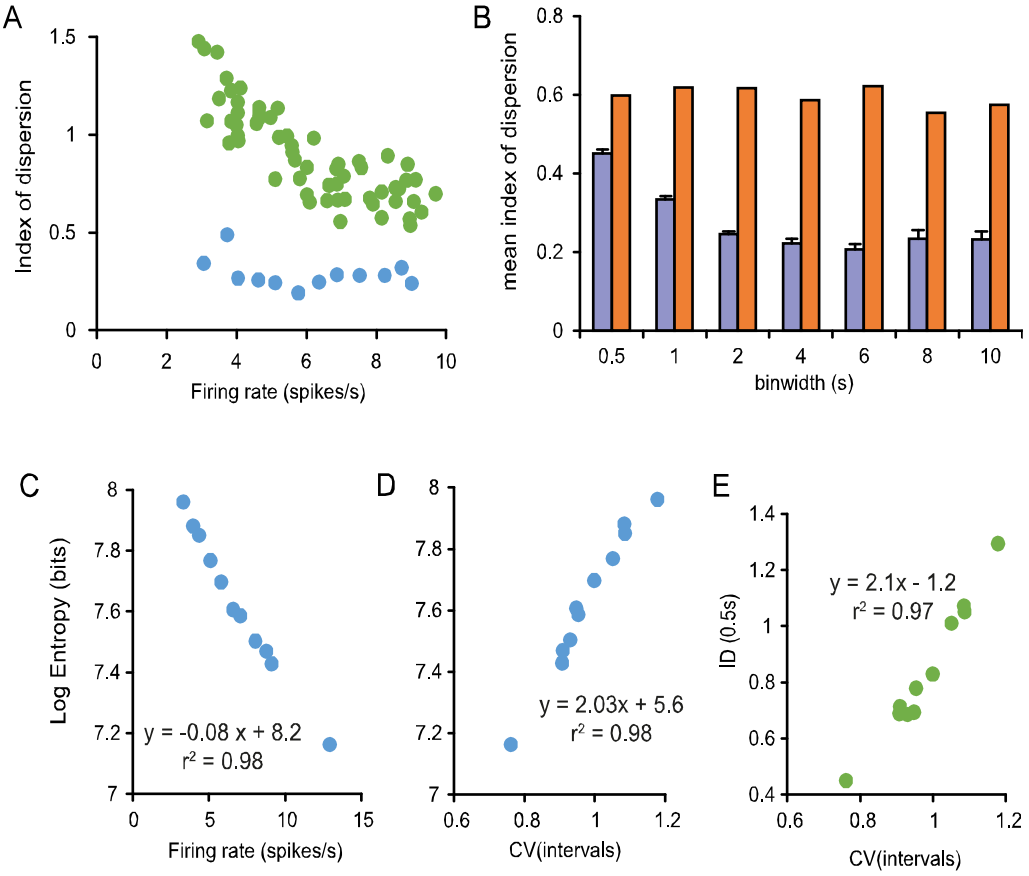

Figure 23. Data are from 3000 s of recording of an oxytocin neurone as its firing rate was increasing linearly in response to an i.v. infusion of 2M NaCl (orange shaded area shown in Figure 22. **A)** The green symbols are the index of dispersion in 0.5-s bins measured every 50-s plotted against the firing rate in that period, and the blue symbols show the index of dispersion in 10-s bins measured every 250 s. The index is consistently higher for data in 0.5-s bins. **B)** shows data from 3000 s of recording of the same neurone firing at a steady rate of 12.9 spikes/s after the end of infusion (blue shaded area in Figure 22). The index of dispersion was measured every 250s at different bin widths (0.5,1,2,4,6,8,10 s), and the blue bars show the mean (SE) index of dispersion at each bin width (n=12). The orange bars show the index of dispersion for shuffled data from this neurone: the ISIs recorded over each 3000 period were randomly shuffled, and the index calculated for the shuffled data. The shuffled data still shows an index of dispersion smaller than 1 due to the effect of the HAP (which largely prevents very short ISIs), but at all bin widths, the index of dispersion for the raw data is lower than that for the shuffled data, and it declines with increasing bin width. **C)** shows the relationship, in this neurone, between log entropy of ISIs (a measure of variability) and firing rate over this period, and **D)** shows the relationship between the coefficient of variation (CV, an alternative measure of variability) and log entropy. The two measures show a strong linear correlation with each other and

with firing rate, implying that they are essentially equivalent measures and that neither is independent of firing rate. **E)** shows the relationship between CV and the index of dispersion (ID) measured in 0.5-s bins, also showing a linear relationship.

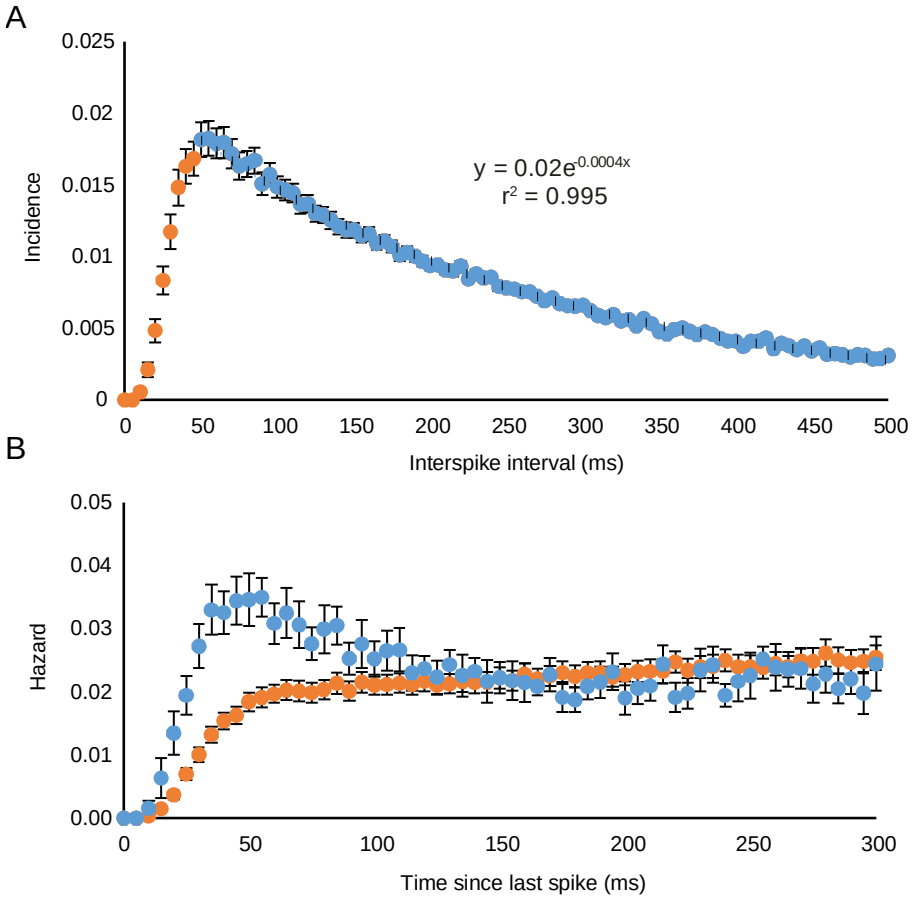

Figure 24 A) Consensus ISI distribution for 76 oxytocin neurones from virgin female rats. Histograms were normalised to the total number of ISIs in the period analysed, and the graph plots the mean (SE) incidence in 5-ms bins. The black dotted line shows a negative exponential fitted to the data from 50 ms onwards (blue symbols). **B)** shows the mean (SE) hazard functions for 9 of the 76 neurones that showed a clear post-spike hyperexcitability (blue symbols and for the other 67 neurones (orange symbols).

To test the generality of the inferences drawn from this initial exploratory analysis, we analysed 76 oxytocin neurones from virgin female rats (Brunton *et al.*, 2006; Velmurugan *et al.*, 2010, 2013). These had firing rates between 1.3 and 8.9 spikes/s (mean (SD) 3.9 (1.8) spikes/s), and the ISI distributions were skewed with modes between 17.5ms and 112.5 ms (mean (SD) 61 (17) ms).

To obtain an ‘average’ distribution, histograms were normalised to the total number of events and averaged. The resulting ‘consensus’ distribution (Figure 24.A) has a mode at 50 ms and a tail that is also well fitted by a single exponential with a time constant of 250 ms (r^2= 0.995 for the fit to ISIs from 50 to 500 ms). The mean hazard function (Figure 24.B) shows a constant hazard after a post-spike interval of about 50 ms. Thus, for most neurones, the ISI distributions and hazard functions conformed closely to the description we published for a sample of 23 oxytocin neurones from male rats (Sabatier *et al.*, 2004).

However, within this larger sample of 76 neurones, heterogeneity was apparent, and nine of the neurones had hazard functions with a conspicuous peak of post spike excitability that was very like that previously described as typical of magnocellular vasopressin neurones (Sabatier *et al.*, 2004), and which apparently reflects a pronounced depolarising afterpotential (DAP). These nine neurones had all shown a clear excitation in the 5 min after intravenous injection of CCK (mean change 1.3 ± 0.4 spikes/s) that was similar to the responses of the remainder of the sample (mean change 1.1 ± 0.2 spikes/s).

To calculate the index of dispersion values for the 76 neurones, we analysed 10-min periods of apparently stationary activity recorded before testing with CCK (Figure 25), and calculated the values of the index for 0.5-s and 10-s bin sizes (Figure 25.A) At a bin width of 0.5 s, the index of dispersion was strongly correlated with the coefficient of variation of ISIs (Figure 25.D). Values of the index of dispersion in 10-s bins were generally lower than in 0.5-s bins (Figure 25.B), consistent with a greater regularity in 10-s bins than expected from the regularity observed in 0.5-s bins. There was only a weak correlation between the index of dispersion in 0.5-s bins and that in 10-s bins (Figure 25.C), suggesting heterogeneity between neurones in the mechanisms underlying this increased regularity.

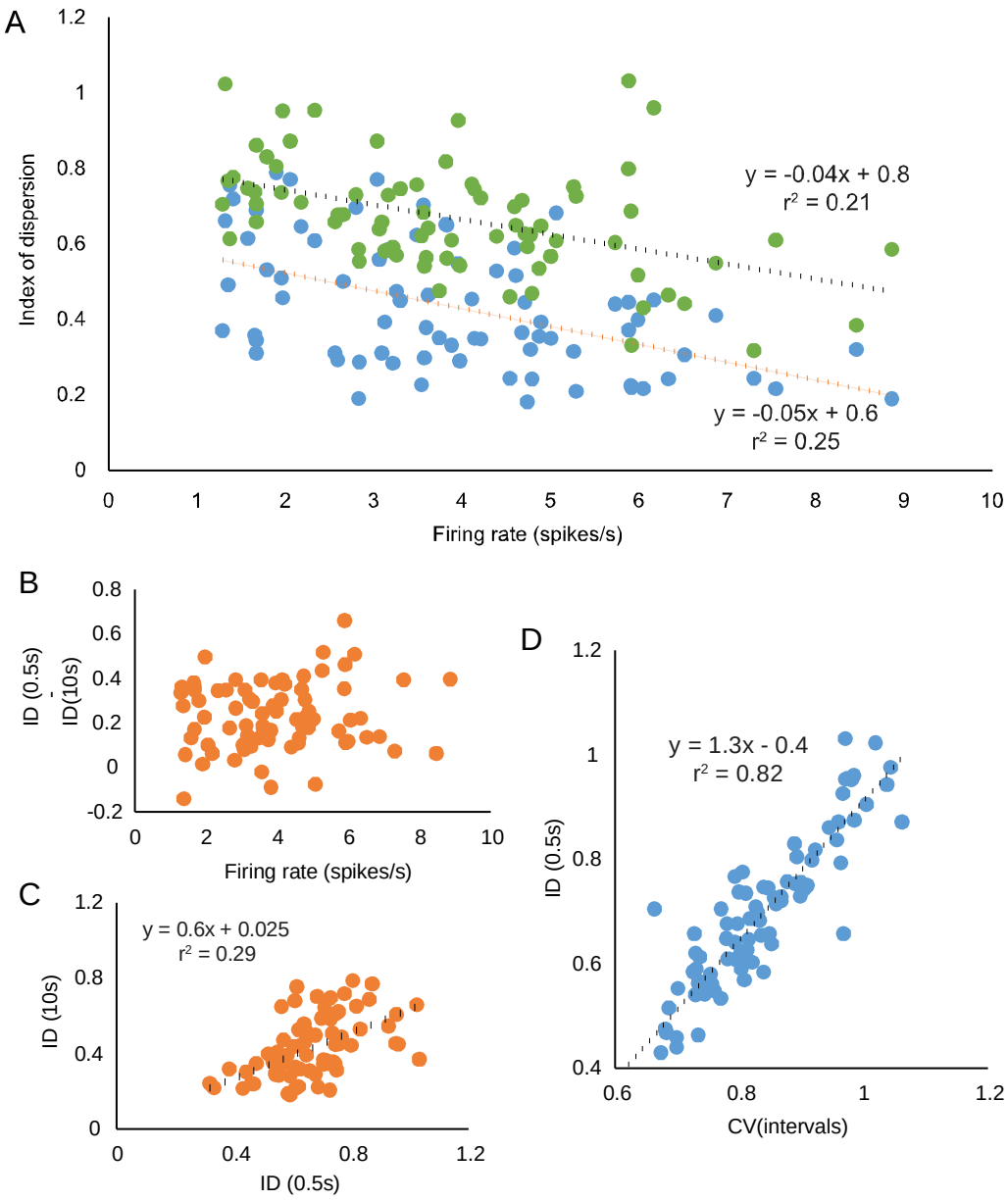

Figure 25. Data from the sample of 76 oxytocin neurones from virgin female rats. A) shows the mean firing rate plotted against the index of dispersion (ID) measured in 0.5s bins (blue symbols) and in 10s bins (green symbols). **B)** plots the difference between the index in 0.5s bins (ID(0.5s) and that in 10-s bins (ID(10s). **C)** shows a weak linear correlation between ID(0.5s) and ID(10s). **D)** shows a strong linear correlation between ID(0.5s) and CV.

Model simulations

We then tested whether model-generated spike data would show the same characteristics of reduced variability with increasing bin width. The integrate-and-fire based model includes mixed random excitatory and inhibitory synaptic inputs and an HAP, and can be extended by adding an AHP and a DAP; the standard parameters

that we used are given in Table 4. For each neurone modelled, we attempted to match the mean firing rate, the ISI distribution, and the index of dispersion for different bin widths. For “typical” oxytocin neurones (i.e. those with hazard functions like the average function shown in Figure 24.B), parameters could be found for model neurones with no AHP, that gave very close fits to the ISI distributions (Figure 26.C1). For neurones where the index of dispersion was independent of bin width, it was possible to match both the index of dispersion and the ISI distribution with just a HAP (Figure 26.B1-B2). When the index of dispersion followed the “typical” decreasing pattern, adding an AHP to the model could result in good fits to the index of dispersion data for all neurones. However, only for some neurones was it possible to simultaneously obtain good fits to the ISI distribution (Figure 26.A1, A2). Specifically, good fits to both could generally be achieved when the index of dispersion was less than 0.6 at a bin width of 0.5 s, but for neurones with an initially high index of dispersion that fell steeply with increasing bin width we could not get good fits to both. For example, for the neurone shown in Figure 26.C, the ISI distribution could be closely matched by a model with a HAP alone (Figure 26.C1), but when we added an AHP to match the index of dispersion data (Figure 26.C4), we could no longer match the ISI distribution (Figure 26.C3).

For these neurones, the difficulty in simultaneously fitting the index of dispersion data and the ISI distribution arose because an AHP that can account for a low index of dispersion at large bin widths also reduces the index of dispersion at short bin widths. To increase the index of dispersion for low bin widths only, the HAP can be reduced, but this results in an excess of short ISIs in the ISI distribution.

This suggested that we were neglecting another factor that increased variability at short bin widths, and an obvious candidate was the DAP, which tends to amplify high frequency firing. In these neurones, we could fit both the ISI distribution and the index of dispersion data with a model that incorporates a DAP as well as a HAP and an AHP (Figure 26.C5-C6).

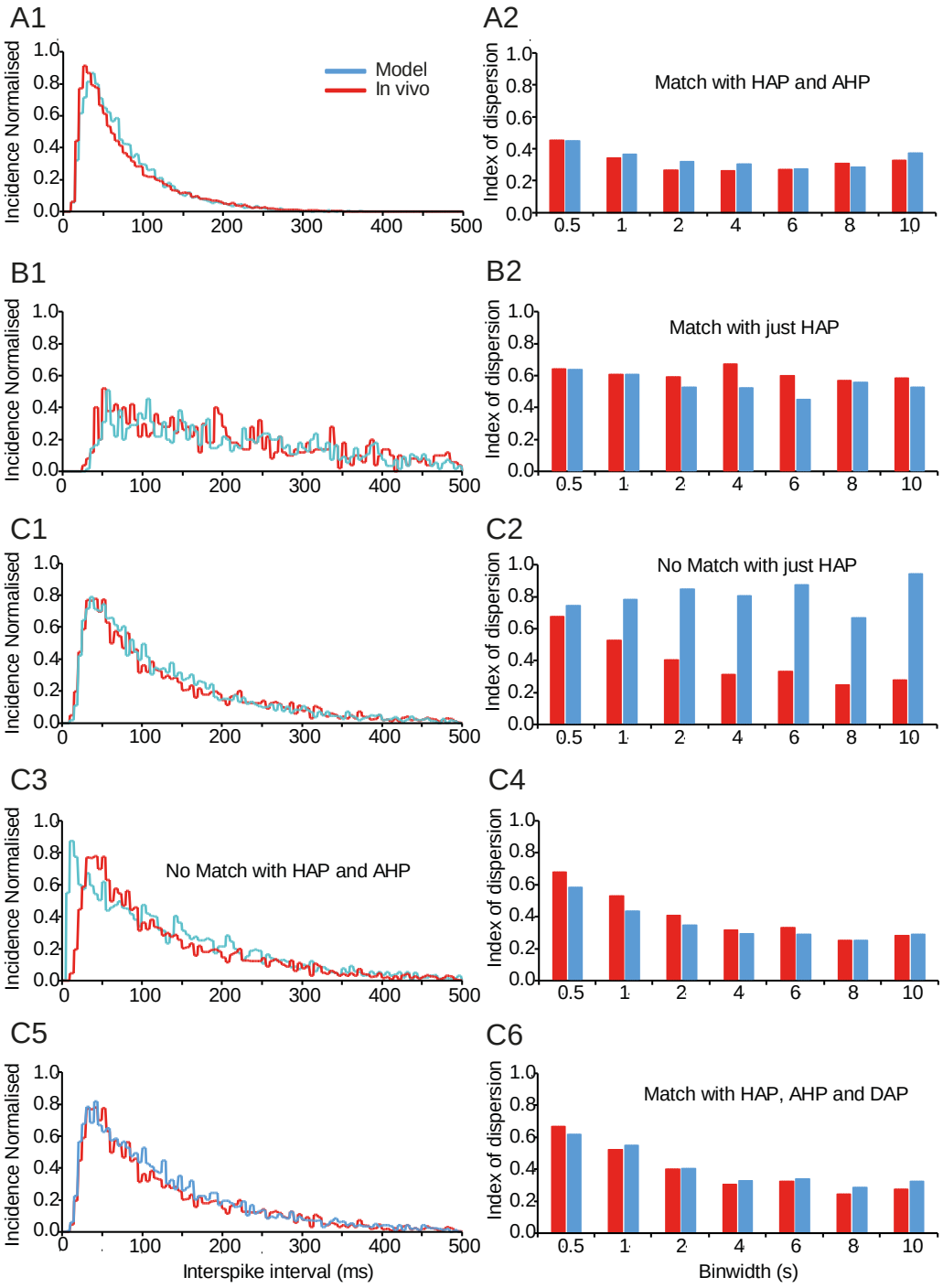

Figure 26. Matching three different neurone baseline intervals. **A)** shows fits for the neurone shown in Figure 22, for the period of spiking activity indicated by the blue shaded area in that figure. A good match was obtained to both the ISI distribution **A1)** and the index of dispersion data **A2)** with a model that had a HAP and an AHP but no DAP (parameters given in Table 5). Notice that the index of dispersion is less than 0.5 for every bin width. B shows an oxytocin neurone (one of the five subsequently exposed to apamin) where the index of dispersion is similar for every bin width. In this case, is possible to match both the ISI distribution **B1)** and the index of dispersion data **B2)** with a model that has just a HAP. **C)** shows another of the neurones that was tested with apamin. In this case, the index of dispersion decreases as bin width increases (from more than 0.6 for 0.5-s bins to less than 0.3 for 10-s bins). To get a match of both index of dispersion and

Table 5. Model parameters to match to the three different neurones shown in Figure 26. Parameters not given here were fixed for all neurones as in Table 4.

	A1, A2	*B1,B2*	*C1,C2*	*C3,C4*	*C5,C6*
Mean rate (spikes/s)					
Model neurone	12.90	3.79	7.40	7.30	7.37
Real neurone	12.93	3.73	7.38	7.38	7.38
Parameters					
I_{re}	752	255	352	540	470
λ_{HAP}	5.4	9.3	4.9	2	4.7
k_{AHP}	0.17	0	0	0.46	0.62
λ_{AHP}	350	-	-	350	350
k_{DAP}	0	0	0	0	0.6
λ_{DAP}	-	-	-	-	215

ISI distributions all three currents -HAP, AHP and DAP- are needed. The model parameters are given in Table 5.

Blocking the medium AHP

The model data thus indicated that the index of dispersion data could be explained by the effects of an AHP. However, an AHP large enough to explain the index of dispersion data has, for some neurones, effects apparently inconsistent with the shape of the ISI distribution. The modelling suggested that in addition to the HAP and the AHP, at least some oxytocin neurones may also have a DAP, the overt effects of which may be occluded by the superimposed HAP and AHP.

To test these inferences, we analysed five identified oxytocin neurones which had been exposed to apamin to block one component of the AHP. In these published experiments (Bull et al., 2011), neurones had been successively exposed over prolonged periods to two concentrations of apamin administered directly to the supraoptic nucleus by retrodialysis. In each of these neurones, exposure to apamin unmasked a period of post-spike hyperexcitability consistent with a DAP. Accordingly, we added a DAP to the model, and looked for a fit to the observed distributions before and after each exposure to apamin, and also a fit to the index of dispersion data.

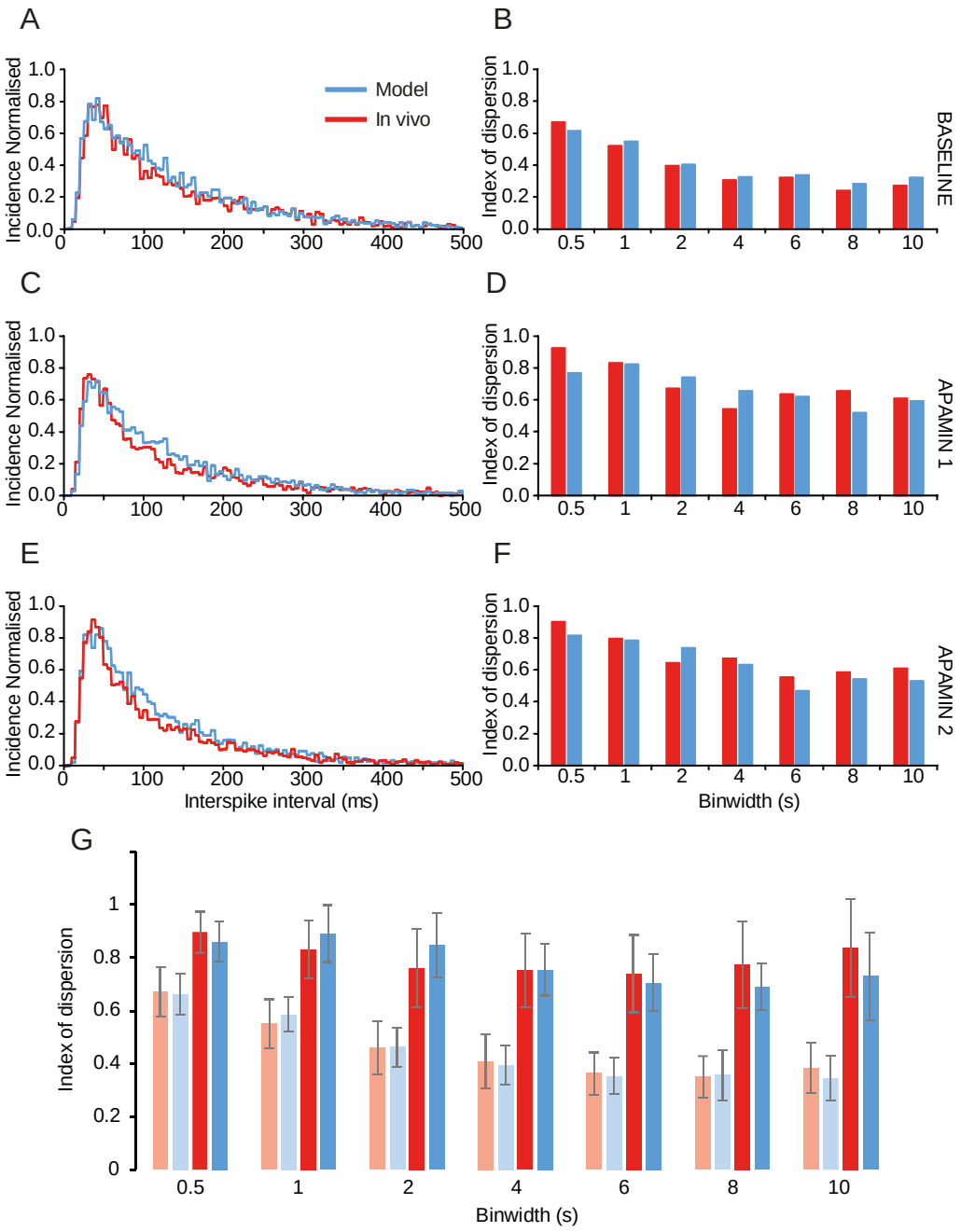

Figure 27. Model fits to five oxytocin neurones that were recorded in basal conditions and during exposure to two concentrations of apamin, given by retrodialysis to the supraoptic nucleus. For each of the five neurones, spike data was fitted by model that included a HAP, AHP and DAP; the parameters varied between neurones, but for each of the neurones, we varied only the amplitude of the AHP and the synaptic input frequency to fit the data after apamin. The model parameters are given in Table 6. **A-F)** shows the fits (in blue) to data (red) from one of these five neurones (neurone 1 in Table 6); the ISI distributions (A, C and E) are normalised to the total number of events in the period analysed. **G)** shows the mean index of dispersion at different bin widths for the five neurones in basal conditions (light red bars) and after the higher dose of apamin (dark red bars), and the corresponding data from the model neurones (light blue for matches to basal data, dark blue for matches to apamin data).

We matched the model to each neurones by finding parameters for the HAP, AHP, DAP and synaptic input rate (I_{re}) that closely matched the ISI distribution and the index of dispersion data at baseline (before any exposure to apamin). For the HAP, changing the amplitude has similar effects to changing the half-life, so we fixed the amplitude at 30 and varied the half-life. We thus sought to find a good match to the three ISI distributions and sets of index of dispersion data for each of the five neurones with fixed values for the half-life of the HAP, the half-life of the AHP and the amplitude and half-life of the DAP but different values for the amplitude of the AHP and I_{re}.

We found parameter sets that produced good fits for each of the five neurones (Figure 27; Table 6). In each case, good fits were obtained to the data after exposure to apamin by reducing both the amplitude of the AHP and the synaptic input rate. The parameter sets that produced good fits are not unique, as different combinations of parameters often give equivalent effects, but in every case, including a DAP was essential to fitting the ISI distributions after apamin, and, in all but one of the five neurones, including an AHP was essential to fitting the index of dispersion data at baseline. Figure 27.A-F shows all the fitted data for one of the five neurones under baseline and apamin conditions, and Figure 27.G shows the mean index of dispersion data for the five neurones and for the five corresponding model neurones.

Table 6 Parameters of models matched to data from neurones exposed to apamin. Three periods of data were matched: baseline (Bsl), apamin 1 (Ap1) and apamin 2 (Ap2). FR - recorded firing rate FR M - modelled firing rate. Parameters not given here were fixed as in Table 4.

	Neuron 1			*Neuron 2*			*Neuron 3*			*Neuron 4*			*Neuron 5*		
Interval	**Bsl**	**Ap1**	**Ap2**	**Bsl**	**Ap1**	**Ap2**	**Bsl**	**Ap1**	**Ap2**	**Bsl**	**Ap1**	**Ap2**	**Bsl**	**Ap1**	**Ap2**
FR M	7.37	7.40	8.00	3.75	4.24	3.68	2.86	2.73	2.17	6.55	8.01	10.24	6.12	5.24	4.57
FR	7.38	7.46	7.91	3.73	4.28	3.61	2.80	2.46	1.87	6.50	8.01	10.20	6.10	5.25	4.89
I_{re}	470	365	350	255	295	245	245	210	190	470	454	414	610	430	315
λ_{HAP}	4.7			7.5			6.0			6.0			11.3		
k_{AHP}	0.62	0.40	0.30	0.42	0.54	0.36	0.94	0.78	0.73	1.39	1.15	0.93	1.13	0.95	0.77
λ_{AHP}	350			350			500			300			495		
k_{DAP}	0.6			0.37			1.1			1.53			1.22		
λ_{DAP}	215			350			350			200			295		

Discussion

In these experiments we have shown that the spiking activity in oxytocin neurones, when measured in bins of 5-10s, is much more regular than we would expect from the variability of ISIs. This is consistent with a slow activity-dependent negative feedback and seems likely to reflect the actions of the AHP that arises by activation of Ca^{2+}-dependent K^+ channels. The best fits with the model, with λ_{AHP} in the range 350 to 500 ms, correspond most closely to the time course of the apamin sensitive SK channel based medium AHP. The half-life of the AHP determines how quickly it changes, and because it is relatively slow, taking several seconds to accumulate, its effect on reducing spike interval variability is only detectable in the larger bin-sizes. However, a value for λ_{AHP} of 1000ms or greater, which would more closely correspond to the slow AHP is unable to fit the index of dispersion at the medium bin widths of 2, 4, and 6 s.

However, adding to the model an AHP which is large enough to account for the values of index of dispersion significantly impacts upon the ISI distribution, delaying the mode and impinging on the ability of the model neurones to display high frequency firing, especially as seen during the milk-ejection reflex. It appears therefore that oxytocin neurones also have an activity-dependent depolarisation superimposed upon the HAP and AHP, with an intermediate timescale. Together, these three features allow the neurones to maintain a relatively regular firing rate in basal conditions while retaining the ability to generate bursts of activity.

In fitting models to the data from oxytocin neurones exposed to apamin, we sought parameters that fitted the behaviour of each of five neurones in three conditions (at baseline and after exposure to two concentrations of apamin). Hazard function based spike interval analysis shows that apamin removes any hazard detectable AHP, and unmasks a distinct DAP, that is enhanced further with an increased dose of apamin (Bull *et al.*, 2011). For each neurone, we found a parameter set that would fit all three conditions well with changes in just two parameters – the synaptic input rate and the amplitude of the AHP. In each case, the fits involved reducing the AHP amplitude progressively with increasing apamin concentration, consistent with the established actions of apamin to block one component of the AHP, but the fits also required a progressive reduction in synaptic input. This suggests that, in the experimental conditions, apamin also had presynaptic actions, either reducing excitatory input or increasing inhibitory input. The latter seems more likely, as

apamin's actions would be generally expected to increase neuronal excitability, increasing spike rate as is observed *in vitro* (Kirkpatrick & Bourque, 1996), and supraoptic neurones receive an extensive inhibitory input from GABA neurones in the perinuclear zone immediately adjacent to the supraoptic nucleus (Herbison, 1994; Wang *et al.*, 2015).

Importantly, to obtain these good fits in all conditions, it was necessary in all neurones to include a DAP in the model. The DAP has the opposite effect to the AHP on the index of dispersion; by acting as a positive feedback it increases spike interval variability at short bin widths. Whereas vasopressin neurones in the supraoptic nucleus typically display a conspicuous DAP, oxytocin neurones generally do not. However the presence of a fast DAP has been reported in about 20% of oxytocin neurones (Teruyama & Armstrong, 2007), which seems consistent with the observation here of a conspicuous post-spike hyperexcitability in nine of 76 neurones (12%). In supraoptic neurones generally, DAPs are triggered by Ca^{2+} influx during spikes (Andrew & Dudek, 1984; Smith & Armstrong, 1993; Li & Hatton, 1997; Greffrath *et al.*, 1998), but their ionic basis is poorly understood. One study suggested that they may result from the Ca^{2+}-dependent reduction of a resting K^+ conductance (Li & Hatton, 1997), but subsequent work suggested that a Ca^{2+}-activated nonselective cation channel is involved (Ghamari-Langroudi & Bourque, 2002; Teruyama & Armstrong, 2007). The effect of a DAP on oxytocin neurone activity is to increase irregularity of firing, especially when measured in short bin widths; it thus appears that the combination of a DAP and an AHP has the effect of increasing the regularity of firing in long bin widths while protecting the ability to fire at high frequencies during milk-ejection bursts.

The parameters that we found for the DAP correspond approximately to those reported for the fast DAP (Teruyama & Armstrong, 2007). A larger subset of oxytocin neurones *in vitro* have been reported to express a slow DAP, with a much longer duration (~2 s) than the fast DAP (Stern & Armstrong, 1996; Armstrong *et al.*, 2010). Because the duration of the slow DAP is similar to that of the slow AHP, it seems possible that their effects upon spike excitability largely cancel out in the circumstances that we are exploring them (stable spontaneous activity).

How important it is for an oxytocin neurone to maintain a regular firing rate in constant conditions is hard to judge. For oxytocin neurones generally, slow activity-dependent mechanisms reduce the index of dispersion in 10-s bins from about 1 to

about 0.4 at a firing rates of 4 spikes/s. This is equivalent to reducing the standard deviation from 6.3 to 2.8 – a substantial reduction, but the plasma oxytocin concentration reflects the averaged secretion of several thousand oxytocin neurones, so is this reduction physiologically meaningful? It may be, because for any one oxytocin neurone, the relationship between firing rate and secretion is complex and non-linear: for short bursts of spikes, secretion increases disproportionately with spike frequency (MacGregor & Leng, 2013), so that, in a 1-s burst at 50 Hz, triggers secretion of, on average about 100 times as much oxytocin as is released by the same number of spikes at 1 Hz (Bicknell, 1988). Moreover, subsets of magnocellular neurones project to sites within the brain, and these sites receive relatively few oxytocin fibres (Knobloch & Grinevich, 2014). Accordingly, mechanisms that reduce the "burstiness" of firing that arises from random variation in synaptic input may be very important in ensuring that the secretion rate at these sites accurately reflects the mean firing rate.

We can also look more generally at the possible utility of these mechanisms, remembering that subpopulations of magnocellular oxytocin neurones project to many different brain sites, and that at these central projections they appear to use glutamate as a conventional synaptic neurotransmitter. The mean firing rate of any particular oxytocin neurone is proportional to the plasma sodium concentration, and increases by an average of about 0.7 spikes/s for every 1mM increase. We can therefore ask, if the plasma Na^+ concentration is raised by 1mM, for how long do we need to measure the firing rate of an oxytocin neurone to know with 95% confidence that plasma sodium has increased (given no change in any of the other stimuli that influence oxytocin neurones)? Suppose that the starting firing rate a is 3 spikes/s, that we know this with certainty, and that the true rate b after osmotic stimulation is 3.7 spikes/s. If the index of dispersion is 1, it will be necessary to measure the neurone's firing rate for at least 30 s to have 95% confidence that the firing rate is actually higher than a. By contrast, if the index of dispersion is 0.2, then just 8 s is enough. In practice, neurones do not have good mechanisms for averaging synaptic inputs over prolonged periods. Thus, if it is important for neuronal networks to respond to small but sustained changes in external signals swiftly and reliably, then cellular mechanisms for reducing the variability of discharge patterning may be very important.

Acknowledgements.

This project has received funding from the European Union's Seventh Framework Programme for research, technological development and demonstration under grant agreement no 607310. The apamin experiments were funded by Wellcome Trust Grant Number 070118. Trystan Leng assisted in the oxytocin neurone spike interval analysis.

Conclusions to the first paper

This first paper (Maícas-Royo *et al.*, 2016) supported the robustness of the LIF model to simulate the spiking activity of oxytocin neurones. Besides, it showed the model's ability to differentiate the contribution of the different currents involved in the membrane response to the action potential. In particular, it showed the importance of the AHP in the reduction of the variability in the spiking activity and also the necessity of a DAP in some neurones. The model also showed how the DAP could be unmasked in more neurones, once the AHP contribution was made zero.

Moreover, by seeing how the index of dispersion could be matched by modifying the different currents, it also supported the choice of simulating the PSP as randomly arriving inputs that follow a Poisson distribution.

Summing up, the model showed it was working well to mimic the spiking activity of any single oxytocin neurone and, at the same time, reveal the membrane characteristics that were making a neurone behave in a particular way. Being certain that the spiking model was a stable pillar to build on, we started wondering what would be next. Following the findings we got about the role of the AHP, we had two natural options. To see how the AHP could affect in a more complex context we could choose between developing a model that would simulate a population of neurones or, before doing that, try to simulate first the secretion dynamics of oxytocin neurones.

Chapter 4 (paper):

A predictive, quantitative model of spiking activity and stimulus-secretion coupling in oxytocin neurons.

Introduction to the second paper.

Maícas-Royo J, Leng G & MacGregor DJ (2018). A Predictive, Quantitative Model of Spiking Activity and Stimulus-Secretion Coupling in Oxytocin Neurons. *Endocrinology* **159,** 1433–1452.

Taking advantage of the work of my supervisors (MacGregor & Leng, 2013), we decided that the best way to build upon the spiking model for single oxytocin neurones would be to use the secretion model of vasopressin neurones, developing a secretion model for oxytocin neurones.

Thus, our main assumption was that we could model the spiking activity of the whole population of magnocellular oxytocin neurones as the average of all of them that would be simulated by our model for single neurones.

The secretion model would be fed by the single oxytocin neuron model and, at the end, the resultant secretion would be the input of the plasma oxytocin. As the plasma oxytocin is cleared and it can diffuse as well to the extravascular fluid, we also made a model to simulate that dynamics.

After developing the three models separately, I fitted them individually by trial and error to experimental data that evaluated the physiology of each of them. Once that was done, I integrated in a single model the spiking, secretion and plasma model, testing the resultant model by comparing its dynamics with the well described response of oxytocin neurones to CCK.

I soon obtained good results and we decided to publish them. However, writing took me one year. Partly because my writing abilities are not the best and partly because, in the process, we incorporated other experiments we found in the literature. And every time I incorporated new experiments, I adjusted the new fitting to all the previous experiments.

When I was finally certain of the robustness of the model, I used it to elucidate what the role of the AHP was in secretion and plasma oxytocin.

Finally, I introduced a bit of heterogeneity in our model, running simulations with small populations of 20 neurones to check the effect that the variability of postsynaptic inputs could have on the final response.

Abstract

Oxytocin neurons of the rat hypothalamus project to the posterior pituitary where they secrete their products into the bloodstream. The pattern and quantity of that release depends on the afferent inputs to the neurons, on their intrinsic membrane properties, and on non-linear interactions between spiking activity and exocytosis: a given number of spikes will trigger more secretion when they arrive close together. Here we present a quantitative computational model of oxytocin neurons that can replicate the results of a wide variety of published experiments. The spiking model mimics electrophysiological data of oxytocin cells responding to cholecystokinin (CCK), a peptide produced in the gut after food intake. The secretion model matches results from *in vitro* experiments on stimulus-secretion coupling in the posterior pituitary. We mimic the plasma clearance of oxytocin with a two-compartment model, replicating the dynamics observed experimentally after infusion and injection of oxytocin. Combining these models, allows us to infer, from measurements of oxytocin in plasma, the spiking activity of the oxytocin neurons that produced that secretion. These inferences we have tested with experimental data on oxytocin secretion and spiking activity in response to intravenous injections of CCK. We show how intrinsic mechanisms of the oxytocin neurons determine this relationship: in particular, we show that the presence of an after-hyperpolarization (AHP) in oxytocin neurons dramatically reduces the variability of their spiking activity, and even more markedly reduces the variability of oxytocin secretion. The AHP thus acts as a filter, protecting the final product of oxytocin cells from noisy fluctuations.

Introduction

Magnocellular oxytocin neurons in the supraoptic nucleus (SON) and paraventricular nucleus of the hypothalamus project their axons to the posterior pituitary where they secrete their hormones into the bloodstream. Oxytocin has an indispensable role in breastfeeding and an important one in parturition (Leng *et al.*, 2015), but the secretion of oxytocin is also regulated by a variety of metabolic signals arising from the gastrointestinal tract, and, in the rat, oxytocin secretion also regulates sodium excretion and gut motility (Leng & Sabatier, 2017).

The membrane properties of these neurons have been studied extensively by electrophysiological studies *in vitro* (Hatton & Li, 1999; Pittman *et al.,* 1999;

Armstrong *et al.*, 2010; Brown *et al.*, 2013). In these neurons, spikes are typically triggered by the arrival of excitatory inputs (excitatory postsynaptic potentials; EPSPs) from diverse brain areas. Whenever a spike is produced, Ca^{2+} enters the cell through voltage-activated channels and subsequently activates K^+ channels that mediate post-spike hyperpolarisations. Large conductance (BK) channels open and close rapidly, producing a short hyperpolarizing afterpotential (HAP) which makes the neurons relatively inexcitable for 30-50ms (Leng *et al.*, 2017). Small conductance (SK) channels produce a medium afterhyperpolarization (AHP). This is much smaller than the HAP, but the half-life is much longer (about 350ms), so the AHP accumulates over successive spikes, and the resulting level of activity-dependent hyperpolarization will reflect the average level of spike activity over the preceding few seconds (Leng *et al.*, 2017). Some oxytocin neurons also generate an activity-dependent depolarising afterpotential (DAP) (Teruyama & Armstrong, 2007), but this is usually quite small and masked by the larger activity-dependent hyperpolarisations.

The patterning of spikes generated by these neurons has also been studied extensively *in vivo* (Richard *et al.*, 1997; Leng *et al.*, 1999; Hatton & Wang, 2008; Brown *et al.*, 2013). In lactating rats, suckling induces brief intense bursts of spikes in oxytocin cells, but other stimuli produce graded increases in spike activity. For example, intravenous (i.v.) injections of cholecystokinin (CCK) produce a dose-dependent increase in spike activity that lasts for 10-15 min (Renaud *et al.,* 1987; Leng *et al.*, 1992; Brown *et al.*, 1996; Velmurugan *et al.*, 2010, 2013), producing a transient increase in plasma oxytocin. CCK is secreted from the duodenum in response to a meal and acts at CCK1 receptors on gastric vagal afferents; these project to neurons in the nucleus tractus solitarii, which in turn project directly to magnocellular oxytocin neurons (Rinaman *et al.,* 1995; Leng *et al.,* 2008). The subsequent secretion of oxytocin is thought to regulate gut motility and sodium excretion at the kidneys (McCann *et al.,* 1989; Verbalis *et al.*, 1991).

The spontaneous spiking activity of oxytocin neurons can be matched by a modified leaky integrate-fire model, which incorporates a HAP and an AHP (Maícas-Royo *et al.*, 2016; Leng *et al.*, 2017). This model can closely match the statistical features of spike patterning in oxytocin neurons, as reflected by the interspike interval distribution and the index of dispersion of spike rate. Given this, it should be possible to use the model to infer the synaptic input that oxytocin cells receive when

responding, for example, to CCK, if we assume that the CCK-evoked input consists solely of a change in excitatory input rate.

Our previous work indicates that the AHP in oxytocin neurons, by acting as an activity-dependent negative feedback, reduces the second-by-second variability (index of dispersion) in the firing rate of oxytocin cells (Maícas-Royo *et al.*, 2016). Because of particular features of stimulus-secretion coupling in these neurons, this "regularisation" of firing rate is likely to be most important during dynamic challenges to oxytocin cell activity. In oxytocin neurons, secretion is a non-linear function of spike activity: a given number of spikes secrete more oxytocin when they are close together than when sparsely distributed. This nonlinearity is marked: during a reflex milk ejection, oxytocin cells fire about 100 spikes in just 2 s (Wakerley & Lincoln, 1973), and during this burst, each spike releases, on average, about 100 times as much oxytocin as spikes that occur at the typical basal firing rate of 2 spikes/s (Leng & Brown, 1997). Because of this non-linearity, the oxytocin secretion from a single cell depends not only on its mean firing rate but also on the variability of its firing rate, due to the disproportionate influence of high firing rate fluctuations.

The mechanisms of stimulus-secretion coupling are complex, but we recently published a model of stimulus-secretion coupling in magnocellular vasopressin cells fitted to data on stimulus-evoked vasopressin secretion (MacGregor & Leng, 2013). The properties of vasopressin terminals differ quantitatively from those of oxytocin terminals, and here we modified the vasopressin secretion model to fit the properties of oxytocin terminals (Bicknell et al., 1984; Carolyn A. Bondy, 1987; Bicknell, 1988). Combining the spiking model of oxytocin neurons with this secretion model allows us to model the activity-dependent output of oxytocin cells. To predict the consequences for plasma concentrations, we also introduced a model of the clearance of oxytocin from plasma. For this there is good historical data (Ginsburg & Smith, 1959; Fabian *et al.*, 1969*a*; Leng & Sabatier, 2016). Applying this allows us to predict, from the model, the plasma oxytocin concentration that will result from a given stimulus to the oxytocin cells. In the case of CCK, again there is published data to compare with the model. This allows us to assess the importance of the AHP not only for spike activity but also for the important biological signal – the resulting change in plasma oxytocin concentration.

Methods

We used a previously described model for the spiking activity of oxytocin neurons ((Maícas-Royo *et al.*, 2016); parameters given in Table 7) and adapted a published model of stimulus-secretion coupling in vasopressin neurons to model oxytocin secretion (MacGregor & Leng, 2013). We also added a two-compartment model to mimic the dynamics of oxytocin concentration in plasma (

Figure **28**). The models were developed using software written in C++ and a graphical interface based in the open source wxWidgets library. Simulations were run for up to 10,000 s using a 1-ms step.

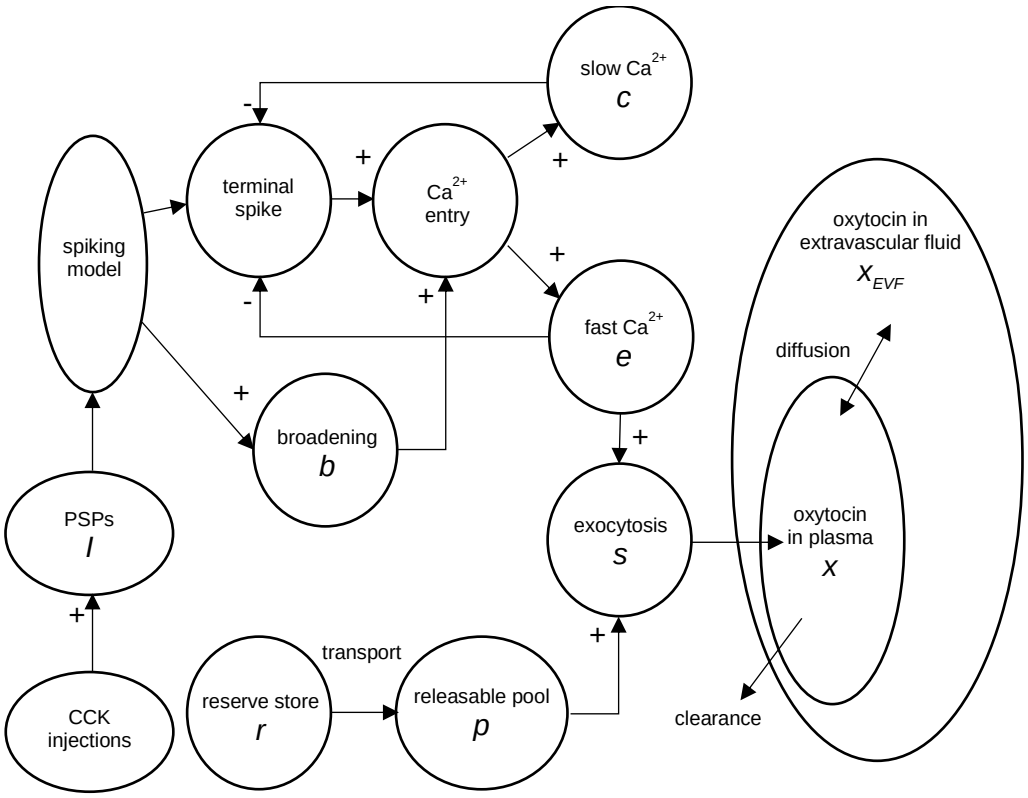

Figure 28 The combined spiking, secretion, and diffusion model. The integrate-and-fire based spiking model responds to randomly arriving PSPs. The i.v. injection of CCK is simulated as an exponentially decaying increment in the mean arrival rate of EPSPs. The resulting spikes become the input of the secretion model. In that model, spike-induced Ca^{2+} entry at secretory terminals is positively modulated by activity-dependent spike broadening (b), and negatively modulated by fast (e) and slow (c) Ca^{2+} variables that inhibit spike-induced opening of Ca^{2+} channels (MacGregor & Leng, 2013). The secretion rate (s) is the product of the releasable pool (p) and e. When depleted, pool p is refilled from a reserve pool (r) at a rate dependent on the pool content. Oxytocin in plasma (x) is cleared with an exponential decay, and diffuses between the plasma and extravascular fluid (x_{EVF}) according to the concentration gradient.

Spiking model

The integrate-and-fire based spiking model (Maícas-Royo *et al.*, 2016) simulates the firing activity of oxytocin cells in response to EPSPs and inhibitory postsynaptic potentials (IPSPs). We model PSPs as arriving randomly at mean rates I_{re} and I_{ri}, and in this study, we fixed I_{ri} to be equal to I_{re}. Thus, the time an EPSP arrives, $epsp_{time}$ is defined by:

$$epsp_{time} = \frac{-\log(1 - rand)}{I_{re}}, \qquad \text{where } rand \text{ is a random number between 0 and 1} \qquad (12)$$

The IPSP arrival times follow the same formula.

Table 7 Spiking Model Parameter Values Top) Parameters of the integrate-and-fire spiking model, with values chosen from (Maícas-Royo *et al.*, 2016) and CCK parameters, as used for the simulations in Figure 29.B. **Bottom)**. Parameter changed from Top) to match a single oxytocin neuron recording as seen in Figure 29.C. In subsequent simulations, I_{re} and I_{ri} were kept equal to each other but were varied to produce different basal firing rates as appropriate; the other parameters were unchanged from the upper table.

Name	Description	Value	Units
I_{re}	excitatory input rate	292	Hz
I_{ri}	inhibitory input rate	292	Hz
$epsp_h$	EPSP amplitude	2	mV
$ipsp_h$	IPSP amplitude	-2	mV
λ_{syn}	PSP half-life	3.5	ms
k_{HAP}	HAP amplitude per spike	30	mV
λ_{HAP}	HAP half-life	7.5	ms
k_{AHP}	AHP amplitude per spike	1	mV
λ_{AHP}	AHP half-life	350	ms
V_{rest}	resting potential	-56	mV
V_{thresh}	spike threshold potential	-50	mV
λ_{CCK}	CCK half-life in plasma	230	s
CCK_{dur}	CCK injection duration	20	s
k_{CCK}	CCK i.v. injection	20	µg/kg
I_{re}	excitatory input rate	210	Hz

Responses to CCK

We mimicked the effect of i.v. injection of CCK by adding an additional random EPSP contribution, with mean rate I_{rCCK}. The total EPSP rate is the sum of I_{re} and I_{rCCK}.

The increase in EPSP rate during simulated CCK injection follows a linear function k_{CCK}/CCK_{dur} defined by the quantity of CCK injected, k_{CCK}, and the duration of the injection, CCK_{dur}.

We assume that CCK is cleared from plasma following an exponential decay with time constant τ_{CCK}.

$$\frac{dI_{rCCK}}{dt} = \frac{\left({}^{k_{CCK}}/_{CCK_{dur}}\right) - I_{rCCK}}{\tau_{CCK}} \text{ when } CCK_{\text{start}} \leq t \leq CCK_{\text{start}} + CCK_{\text{dur}} \quad (13)$$

$$\frac{dI_{rCCK}}{dt} = \frac{-I_{rCCK}}{\tau_{CCK}} \text{ when } t > CCK_{\text{start}} + CCK_{\text{dur}} \quad (14)$$

where CCK_{start} is the injection's start time.

Time constants are calculated from half-life parameters by:

$$\tau_x = \frac{\lambda_x}{ln(2)} \quad (15)$$

We fixed the magnitude of EPSPs and IPSPs, $epsp_h$ and $ipsp_h$, at 2 mV, having an opposite sign for EPSPs and IPSPs. The final input depends on the number of inputs, $epsp_n$ and $ipsp_n$, per unit of time (fixed at 1ms in our simulations). $epsp_n$ is the number of EPSPs obtained in a given time unit from a random process with mean rate I_{re}.

$$I = epsp_h.epsp_n + ipsp_h.ipsp_n \quad (16)$$

V_{syn} represents the contribution of synaptic input to the membrane potential V, and decays to 0 with time constant τ_{syn} corresponding to a half-life λ_{syn} of 3.5 ms.

$$\frac{dV_{syn}}{dt} = -\frac{V_{syn}}{\tau_{syn}} + I \qquad (17)$$

Initially, the model neuron is at a resting potential, V_{rest} = -56mV. If inputs summate to increase the membrane potential V above a threshold V_{th} = -50mV, the neuron produces a spike. Then, the model triggers a HAP and an AHP, and V evolves according to

$$V = V_{rest} + V_{syn} - HAP - AHP \qquad (18)$$

HAP has a fixed amplitude (k_{HAP} = 30mV) and a time constant, τ_{HAP} , that corresponds to a half-life of 7.5 ms, following values from previous work (Maícas-Royo *et al.*, 2016). *AHP* also has a fixed amplitude (k_{AHP} = 1) and τ_{AHP} was set to correspond to a half-life λ_{AHP} of 350 ms as used previously (Maícas-Royo *et al.*, 2016); we explored different values of k_{AHP} in the range of values (0.2-1.4) found previously from fits to individual oxytocin neurons (Maícas-Royo *et al.*, 2016); the results were qualitatively similar for other values of k_{AHP}.

$$\frac{dHAP}{dt} = -\frac{HAP}{\tau_{HAP}} + k_{HAP} \cdot \delta \qquad (19)$$

$$\frac{dAHP}{dt} = -\frac{AHP}{\tau_{AHP}} + k_{AHP} \cdot \delta \qquad (20)$$

where δ = 1 if a spike is fired at time t, and δ = 0 otherwise.

Secretion model

The secretion model is an adaptation of the model of MacGregor and Leng (MacGregor & Leng, 2013), developed to mimic stimulus-secretion coupling in vasopressin neurons. When spikes invade the secretory terminals, exocytosis occurs at sites close to clusters of voltage-gated Ca^{2+} channels. These sites experience transiently high Ca^{2+} concentrations in response to spikes, but the Ca^{2+} swiftly diffuses into the cytosol (Nowycky *et al.,* 1998). This is represented by making secretion proportional to a 'fast' Ca^{2+} variable e. At increased frequencies,

the spikes broaden (Bourque, 1990; Muschol & Salzberg, 2000), producing a larger rise in *e*.

Table 8. Secretion model parameter values, modified from the parameters used for a model of vasopressin secretion (MacGregor & Leng, 2013) as described in the Results.

Name	Description	Value	Units
k_b	broadening per spike	0.021	-
λ_b	broadening half-life	2000	ms
b_{base}	basal spike broadening	0.5	-
k_c	max cytosolic Ca^{2+} per spike	0.0003	-
λ_c	cytosolic Ca^{2+} half-life	20000	ms
k_e	max submembrane Ca^{2+} per spike	1.5	-
λ_e	submembrane Ca^{2+} half-life	100	ms
c_θ	threshold, terminal inhibition by *c*	0.14	
c_n	gradient, terminal inhibition by *c*	5	
e_θ	threshold, terminal inhibition by *e*	12	
e_n	gradient, terminal inhibition by *e*	5	
β	pool refill rate scaling factor	120	
r_{max}	reserve store maximum	1000	ng
p_{max}	reserve pool maximum	5	ng
α	Secretion scaling factor	3	
φ	cooperativeness of the Ca^{2+} activation of exocytosis	2	

The resulting facilitation of secretion is limited by activity-dependent attenuation of secretion, modelled as arising from Ca^{2+}-dependent inactivation of Ca^{2+} channels in the submembrane compartment, and by activation of Ca^{2+}-dependent K^+ channels. The model consists of differential equations which take as input the spike events generated by the spiking model. Variables representing spike broadening (*b*), cytosolic Ca^{2+} concentration (*c*) and submembrane Ca^{2+} concentration (*e*) are all incremented with each spike. The Ca^{2+} variables model Ca^{2+} mediated signals at specific action sites: we did not attempt to represent the full dynamics of intracellular calcium changes.

We model spike broadening *b* by increasing it by k_b = 0.021 when a spike arrives, and with an exponentially decay with half-life λ_b = 2 s:

$$\frac{db}{dt} = -\frac{b}{\tau_b} + k_b \cdot \delta \qquad (21)$$

where $\delta = 1$ if a spike is fired at time t, and $\delta = 0$ otherwise.

The Ca^{2+} entry, Ca_{ent}, provoked by spikes has two other effects. *c* and *e* measure how the concentration of Ca^{2+} changes at the cytosol and in the submembrane compartment. They are incremented by $k_c = 0.0003$ *and* $k_e = 1.5$ with every spike and decay with half-lives λ_c = 20 s and λ_e = 100 ms:

$$\frac{dc}{dt} = -\frac{c}{\tau_c} + k_c \cdot Ca_{ent} \cdot \delta \qquad (22)$$

$$\frac{de}{dt} = -\frac{e}{\tau_e} + k_e \cdot Ca_{ent} \cdot \delta \qquad (23)$$

where δ=1 if a spike is fired at time *t*, and δ=0 otherwise.

Ca^{2+} entry depends on spike broadening (*b*), and is subject to Ca^{2+}-dependent inhibition:

$$Ca_{ent} = e_{inhib} \cdot c_{inhib} \cdot (b + b_{base}) \qquad (24)$$

The basal level of spike broadening is given by $b_{base} = 0.5$. Ca^{2+} entry is inhibited by *c* and *e* using two inverted Hill equations with threshold and coefficient parameters, c_θ = 0.14, e_θ = 12, c_n = 5 and e_n = 5:

$$c_{inhib} = 1 - \frac{c^{c_n}}{c^{c_n} + {c_\theta}^{c_n}} \qquad (25)$$

$$e_{inhib} = 1 - \frac{e^{e_n}}{e^{e_n} + {e_\theta}^{e_n}} \qquad (26)$$

The releasable vesicle pool (*p*) is depleted with secretion, *s*, and refilled when not full (p_{max} = 5 ng) at a rate proportional to the remaining reserve pool (*r*) divided by its maximum capacity (r_{max} = 1 µg). The refill rate is scaled by β = 120:

$$\frac{dp}{dt} = -s + \beta \cdot \frac{r}{r_{max}} \quad \text{when } p < p_{max}, \qquad -s \text{ otherwise} \qquad (27)$$

The reserve pool is depleted exponentially as it refills *p*, with its maximum (initial) value defined by r_{max}:

$$\frac{dr}{dt} = -\beta \cdot \frac{r}{r_{max}} \quad \text{when } p < p_{max}, \qquad 0 \text{ otherwise} \tag{28}$$

The rate of secretion (*s*) is the product of *e* raised to the power φ (because of the cooperativeness of the Ca^{2+} activation of exocytosis) (Neher, 2012), the releasable pool (*p*) and a scaling factor α

$$s = e^{\varphi} \cdot \alpha \cdot p \tag{29}$$

The parameters of the vasopressin model were fitted to data obtained for secretion from the whole neural lobe – containing the axons of up to 9000 neurons (Bandaranayake, 1971; Rhodes *et al.*, 1981). Thus, parameters relevant to *quantities* of secretion (*p*, p_{max} , *r* and r_{max}) from the whole population are about nine thousand times higher than would be appropriate for single cells. The same approach was taken here, and the same 'correction factor' applies.

To adapt this model to match oxytocin secretion, we made six changes from the parameters of the vasopressin model (MacGregor & Leng, 2013); the new parameters are given in Table 8.

1) We decreased k_b from 0.05 to 0.021, reducing the spike broadening.
2) We reduced the sensitivity to Ca^{2+} entry in the submembrane compartment, by increasing e_θ from 2.8 to 12.
3) We increased c_θ from 0.07 to 0.14.
4) We reduced the cooperativeness of the Ca^{2+} activation of exocytosis from φ = 3 to φ = 2.
5) We increased α, a scaling factor, to 3 to match the levels of oxytocin measured in plasma.
6) We increased β, the refill rate of the pools from the reserve, from 50 to 120.

The results mimic the secretion of the entire population by considering that the average response of the population can be mimicked by the response of a single oxytocin cell multiplied by a scaling factor.

Two-compartment diffusion model

To simulate how the oxytocin that enters the plasma (*x*) is cleared, we developed a two-compartment model. Secreted oxytocin enters the plasma volume (C_{plasma}) and is cleared from it mainly through the kidneys and liver. The second compartment represents the extravascular fluid compartment (C_{EVF}), and oxytocin diffuses between these two compartments according to the concentration gradient. The clearance from plasma and the diffusion between compartments follow exponential differential equations with a clearance half-life λ_{cl}, of 68s and a diffusion half-life λ_{diff} of 61s (Table 9), values derived from reference data described below:

$$\frac{dx}{dt} = s - \frac{x}{\tau_{clr}} - \frac{DiffRate}{\tau_{diff}} \qquad (30)$$

The oxytocin content in plasma (*x*) and extravascular fluid (x_{EVF}) change due to diffusion between the compartments following the oxytocin concentration gradient (*DiffRate*):

$$DiffRate = \left({}^{x}/_{C_{plasma}} - {}^{x_{EVF}}/_{C_{EVF}}\right) \cdot \frac{C_{plasma} + C_{EVF}}{2} \qquad (31)$$

$$\frac{dx_{EVF}}{dt} = \frac{DiffRate}{\tau_{diff}} \qquad (32)$$

Reference data.

To fit the spiking model, we used a library of recordings of oxytocin neurons in urethane-anesthetised rats. Full details of these experiments have been published previously (Sabatier *et al.*, 2004; Velmurugan *et al.*, 2010, 2013). In brief, neurons were recorded from the supraoptic nucleus using a transpharyngeal surgical approach, and were antidromically identified as projecting to the posterior pituitary. Oxytocin neurons were identified by their excitatory responses to i.v. injection of CCK, and spike times were collected using Spike2 software (Cambridge Electronic Design Ltd.). Model data was compared to recorded spike activity by comparing the interspike interval distributions (in 5-ms bins) and by comparing the index of dispersion of firing rate, calculated as the ratio of variance to mean rate for binwidths of 0.5, 1, 2, 4 and 8 s.

To fit the secretion model, we used data from three independent data sets:

In Bicknell et al. (Bicknell *et al.,* 1984) and Bicknell (Bicknell, 1988), oxytocin release from isolated rat posterior pituitaries was measured by radioimmunoassay after:

- 20-min periods of 13 Hz stimulation
- 18, 36, 54 and 72-s periods at 13 Hz
- 156 pulses at 6.5, 13, 26 and 52 Hz

In Bondy et al. (Carolyn A. Bondy, 1987), rat posterior pituitaries were stimulated with 600 pulses at 1, 4, 8, 12, 20 and 30 Hz. The released oxytocin was measured by radioimmunoassay and normalized to release evoked by 600 pulses at 12 Hz.

Table 9. **Diffusion model parameter values.** The upper section gives values measured experimentally. The middle section gives parameter values used in the diffusion model. The bottom line shows model measurements from simulations of the experiments.

Parameter	Description	Normal rat	Kidneys or splanchnic clamped	Both clamped	Normal rat
	Experiments	(Fabian *et al.*, 1969*a*)			Ginsburg & Smith (1959)
	Plasma oxytocin half-life (s)	126	380	480	99
	Total fluid volume (ml)	18.25	37.5	35.75	No data
	Duration of oxytocin infusion (s)	1800	-	-	2
λ_{clr}	clearance half-life (s)	68	135	188	68
λ_{diff}	diffusion half-life (s)	61	-	-	-
C_{plasma}	plasma volume (ml)	8.5	-	-	-
C_{EVF}	Extravascular fluid volume (ml)	9.75	-	-	-
	Plasma oxytocin half-life (s)	126	379	479	91

To fit the diffusion model, we matched data from experiments in rats described by Fabian et al. (Fabian *et al.*, 1969*a*) and Ginsburg and Smith (Ginsburg & Smith, 1959), who measured plasma oxytocin by bioassays. Ginsburg and Smith reported that in male rats, a 440 ng/100 g bolus injection of oxytocin disappears from plasma with an apparent half-life of 1.65 ± 0.13 min (1.73 ± 0.1 min in female rats). Fabian *et al.* found that, after a constant 30 min infusion of oxytocin at rates between 550

and 13200 pg/min/100 g body weight, plasma oxytocin concentrations fell to 50% of the initial value in a median time of 126 s, and continuously infused oxytocin was distributed in an apparent volume of 7.3 ml/100 g body weight. Assuming a plasma volume of 3.4 ml/100g body weight, we calculate a plasma compartment, C_{plasma} = 8.5 ml for a 250 g rat, and an extravascular fluid compartment C_{EVF} = 9.75 ml. Fabian *et al.* measured the peak concentrations just before they stopped their infusions (Table 9). Ginsburg and Smith measured the peak value 1 min after the injection of 440 ng/100 g oxytocin in male rats (average 46 ng/ml). Finally, we mimic the clearance found in rats with the kidneys or the splanchnic area clamped and with both areas clamped (Table 9 and Table 10).

To fit the combined model, which includes the spiking, secretion and diffusion, we used four sets of plasma measurements of oxytocin from independent experiments in which rats were given an i.v. injection of CCK.

- conscious virgin female rats, in which blood samples were taken before and after i.v. injection of 20 µg/kg CCK (Leng *et al.,* 1997).
- conscious male rats in which blood samples taken before and after i.v. injection of 10 µg/kg CCK (McCann *et al.,* 1989).
- two groups of anaesthetized female rats, in which blood samples were taken before and after i.v. injection of 20 µg/kg CCK (Luckman *et al.,* 1993).

Table 10. Peak concentration for the two-compartment diffusion model.

	Oxytocin Infusion ng/100g/ml	**Peak concentrations (ng/ml)** (Fabian *et al.*, 1969*a*)	Model
Fabian *et al.* (1969*a*) **30 min infusion**	0.550	0.220	0.270
	3	-	1.447
	13.2	6.160	6.347

	Oxytocin injection ng/100g	**Peak concentration after 60 s (ng/ml)** Ginsburg & Smith (1959)	Model
Ginsburg & Smith (1959**) Injection**	440	45.32 (+/- 6.27)	43.48

Results

Reference data

We selected 23 recordings from oxytocin neurons that showed a fast and clear response to CCK and in which the firing rate subsequently returned to the initial level. The 23 cells had a mean (SD) spontaneous firing rate of 2.5 (0.39) spikes/s (range 0.02-7.9 spikes/s), measured as the average over 4-min before injection. The cells responded to i.v. injections of 20 µg/kg CCK with a mean increase of 1.46 (0.74) spikes/s (range 0.57-3.6 spikes/s), measured as the difference between the basal firing rate and the average over the 5-min after the injection (Figure 29.A). The decay of the mean response from 50 s after injection was well fitted by a single exponential equation with a half-life of 230 s (R^2 =0.88) (Figure 29.A).

Spiking model

For the spiking model we chose a basal mean PSP rate of 292/s (basal EPSP rate is equal to basal IPSP rate) to match the spontaneous firing rate of 2.5 spikes/s. After 5 min of basal activity, we simulated an injection of CCK as a linear increase in mean EPSP frequency over 20 s that declined exponentially to the basal EPSP rate with a half-life of 230 s. These values gave a close match to the average response profile of the reference set of oxytocin neurons to CCK (Figure 29.B). Figure 29.B shows the average of 23 runs of the spiking model. The variability of this average is less than the variability of the average of the reference data: the 23 model neurons are all identical and firing at the same mean rate, while the neurons in the reference data differed in intrinsic properties and mean firing rates.

The spiking model reproduces various statistical characteristics of single oxytocin cells (Figure 29.C). Thus, for the neuron shown in Figure 29, by modifying only the basal PSP rate (Table 7b), the model matches mean spike rate over the whole recording (Figure 29.C1), simulating the firing rate increment response as an increase in EPSP rate that modifies the oxytocin neuron spiking activity (Figure 29.C2). The model also matches well the interspike interval distribution (Figure 29.C3), and mimics the index of dispersion of the firing rate during the complete recording, which measures the variability of spike rate at different bin widths (Figure 29.C4).

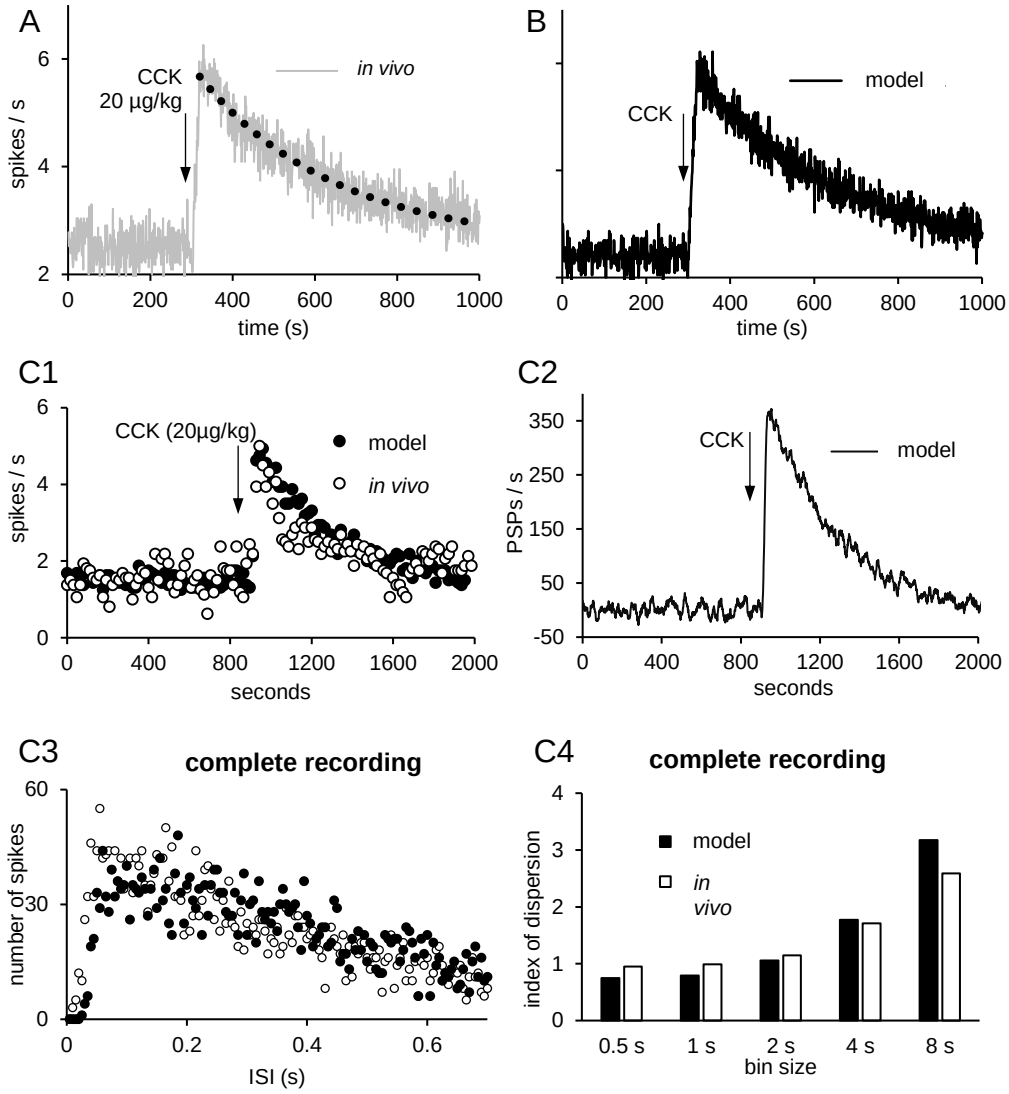

Figure 29. Responses of oxytocin neurons to CCK, and simulation in model cells. **A)** The average response (in 1-s bins) of 23 oxytocin neurons to i.v. injection of 20 µg/kg CCK. The response decays exponentially with a best-fit half-life of 230 s (dotted line). **B)** Response of a model oxytocin cell to a simulated challenge with CCK, simulated as an increase in PSP rate that decays exponentially with a half-life of 230 s, matching the measured half-life of CCK in plasma. The simulation was run 23 times with different random seeds, and the figure shows the average (see Tables 1&2 for model parameters). **C1)** A typical response to CCK from a single oxytocin cell (white dots). With a model cell (black dots) that has a HAP and an AHP it is possible to match this response closely. Parameter values for the model are in Table 1. **C2)** In this simulation, CCK increases the EPSP rate: the increase decays exponentially with a half-life of 230 ms. **C3)** The ISI distribution, constructed from the complete activity shown in C1, shows how often two consecutive spikes have a particular interval between them; the distribution from the model cell (black dots) closely matches that of the recorded cell (white dots). **C4)** The index of dispersion measures longer timescale spike patterning, showing how spike rate variability changes using different bin widths, again from the entire activity shown in C1). The model (black bars) closely matches the values measured in the recorded oxytocin neuron (white bars).

Secretion model

To model stimulus-secretion coupling, we modified the previously published vasopressin secretion model (MacGregor & Leng, 2013) to match data from three experiments where oxytocin secreted from isolated posterior pituitaries was measured. We mimicked these protocols in the spiking model, progressively adapting the secretion model to fit the oxytocin data by changing six parameter values (k_b, c_θ, e_θ, β, α and φ).

In the first of these experiments (Bicknell, 1988), 156 pulses at 6.5, 13, 26 and 52 Hz were applied to the posterior pituitaries (Figure 30.A1).

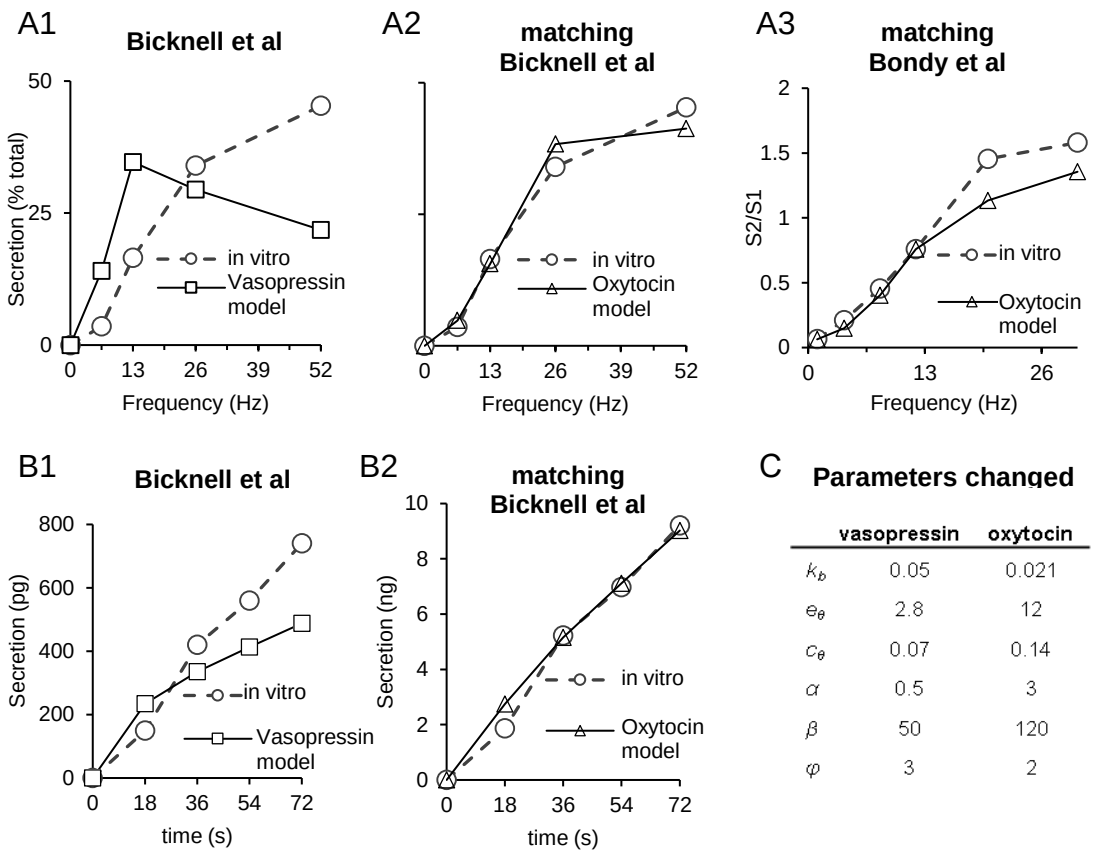

Figure 30. Oxytocin secretion model dynamics. Oxytocin secretion follows a non-linear function of the spiking activity. We adapted a previous model of vasopressin secretion (white squares) (MacGregor & Leng, 2013), modifying six parameter values to obtain our oxytocin model (white triangles). With those changes, we matched the oxytocin secretion from experiments (white circles). **A1)** In Bicknell's experiments (Bicknell, 1988), when posterior pituitaries were electrically stimulated with 156 pulses at 6.5, 13, 26 and 52 Hz, vasopressin secretion (white squares) was maximal at 13 Hz. By contrast, oxytocin secretion (white circles) continued to increase up to 52 Hz. **A2)** Matching the data from Bicknell (Bicknell, 1988) with the oxytocin model. **A3)** Using the same parameters, we also obtained a good match to data from Bondy et al. (Carolyn A. Bondy, 1987). In those experiments, glands were stimulated with 600 pulses at 1, 4, 8, 12, 20 and 30 Hz, and evoked secretion (S2) was

expressed as a ratio of S1, a reference secretion produced by a preceding stimulus at 12 Hz. **B1)** In Bicknell et al. (Bicknell et al., 1984), glands were stimulated at 13 Hz for 18-72 s: vasopressin secretion peaked during the first 18 s and showed subsequent fatigue (white squares), whereas oxytocin showed a consistent response (white circles). **B2)** We matched that response with the model using the same parameters as in A2) and A3). **C)** The six parameters changed from the model of vasopressin secretion (MacGregor & Leng, 2013).

The second source of experimental data (Carolyn A. Bondy, 1987) followed a similar protocol, this time stimulating with 600 pulses at 1, 4, 8, 12, 20 and 30 Hz (Figure 30.A3).

In the third set of data (Bicknell et al., 1984), isolated rat posterior pituitaries were stimulated *in vitro* at 13 Hz for 18, 36, 54 and 72 s in a randomised order (Figure 30.3B1). This third set of data are critical for estimating the temporal profile of secretion, and they showed that, unlike vasopressin secretion, which shows fatigue, oxytocin secretion is relatively stable over time in response to a constant frequency of stimulation. The modified model fits all three sets of data well (Figure 30.A2, A3, B2).

How the changes in model parameters were arrived at is illustrated in Figure 31. In the vasopressin model, the submembrane Ca^{2+} concentration (e), which has a direct role in exocytosis (equation *(30)*, displays fatigue at a firing rate of 13 spikes/s, and the rate of secretion declines during constant stimulation (Figure 31.A).

This is inconsistent with the experimental oxytocin data. In addition, vasopressin secretion per pulse declines at frequencies above 13 Hz, whereas oxytocin secretion is facilitated. Reducing the broadening of spikes k_b (Figure 31.B1) reduces secretion at low frequencies and increases secretion at high frequencies by reducing Ca^{2+}-induced inhibition of Ca^{2+} entry, and reduces but does not eliminate the fatigue. Increasing e_θ to weaken the Ca^{2+}-induced inhibition of Ca^{2+} entry enhances secretion, particularly at high frequencies (Figure 31.B2), but fatigue is much more prominent after this change. Raising c_θ, to reduce the sensitivity to cytosolic Ca^{2+}, reduces Ca^{2+}-induced inhibition of Ca^{2+} entry and so eliminates fatigue. Combining these three changes matched the frequency response (Figure 31.C). To match the slope of the temporal response to a constant frequency of 13 Hz, we also needed to change the exponent in the secretion equation, φ, from 3 in the vasopressin model to 2, indicating a smaller cooperative activation of exocytosis (Neher, 2012).

The constant factor α scales the output of the model quantitatively to measured oxytocin levels. In rats, milk-ejection bursts typically contain about 100 spikes over about 2 s and release about 1 mU (2.2 ng) of oxytocin (Wakerley & Lincoln, 1973). Setting $\alpha = 3$, the model simulates a release of ~2.27 ng in response to 2 s of stimulation at 50 spikes/s.

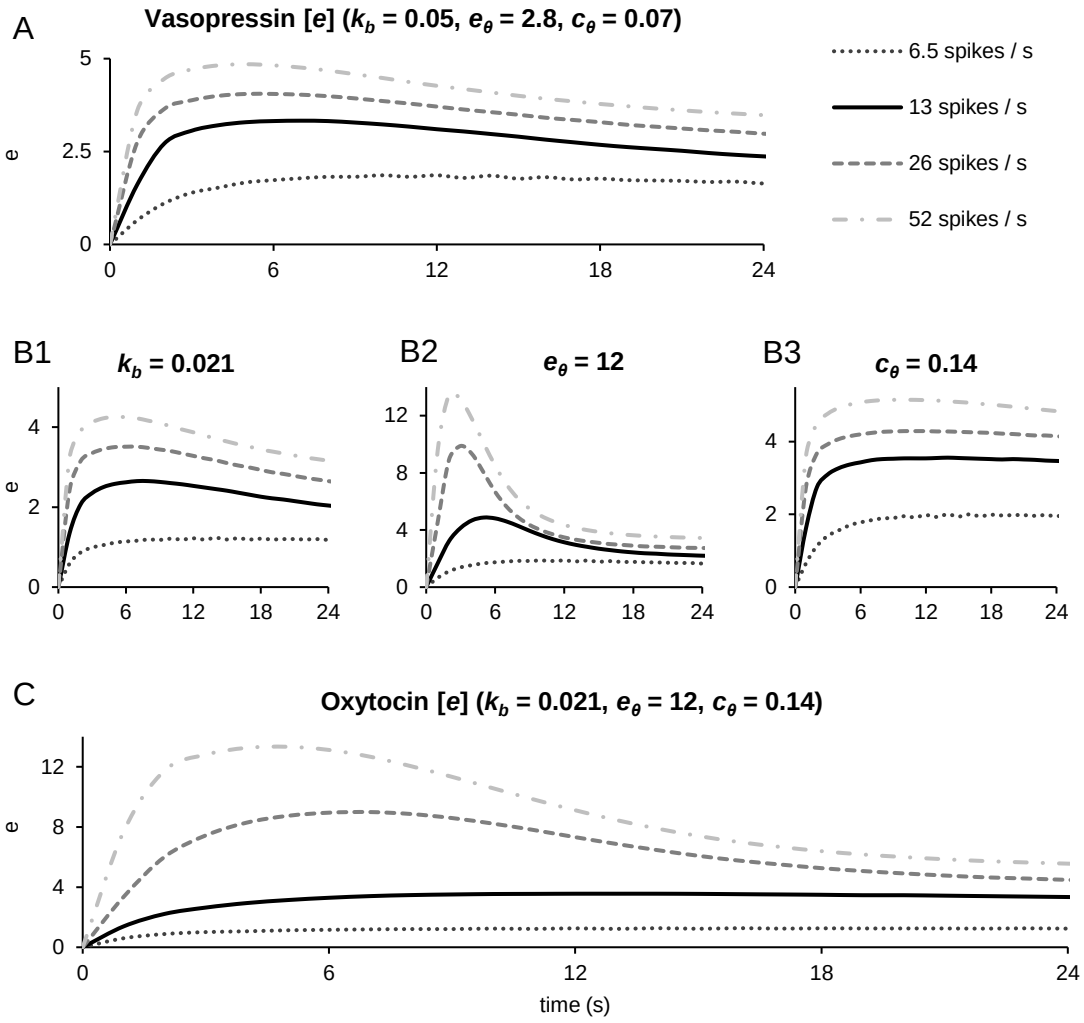

Figure 31. Transition from a vasopressin secretion model to an oxytocin secretion model. In both models, secretion is proportional to the submembrane Ca2+ concentration e. We show here how e changes during 24-s of stimulation at constant rates of 6.5, 13, 26 and 52 spikes/s. **A)** In the vasopressin model, for stimulations at 13, 26 and 52 spikes/s, e reaches a peak during the first 2 s of stimulation, followed by fatigue. Neither the fatigue, nor the early peak is present at 6.5 spikes/s. To obtain the frequency facilitation seen in Figure 30, we need to eliminate the fatigue at 13 spikes/s and increase the response at higher frequencies. **B1)** Decreasing k_b produces less saturation at high frequencies, increasing the difference between responses. **B2)** Increasing e_θ increases the peak response, especially at higher spike rates, but does not reduce the fatigue. **B3)** Increasing c_θ eliminates the fatigue but does not separate the responses to different stimulation frequencies. **C)** Combining these three changes reproduces the frequency-facilitation of secretion while eliminating fatigue at 13 spikes/s.

This increase necessitated an increase in the scaling factor for the pool refill rate, β, from 50 to 120.

Spiking plus secretion model

We used the combined model to explore how the spiking response to CCK varies with the dose of CCK and with the basal firing rate, and how that response affects secretion. We chose basal firing rates 1, 3 and 5 spikes/s, spanning the range in the reference data, and simulated CCK injections of 5, 10 and 20 µg/kg. Each combination was run 20 times (differing by the random differences in PSP arrival times) and the results were averaged. Each response was calculated as the difference between the average firing rate in the 25 s after the peak response and the basal firing rate (determined after allowing enough time for the model simulation to reach equilibrium of secretion). Comparing responses for the same CCK dose and different basal firing rates (Figure 32.A1), the response to CCK is largely independent of the basal firing rate in the range 1-7 spikes/s. At 20 µg/kg, where there is the biggest difference, the response from a basal firing rate of 1 spike/s (3.5 spikes/s) is 30% greater than that from a basal rate of 7 spikes/s (2.7 spikes/s).

This consistency in firing rate responses to a given dose of CCK is not present in the secretory response, similarly calculated as the difference between basal levels and evoked levels. At higher basal firing rates, the secretory response is much greater than from a basal firing rate of 1 spike/s for all doses of CCK (5, 10, 20 µg/kg; Figure 32.A2). The relationship between EPSP rate and firing rate in the oxytocin cell model is approximately linear over the range modelled here (7) so the firing rate increment in response to CCK is relatively independent of basal firing rate. However, the frequency dependence of stimulus-secretion coupling makes the secretory response to CCK non-linearly dependent on the absolute firing rate achieved in response to CCK. Hence the secretory response to CCK depends on both the basal firing rate and the dose of CCK.

The influence of the AHP was examined by comparing the response of the model with and without an AHP (i.e. setting $k_{AHP} = 0$) for a CCK injection of 20 µg/kg. With an AHP, the spiking response to CCK (about 4 spikes/s at peak; Figure 32.B1) is much less than without an AHP (about 11 spikes/s; Figure 32.B2). In the presence of an AHP, the profile of secretion follows that of spike activity smoothly (Figure 32.B3).

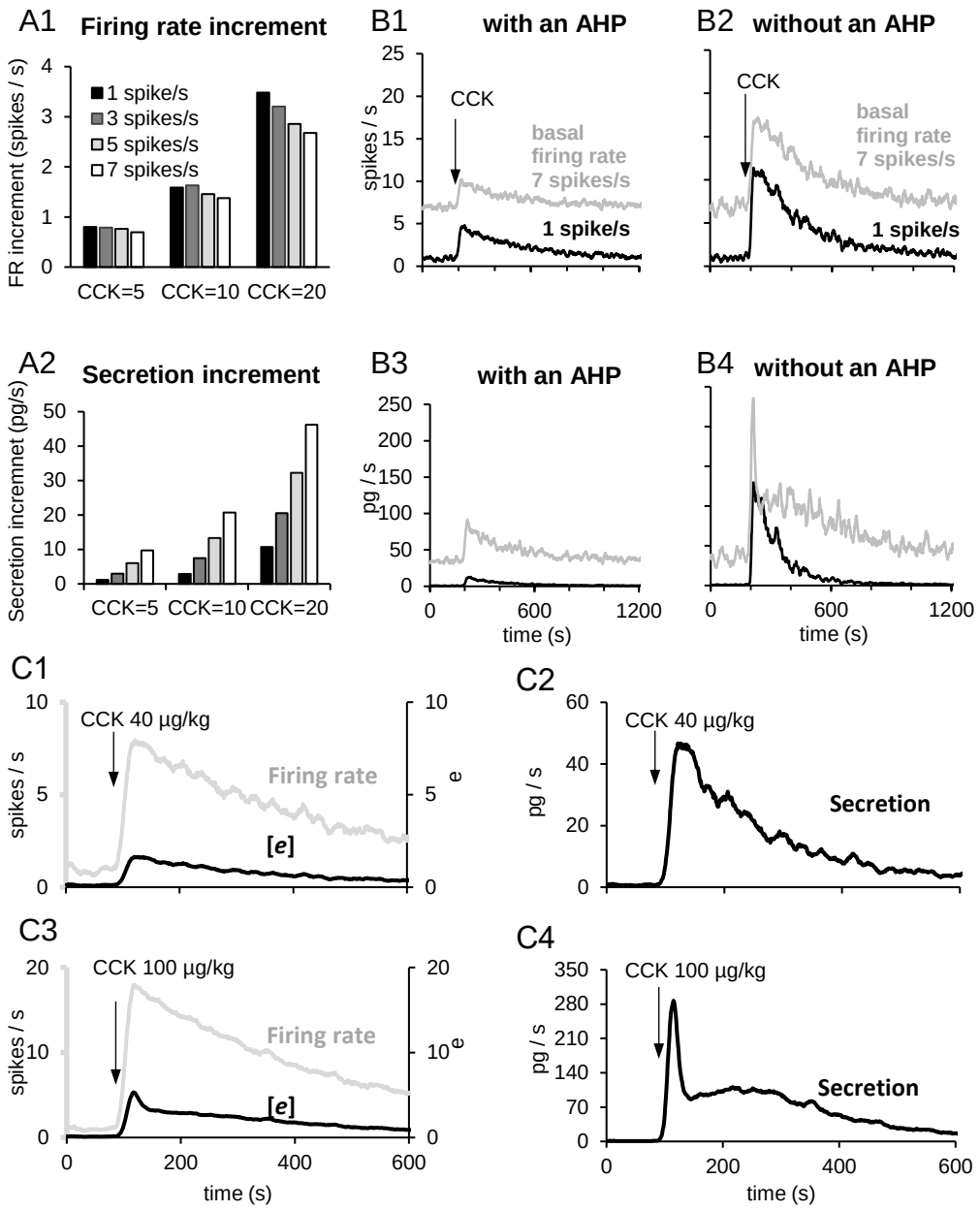

Figure 32. **Oxytocin spiking and secretion response to CCK**. **A1)** Model oxytocin neurons respond to CCK by increasing their spike activity independently of the basal firing rate. The graph shows the increments in spike activity of a model cell responding to simulated challenges with different amounts of CCK (5, 10 and 20 µg/kg), from different basal firing rates (1, 3, 5 and 7 spikes/s). The same model neuron was tested 20 times, receiving random PSPs with the same average rate of 165, 348 583 and 895 PSPs/s. **A2)** In the same simulations as in A1, the secretion response depends on the basal firing rate. **B1)** Large differences in basal firing rate (1 spike/s in black, 7 spikes/s in grey) do not drastically change the firing rate response to CCK. **B2)** The same simulations as in B1 but in a model cell without an AHP. The presence of an AHP greatly reduces the response to CCK. **B3,4)** Secretion corresponding to the simulations in B1,2. The evoked secretion is strongly affected by the basal firing rate due to the non-linearity of the secretion response. In B4, the secretory response to CCK in a model cell with a basal firing rate of 7 spikes/s and no AHP shows a marked initial peak. **C1)** When a model cell firing at 1 spike/s is challenged with a large CCK injection (40 µg/kg), the firing rate response closely follows the change in the model variable e. **C2)** The secretory response to the challenge

illustrated in c1. **C3)** In response to a still larger challenge (100 µg/kg CCK), the firing rate response has a similar shape as in C1). However, e follows an acute initial increment that is not maintained, due to the negative feedback provoked by [Ca^{2+}]. **C4)** Due to those changes in e, amplified because secretion is proportional to e^2, oxytocin secretion follows the biphasic pattern observed in B4.

By contrast, without an AHP, when the basal firing rate is 7 spikes/s, the initial high level of secretion evoked by CCK rises sharply from 40 pg/s to 235 pg/s in response to CCK, but decreases abruptly to 110 pg/s within 20 s before declining more smoothly (Figure 32.B4). To understand this behaviour, we simulated a similarly large spike response in the presence of an AHP. From a basal firing rate of 1 spike/s, a simulated CCK injection of 40 µg/kg evoked a response of 8 spikes/s (Figure 32.C1), and was accompanied by a smooth secretory response (Figure 32.C2).

A larger CCK injection (100 µg/kg) evoked a response of 18 spikes/s (Figure 32.C3), and the accompanying secretory response rose sharply and decreased abruptly (Figure 32.C4), as observed in the model without an AHP (Figure 32.B4). This feature is because of the fatigue associated with Ca^{2+}-induced inhibition of Ca^{2+} entry (Figure 32.C1, C3), which becomes noticeable only above firing rates of 13 spikes/s. Thus, in the model, an abrupt pulse of oxytocin secretion can arise at the onset of a sustained increase in activity to a level exceeding 10 spikes/s.

The diffusion model

To model the oxytocin concentration in plasma, we simulated experiments that measured the half-life of oxytocin in plasma and its apparent volume of distribution following i.v. infusions of oxytocin in normal rats and in rats where the blood supply to the kidneys and/or the splanchnic was clamped (Figure 33.A). We created a two-compartment model where oxytocin secretion first enters a plasma compartment with volume C_{plasma} = 8.5 ml from which it is cleared, and from which it diffuses to an extravascular compartment of volume C_{EVF} = 9.75 ml (

Figure **28**); these volumes are as estimated by Fabian *et al.* (1969a). We chose a diffusion half-life (λ_{diff} = 61s) compatible with the diffusion of NaCl between plasma and extravascular fluid (Leng et al., 2001). With those parameters, we matched the experimental data from continuous infusion studies (Fabian *et al.*, 1969*a*) with a clearance half-life λ_{clr} = 68 s (Table 9). Using the same parameter values, we can

also match the observed oxytocin clearance after a bolus injection of oxytocin (Ginsburg & Smith, 1959) (Figure 33.B).

Spiking, secretion and diffusion models combined

Combining the spiking, the secretion and the diffusion models, we tried to match the plasma oxytocin concentration measured in experiments where CCK was injected in rats. In the first experiment (Leng *et al.,* 1997), 23 rats were injected with 20 µg/kg CCK. In the second, seven rats were injected with 10 µg/kg CCK (McCann *et al.,* 1989). Lastly, two groups of 39 and 25 rats were injected with 20 µg/kg CCK (Luckman *et al.,* 1993). In all cases, oxytocin was measured by radioimmunoassay, but in the first, third and fourth cases, the assay used was that of Higuchi *et al*. (Higuchi *et al.,* 1985) and oxytocin was measured in unextracted plasma. The second set of data measured oxytocin after plasma extraction using a different antibody.

We matched the first set of data (Figure 33.C1) by simulating a basal firing rate of 2.4 spikes/s, increasing the EPSP rate after 5 min with a simulated injection of 20 µg/kg CCK (i.e. by the amount determined by the fits of the spiking model to neuronal responses to CCK; Figure 29). In the second set of data, the oxytocin concentration did not return to the original baseline level after the CCK injection, and we simulated a basal firing rate of 0.8 spikes/s that fit the final oxytocin concentration, not the initial concentration (Figure 33.C2). In the third set of data, we simulated a basal firing rate of 1.7 spikes/s to match the average of initial and final oxytocin concentrations (Figure 33.C3) and in the final set, we matched initial and final oxytocin concentrations with a basal firing rate of 0.9 spikes/s (Figure 33.C4). For each set of data, there is a close match to the oxytocin concentrations measured in the 15 min after CCK injection.

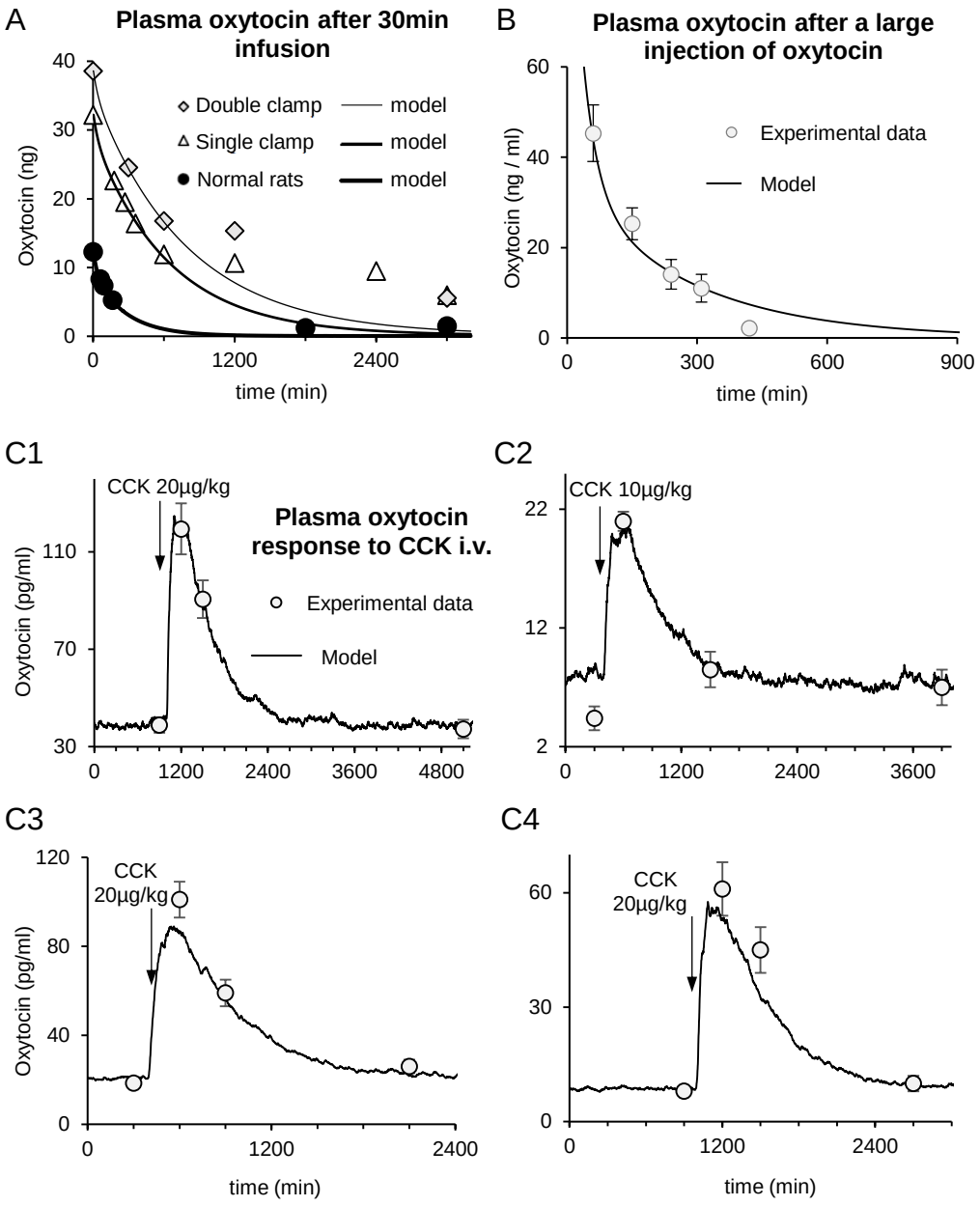

Figure 33. **Two-compartment diffusion model and plasma oxytocin response to CCK.** We calibrated our two-compartment diffusion model with data from two i.v. oxytocin protocols: after a long infusion and after a bolus injection. We then simulated the plasma oxytocin response to CCK to compare with four experimental datasets. **A)** Oxytocin clearance after 30-min infusion of 3 ng/100g body weight/min oxytocin. Black dots, white triangles and light grey diamonds show the plasma oxytocin measured (Fabian *et al.*, 1969*a*) in normal rats (black circles), rats with the kidneys or the splanchnic area clamped (grey triangles) and rats with both set of organs clamped (grey squares). Thick, normal, and thin black lines are the model results following simulations of the same protocol. The parameter values are given in Table 3. **B)** Mean (SE) plasma oxytocin after bolus (2-s) injection of 440 µg/100g of oxytocin (Ginsburg & Smith, 1959), white dots), matched (black line) by a model with the same parameter values as used in a). **C)** Adding the diffusion model to the spiking and secretion models (solid lines), we can match the CCK experimental response in plasma (open circles with SE shown) from four data sets by changing the basal PSP rate to match the first experimental point, and emulating the

amount of CCK injected. **C1)** Data from 23 conscious female rats injected with 20 µg/kg CCK (Leng et al., 1997). **C2)** Data from 5-10 conscious male rats given 10 µg/kg CCK (McCann et al., 1989). **C3)** and **C4)** Anesthetized female rats injected with 20 µg/kg CCK from (Luckman et al., 1993). Modelled data are shifted by 60 s in C1 to C4, assuming that the CCK injections were given slowly. The other model parameters are as obtained to match the spiking response to CCK (Table 1).

The role of the AHP

As shown previously (Maícas-Royo *et al.*, 2016), the AHP "smooths" the firing rate of oxytocin cells reducing its variability, and it reduces the amplitude of the response to CCK (Figure 34.A). As we predicted, the AHP has an even bigger effect in reducing the variability (SD) of basal oxytocin secretion (Figure 34.B) and basal oxytocin concentrations (Figure 34.C).

We went on to study why this reduction in variability might be important. We used the model to mimic the same firing rate response to a simulated challenge with and without an AHP. We ran the model with an AHP 20 times (randomising the PSP arrival times) to produce an average basal firing rate of 1.5 spikes/s, and simulated the response to 10 µg/kg CCK. Then, we ran the model without an AHP, adjusting the mean PSP rate to produce the same average basal firing rate, and challenged it with a simulated injection of 5 µg/kg CCK to evoke a similar firing rate response. Although the firing rate responses to CCK are similar in magnitude, they differ in variability.

To illustrate how this reduction in variability helps to distinguish between different levels of mean activity, we ran the model with and without an AHP for 20 min at mean firing rates of 1, 4, and 7 spikes/s. The modelled secretion varies according to the history of activity and secretion, so we plotted the actual firing rate in each 6-s bin against the secretion in that bin (Figure 35.E-F). In the model with an AHP, the rates of secretion are consistently separated (Figure 35.E), but in the model without an AHP they overlap substantially (Figure 35.F).

Finally, we considered how the AHP affects the reliability of the signal from a single oxytocin neuron. We ran the model with and without an AHP, as a single neuron firing on average at 1, 3 and 7 spikes/s. We calculated what increase in EPSP rate in each condition would raise the mean firing rate by 1 spike/s on average.

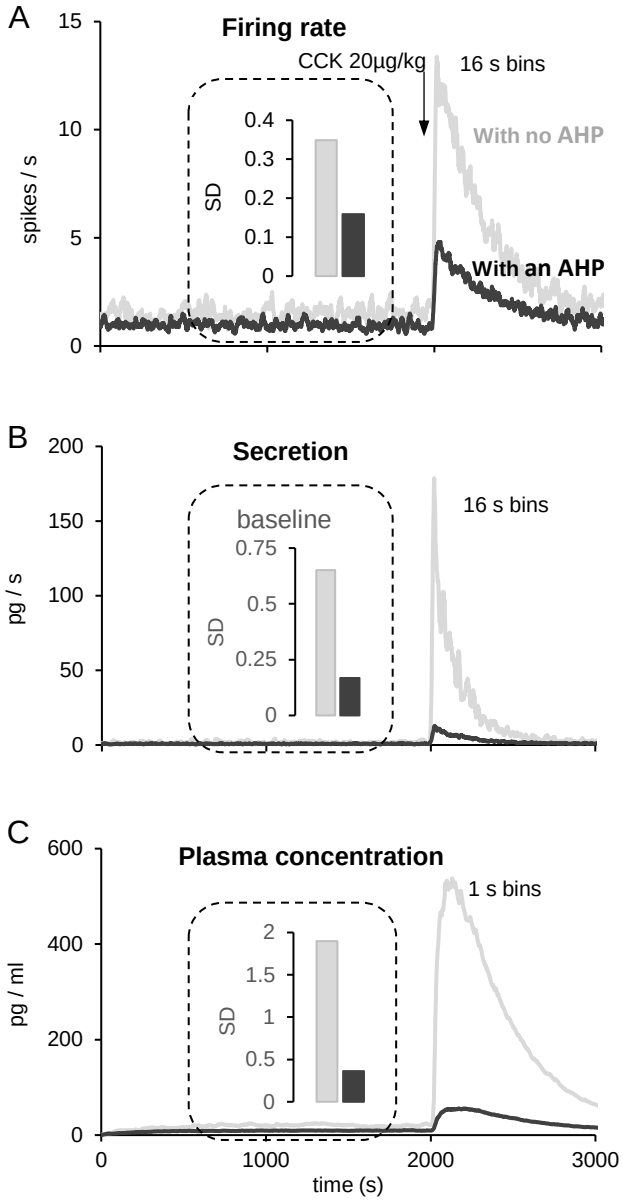

Figure 34. The effect of the AHP. The AHP affects the baseline behaviour and the response to CCK (20 µg/kg i.v.) in the spike rate (A), secretion (B) and plasma concentration (C). SD: standard deviation during the 1200-s period before CCK injection. **A)** The model was set to produce a basal mean firing rate of 1 spike/s, which increased to 4.9 spikes/s after CCK (black). Removing the AHP (grey), but keeping the same initial PSP rate, produces a slightly higher basal firing rate and a much greater response to CCK. The basal firing rate, measured between 800 and 2000 s, is less variable with an AHP than without it as apparent from the SD (bars). **B)** Secretion is a non-linear function of the firing rate. When there is a fast change in firing rate, the non-linearity provokes a very much larger secretory response in a model without an AHP. The basal secretion rate is much less variable with an AHP than without it. **C)** Without an AHP, the plasma oxytocin concentration increases hugely in response to CCK injection. Before CCK, the basal oxytocin concentration in plasma is much less variable with an AHP than without it.

We then tested the model with a pattern of EPSPs that alternated between the higher (challenge) and lower (basal) level, for different durations (1-50 s), and for a total run of 100 min (Figure 36), and compared the modelled total secretion during each challenge episode with that in the preceding basal episode. If the secretion during the challenge episode did not exceed that during the corresponding basal episode, we registered this as a “detection error”, and counted the number of such errors in each trial.

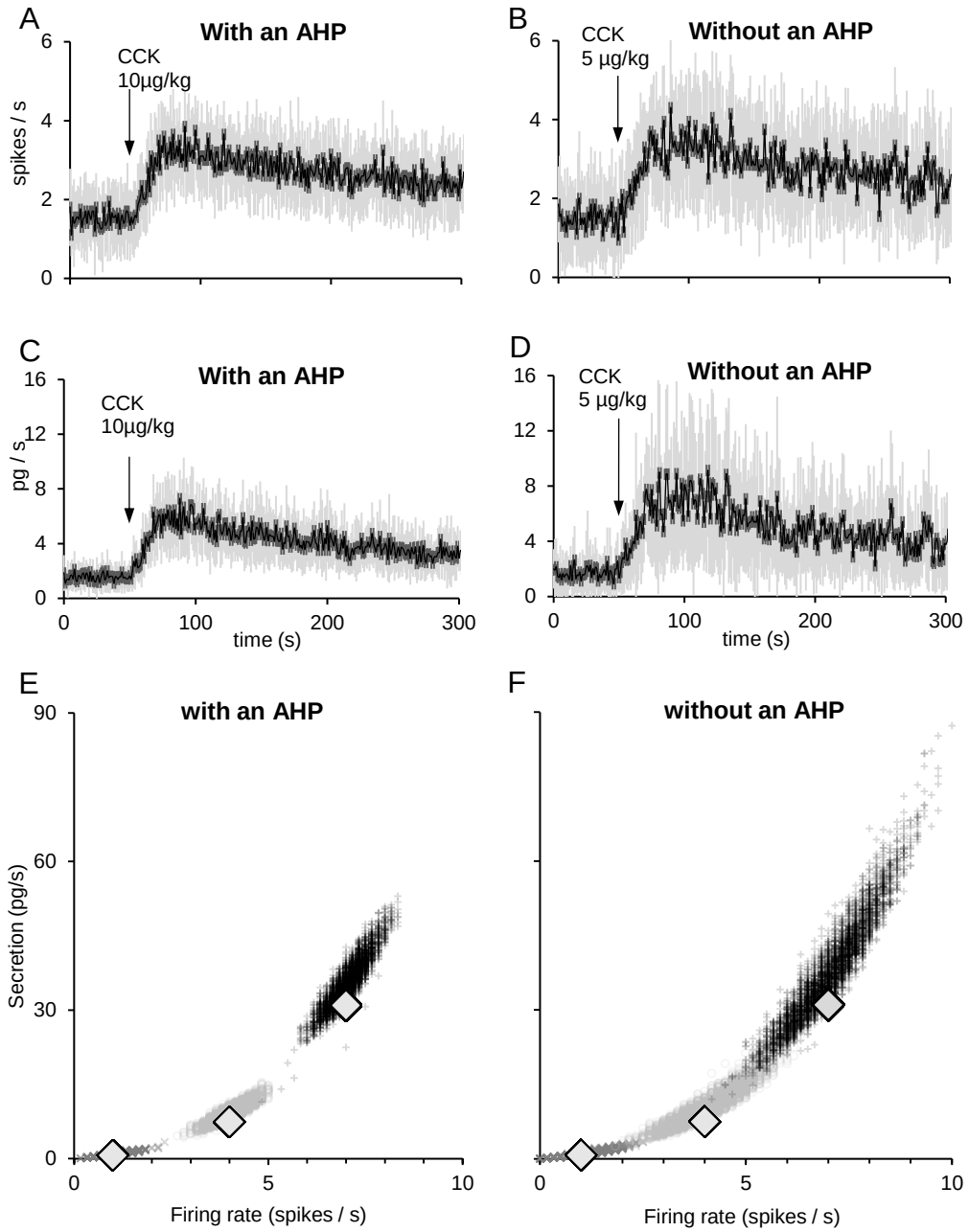

Figure 35. The role of the AHP in signal response. (A-B) Average firing rate of 20 runs of the same model cell. We compare average spiking and secretion responses to CCK when there is an AHP in the model (A and C) and when there is not (B and D). Means are in black and SD in grey. **A)** Modelling a basal firing rate of 1.5 spikes/s with a PSP rate of 210/s and an AHP. In response to a simulated injection of 10 µg/kg, the model cell responds with an increment of ~ 2 spikes/s. b) To obtain a similar average response without an AHP, we reduced the PSP rate to 165/s and the CCK injection to 5 µg/kg. Although the mean responses are similar, the SD (grey) is much larger without an AHP. **C)** and **D)**. Secretion rates accompanying the firing rate simulations in A) and B). Secretion shows an even bigger difference in variability without an AHP due to the non-linearity between secretion and firing rate. **E)** Another way to see the role of the AHP is to look at oxytocin secretion in 4-s intervals in response to PSPs at a constant mean rate. In models with and without an AHP, PSP rates were chosen to produce mean firing rates of 1, 4 and 7 spikes/s (large diamonds). Because of the randomness of PSP arrival times, the firing rate varies from interval to interval around these means, and this variability is

greater without an AHP. This variability is amplified by the non-linearity of stimulus-secretion coupling. The dot clouds represent the firing rates in 6-s intervals and the concurrent secretion during 1200s when the modelled neuron produces average firing rates of 1 (dark grey crosses), 4 (grey circles) and 7 spikes/s (black pluses). In a model with an AHP, the firing rates and secretion measured in every interval both consistently distinguish the three levels of PSP rate. **F)** In a model without an AHP, there is extensive overlap.

The error rate is consistently much higher without an AHP: for example, at 3 spikes/s, 1-s challenge episodes are not detected in 37% of trials of a neuron without an AHP, but in only 20% of trials of a neuron with an AHP (Figure 36.C-D).

With an AHP, the mean (SD) second-by second coefficient of variation of firing rate (SD/mean) in the 20 runs for the 50 s before CCK plus the 300 s after is 0.43 (0.11) (Figure 35.A), compared to 0.60 (0.13) for the model without an AHP (Figure 35.B). For secretion: the corresponding coefficient of variation is 0.54 (0.12) in the model with an AHP (Figure 35.C), compared to 0.81 (0.17) in the model without an AHP (Figure 35.D).

Heterogeneity in basal firing rate and response to CCK

In the reference data, the basal firing rate and the response to CCK are both heterogeneous: the mean SD of the basal firing rate (in 1-s bins) was 2.34, close to the SD = 2 reported previously for oxytocin neuron firing rates (Sabatier *et al.*, 2004). This increased to 2.84 over the 5 min after injection of CCK, also consistent with previous data (Velmurugan *et al.*, 2010). To evaluate how that heterogeneity affects secretion, we ran the model with the recorded spike times of those 23 neurons, obtaining the predicted secretion and its mean SD (Figure 37.A).

In Figure 29, we simulated the average response of those 23 neurons using 23 runs of a single model neuron with randomised input arrival times at the same mean rate. This gives a much lower SD of firing rate (Figure 37.B1). Moreover, although the averaged modelled secretion was close to the predicted *in vivo* secretion (Figure 37.B1), the mean basal secretion (3.34) is much lower than the predicted mean basal secretion (7.11). That leads to an overestimate of the predicted basal firing rate when fitting the model to plasma oxytocin measurements, as we did in Fig 6c. The SD of the secretion rate was also much lower.

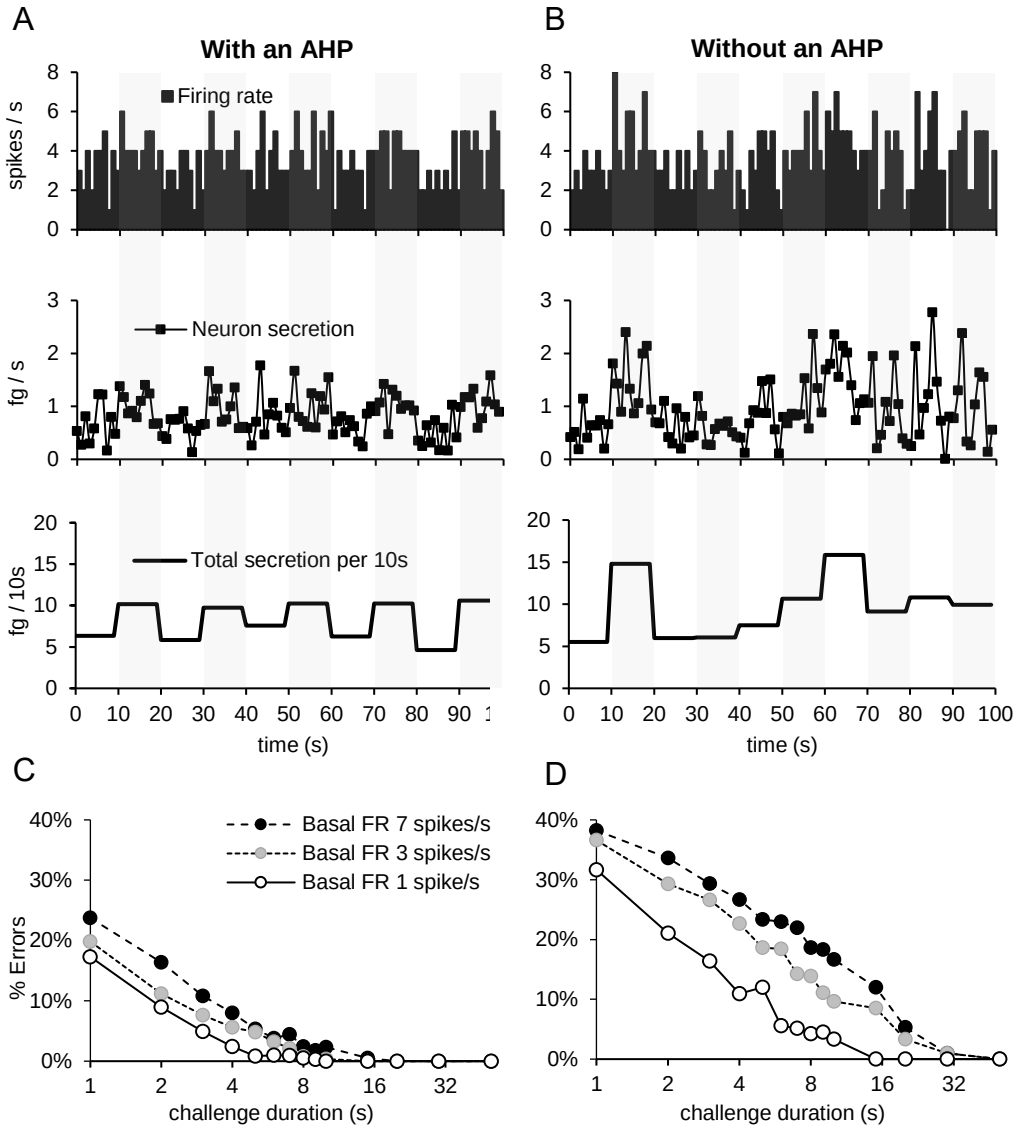

Figure 36. The role of the AHP in the detection of a transient signal. A) We ran the model as a single neuron with a mean basal firing rate (FR) of 1, 3 and 7 spikes/s. By modifying the EPSP rate, we raised the firing rate by an average of 1 spike/s for a 10-s challenge episode every 20 s for 100 min. The graphs plot the model outputs (firing rate, secretion per second and secretion per 10-s) for a model neuron firing at 3 spikes/s for the first 100 s of the simulation. **B)** as in A) but for a model with no AHP. Note that in A), episodes of greater EPSP rate are consistently associated with greater secretion (as measured in 10-s bins), but this is not true of a model with no AHP. **C)-D)** Similar experiments to those in A) and B) were performed to assess challenge episodes of different duration (1, 3, 5, 10, 15, 30 and 50 s). **C)** Shows the percentage of errors for a neuron firing at a basal firing rate of 1, 3 and 7 spikes/s when there is an AHP. **D)** Same but without an AHP. In all cases, there is a much smaller error rate when there is an AHP.

Therefore, we introduced heterogeneity in our model by simulating a population of 23 neurons with independently generated values for PSP rate (I_{re} and I_{ri} sampled from a lognormal distribution with mean (SD) = 292 (292), see Table 11) to closely match both the average firing rate of the reference neurons and the SD of their basal firing rate (Figure 37.B2). However, the SD of the firing rate of the heterogeneous model cells did not change after CCK (2.23 at basal level and 2.24 after CCK). Consequently, the secretion rate is similar to the predicted secretion from the reference neurons at the baseline, but does not reach the predicted levels of CCK response.

We therefore also introduced heterogeneity to the CCK response by simulating a lognormally distributed k_{CCK} of mean (SD) = 20 (20). With that change, the match to the firing rate was still good and the SD of the basal firing rate (2.21) and the SD during the 5 min after CCK (2.93) were close to the reference data (Figure 37.B3). In addition, the model mimicked the predicted *in vivo* secretion closely in both average and SD (see Table 11 for the parameter values of the 23 neurons).

To study the impact of the AHP, we made the AHP = 0 and, in the model without heterogeneity we reduced the basal PSP rate from 292 to 203.5 and k_{CCK} from 20 to 7 to match the mean firing rate of the reference data (Figure 37.C1). The resulting SD of the firing rate was 1.33 at the basal level and 1.71 after CCK (Figure 37.C1). The secretion still matched the predicted *in vivo* reference data but not the SD. We then introduced heterogeneity by varying the PSP rate (lognormal distribution with mean (SD) = 203.5 (203.5)) and k_{CCK} (lognormal distribution with mean (SD) = 7 (7)). This gave a raised mean basal firing rate of 3.06 spikes/s, and a mean response magnitude of 1.2 spikes/s over the 5 min after CCK (Figure 37.C2). The firing rate SD was 4.27 at basal and 4.9 after CCK, much higher than in the reference data. The close match to predicted secretion was lost (see Table 5 for the parameter values of the 23 neurons without an AHP). Thus a close match to both the mean and the variability of the reference data (Figure 37.A) was obtained by modelling a population of neurons matching the heterogeneity of those data using a model with an AHP, but not by using a model without an AHP.

Table 11. Spiking parameter values to simulate heterogeneity in an oxytocin neuron population as shown in Figure 37.

	With an AHP						Without an AHP			
Neuron	Model		Random basal firing rate		Random basal FR and CCK response		Model		Random basal FR and CCK response	
	I_{re} & I_{ri}	k_{CCK}	I_{re} & I_{ri}	k_{CCK}	I_{re} & I_{ri}	k_{CCK}	I_{re} & I_{ri}	k_{CCK}	I_{re} & I_{ri}	k_{CCK}
1	292	20	112	20	112	13.9	203,5	7	71	16.1
2			63		63	7.5			322	3.7
3			68		68	5.6			101	2.5
4			92		92	55.3			490	1.7
5			180		180	18.0			71	5.2
6			74		74	12.0			292	6.1
7			278		278	8.2			208	5.1
8			488		488	5.5			85	8.0
9			203		203	8.0			43	6.5
10			69		69	8.7			335	5.4
11			237		237	10.5			587	12.3
12			279		279	16.8			104	3.8
13			411		411	41.0			622	1.1
14			156		156	14.0			114	13.2
15			494		494	23.4			83	25.5
16			383		383	41.7			63	3.9
17			218		218	35.1			240	4.0
18			699		699	2.3			36	3.5
19			204		204	27.3			410	12.7
20			1026		1026	20.6			104	3.2
21			67		67	15.8			127	5.0
22			335		335	38.9			129	10.8
23			574		574	37.2			45	2.0
Average			291.7		291.7	20.3			203.7	7.0

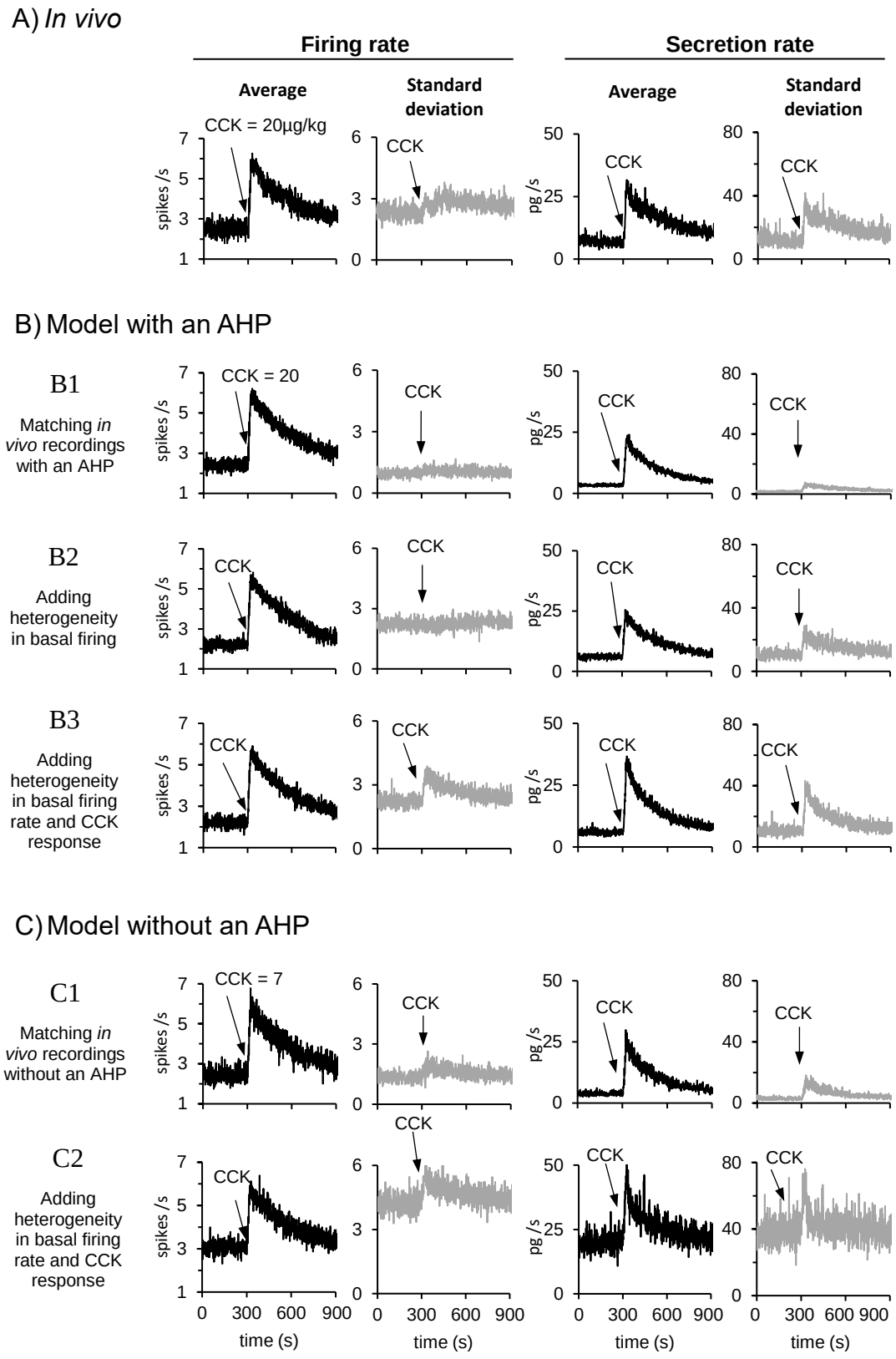

Figure 37. Heterogeneity in oxytocin spiking activity and response to CCK. From left to right, each set of panels shows the average firing rate of the 23 neurons (in 1-s bins), the SD of the firing rate, the predicted *in vivo* secretion (in 1-s bins), and the SD of the predicted secretion **A)** shows data from the 23 reference neurones. **B1)** Averages of 23 runs of the

model with random PSP arrival times at a fixed PSP rate. The SD of the basal firing rate is much smaller than in a, and does not increase after CCK. The basal secretion is lower than in a but the increment after CCK (~20 pg/s) is similar. The SD in the model is also much lower than in a. **B2)** To simulate heterogeneity in oxytocin neurons, we varied the basal PSP rate using a lognormal distribution. The heterogeneity elevates the SD to the level in a, but the SD still does not increase after CCK. The secretion is close to that in a. **B3)** Adding heterogeneity to the response to CCK gives a very close match to all panels in a. **C1)** In 23 homogeneous model cells without an AHP, a match to the mean firing rates of the reference neurons is obtained by reducing the basal PSP rate and kCCK. The SD of the firing rate is lower than in a but higher than in B1. The basal secretion and the SD of secretion are lower than in a. **C2)** Adding heterogeneity to the model without an AHP produced a higher basal firing rate and smaller response to CCK, but greatly increased the SD of the firing rate and the secretion rate to levels much higher than in a. Thus, a close match to both the mean and the variability of the reference data (A) was obtained by modelling a population of neurons matching the heterogeneity of those data using a model with an AHP, but not by using a model without an AHP. The parameter changes used for the simulations shown are given in Table 11.

Discussion

In the present study, we used a previously published integrate-and-fire based model of oxytocin neuron activity. We have shown elsewhere that this model is closely consistent with a Hodgkin-Huxley type model that represents the AHP and HAP in a biophysically meaningful way consistent with experimental data from *in vitro* experiments (Leng *et al.*, 2017). Real oxytocin neurons vary in their intrinsic properties, in their basal firing rates, and in their responsiveness to CCK. In the present study, we began by considering the population of oxytocin neurons as identical, differing in their behaviour only as a result of differences in the random arrival times of PSPs. The model neurons are however ‘typical’ of real oxytocin neurons, and we simulated a response to CCK that matches the average response of real neurons to CCK. We did so by the minimalist assumption that the mean rate at which EPSPs arrive is proportional to the CCK concentration in plasma, which decays exponentially to zero after bolus injection. The decay of plasma CCK estimated in the present study from the recordings of oxytocin cells (230 s) is close to the half-life of CCK measured in human plasma (about 4 min) (Jebbink et al., 1990).

To this spiking model, we added a model of stimulus-secretion coupling adapted from a model used previously to model stimulus-secretion coupling in vasopressin neurons. We adapted that model to match four sets of published data on oxytocin secretion from isolated posterior pituitaries.

The model expresses the rate of oxytocin secretion from a single neuron as a continuous variable. This understates the variability of secretion from a single cell. Oxytocin is secreted in discrete packets – vesicles that each contain about 85,000 molecules of oxytocin - and the rate at which these vesicles are secreted from a single cell at baseline is low – about 1-4/s (Leng & Ludwig, 2008). A more accurate model would represent secretion as a stochastic process, not as a continuous deterministic process. In the context of the present model, we can better understand the variable (*s*), described here as representing the rate of secretion, as rather reflecting the instantaneous probability of vesicle exocytosis. However, as we are using this model to simulate the total secretion from the population, it seemed reasonable to accept a continuous representation of secretion as approximating the average of many stochastic processes.

The secretion model is a highly simplified representation of mechanisms in the nerve terminals. The terminals express a variety of Ca^{2+} channels (Lemos *et al.*, 2012) and there is evidence that Ca^{2+} release from intracellular stores also has a role (McNally *et al.*, 2014). Exocytosis is also modulated by activity-dependent secretion of several modulators, including ATP (Knott *et al.*, 2008), adenosine (Knott *et al.*, 2007) and endogenous opioids (Brown *et al.*, 2000; Velázquez-Marrero *et al.*, 2010). The terminals do not contain clearly separate pools of readily-releasable and reserve vesicles, but rather a heterogeneous population differing in releasability (Seward *et al.*, 1995). Other mechanisms also affect stimulus-secretion coupling, including changes in axonal excitability that result from activity-dependent changes in extracellular potassium concentration (Dyball *et al.*, 1988; Dyball & McKenzie1, 2000). In this study our purpose was not to construct a detailed model of all of the mechanisms that contribute to stimulus-secretion coupling, but rather to produce a minimalist model that by matching available data on stimulus-secretion coupling would enable us to predict secretion from spiking activity (Gainer *et al.*, 1986; Nowycky *et al.*, 1998; Dyball & McKenzie1, 2000; Marrero & Lemos, 2003).

Combining the spiking model with this secretion model allowed us to model the activity-dependent output of oxytocin cells. To relate this to measurements of secretion *in vivo,* we needed to scale the output of the model by choosing an appropriate value for the scaling factor α. The *in vitro* measurements used to fit the model report variable absolute levels of oxytocin secretion; in these experiments glands are impaled on stimulating electrodes, and exactly where the glands are

impaled will determine what proportion of the axons are stimulated, and there will be variable damage to axons. Stripping neural lobes from the adjacent intermediate lobe reduces the volume of tissue impaled and makes it more likely that the tissue is effectively stimulated, but entails greater tissue damage. In such experiments (Bicknell et al., 1983), 6 min of stimulation at 13 Hz released up to 9 ng oxytocin. Matching this with the secretion model suggests a value of α = 1.5 as a lower bound of plausible values. Wakerley and Lincoln (Wakerley & Lincoln, 1973) estimated stimulus-evoked release in lactating rats by stimulating the neural stalk and comparing the resultant increase in intramammary pressure with that evoked by i.v. injections of oxytocin: they estimated that about 1 mU was released by 4 s of stimulation at 50 Hz, consistent with α = 2. However, the response to stimulation *in vivo* varies with the precise placement of the electrode and with the stimulus current used. There is one circumstance, which does not involve that uncertainty. In the anesthetised lactating rat, suckling evokes intermittent milk-ejection bursts in oxytocin neurons which typically contain between 50 and 100 spikes and which last for about 2 s. These bursts produce an abrupt rise in intramammary pressure that can be mimicked by i.v. injection of 0.5 - I mU oxytocin (1.1 - 2.2 ng). The release of 2.2 ng oxytocin by 2 s of stimulation at 50 Hz in the model is closely approximated by a value of α = 3, which was chosen for subsequent tests of the model.

To predict the consequences of oxytocin secretion for plasma concentrations, we also needed to model the clearance of oxytocin. Early studies in the rat studied clearance in two ways: by infusing oxytocin continuously and measuring the achieved concentration at equilibrium and the decline after stopping infusion (Fabian *et al.*, 1969*a*), and by injecting large amounts as a bolus and measuring the decline (Ginsburg & Smith, 1959). In the former case, experiments studied the mechanisms of clearance by clamping vessels to the kidneys and splanchnic area. These two sets of data could mostly be well matched by a two-compartment model, except that, in data from rats with venous clamps, oxytocin concentrations remained elevated above predicted levels in a way that (Fabian *et al.*, 1969*a*) proposed arose from a time and surgery-dependent increase in the apparent distribution volume. This, we did not attempt to mimic in the model.

Having selected a value for α, and with a validated model for plasma clearance of oxytocin, we could use the model to predict the changes in plasma concentration that result from the response of oxytocin neurons to CCK. For this, we had four sets

of data in which oxytocin was measured in different conditions (conscious and anaesthetised rats, male and female rats) at two different doses of CCK and using two different radioimmunoassays.

Matching the initial basal level of secretion in these data implied differences in the basal firing rates of oxytocin neurons in the four conditions. The mean basal firing rates inferred from the model were 2.4 spikes/s for conscious female rats (Figure 33.C1), 0.8 spikes/s for conscious male rats (Figure 33.C2), and 1.7 spikes/s and 0.9 spikes/s for urethane-anaesthetised female rats (Figure 33.C3-4). These are lower than the basal firing rates recorded from the supraoptic nucleus of urethane-anaesthetised virgin female rats which are generally about 2.5 spikes/s (Bhumbra & Dyball, 2004; Sabatier *et al.*, 2004), but this difference is as expected, given that the electrophysiological recordings are from rats in which the hypothalamus has been exposed by transpharyngeal surgery. The trauma and blood loss entailed in this surgery increases the basal activity of both oxytocin and vasopressin neurons. Across these four sets of data there is good agreement between model predictions of the response to CCK and experimentally measured levels.

We went on to use the model to investigate the role of the AHP. This activity-dependent potential, which is pronounced after high frequency spiking, is important in shaping the profile of milk-ejection bursts (Rossoni *et al.*, 2008). However, the AHP is also active at low basal firing rates, and it both restrains basal activity and reduces the variability of firing rate (Maícas-Royo *et al.*, 2016). Secretion is coupled non-linearly to firing rate, and as a result, variability of firing rate produces an amplified variability of secretion.

The extent of this variability is illustrated in Figure 35, which shows that for an oxytocin neuron firing at 7 spikes/s, the secretion in 6-s bins is very variable, but is always distinct from the secretion resulting from a firing rate of 4 spikes/s. However, for a neuron without an AHP there is considerable overlap: the mean spike rate cannot be reliably estimated from the secretion measured in a given 6-s bin. This variability is of little consequence to plasma levels in the rat: oxytocin in plasma has a half-life of about a minute, and levels reflect the activity of about 9000 neurons. However, for smaller animals, such variability may be more problematic. In zebrafish for example, the ortholog of oxytocin, isotocin, is expressed in only a few tens of neurons (Herget *et al.,* 2017).

In mammals, small subsets of magnocellular neurons project to diverse sites in the brain, and at these sites, stability of oxytocin secretion rates might also be important. We have shown (Figure 36) that even changes in spike activity that have large functional consequences (1 spike/s) cannot be consistently detected as changes in secretion from a single neuron unless secretion is averaged over many seconds. Without an AHP, only the average secretion over 30 s will consistently reveal a rise in mean firing rate. Thus, the output of a single oxytocin neuron is a very noisy reflection of the signal that determines the mean level of its afferent inputs, but the presence of an AHP markedly enhances its signal detection ability. This may be important for a small population of neurons, including for the small subsets of oxytocin neurons that project to various forebrain sites, but is much less important for the large population that projects to the pituitary.

An important consideration in inferring physiological significance to the behaviour of a single neuron is how population heterogeneity may temper those inferences. Oxytocin neurons are certainly heterogeneous – in their basal firing rates, in their responsiveness to physiological stimuli, and in their intrinsic membrane properties including those that determine the HAP and the AHP. Here we simulated some of this heterogeneity by running our single neuron model with varied synaptic input rates, and by introducing variability into the simulated CCK challenge. The activity dependence of the AHP means that it has a stronger inhibitory effect on more active neurons, pulling them closer to the mean firing rate. Thus, as well as reducing signal variability within single neurons, the AHP reduces the variability of firing rate of a heterogeneous population (Figure 37), with an even larger effect on the variability of secretion rate because of the non-linear coupling of firing rate to secretion.

A full appreciation of the effects of heterogeneity is beyond the scope of the present paper. It remains to be determined how variability in intrinsic properties interacts with variability in input rates, and how variability in the population signal affects secretion might depend on assumptions about the independence of input signals. Each oxytocin neuron receives many synaptic inputs, and it is likely that these are from overlapping subsets of a larger pre-synaptic population, resulting in many neurons receiving the same input noise. There is extensive data already in the literature on both the electrophysiological responses of oxytocin neurons to different stimuli and on associated plasma oxytocin responses, giving a potentially rich source of material to test and refine the present model.

Acknowledgements

This project has received funding from the European Union's Seventh Framework Programme for research, technological development and demonstration under grant agreement n 607310.

Conclusions to the second paper

This paper took time. At least two years of work before we were happy with it. It involves three models, connected but also independent: spiking, secretion and plasma dynamics. Thus, the test results on one of them were always affecting the others. If one parameter value was changed in the spiking activity, every test for every model had to be run again. Due to the amount of experimental data we were trying to mimic, that happened many times.

In the end, it was worth the effort. The computational model mimicked remarkably well the experimental data. Sometimes the results were so good that it looked like we were fitting the model for every experiment to get a perfect match. However, the only thing we were changing was the basal firing rate and the amount of CCK injected, according to the experimental data.

That robustness and accuracy matching different experiment results, legitimates the second part of the work, where we showed the role of the AHP and heterogeneity in secretion and plasma oxytocin.

In addition, it gave us a powerful tool to explore the role of magnocellular oxytocin neurones in other physiological processes: osmotic pressure and hypovolemia.

Chapter 5 (paper):

Lamina terminalis, oxytocin neurons and the rat osmotic homeostasis. A computational model.

Introduction to the third paper

Maícas Royo J, Leng G & MacGregor DJ (2019). The spiking and secretory activity of oxytocin neurones in response to osmotic stimulation: a computational model. *The Journal of Physiology*;

This chapter is presented in a paper format because it has been accepted and published. I am first author, with my supervisors Gareth Leng and Duncan MacGregor as the other two co-authors. As we submitted the manuscript to the *Journal of Physiology*, there is a different notation than in the rest of the thesis. When expressing units in formulas or in the text, units in the quotient are expressed as $^{-1}$. For instance, spikes s^{-1} is written instead of spikes/s.

In this chapter/paper it is shown how the oxytocin model described in the previous chapter is used to mimic experimental data related with the role of oxytocin in the regulation of osmotic pressure and hypovolemia.

We focused on those topics because the response of oxytocin neurones to them has been described extensively in the literature, while, at the same time, it is not clear what is the exact origin and nature of the inputs that oxytocin neurones respond to in those circumstances.

The model was used as described in the previous papers, only changing the basal firing rate and the ratio between excitatory and inhibitory postsynaptic potentials, which are key to interpret the inputs that oxytocin neurones receive from osmoreceptors in the circumventricular organs. As I was mimicking experiments where the rats had different weights, I introduced that variable in our model.

I also present a new model that is an attempt to mimic the Na^+ dynamics in the rat, as the oxytocin neurones seem to respond linearly to that concentration.

The model simulates populations of up to 100 neurones, programmed by parallel computing. Importantly, heterogeneity is also present in this last version of the model. The models allow us to introduce heterogeneity in multiple parameters but I have been focusing on the inputs that every neuron has, reflecting their individual firing rate.

As in the previous papers, I developed the models, ran all the tests, fitted the parameters manually by trial and error and wrote the manuscript. As in the previous papers, my supervisors helped me with the writing by patiently correcting my drafts to improve the English.

Introduction

Oxytocin neurones are large, multifunctional, multisensory neurones in the hypothalamus that subserve a variety of important physiological functions. The great majority of these neurones project an axon to the posterior lobe of the pituitary and some of these have axon collaterals that sparsely innervate diverse forebrain regions. At the pituitary, they secrete oxytocin into the systemic circulation, regulated by action potentials (spikes) propagated in their axons, but they can also release large amounts of oxytocin into the hypothalamus from their dendrites. Dendritic release is semi-independent of spike activity: it can be triggered by peptides that induce intracellular calcium release as well as by voltage-gated calcium entry triggered by spikes (Ludwig, 1998). The coupling of spike activity to dendritic release is plastic: it depends on the availability of dendritic vesicles for spike-dependent release, and this is regulated by peptide actions at the dendrites. Accordingly, central (dendritic) and peripheral (axonal) release of oxytocin are regulated differentially and differently in different physiological states (Ludwig & Leng, 2006).

Oxytocin secretion is essential for milk let-down in lactation and is an important though not essential regulator of the progress of parturition in mammals (Higuchi *et al.,* 1985; Russell & Leng, 1998). At term pregnancy, in response to signals from the contracting uterus; and in lactation, in response to the suckling of young, oxytocin neurones discharge in quasi-synchronous intermittent bursts that lead to pulsatile secretion of oxytocin. The approximate synchrony arises from dendro-dendritic interactions involving oxytocin release (Perlmutter *et al.,* 1984), and it occurs in conditions when dendritic stores of oxytocin have been primed to be available for spike-dependent release (Rossoni *et al.*, 2008). However, at other times, and in the absence of these specific stimuli, oxytocin neurones fire independently and do not show bursting activity. At these times, spike activity primarily governs axonal release, mainly secretion from the pituitary (Ludwig & Leng, 2006).

In rodents and in some but not all other mammals (Rasmussen *et al.*, 2003, 2004), oxytocin is regulated by plasma osmotic pressure and blood volume to control sodium excretion at the kidneys (Zimmerman *et al.,* 2017), and by a wide range of signals that regulate appetite and energy expenditure (Leng & Sabatier, 2017). In response to these stimuli, oxytocin cells fire continuously and proportionately to the challenge, leading to sustained increases in plasma oxytocin concentration.

We now have a good understanding of the intrinsic properties of oxytocin neurones that underlie their spiking activity from electrophysiological studies *in vitro* (e.g. Hatton & Li, 1999; Pittman *et al.,* 1999; Armstrong *et al.*, 2010; Brown *et al.,* 2013). Spikes in these neurones arise from perturbations in membrane potential evoked by synaptic inputs that produce excitatory and inhibitory post-synaptic potentials (EPSPs and IPSPs). When a spike is triggered, a hyperpolarising afterpotential (HAP) is evoked that imposes a relative refractory period of typically about 30 ms. Spikes also evoke a small but long lasting afterhyperpolarisation (AHP) that is the result of Ca^{2+}-activated K^{+} conductances. These two spike-dependent changes in excitability account for the spontaneous spiking activity of most oxytocin neurones *in vivo* (Richard *et al.*, 1997; Leng *et al.*, 1999; Hatton & Wang, 2008; Brown *et al.*, 2013), as indicated by the excellent fit to recorded patterns of spike activity that can be achieved with a Hodgkin-Huxley type model of the oxytocin neurone stimulated by a randomly arriving mixture of simulated EPSPs and IPSPs (Leng *et al.,* 2017). This model in turn can be well approximated by a leaky integrate-and-fire single neurone model adapted to include a simulated HAP and AHP (Maícas-Royo *et al.*, 2016). The stimulus-secretion properties of the neurosecretory terminals have also been well characterised (Bicknell *et al.,* 1984; Bicknell, 1988). Stimulus-secretion coupling is highly non-linear, but the features of this can also be modelled in a way that matches experimental data closely (MacGregor & Leng, 2013). Finally, the clearance of oxytocin from the blood has been extensively characterised (Ginsburg & Smith, 1959; Fabian *et al.*, 1969*a*; Leng & Sabatier, 2016) .

We have recently described a model linking oxytocin neurone properties to spike activity, spike activity to secretion, and secretion to the dynamics of oxytocin in plasma (Maícas-Royo *et al.,* 2018). This model gives a close quantitative match to the behaviour of oxytocin neurones in response to an appetite-related challenge (systemic injection of the gut hormone cholecystokinin) and to the ensuing changes in plasma oxytocin concentration. In that work, we used experimental data to fit the

model. Here we have *tested* this combined model. To do so we needed independent data comprising measurements of oxytocin neurone spiking activity and measurements of plasma oxytocin concentration.

The greatest abundance of such data in the published literature comes from studies of the osmotic responsiveness of oxytocin neurones. These neurones respond to increases in plasma osmotic pressure partly as a result of intrinsic osmosensitivity, but also as a result of increased afferent input arising directly and indirectly from osmoreceptors in other forebrain regions (Bourque, 2008; Zimmerman *et al.,* 2017). Specifically, osmosensitive neurones in the subfornical organ and organum vasculosum of the lamina terminalis (OVLT) project directly to the oxytocin (and vasopressin) neurones of the supraoptic and paraventricular nuclei, and also indirectly via the nucleus medianus (Prager-Khoutorsky & Bourque, 2015; Choe *et al.*, 2016). It appears that the osmotically regulated input involves a direct excitatory glutamatergic component, but also an inhibitory component, as osmotic stimuli result in increases in both GABA and glutamate release in the supraoptic nucleus as measured by microdialysis *in vivo*. In earlier modelling work, we showed that the combined presence of EPSPs and IPSPs in the osmotically regulated input linearises the response of the oxytocin neurones and extends their dynamic range (Leng *et al*., 2001).

Using these data to test the combined model presented a fresh challenge. The published experiments used a variety of experimental protocols: some measured activity and secretion in conditions of chronic challenge (Wakerley *et al.,* 1978; Verbalis *et al.,* 1986; Stricker *et al.,* 1987; Verbalis & Dohanics, 1991), others used an acute (Higuchi *et al.*, 1988) or a slow intravenous sodium load (Leng et al., 2001), others again an acute i.p. injection of hypertonic saline (Brimble & Dyball, 1977). To make full use of the data we had to first model the experimental challenges themselves. We did so by assuming that oxytocin cells increase their activity as a consequence of changes in $[Na^+]$ in the extracellular environment of osmoreceptive neurones, and that this results in an increase in EPSP and IPSP rate that is linearly proportional to $[Na^+]$. We therefore had to infer the dynamic profile of changes in local $[Na^+]$ arising in the different experimental circumstances from available data on plasma $[Na^+]$ and osmotic pressure. We neglected the intrinsic osmosensitivity of oxytocin neurones (Prager-Khoutorsky & Bourque, 2015), but this simplification has no substantial consequence as in the model the effects of a small

direct depolarisation that is linearly proportional to osmotic pressure is very similar to that of an increase in mean EPSP rate.

Given this model of the experimental challenges, we show here that the previously published model of the oxytocin system appears to be fully quantitatively predictive. From spike activity, the changes in plasma oxytocin concentration can be reliably inferred and vice versa. We also show how the model can give predictive insight into features of physiological behaviour, in particular by revealing a likely mechanism by which hypovolemia alters the gain of osmoresponsiveness.

Methods

We used our previous models for the spiking (Maícas-Royo *et al.*, 2016), secretion, and plasma oxytocin dynamics (Maícas-Royo *et al.*, 2018), adding a new model to mimic how osmotic pressure changes due to either intra ventricular (i.v.) or intra peritoneal (i.p.) NaCl injection or infusion, and how that osmotic pressure is encoded as an input signal to the spiking model. The models were developed using software written in C++ with a graphical interface based in the open-source wxWidgets library. The software is able to simulate a population of oxytocin neurons by running multiple threads in parallel, summing individual neurons' secretion output to drive a single thread running the plasma oxytocin model. Population simulations were run with 100 neurones for up to 10,000 s, using a 1-ms step size. A single run simulating 10,000s of activity of 100 neurones responding to a hyperosmotic infusion takes 60 s, running on a quad core Intel i7-2600K at 3.40 GHz processor.

Post synaptic potentials

The integrate-and-fire based spiking model (Maícas-Royo *et al.*, 2016) simulates the firing activity of oxytocin cells in response to excitatory and inhibitory postsynaptic potentials (EPSPs and IPSPs). We model PSPs as exponentially decaying perturbations to the membrane voltage V, arriving at Poisson random intervals at mean rates I_{re} and I_{ri}. Thus, the time elapsed since the previous EPSP, e_{time}, is defined:

$$e_{time} = \frac{-\log(1 - N_{rand})}{I_{re}}$$

where N_{rand} is a uniform random between 0 and 1. IPSP arrival times, i_{time}, follow the same formula.

The osmotic model alters the PSPs

In our new model, both I_{re} and I_{ri} can be modified by changes in osmotic pressure. We simulated the effect of an injection or infusion of NaCl, either i.v. or i.p., by a multi-compartment model, representing the amount of Na^+ in plasma (Na_p), in the extravascular fluid (Na_{EVF}), the EVF volume ($Vol_{EVF(Na)}$) and the ICF volume (Vol_{ICF}). Na^+ has a larger EVF volume of distribution than oxytocin ($Vol_{EVF(oxy)}$), but the plasma volume (Vol_p) is the same for both oxytocin and Na+. The EVF volume of distribution for oxytocin is as calculated in our previous work (Maícas-Royo *et al.,* 2018). Depending on differences in [Na^+], Na^+ diffuses between plasma and the EVF compartment. At the same time, water diffuses between the EVF and the ICF to maintain osmotic equilibrium, shifting the EVF and ICF volumes (Figure 38). Plasma volume is given a fixed value, dependent only on body weight.

Table 12. **Top) Parameters of the integrate-and-fire spiking model**, with parameter values chosen from (Maícas-Royo et al., 2018) **Bottom)**. Parameters to fit the osmotic model. In subsequent simulations, $\boldsymbol{I_{re}}$ varied to produce different basal firing rates as appropriate; I_{ratio} was varied to simulate the experiments where IPSPs were reduced; the other parameters were unchanged from the upper table.

Name	Description	Value	Units
$I_{reBasal}$	Basal excitatory input rate	292	Hz
I_{ratio}	Ratio between IPSP and EPSP	0.75	
e_h	EPSP amplitude	2	mV
i_h	IPSP amplitude	-2	mV
λ_{syn}	PSP half-life	3.5	ms
k_{HAP}	HAP amplitude per spike	30	mV
λ_{HAP}	HAP half-life	7.5	ms
k_{AHP}	AHP amplitude per spike	1	mV
λ_{AHP}	AHP half-life	350	ms
V_{rest}	resting potential	-56	mV
V_{thresh}	spike threshold potential	-50	mV
$\lambda_{i.p.}$	Na^+ half-life after i.p. injection	1150	s
$\lambda_{i.v.}$	Na^+ half-life after i.v. injection	190	s
λ_w	membrane crossing half-life of water	0.43	s

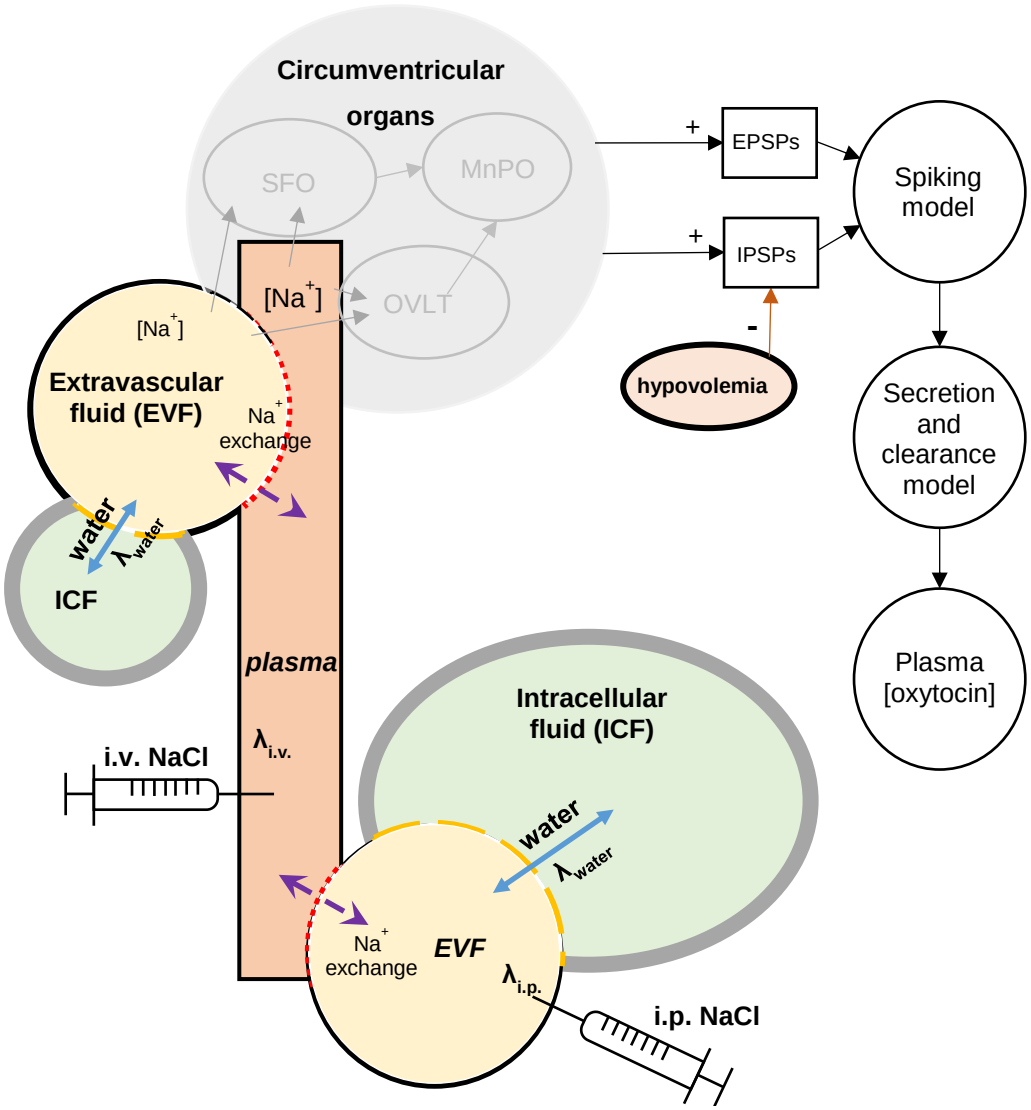

Figure 38. Schematic model. The spiking, secretion and clearance models for oxytocin neurons (Maícas Royo et al., 2016; Maícas-Royo et al., 2018), incorporate here the ability to respond to osmotic or volumetric pressure. Modelled changes in osmotic pressure are mimicked by simulating the injection or infusion of intravenous (i.v.) or intra peritoneal (i.p.) hypertonic solutions of NaCl. A [Na^+] rise close to the circumventricular areas provokes an increment in the PSPs the oxytocin neurones receive from the circumventricular organs. When NaCl is injected i.p. to the extra vascular fluid (EVF), Na^+ diffuses to plasma and water moves by osmosis from the intra cellular fluid (ICF) to the EVF, to maintain the same osmolality in every compartment. When NaCL is injected i.v. or once Na^+ has diffused from the body's EVF, Na^+ diffuses to a small EVF compartment in contact with the brain's circumventricular organs. The model does not simulate what happens in the circumventricular organs. It considers them as a black box which produces a combination of excitatory and inhibitory post synaptic potentials (EPSPs and IPSPs) in response to changes in osmolality or volume pressure. Volume pressure is simulated by changing the amount of IPSPs coming from the circumventricular organs and by reducing the plasma volume and increasing the EVF volume associated with the [oxytocin].

An injection or infusion of NaCl is modelled first by setting its duration (T_{NaCl}) and its quantity (k_{NaCl}) in mM. The quotient gives the rate of the injection ($R_{i.v.} = k_{NaCl} / T_{NaCl}^{-}$). Second, the model distinguishes between i.v. and i.p. by assigning different entrance compartments. The compartment receiving the NaCl is the plasma in the case of i.v. infusions and the EVF in the case of i.p. injection, having different diffusion half-lives, $\lambda_{i.v.}$ of 190 s and $\lambda_{i.p.}$ of 1150 s, to take into account how long it takes for Na^+ to diffuse to the final EVF compartment (not explicitly modelled) where the circumventricular organs' neurons sense changes in extracellular [Na^+]. Thus, in the case of an i.v. injection:

$$\frac{dNa_p}{dt} = R_{i.v.} \cdot \delta_{i.v.} - \frac{G_d}{\tau_{i.v.}}$$

Where $\delta_{i.v.} = 1$ if $T_{iv} \leq t \leq T_{iv} + T_{NaCl}$, otherwise $\delta_{i.v.} = 0$.

Time constants are calculated from half-life parameters using:

$$\tau_x = \frac{\ln(2)}{\lambda_x}$$

The Na^+ diffusion gradient, G_d, is defined as:

$$G_d = [Na]_p - [Na]_{EVF}$$

Where [Na^+] in plasma, $[Na]_p$, is calculated as:

$$[Na]_p = {Na_p}\Big/{(Vol_P \cdot MW_{Na})}$$

MW_{Na} is the molar weight of Na^+, 22.9898 g mol^{-1}. The $[Na]_{EVF}$ follows a similar relationship:

$$[Na]_{EVF} = {Na_{EVF}}\Big/{(Vol_{EVF(Na)} \cdot MW_{Na})}$$

Where Na_{EVF} varies as:

$$\frac{dNa_{EVF}}{dt} = \frac{G_d}{\tau_{i.v.}}$$

In the case of i.p. infusion or injection:

$$\frac{dNa_{EVF}}{dt} = R_{i.p.} \cdot \delta_{i.p.} - \frac{G_d}{\tau_{i.p.}}$$

Where $\delta_{i.p.} = 1$ if $T_{ip} \leq t \leq T_{ip} + T_{NaCl}$, otherwise $\delta_{i.p.} = 0$ and:

$$\frac{dNa_p}{dt} = \frac{G_d}{\tau_{i.v.}}$$

The initial volumes for the different compartments, plasma, EVF and ICF, depend on the body weight of the rat, *B*, but not on its sex (Sheng & Huggins, 1979). Following Sheng & Huggins, we fixed the total amount of water as 60% of body weight. Of that 60%, two thirds is in the ICF and the rest in the EVF and plasma. In our previous work, we used a plasma volume, Vol_p, of 8.5ml in rats of 250g. (Maícas-Royo *et al.*, 2018). We maintain that proportion in this work. Thus, initially:

$$Vol_{ICF} = 0.6 \cdot B \cdot 0.67$$

$$Vol_p = 8.5 \cdot \frac{B}{250}$$

$$Vol_{EVF(Na)} = (0.6 \cdot B \cdot 0.33) - Vol_p$$

Table 13. Volume distributions depending of the rat's weight for the different experiments simulated.

Name	%	Rat #1	Rat #2	Rat #3	Rat #4
Body Weight (g)	100 %	190	250	300	350
Total Body Fluid (ml)	60 %	114	150	180	210
Plasma (ml)	3.4 %	6.46	8.5	10.2	11.9
$EVF_{(oxy)}$ (ml)	3.9 %	7.41	9.75	11.7	13.65
$EVF_{(Na+)}$ (ml)	16.4 %	31.16	41	49.2	57.4
ICF (ml)	40.2%	76.38	105	120.6	140.7

When the model simulates injection or infusion of NaCl, the plasma volume remains invariant, but the EVF and ICF volumes change as $[Na^+]$ in the EVF changes. The model simulates the fast osmotic movement of water through cell membranes between the EVF and the ICF (Sidel & Solomon, 1957), with a half-life λ_{osmo} = 0.43 s. The water movement follows the gradient, G_w, between the current $[Na^+]$ in the EVF and the averaged $[Na^+]$ in the EVF during the previous 2 s, $[Na]_{EVF\text{-}2s}$. That averaged value allows the model to buffer water osmotic passage between the ICF and the EVF, avoiding instability in the model:

$$G_w = ([Na]_{EVF} - [Na]_{EVF-2s})$$

$$\frac{dVol_{EVF(Na)}}{dt} = Vol_{EVF(Na)} + \frac{G_w}{\tau_{osm}}$$

$$\frac{dVol_{ICF}}{dt} = Vol_{ICF} - \frac{G_w}{\tau_{osm}}$$

Osmotic signal to the spiking model

An increased extracellular $[Na^+]$ generates an increase in osmotic pressure, which is sensed by osmosensitive neurons of the circumventricular organs. These send excitatory and inhibitory synaptic signals to the oxytocin neurones. To simulate this input signal we added a new input component to the spiking model, using a linear relationship between PSP rate due to the osmotic pressure, I_{osmo}, and the osmotic pressure (*OP*):

$$I_{osmo} = 44 \cdot (OP - 310)$$

The gradient (44) and the baseline (310) were fitted based on experimental data showing a linear increase in spike rate in response to increasing osmotic pressure,

described in detail below. Osmoreceptors in the circumventricular organs sense both the ventricular EVF and the plasma that vascularizes some walls of the ventricles. We calculate *OP* as $(2 \cdot [Na]_p)$, if the NaCl injection is i.p. or $(2 \cdot [Na]_{EVF})$, if the injection is i.v., assuming that diffusion from the entrance compartment to the second Na^+ compartment implicitly includes diffusion to the cerebroventricular EVF compartment.

The rates of EPSPs and IPSPs arriving at the oxytocin cells are defined by a combination of osmotically dependent and non-osmotically dependant PSPs. In the case of EPSPs:

$$I_{re} = I_{reBasal} + I_{osmo}$$

Where $I_{reBasal}$ is the PSP rate of non-osmosensitive inputs. The IPSP rate is a function of the EPSP rate:

$$I_{ri} = I_{ratioBasal} \cdot I_{reBasal} + I_{ratioOsmo} \cdot I_{osmo}$$

where $I_{ratioBasal}$ and $I_{ratioOsmo}$ can be modified independently to separately affect osmotically or not osmotically IPSPs, taking by default the same value, I_{ratio} = 0.75.

Spiking model

The rest of the model is exactly as described in our previous work (Maícas-Royo *et al.*, 2018). We fix the PSP magnitudes, e_h and i_h, at 2 mV, having opposite sign for EPSPs and IPSPs. At each time step (fixed at 1 ms in our simulations) the number of PSPs, e_n and i_n, arriving at random intervals e_{time} and i_{time} is counted and summed to give the final input *I*:

$$I = e_h.e_n + i_h.i_n$$

Variable V_{syn} represents the contribution of synaptic input to the oxytocin cell membrane's voltage (*V),* and decays to 0 with time constant τ_{syn} corresponding to a half-life λ_{syn} of 3.5 ms:

$$\frac{dV_{syn}}{dt} = -\frac{V_{syn}}{\tau_{syn}} + I$$

Initially, the model neurone is at resting potential V_{rest} = -50mV. If inputs raise the membrane potential V above a threshold V_{th} = -56mV, the neurone produces a spike. The model then triggers an HAP and an AHP, and V evolves according to:

$$V = V_{rest} + V_{syn} - HAP - AHP$$

HAP has a fixed step amplitude (k_{HAP} = 30mV) and time constant (τ_{HAP}) that corresponds to a half-life of 7.5 ms, following previous work (Maícas-Royo *et al.*, 2016, 2018). *AHP* also has a fixed step amplitude (k_{AHP} = 1mV) and τ_{AHP} set to correspond to a half-life λ_{AHP} of 350 ms, as used previously (Maícas-Royo et al., 2018):

$$\frac{dHAP}{dt} = -\frac{HAP}{\tau_{HAP}} + k_{HAP} \cdot \delta$$

$$\frac{dAHP}{dt} = -\frac{AHP}{\tau_{AHP}} + k_{AHP} \cdot \delta$$

where δ = 1 if a spike is fired at time t, and δ = 0 otherwise. Unlike the conventional integrate-and-fire model, there is no reset to V_{rest} following a spike. The HAP and AHP are thus able to accumulate across spikes and modulate activity dependent excitability.

Secretion and plasma models

In our previous paper (Maícas-Royo et al., 2018) we modelled 250-g rats, and set a fixed plasma volume for oxytocin, Vol_p = 8.5 ml, and for the EVF volume of distribution for oxytocin, $Vol_{EVF(oxy)}$ = 9.75 ml. Here we defined these values as a function of the rat body weight (B) which varies from 190 to 400 g in the experimental data we used.

$$Vol_p = 8.5 \cdot \frac{B}{250}$$

$$Vol_{EVF(oxy)} = 9.75 \cdot \frac{B}{250}$$

The rest of the equations and parameter values are as in the previous work, for both the oxytocin secretion and clearance models.

Reference data

Both spiking activity and plasma oxytocin have been measured in studies of osmotically regulated secretion. Some of these experiments used i.p. injections of hypertonic NaCl as a challenge, others used i.v. infusion, and some reported correlations between plasma osmotic pressure and oxytocin cell activity from conditions of chronic osmotic challenge. To use as much of these data as possible, we needed to model the experimental challenges themselves.

To fit the osmotic model we used data from experiments described by Leng *et al.* (2001) and Brimble & Dyball (1977). To connect the osmotic model with the oxytocin spiking model we used data from Leng et al. (2001) and Brimble & Dyball (1977). We also tested the coupling of the osmotic model, plus the oxytocin spiking model, with the oxytocin secretion and plasma oxytocin models. To do it we simulated experiments from (Leng *et al.,* 2001) and Higuchi *et al.* (1988). Finally, we simulated the effect of bicuculline and hypovolemia in oxytocin neurones under osmotic challenges, mimicking data from (Leng *et al.,* 2001) and Stricker & Verbalis (1986).

Results

In our previous work (Maícas-Royo *et al.*, 2018), we developed a model of the spiking activity of oxytocin cells. We linked this to a model of the stimulus-secretion properties of the terminals in the posterior pituitary, and to a model of clearance of oxytocin from the plasma, to relate spiking activity to plasma oxytocin concentrations. The integrated model was fit to data associating spiking activity to plasma oxytocin levels in response to systemic injections of cholecystokinin, and to data on stimulus-secretion coupling in the posterior pituitary. Here we *tested* this model by assessing how well predictions of the model match experimental measurements of spike activity and plasma oxytocin.

In the experimental conditions mimicked here, we varied the PSP rate as a linear function of extracellular [Na^+]. The plasma [Na^+] is *not* directly the stimulus, because when hypertonic NaCl is infused slowly i.v., there is a rapid increment in plasma [Na^+] that is not accompanied by a corresponding increment in spike activity, but there is a slow linear and parallel increase in spike activity and plasma [Na^+] during continued infusion (Leng *et al.*, 2001). The change in plasma [Na^+] during infusion implies a rapid transfer of Na^+ from plasma to EVF, so it appears to be changes in an extravascular compartment that are seen by the oxytocin cells and their inputs – presumably changes in the surrounding extracellular fluid (Figure 38).

Multi-compartment model for Na^+ diffusion

We first simulated a 30-min i.v. infusion of 2M NaCl at 0.26 µl min^{-1}. As reported in Leng *et al.* (2001), such infusions produced a rise in plasma [Na^+] from 134.5 to 146 mM during the first 5 min of infusion, followed by a linear rise of 8.5 mM in the next 25 min, consistent with rapid diffusion from plasma into EVF. To model this, we needed to estimate the volumes of the EVF, plasma and ICF, and we assumed that equilibration of osmotic pressure between intracellular and extracellular compartments involves the passage of water from the intracellular to the extracellular space.

These experiments were on urethane-anaesthetized rats; urethane is a sodium salt, and the basal plasma [Na^+] was 134.5 mM and assumed to be the same in the EVF. The mean body weight of the rats was 350 g. The model EVF volume, estimated as 16.4 % of body weight, was set at 57.4 ml, the plasma volume, (3.4 % of body weight) at 11.9 ml and the ICF volume (40.2% of body weight) at 140.7 ml (see Methods). Assuming that plasma volume is constant throughout the infusion, the data are closely matched (Figure 39.A) by assuming that plasma [Na^+] equilibriates with EVF [Na^+] with a half-life $\lambda_{i.v.}$ of 190 s. When the infusion stops, plasma [Na^+] decreases to 144.7 mM over 10 min as it equilibriates with the EVF [Na^+] (Figure 39.A). EVF [Na^+] rises linearly throughout the infusion as a consequence of diffusion of Na^+ from plasma, accompanied by the transfer of 16.2 ml water from ICF (Figure 39.B). The amount of water transfer was calculated to be that required for equilibriation of osmotic pressure in all compartments.

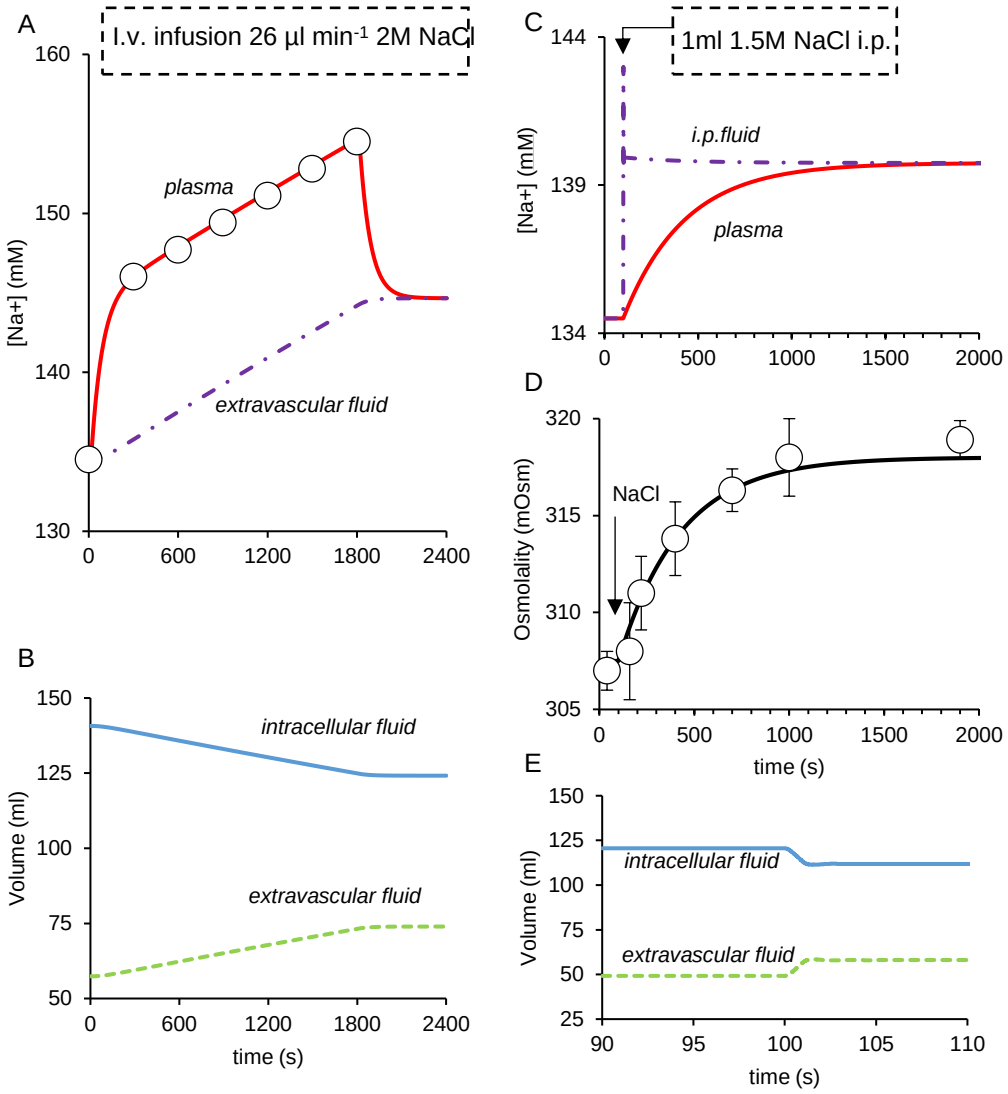

Figure 39. **The diffusion model of Na^+. A)** [Na^+] dynamics in plasma and extra vascular fluid (EVF) during a 30 minutes i.v. infusion of 26µl min^{-1} 2M NaCl. White dots show *in vivo* plasma [Na^+] as seen in Leng *et. al* (2001). The red line represents the plasma [Na^+] simulated by the model. The purple line shows the modelled [Na^+] in the EVF. The parameter values to match the *in vivo* data are the same for the rest of the figures. **B)** Modelled volume dynamics in the EVF and intra cellular fluid (ICF) during the i.v. infusion. **C)** Using the same parameter values as in A and B, the model can simulate the [Na^+] dynamics after an i.p. NaCl injection, as described in Brimble & Dyball (1977). **D)** The resultant *in vivo* osmolality (white dots) can be mimicked (black line) as a linear function of the simulated [Na^+] in plasma from C. **E)** shows the volume dynamics near the injection time.

We then modelled the i.p. injection of 1 ml 1.5M NaCl described in Brimble & Dyball (1977) who used urethane-anaesthetized rats of 300 g body weight. [Na^+] was not measured in these experiments, but plasma osmotic pressure was. We ran our model assuming the same initial plasma [Na^+] as above (134.5 mM). Sodium moves

rapidly from plasma to EVF because plasma is under positive orthostatic pressure, but movement from EVF into plasma is much slower. The model was fit to measures of plasma osmotic pressure reported by Brimble & Dyball (1977) by multiplying the plasma [Na^+] by two to convert to osmolality, and adding a constant of 38.5 mOsmol (Figure 39.D) to reflect other osmolytes in plasma. The data were fit by an inferred half-life time of diffusion from EVF to plasma, $\lambda_{i.p}$ of 1150 s. In the model, the EVF [Na^+] rises rapidly from 134.5 mM to 143 mM after the injection. It then quickly falls, equilibriating with plasma [Na^+] at 139.75 mM at 30 min (Figure 39.C), because of a fast water flux from ICF to the EVF (8.8 ml in 3 s; Figure 39.E).

There is an important difference between the i.v. and i.p. routes. While NaCl is infused i.v. the plasma [Na^+], will always exceed the EVF [Na^+], and we use EVF [Na^+] as the input to the spiking model to model responses to i.v. injections. However, when NaCl is injected i.p., the EVF [Na^+] in the peritoneum will initially greatly exceed the plasma [Na^+], but [Na^+] in the brain will change more slowly, as Na^+ enters the brain from both the blood and EVF. For i.p. injections, we assume that plasma [Na^+] approximates the changes in brain extracellular [Na^+] – i.e., we assume that the brain extracellular [Na^+] equilibriates with the EVF [Na^+] at the same rate as plasma [Na^+] does.

Integration with the spiking and secretion model

The next step was to fit the relationship between brain extracellular [Na^+] and the spiking activity of oxytocin cells. The firing rate of oxytocin cells increases linearly during i.v. infusion of hypertonic NaCl, and we assumed that this arises from a linear relationship between extracellular [Na^+] and synaptic input rate (PSP rate). In our model, this relationship depends on both intrinsic neuronal properties and on the nature of the input. Neurones without an AHP show a non-linear increase in spike activity in response to a linearly increasing PSP rate, but this nonlinearity is abated by the presence of an AHP, or if the stimulated input comprises a mixture of EPSPs and IPSPs. Here we used an oxytocin cell model with the same intrinsic properties as defined previously (Maícas-Royo *et al.*, 2018), including the same AHP parameters, and we set the basal PSP rate to match the observed basal firing rate. We also assumed that osmotic stimuli increase the rate of both EPSPs and IPSPs, as inferred previously (Leng *et al.*, 2001). This left two free parameters to fit: the slope of the relationship between PSP rate and extracellular [Na^+], and the ratio (I_{ratio}) of EPSPs and IPSPs in that signal. As detailed below, the response of

oxytocin cells to i.v. NaCl could be well fit with I_{ratio} = 0.75 and we set the slope with a value of 44. We kept these values for the rest of the simulations.

We first compared the response of the model to the response of a typical oxytocin cell exposed to i.v. injection of 20 µg kg^{-1} CCK followed by an i.v. infusion of 26 µl 2M NaCl (Figure 40.A). We adjusted the basal PSP rate, to match the basal firing rate of 2.9 spikes s^{-1}. We simulated the CCK injection, as in Maícas-Royo *et al.* (2018), and the NaCl infusion, adjusting the model for a body weight of 350 g. The model response is very similar to the observed responses to CCK and NaCl. Importantly, we made no attempt to fit the oxytocin cell model to the experimentally observed response; the comparison shown is the prediction from the generic oxytocin cell model described in (Leng *et al.,* 2017). In the simulation, the firing rate responds to the 60 minutes infusion by raising from 2.3 spikes s^{-1} (Figure 40.B left) to 10.5 spikes s^{-1} (Figure 40.B right). At its basal firing rate, the model simulates a single neuron average secretion of 0.13 fg s^{-1}, fluctuating between secretion rates of 0 and 1 fg s^{-1} (Figure 40.C left). Because of the non linear coupling between spiking activity and secretion, after the infusion, the modelled secretion for the single neuron has a mean of 9.75 fg s^{-1}, 77 times more than during basal activity, whereas secretion excursions vary from 5.5 to 16.7 fg s^{-1} (Figure 40.C right).

Oxytocin cells are heterogeneous in their basal firing rates. We simulated populations to mimic the numbers of cells recorded in experiments and their variation in basal firing rate, and to fit the measured basal plasma oxytocin concentration. We made the populations heterogeneous by varying the basal PSP rate using a lognormal distribution to match the mean and SD of experimental data.

We started by mimicking the response of 12 oxytocin cells to a 60-min i.v. infusion of 2M NaCl at 26 µl min^{-1} as reported by (Leng *et al.*, 2001). We simulated a 350-g rat, setting a mean (SD) PSP rate of 305(150) s^{-1} to obtain a basal firing rate of 3.1 spikes s^{-1}, matching exactly the reported basal rate. Our model showed a linear increase in the mean firing rate, matching the experimental data very closely (Figure 41.A).

Leng *et al* also reported measurements of plasma oxytocin during similar infusions, but in different experimental conditions: these rats were also anaesthetized with urethane, but the transpharyngeal surgery involved in recording was not performed. In these conditions, basal oxytocin concentrations are lower, apparently because the stress of surgery and associated blood loss elevates basal neuronal activity.

Accordingly, it was necessary to estimate the basal firing rate from the plasma concentration at rest.

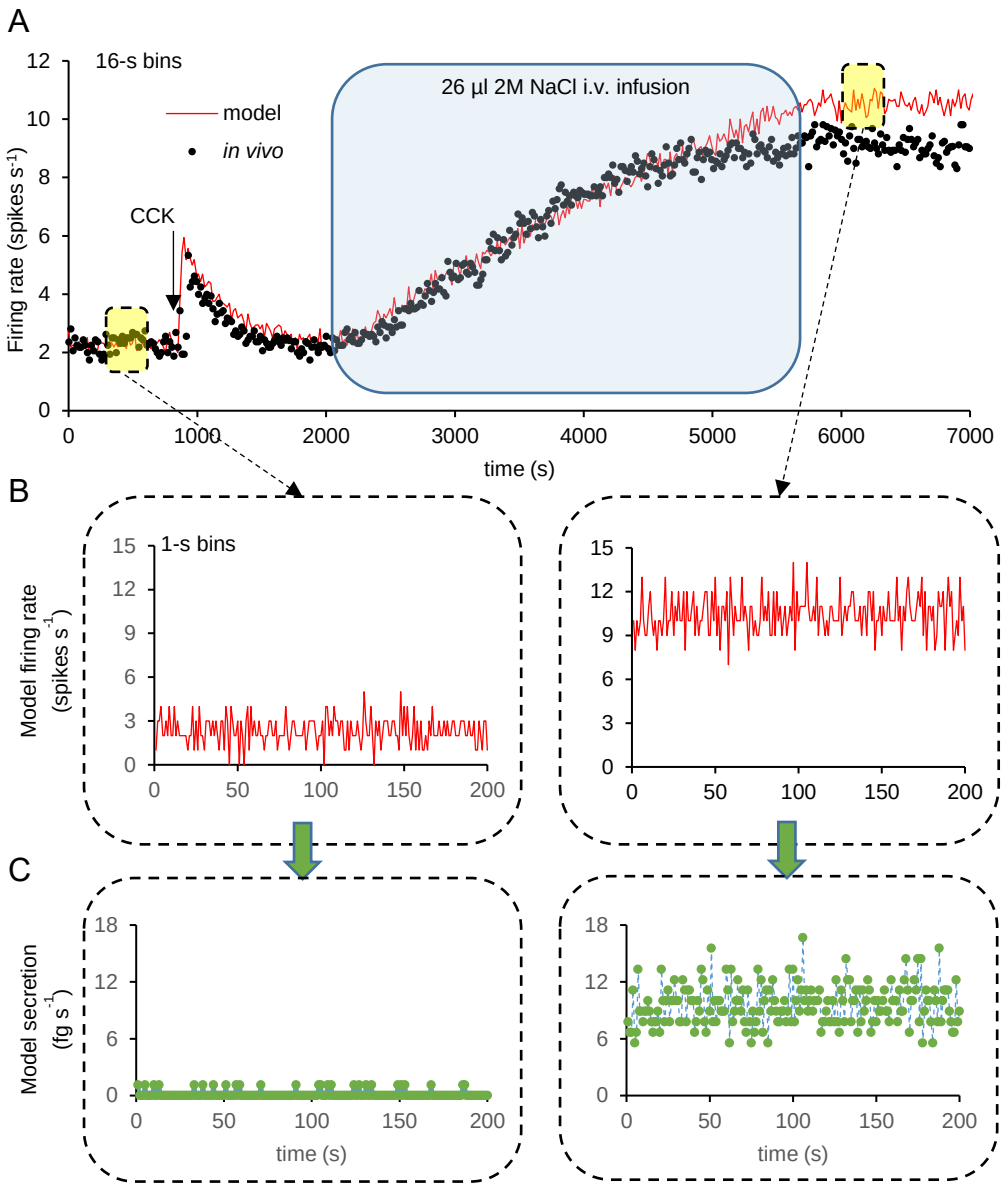

Figure 40. The single neuron model. A) By adjusting the rat weight, the initial firing rate (2,29 spikes s-1), the cholecystokinin (CCK) as in Maícas-Royo *et al*., (2018) and NaCl infused as in Leng *et al*. (2001), the oxytocin neuron model (red line) can mimic *in vivo* spiking data (black circles) from a oxytocin neuron responding both to an injection of CCK, and to an i.v. infusion of NaCl. **B)** The basal firing rate of the neuron (left), is 2.29 spikes s^{-1}. After the NaCl infusion finishes, the model predicts an average increment of 8 spikes s-1 (right). **C)** Exocytosis is triggered by the spikes' arrival to the axon terminal. Because of the non-linear coupling between spike rate and secretion (Maícas-Royo *et al.,* 2018), the model predicts a much larger exocytosis at higher firing rates.

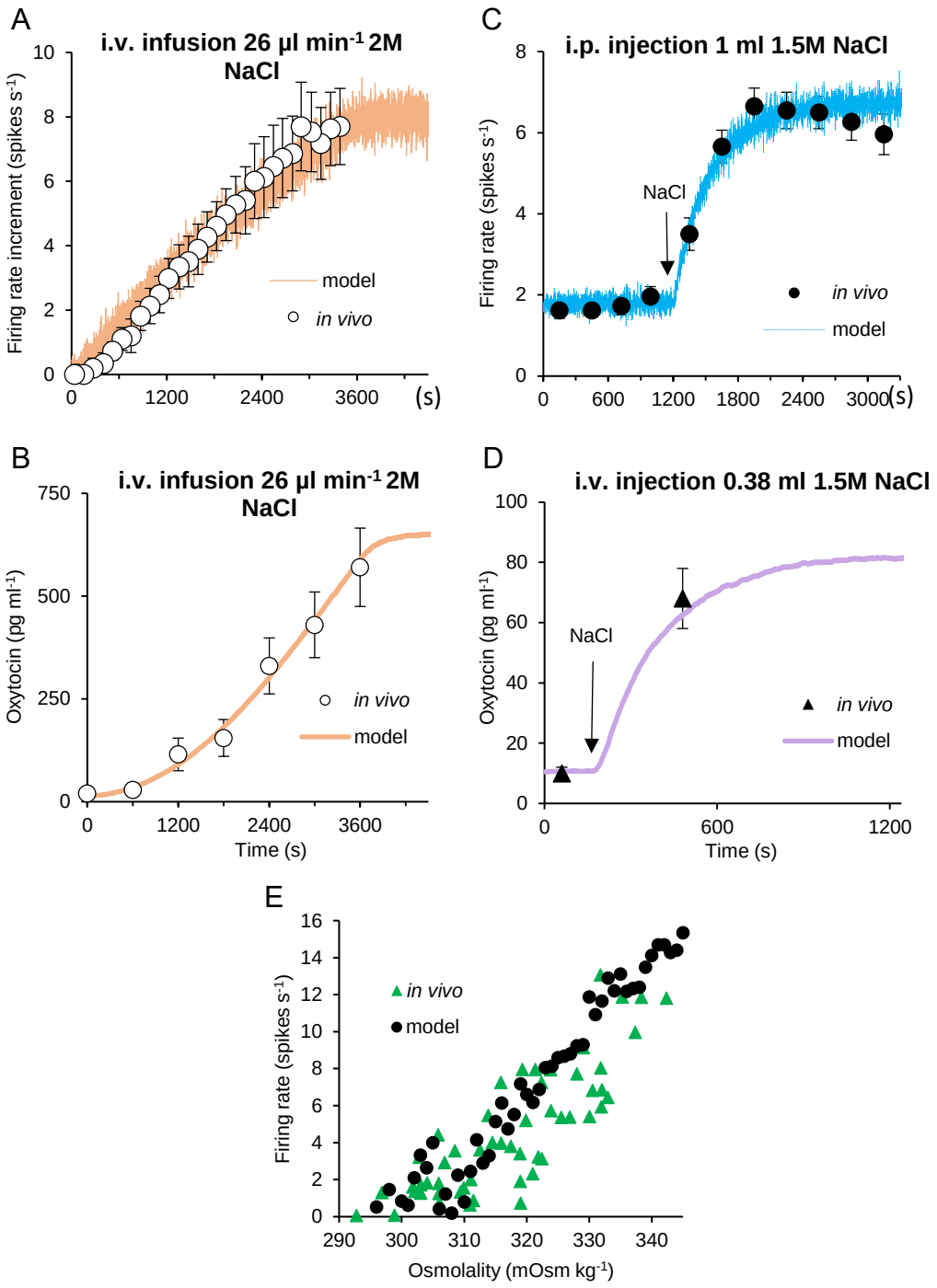

Figure 41. Oxytocin spiking and plasma responses to changes in osmolality. We run the model using the same parameter's values as in **Figure 40**, adjusting just the basal firing rate, the rat's weight and the amount and origin of NaCl injected. **A)** White dots show the averaged *in vivo* firing rate increment of 12 oxytocin neurones during a 60 min i.v. infusion of 2M NaCl at 26 µl min^{-1} (Leng *et al.,* 2001). In orange, the response of a modelled population of 30 oxytocin neurones with lognormally randomised PSP arrival rates matches it closely. **B)** Here, the simulated plasma oxytocin (orange line) of a 100 neurones population matches perfectly the *in vivo* data of plasma oxytocin (white dots) when the same infusion than in A is simulated. **C)** The simulated response of 30 oxytocin neurons (blue line) matches the averaged *in vivo* firing rate response of 11 oxytocin neurones after an i.p. injection of 1.5 ml 1M NaCl (black dots) (Brimble & Dyball, 1977). **D)** The *in vivo* plasma oxytocin response

after an i.v. injection (black dots) (Higuchi *et al.,* 1985). is also mimicked by a population of 100 neurones with the same parameter values as in A,B and C. **E)** Green triangles show *in vivo* firing rates of 53 oxytocin neurones in rats with different osmolality (Brimble & Dyball, 1977). In this case, 50 modelled neurones responding to increasing levels of NaCl in plasma (black circles) draws a very similar osmolality-firing rate curve.

We used plasma oxytocin data from experiments reported in Leng *et al*. (2001), including a set of serial measurements from rats. To match the basal concentration of oxytocin, we set the mean PSP rate at 190 s^{-1}, randomizing lognormally the PSP rate from neuron to neuron with a SD of 95 s^{-1}.That gave a mean firing rate of 1.38 spikes s^{-1} and a plasma concentration oxytocin of 15.7 pg ml^{-1} (Figure 41.B). With the predicted osmotically induced increment of 20.2 mOsm, the model simulates oxytocin concentrations remarkably close to observed levels.

Brimble & Dyball (1977) recorded from 11 oxytocin cells in rats of 300 g body weight, and gave an i.p. injection of 1 ml 1.5M NaCl. The mean spike activity increased from 1.8 to 6.6 spikes s^{-1} in the 12 min after the injection (Figure 41.C). We simulated this experiment for a 300-g rat and 30 model neurones with a mean basal firing rate of 1.79 spikes s^{-1}, obtained by a lognormally randomized PSP mean (SD) rate for the population of 215 (100) s^{-1} (Figure 41.C). The predicted change in firing rate is remarkably close to the experimentally reported data.

We also matched the plasma oxytocin response after i.v. injection of 0.38 ml 1.5M NaCl in 190-g rats reported by Higuchi et al. (1988) who used the same oxytocin immunoassay as (Leng *et al.*, 2001). In these experiments, the basal oxytocin concentration was lower, mimicked with a PSP rate of 132 (65) s^{-1}, producing a mean basal firing rate of 0.75 spikes s^{-1}, associated with a basal plasma oxytocin of 10.6 pg ml^{-1}. We simulated the i.v. injection, obtaining a close match (Figure 41.D).

To this point, we mimicked the time response of experimental data after a hypertonic injection or during a hyperosmotic infusion. However, we also simulated stationary experiments. Brimble & Dyball (1977) showed the recorded firing rates of 50 oxytocin cells from rats with different osmotic pressures. We ran the model with 50 neurones to construct the relationship of mean firing rate to osmotic pressures between 305 and 345 mOsm kg^{-1}. We obtain the values by averaging the firing rate of the cells over an hour, during which the cells produce a regular spike activity. The model prediction matches the experimental data closely (Figure 41.E).

The role of IPSPs in the osmotic response

We used the combined model to simulate the effect of bicuculline, delivered to the dendritic zone of the supraoptic nucleus, as described in Leng *et al.* (2001). In that work, five oxytocin cells were challenged with two 10-min infusions of 2M NaCl i.v. at 26 µl min^{-1}, before and after a 25-min application of bicuculline by retrodialysis. Bicuculline blocks GABA receptors in neurons. Leng *et al.* found that the response to osmotic pressure after bicuculline was greater than before, implying that the IPSPs are involved in the oxytocin response to osmotic pressure (Figure 42.A). We simulated that experiment by running our model with two populations of 20 neurones with a PSP rate of 210 (100) s^{-1}, and mimicked the effect of bicuculline by making the IPSPs equal to 0 in one of the populations. After 10-min infusion, the difference in firing rate increment between the populations was ~1.5 spikes s^{-1}, very close to that observed experimentally (Figure 42.B).

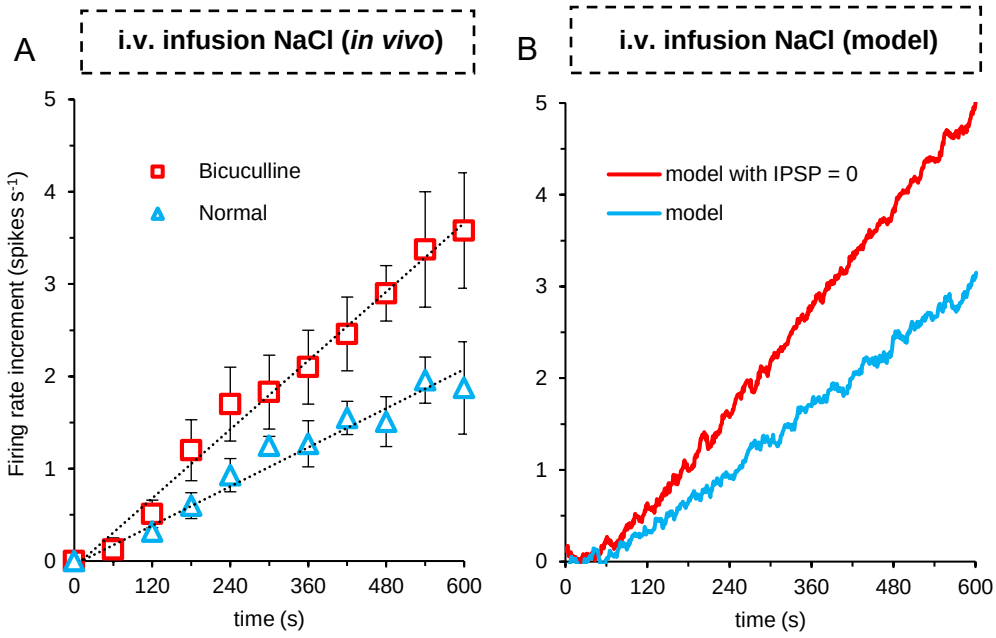

Figure 42. Response to bicuculline. Bicuculline blocks the effects of GABA. **A)** Blue triangles with white centre show the firing rate increment response of 5 oxytocin neurones to *in vivo* infusion of 2M NaCl at 26 µl min^{-1} Red squares with white centre show the increment in firing rate under the same circumstances after bicuculline had been injected (Leng *et al*., 2001). **B)** We can simulate the effect of bicuculline by making the IPSPs equal to 0 in the model, while keeping the same amount of EPSPs. The blue line shows the firing rate increment to the simulated hypertonic saline infusion in oxytocin neurones with IPSPs. The red line shows the simulation when the IPSPs are 0.

Simulating the osmotic response in hypovolemic rats

Using polyethylene glycol (PEG) to reduce the plasma volume by 35-40%, Stricker & Verbalis (1986) and Stricker *et al.* (1987) found a steeper slope in the relationship between plasma oxytocin concentration and osmotic pressure (Figure 43.A). Our model is fitted to plasma oxytocin concentrations measured with the Higuchi radioimmunoassay (Higuchi *et al.*, 1985), but the studies above used a radioimmunoassay with the antibody Pitt Ab-2, which consistently reported lower plasma oxytocin concentrations (Amico *et al.*, 1985). Therefore, here we matched trends more than absolute values, which in the model are ~20 times bigger than in the experimental data. To simulate hypovolemia, we first obtained a good approximation by running the model for different osmotic pressures, whilst making IPSPs = 0 (Figure 43.B). However, we found a closer fit by both using the reduction in IPSPs and reducing a 35% the plasma volume, increasing the EVF volume by the same amount lost by the plasma, as it happens with PEG (Figure 43.C).

That latter result means that, when using PEG, the reduction in plasma volume, and increment in EVF is responsible for at least, part of the higher plasma oxytocin concentrations in hypovolemic animals. Moreover, that happens independently of the IPSP inputs that oxytocin neurones receive. The model helps to elucidate how that happens by showing that the oxytocin concentration is the same in plasma and in the EVF under any level of hypovolemia (Figure 43.D) and that, counterintuitively, the oxytocin in plasma would eventually reach the same level under different hypovolemic conditions too (Figure 43.E), even if hypovolemic animals will reach that level later. In our previous model, oxytocin clearance is exclusively produced from the plasma compartment (Maícas-Royo *et al.*, 2018). That, in conjunction with the larger values of oxytocin moving to the EVF in hypovolemic conditions (Figure 43.F) is responsible for the higher oxytocin concentrations observed experimentally.

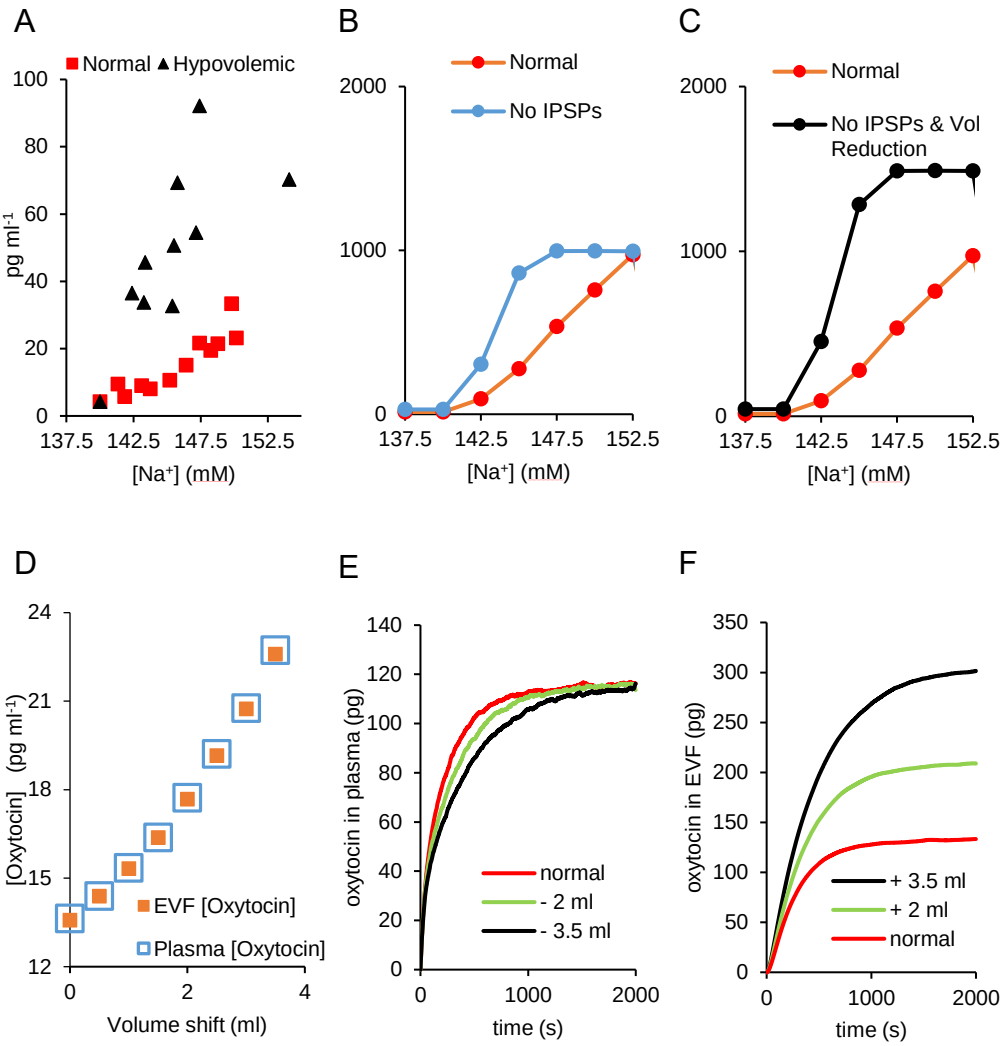

Figure 43. Hypovolemia is often achieved in experiments by injecting animals with polyethylene glycol (PEG). As a result, some plasma volume moves into the EVF producing and edema **A)** After injecting them with PEG, hypovolemic rats (black triangles) show higher plasma oxytocin levels than normal rats (red squares), and the difference increases with osmotic pressure (Stricker & Verbalis, 1986). **B)** We can partially simulate that effect by making IPSPs = 0 in the modelled oxytocin neurones (blue dots and line), seeing that the response is higher than with a normal IPSP rate (red dots and line). **C)** The effect is better achieved when, in addition to make IPSP = 0, we both reduce the plasma volume and increase the extra vascular volume (EVF) in the model (black dots and line), mimicking the conditions in A. This result suggests that, independently of the IPSPs, a reduction of plasma volume will trigger a response to osmotic pressure. Note: our model (B and C) gives values of plasma oxytocin ~20 times bigger than A because it simulates the plasma oxytocin levels assessed by the Higuchi immunoassay (Higuchi et al., 1985) that gives larger values than the radioimmunoassay with the antibody Pitt-Ab-2 used in A. **D)** This phenomenon is produced because the plasma oxytocin (blue squares) maintains the equilibrium with the [oxytocin] in the EVF (red squares). **E)** Our model shows that, simulations with volume reductions, 2 ml (green line) and 3.5 ml (black line), take more time to reach the equilibrium than normal volume (red line). However, under the same constant secretion rate, a shift of volume and a punctual increment of [oxytocin] plasma does not affect the final amount of oxytocin in plasma. **F)** To maintain the same [oxytocin] than in plasma, when the EVF increases its volume by the same amounts (as indicated) the plasma volume is reduced, the equilibrium points for the total amount of oxytocin in the EVF are different.

Discussion

In this work, we used our oxytocin spiking, secretion and plasma clearance model to simulate the response of oxytocin cells, and their secretion in plasma, to hypertonic saline challenges.

To simulate the dynamics of Na^+ in the rat body until equilibrium is reached in the EVF of the LT, we adapted the two-compartment model for oxytocin clearance that we had implemented in our previous work by adding a third compartment, the ICF, which maintains osmotic equilibrium with the EVF by exchange of water. To find a biologically valid value for the time it takes water to cross from the ICF to the EVF we used the classical work from Sidel & Solomon (1957). We also compared our fit with the results from Mazzoni *et al.* (1988). From experiments in healthy humans we know that large hypertonic infusions produce an important water transfer from the ICF to both plasma and EVF, up to a 20% of plasma volume with a 7.5% saline infusion (Järvelä *et al.*, 2003). For simplicity, we implemented that osmotic transfer occurs only between the ICF and the EVF, making the plasma volume stable, obtaining an increment of a 28% in the EVF volume after a 30 min infusion of 26µl.min^{-1} 2M NaCl.

Once the Na^+ model was developed, we coupled it with our previous model for oxytocin cells. As this study was conceived as a test of the published model, we changed only parameters necessary to simulate the experimental conditions. We have only modified the ratio between the EPSPs and the IPSPs (I_{ratio}), decreasing it from the value of 1 that it had in our previous work to a value of 0.75. With a smaller I_{ratio} the firing rate follows a more linear function of the arriving PSPs, making the relationship increasingly quadratic with a larger I_{ratio}. However, a smaller I_{ratio} would reduce the difference between the simulations of the responses to hyperosmotic infusions with and without bicuculline, making a larger ratio produce the opposite effect (Figure 42.B). An alternative way to increase the linearity between PSP and firing rate would be to have either a smaller AHP or the presence of a depolarisation afterpotential (DAP), that we have shown is necessary to model at least some oxytocin neurones (Maícas-Royo *et al.*, 2016). However, in those cases, the firing rate response, apart from being more linear, also has a larger slope, making other firing rate matches not suitable (Figure 41A, C, E). To make those fits possible with a reduced AHP or with a DAP we should increment the I_{ratio} but in that case we

would lose the match between the differences in response when bicuculline was injected (Figure 42.B).

Partly because oxytocin may not be involved in the fluid balance in humans (Rasmussen *et al.*, 2003, 2004), the role of oxytocin in that homeostatic process has not been studied as extensively as that of vasopressin. However, oxytocin cells are involved in fluid balance in the rat and have many similarities with vasopressin cells in their firing rate responses to osmotic challenges (Brimble & Dyball, 1977), and oxytocin and vasopressin are almost identical in their plasma response in the rat (Stricker & Verbalis, 1986; Verbalis *et al*., 1986; Stricker *et al.*, 1987; Verbalis & Dohanics, 1991).

When fitting the model we have found that many of the experimental data show substantial differences. For instance, the data we show in Figure 42.E, from Brimble & Dyball (1977), follows the same linear relationship between osmotic pressure and spike rate as the findings from Wakerley *et al.* (1978). However, the latter suggests a much smaller slope and a different osmotic pressure set point. Something similar happens with the plasma oxytocin concentration. The absolute measurements of oxytocin differ with different assays (Leng & Sabatier, 2016). In this work, we have matched experimental data *(*Higuchi *et al.*, 1988; Leng *et al*., 2001) to data obtained with the Higuchi immunoassay (Higuchi *et al.*, 1985), as in our previous work (Maícas-Royo *et al*., 2018) and we used other experimental results as indicators for the response slope but not for the exact values we should obtain with our model.

Finally, to model systemic changes in osmolality we developed a new model that calculates the $[Na^+]$ dynamics in the plasma, EVF and IVF. The model needs to be improved to be physiologically accurate. Possible alternatives to achieve a better match in the $[Na^+]$ model would include a combined effect of both hypovolemia and osmotic pressure. The structures adjacent to the lamina terminalis have receptors for both, however, when there is a rapid decrease in plasma volume, angiotensin II receptors in these structures activate quickly, which corresponds better with an i.p. infusion or injection, where water will be shifted from plasma to equilibrate osmolality. Whereas, an i.v. infusion or injection would hypothetically increase the plasma volume by a shift of water from the plasma ICF and also from the ECF, producing a smoothed response that we have attributed totally to the shift in Na^+ to the EVF which includes the cerebral ventricles in our model.

Chapter 6:

General Discussion

"It's the questions we can't answer that teach us the most. They teach us how to think. If you give a man an answer, all he gains is a little fact. But give him a question and he'll look for his own answers".

Patrick Rothfuss. TWMF

Magnocellular oxytocin neurones have particular characteristics that make them an excellent study target (Leng *et al.*, 1999). They are big in comparison with many other neurones, as their own name indicates, and that makes it easier to identify them and also to study their electrophysiological characteristics. Another advantage they have is that they are mainly in two nuclei, the SON and the PVN of the hypothalamus. In fact, in the SON there are only either oxytocin or vasopressin magnocellular neurones. The fact that the hypothalamus is at the bottom of the brain makes more feasible to do *in vivo* recordings of the neurones, as far as the SON or the PVN are accessed ventrally. Finally, oxytocin neurones secrete their product to the bloodstream, where plasma oxytocin and its fluctuations can be accurately measured. Thus, the result of the oxytocin neuronal activity can be measured with a blood test whilst their spiking activity, if not as easy to measure, is much more accessible than neurones located deeper in the brain. All that makes them better candidates to be studied than other neurones, which are more difficult to localize, whose projections are only central and often quite diffuse and difficult to trace.

All those characteristics have made the behaviour of oxytocin neurones comparatively well described.

Plasma oxytocin levels raise spectacularly during parturition and breastfeeding. That made those two scenarios the first ones to be studied, offering the first lights over oxytocin neurones dynamics.

In a lesser, because plasma oxytocin levels change more smoothly in those circumstances, but not minor extent, we also know that oxytocin neurones also respond to changes in osmotic pressure, hypovolemia and food intake.

Those five physiological functions have been broadly studied. The pathways and the different cells involved in receiving information from the body, sending that information to the brain, integrate that information and finally send it to the oxytocin neurones, are some of the best documented fields in physiology. However, there are still many gaps in the understanding of the pathways and the neurones themselves.

Classic electrophysiology can record one neurone activity each time, with multi-unit techniques making possible to record more than one (Buzsáki, 2004; Takekawa *et al.*, 2010). Alternatively, optogenetics can look into the dynamics of neural networks not as fast as electrophysiology, but still with a precision of milliseconds (Fenno *et al.*, 2011) and techniques such as two photon calcium imaging provide the capacity to selectively choose the neurons whose activity we want to measure (Kim *et al.*, 2017; Stamatakis *et al.*, 2018). Although these techniques can be used more easily to study the cortex of freely moving animals because in those cases the laser beams and the microscope can be attached to the skull, they have also shown their potential in oxytocin and vasopressin neurones (Yoshimura & Ueta, 2018). All these techniques also have their issues, not least because while they obtain more data, new tools need to be developed to analyse it (Takekawa *et al.*, 2010).

However, once we get deeper in the brain, *in vivo* recordings of neural activity become increasingly difficult. For instance, the exact origin of the oxytocin inputs responding to osmotic pressure or hypovolemia is still unclear. It is known that the osmotic inputs come from the lamina terminalis (Zimmerman *et al.*, 2017). The presence of excitatory inputs has been established, and other experiments have indicated inhibitory inputs too (Leng *et al.*, 2001). However, the exact origin of them is still obscure, mainly because the lamina terminalis is less easy to access than the SON, their nuclei's boundaries are not well defined, and their cells are smaller and much heavily interconnected with different parts of the brain. In addition, the techniques to measure plasma oxytocin are far from perfect. That means that the resultant plasma oxytocin after the same hypertonic saline injection, can give a 15 fold difference depending on the assay.

The work described in this thesis has attempted to simulate, to some extent, what is known about oxytocin neurones when they react to food intake, osmotic pressure and hypovolemia. Because a lot is known about oxytocin neurones, but maybe not so much about the neurones that innervate the oxytocin neurones, the focus was set in what it is better known. That way of doing things has shown some advantages. Once the model has been able to simulate the experimental data, it has offered the possibility to advance the scientific knowledge of oxytocin neurones in two different ways.

First, our model has offered a wider perspective of the functionality of the different components of oxytocin neurones.

Experimental data has extensively shown the membrane properties of oxytocin neurones in different circumstances, both in the spiking and the secretion activity. The mathematical models we used describe first simple membrane dynamics, and then they integrate to produce more global spiking, secretion and clearance responses. The fact that the model can describe the different currents and the oxytocin neurone membrane channels, offered the possibility to closely examine the behaviour of each of those currents under a wide variety of physiologically relevant circumstances, but also under other circumstances that would be impossible to replicate in the lab. Moreover, the mathematical model allows to do it very fast: simulating an hour of a single neuron spiking activity takes less than a second and an hour simulation of the spiking and secretion activity of 100 neurones would finish in less than two minutes. In addition, the model allows to do that at any time, and changing any parameter value from experiment to experiment.

However, that speed and versatility has a potential drawback: the immense amount of data that those experiments generate. Because of it, a great part of the work during the PhD has consisted of developing tools to analyse that data.

Combining the robustness of the model, its speed and the automatized statistical tools, I have been able to initially match the model in different ways to the experimental data. And, secondly, I have been able to do certain experiments that would be really difficult in the laboratory.

For instance, the starting point for the first paper I included in this thesis, was to use the index of dispersion on the experimental recording of some oxytocin neurones. My supervisor Gareth Leng wondered why that index of dispersion was smaller for longer bin widths in those oxytocin recordings. At that time, he was probably thinking already that the AHP could be responsible, but to prove it in the lab, he would have needed many excellent recordings, alternately blocking the AHP and not blocking it. Using the computational model allowed us to do those experiments again and again, finding that the AHP was the responsible for the reduction in variability in long bin widths. Moreover, the model supported as well the necessity of a DAP in, at least, some oxytocin neurones (Maícas-Royo *et al.*, 2016).

In addition, we found that the index of dispersion supported another part of our model. It is known that if a sequence of numbers follows a Poisson distribution, its index of dispersion is 1 in every bin width. Our model simulates the arrival of the inputs to the oxytocin neuron following a Poisson distribution. Thus, the fact that the

index of dispersion of the recordings *in vivo* looks similar to the one we obtain in the test, supports the idea that we are producing the inputs in a correct way by using a Poisson distribution.

However, the final product of oxytocin neurones is not the spike. After publishing that first paper, we wanted to know if the AHP role in the spiking activity extended its ability in secretion. Using the vasopressin secretion model that my supervisors had developed before (MacGregor & Leng, 2013) helped us to focus on fitting the model with as many experimental data as we could find. At the end, because I had several sources and not all of them could be matched simultaneously, I obtained a balanced model, which was close enough to every experiment.

The secretion, though, was not the final step of the model. Or at least, not the typical data scientists refer to, when they want to show if an experiment has influenced oxytocin secretion. Thus, I created another model to simulate the clearance of oxytocin from plasma, basing our equations on the fate of oxytocin in the rat described by Ginsburg & Smith (1959) and (Fabian *et al.*, 1969*a*).

Overall, the design of the mathematical equations and the writing of the software that simulate them at a huge speed, did not take much. The biggest task was to fit the parameter values of the mathematical equations to match previous experimental results and the designing and polishing of different statistical and graphic tools that allowed comparative data analysis. All that was done for the spiking model, for the secretion and the clearance models, for the model simulating the Na^+ distribution in the rat's fluids, and finally for the integration of all of them.

Once I had a model to simulate the whole activity of oxytocin neurones, I wanted to do three things. The first one, to know what the role of the AHP in secretion and plasma oxytocin was. Secondly, I wanted to test the model with a physiologically meaningful input. That input ended being CCK, because the response of oxytocin neurones to it is very well described in the literature, and because it is a signal related to food intake. Finally, I wanted to know how heterogeneity in the spiking activity would affect the secretion response.

To achieve all that, several tools were developed to visualize better the noise filtering effect of the AHP in the spiking, secretion and plasma oxytocin dynamics. Several other tools were created to produce responses to different levels of CCK, in different neurones. And other tools to analyse all that data, producing figures

automatically. Finally, heterogeneity was introduced and to compare it with real data, I allowed our model to be fed by experimental recordings, producing a simulated secretion from them.

A predictive model

Probably one of the main strengths of the oxytocin model I have developed is that it can simulate the resultant plasma oxytocin when the oxytocin spiking activity is known, and it can also simulate the spiking activity if what is known is the plasma oxytocin.

Moreover, it does it for different scenarios. In the model both the weight of the rat and the initial osmolality and hypovolemia can be regulated. The model also responds to changes in osmotic pressure and can simulate this as for injections of CCK. Finally, it is straightforward to simulate the (partial) blockage of different currents, as the HAP, the AHP or the DAP or the blockage of excitatory or inhibitory inputs.

In relation to the response to CCK, the model supported something really difficult to notice just analysing electrophysiological data: the response of oxytocin neurones to CCK is quite independent of the basal firing rate. Unlike vasopressin neurones, oxytocin neurones always respond to CCK by increasing their spike activity. Even so, their spiking response to CCK is extremely variable (Maícas-Royo *et al.*, 2018), and it would require a massive amount of good recordings to get to a similar conclusion to the one the model can give in some minutes

Predictions beyond the oxytocin activity

The model allows to predict the behaviour of oxytocin neurones at any point of their dynamics. However, it can do even more. It allows us to infer what should be the necessary inputs, coming from other neurones, and their nature, when certain results are obtained. In other words, once I had an oxytocin model that could replicate the whole process of oxytocin neurones, from the spiking to the clearance in plasma, I had a model also able to predict which kind of input I must have to obtain a certain output. That was particularly useful in different circumstances.

The model suggests several things in relation to the inputs that oxytocin neurones receive. For instance, mimicking the response of oxytocin neurones to a systemic injection of CCK only requires excitatory inputs in the model.

The model also supported the theory that inhibitory inputs coming from the circumventricular organs are necessary for the response of oxytocin neurones under osmotic pressure, giving an idea of the relationship between the excitatory and the inhibitory inputs that oxytocin neurones receive in those circumstances.

Nevertheless, probably the most surprising result of the thesis was to find that the model predicted something, to our knowledge, not proposed before. Previous works found that hypovolemia increases oxytocin secretion. Because the mechanisms related to that are often entangled with osmotic pressure and blood pressure, experimentalists started simulating hypovolemia by injecting PEG. PEG reduces the plasma volume without changing the osmolality or the haematocrit. The resultant hypovolemia increases the concentration of oxytocin in plasma. However, the model is capable of simulating closely the PEG effect and it suggests that, at least, some of that increment in oxytocin concentration is not due to an increment of oxytocin secretion.

Next steps

There are different things that could be the natural steps to take after this work. Some of them would require months and some would probably require years of work, combining it with experiments in the laboratory.

A relatively easy step would include matching the current model with the experimental data that accounts for the oxytocin depletion (Leng *et al.*, 1994). Much bigger challenges would be to include oxytocin dendritic secretion and the synchronization between neurones that is patent during lactation and parturition. Currently, the model is limited to axonal secretion. That means that all the central oxytocin secretion is not contemplated in our model. It is known that oxytocin neurones are involved in processes of bonding and social behaviour in some mammals. They also modulate different processes related with food choice and food reward. That involvement comes from the oxytocin produced and secreted in the brain. Dendritic secretion shares some mechanisms with axonal secretion and it would be a natural next step to complete the model with the dendritic exocytosis.

The secretion and clearance models I have used should work to simulate bursting synchronized activity with some additions. Thus, a model capable of pulsatile secretion should be possible in not so much time considering that Rossoni *et al.* (2008) did that part before. The Rossoni's work also models the dendritic activity

necessary to produce the bursting activity present during breastfeeding or parturition. A more complete model, including dendritic activity associated with central processes, would take a bit longer. However, the effort should be lessened thanks to the work of my supervisor Duncan MacGregor, who has been working on a model for dendritic secretion in vasopressin neurones.

Another field where the model could be improved is the role of heterogeneity in oxytocin neurones. Generalising the behaviour of an average oxytocin cell gives good results in average when I want to simulate a whole population. The good results are robust if I look at the spiking activity. Introducing heterogeneity in the PSP rates does not change the results massively but we know the variability is necessary because it is impossible to mimic the experimental variability without introducing heterogeneity in our model.

Another source of variability could come from the fact that oxytocin neuron inputs are not independent, as I have been assuming in our model. Their inputs do not necessarily have a huge correlation either, but the global processes I have been trying to simulate, as the food intake, osmotic pressure or hypovolemia responses, are supposed to send similar signals to a widespread amount of the oxytocin neurones.

Something that I have not explored either in this work is the heterogeneity in the secretion. Once I fit the model to the experimental data, I kept the same parameter values for the rest of the experiments. Those parameter values made the secretion model for oxytocin neurones show no fatigue at spike rates up to 13 Hz, allowing a maintained secretion over time and a non-linear coupling to the spiking activity. The fact that I obtained very good results with that fitting values for the secretion model supports its robustness when I look at the average dynamics. However, it is probable that oxytocin neurones present heterogeneity in the secretion and that those differences play a role. On the other hand, there is not so much data of secretion from individual oxytocin neurones as there is for the spiking activity. The reason has to do with differences in measuring both dynamics. Spiking activity is measured in a simple way, as changes of voltage in the neurone's membrane. However, the secretion of each oxytocin neurone is related with hundreds of thousands of little signals. Each axon terminal contains about 2000 nerve terminals and swellings, where vesicles each containing ~85000 oxytocin molecules get attached, opening with a higher probability when the spikes arriving to the axon

terminal trigger the entrance of Ca^{2+} and the Ca^{2+} facilitates the exocytosis (Leng & Ludwig, 2008). As result, I decided to work with the average of the final secretion produced by the whole population of oxytocin neurones. However, new techniques such as two photon Ca^{2+} imaging can provide the data necessary to distinguish the secretory dynamics of single cells (Lang *et al.*, 1997) and this model could incorporate that knowledge.

A more complete model would give an interesting stepping stone to explore other populations of neurones which relate with the central activity of oxytocin. In the same way that a complete model for axonal oxytocin secretion led us to discover a hidden mechanism of hypovolemia or to support the necessity for the IPSPs in the osmotic response, a complete model for dendritic oxytocin secretion could help us to understand populations of neurones that are difficult to reach in the brain, but are known to receive or send their signals to oxytocin neurones. In particular, the interconnection between oxytocin and dopamine neurones and the reward system, involved both in eating behaviour and social interactions could be a reasonable medium-term goal.

References

Abrahams VC & Pickford M (1954). Simultaneous observations on the rate of urine flow and spontaneous uterine movements in the dog, and their relationship to posterior lobe activity. *J Physiol* **126,** 329–346.

Amico JA, Ervin MG, Leake RD, Fisher DA, Finn FM & Robinson AG (1985). A Novel Oxytocin-Like and Vasotocin-Like Peptide in Human Plasma after Administration of Estrogen. *J Clin Endocrinol Metab* **60,** 5–12.

Andersson B (1951). Some Observations on the Neuro-Hormonal Regulation of Milk-Ejection. *Acta Physiol Scand* **23,** 1–7.

Andrew RD & Dudek FE (1984). Analysis of intracellularly recorded phasic bursting by mammalian neuroendocrine cells. *J Neurophysiol* **51,** 552–566.

Anon (n.d.). CED Products | Spike2 life sciences data acquisition and analysis system. Available at: http://ced.co.uk/products/spike2 [Accessed October 30, 2015].

Anon (n.d.). wxWidgets: Cross-Platform GUI Library. Available at: http://wxwidgets.org/ [Accessed October 30, 2015].

Antunes-Rodrigues J, De Castro M, Elias LLK, Valença MM & McCANN SM (2004). Neuroendocrine Control of Body Fluid Metabolism. *Physiol Rev* **84,** 169–208.

Antunes-Rodrigues J, Machado BH, Andrade HA, Mauad H, Ramalho MJ, Reis LC, Silva-Netto CR, Favaretto AL, Gutkowska J & McCann SM (1992). Carotid-aortic and renal baroreceptors mediate the atrial natriuretic peptide release induced by blood volume expansion. *Proc Natl Acad Sci U S A* **89,** 6828–6831.

Anyakora C, Oni Y, Ezedinachi U, Adekoya A, Ali I, Nwachukwu C, Esimone C, Abiola V & Nwokike J (2018). Quality medicines in maternal health: results of oxytocin, misoprostol, magnesium sulfate and calcium gluconate quality audits. *BMC Pregnancy Childbirth*; DOI: 10.1186/s12884-018-1671-y.

Armstrong WE (1995). Morphological and electrophysiological classification of hypothalamic supraoptic neurons. *Prog Neurobiol* **47,** 291–339.

Armstrong WE, Stern JE & Teruyama R (2002). Plasticity in the electrophysiological properties of oxytocin neurons. *Microsc Res Tech* **56,** 73–80.

Armstrong WE, Wang L., Li C & Teruyama R (2010). Performance, properties and plasticity of identified oxytocin and vasopressin neurones in vitro. *J Neuroendocrinol* **22,** 330–342.

Arnold D (2013). *The age of discovery, 1400-1600*. Routledge.

Arrowsmith S & Wray S (2014). Oxytocin: Its Mechanism of Action and Receptor Signalling in the Myometrium. *J Neuroendocrinol* **26,** 356–369.

Aruoba SB & Fernández-Villaverde J (2015). A comparison of programming languages in macroeconomics. *J Econ Dyn Control* **58,** 265–273.

Bandaranayake RC (1971). Morphology of the accessory neurosecretory nuclei and of the retrochiasmatic part of the supraoptic nucleus of the rat. *Acta Anat (Basel)* **80,** 14–22.

Bardeen J & Brattain WH (1948). The Transistor, A Semi-Conductor Triode. *Phys Rev* **74,** 230–231.

Baskerville TA, Allard J, Wayman C & Douglas AJ (2009). Dopamine–oxytocin interactions in penile erection. *Eur J Neurosci* **30,** 2151–2164.

Belin V & Moos F (1986). Paired recordings from supraoptic and paraventricular oxytocin cells in suckled rats: recruitment and synchronization. *J Physiol* **377,** 369–390.

Bender KJ & Trussell LO (2012). The Physiology of the Axon Initial Segment. *Annu Rev Neurosci* **35,** 249–265.

Bennett S (1993). *A history of control engineering, 1930-1955*. IET.

Bhumbra GS & Dyball REJ (2004). Measuring spike coding in the rat supraoptic nucleus. *J Physiol* **555,** 281–296.

Bhumbra GS, Inyushkin AN & Dyball REJ (2004). Assessment of Spike Activity in the Supraoptic Nucleus. *J Neuroendocrinol* **16,** 390–397.

Bhumbra GS, Inyushkin AN, Syrimi M & Dyball REJ (2005). Spike coding during osmotic stimulation of the rat supraoptic nucleus. *J Physiol* **569,** 257–274.

Bicknell RJ (1988). Optimizing release from peptide hormone secretory nerve terminals. *J Exp Biol* **139,** 51–65.

Bicknell RJ, Brown D, Chapman C, Hancock PD & Leng G (1984). Reversible fatigue of stimulus-secretion coupling in the rat neurohypophysis. *J Physiol* **348,** 601–613.

Bicknell RJ, Ingram CD & Leng G (1983). Oxytocin release is inhibited by opiates from the neural lobe, not those from the intermediate lobe. *Neurosci Lett* **43,** 227–230.

Blackburn RE, Samson WK, Fulton RJ, Stricker EM & Verbalis JG (1995). Central oxytocin and ANP receptors mediate osmotic inhibition of salt appetite in rats. *Am J Physiol-Regul Integr Comp Physiol* **269,** R245–R251.

Boole G (1854). *An Investigation of the Laws of Thought: On which are Founded the Mathematical Theories of Logic and Probabilities*. Dover Publications.

Borag S & Fernández-Villaverde J (2018). A Comparison of Programming Languages in Economics: An Update. 4.

Borges RR, Borges FS, Lameu EL, Batista AM, Iarosz KC, Caldas IL, Viana RL & Sanjuán MAF (2016). Effects of the spike timing-dependent plasticity on the synchronisation in a random Hodgkin–Huxley neuronal network. *Commun Nonlinear Sci Numer Simul* **34,** 12–22.

Bourque CW (1990). Intraterminal recordings from the rat neurohypophysis in vitro. *J Physiol* **421,** 247–262.

Bourque CW (2008). Central mechanisms of osmosensation and systemic osmoregulation. *Nat Rev Neurosci* **9,** 519–531.

Bourque CW & Brown DA (1987). Apamin and d-tubocurarine block the after-hyperpolarization of rat supraoptic neurosecretory neurons. *Neurosci Lett* **82,** 185–190.

Bourque CW, Randle JC & Renaud LP (1985). Calcium-dependent potassium conductance in rat supraoptic nucleus neurosecretory neurons. *J Neurophysiol* **54,** 1375–1382.

Brimble MJ & Dyball REJ (1977). Characterization of the responses of oxytocin- and vasopressin-secreting neurones in the supraoptic nucleus to osmotic stimulation. *J Physiol* **271,** 253–271.

Brown CH, Bains JS, Ludwig M & Stern JE (2013). Physiological regulation of magnocellular neurosecretory cell activity: Integration of intrinsic, local and afferent mechanisms. *J Neuroendocrinol*; DOI: 10.1111/jne.12051.

Brown CH, Munro G, Murphy NP, Leng G & Russell JA (1996). Activation of oxytocin neurones by systemic cholecystokinin is unchanged by morphine dependence or withdrawal excitation in the rat. *J Physiol* **496,** 787–794.

Brown CH, Russell JA & Leng G (2000). Opioid modulation of magnocellular neurosecretory cell activity. *Neurosci Res* **36,** 97–120.

Brunton PJ, Sabatier N, Leng G & Russell JA (2006). Suppressed oxytocin neuron responses to immune challenge in late pregnant rats: a role for endogenous opioids. *Eur J Neurosci* **23,** 1241–1247.

Buckley CW (1924). Discussion on Diuresis: President's Address and Introduction to the Discussion. *Proc R Soc Med* **17,** 11–17.

Bull PM, Russell JA, Scott V & Brown CH (2011). Apamin increases post-spike excitability of supraoptic nucleus neurons in anaesthetized morphine-naïve rats and morphine-dependent rats: consequences for morphine withdrawal excitation. *Exp Brain Res* **212,** 517–528.

Burkert W (1972). *Lore and science in ancient Pythagoreanism*. Harvard University Press, Cambridge, Mass.

Burkitt AN (2006). A Review of the Integrate-and-fire Neuron Model: I. Homogeneous Synaptic Input. *Biol Cybern* **95,** 1–19.

Buzsáki G (2004). Large-scale recording of neuronal ensembles. *Nat Neurosci* **7,** 446–451.

Carey RM & Siragy HM (2003). Newly Recognized Components of the Renin-Angiotensin System: Potential Roles in Cardiovascular and Renal Regulation. *Endocr Rev* **24,** 261–271.

Carolyn A. Bondy HG (1987). Effects of stimulus frequency and potassium channel blockade on the secretion of vasopressin and oxytocin from the neurohypophysis. *Neuroendocrinology* **46,** 258–267.

Choe KY, Trudel E & Bourque CW (2016). Effects of Salt Loading on the Regulation of Rat Hypothalamic Magnocellular Neurosecretory Cells by Ionotropic GABA and Glycine Receptors. *J Neuroendocrinol*; DOI: 10.1111/jne.12372.

Coote JH (2005). A role for the paraventricular nucleus of the hypothalamus in the autonomic control of heart and kidney. *Exp Physiol* **90,** 169–173.

Cross BA & Green JD (1959). Activity of single neurones in the hypothalamus: effect of osmotic and other stimuli. *J Physiol* **148,** 554–569.

Curry F-RE (2005). Atrial natriuretic peptide: an essential physiological regulator of transvascular fluid, protein transport, and plasma volume. *J Clin Invest* **115,** 1458–1461.

Dale HH (1906). On some physiological actions of ergot. *J Physiol* **34,** 163–206.

Day NC, Hall MD & Hughes J (1989). Modulation of hypothalamic cholecystokinin receptor density with changes in magnocellular activity: A quantitative autoradiographic study. *Neuroscience* **29,** 371–383.

Debanne D, Campanac E, Bialowas A, Carlier E & Alcaraz G (2011). Axon Physiology. *Physiol Rev* **91,** 555–602.

Dicks DR (1970). *Early Greek astronomy to Aristotle*. Cornell University Press, New York.

Donaldson ZR & Young LJ (2008). Oxytocin, Vasopressin, and the Neurogenetics of Sociality. *Science* **322,** 900–904.

Dunn FL, Brennan TJ, Nelson AE & Robertson GL (1973). The Role of Blood Osmolality and Volume in Regulating Vasopressin Secretion in the Rat. *J Clin Invest* **52,** 3212–3219.

Dyball RE, Grossmann R, Leng G & Shibuki K (1988). Spike propagation and conduction failure in the rat neural lobe. *J Physiol* **401,** 241–256.

Dyball REJ & McKenzie1 DN (2000). Synchronized clusters of action potentials can increase or decrease the excitability of the axons of magnocellular hypothalamic neurosecretory cells. *J Neuroendocrinol* **12,** 729–735.

Engels D (1985). The Length of Eratosthenes' Stade. *Am J Philol* **106,** 298–311.

Fabian M, Forsling ML, Jones JJ & Lee J (1969*a*). The release, clearance and plasma protein binding of oxytocin in the anaesthetized rat. *J Endocrinol* **43,** 175–189.

Fabian M, Forsling ML, Jones JJ & Pryor JS (1969*b*). The clearance and antidiuretic potency of neurohypophysial hormones in man, and their plasma binding and stability. *J Physiol* **204,** 653.

Fenno L, Yizhar O & Deisseroth K (2011). The Development and Application of Optogenetics. *Annu Rev Neurosci* **34,** 389–412.

Fisher TE & Bourque CW (2001). The function of Ca2+ channel subtypes in exocytotic secretion: new perspectives from synaptic and non-synaptic release. *Prog Biophys Mol Biol* **77,** 269–303.

Fong CTO, Silver L, Christman DR & Schwartz IL (1960). On the Mechanism of Action of the Antidiuretic Hormone (vasopressin). *Proc Natl Acad Sci* **46,** 1273–1277.

Forsling ML (1986). Regulation of Oxytocin Release. In *Neurobiology of Oxytocin*, ed. Ganten D & Pfaff D, Current Topics in Neuroendocrinology, pp. 19–53. Springer Berlin Heidelberg, Berlin, Heidelberg.

Freund-Mercier MJ, Stoeckel ME & Klein MJ (1994). Oxytocin receptors on oxytocin neurones: histoautoradiographic detection in the lactating rat. *J Physiol* **480,** 155–161.

Gainer H, Wolfe SA, Obaid AL & Salzberg BM (1986). Action potentials and frequency-dependent secretion in the mouse neurohypophysis. *Neuroendocrinology* **43,** 557–563.

Ghamari-Langroudi M & Bourque CW (1998). Caesium blocks depolarizing after-potentials and phasic firing in rat supraoptic neurones. *J Physiol* **510,** 165–175.

Ghamari-Langroudi M & Bourque CW (2002). Flufenamic acid blocks depolarizing afterpotentials and phasic firing in rat supraoptic neurones. *J Physiol* **545,** 537–542.

Ghamari-Langroudi M & Bourque CW (2004). Muscarinic Receptor Modulation of Slow Afterhyperpolarization and Phasic Firing in Rat Supraoptic Nucleus Neurons. *J Neurosci* **24,** 7718–7726.

Ginsburg M (1954). The secretion of antidiuretic hormone in response to haemorrhage and the fate of vasopressin in adrenalectomized rats. *J Endocrinol* **11,** 165–176.

Ginsburg M & Smith MW (1959). The fate of oxytocin in male and female rats. *Br J Pharmacol Chemother* **14,** 327–333.

Goldstein BR (1984). Eratosthenes on the “measurement” of the earth. *Hist Math* **11,** 411–416.

Greffrath W, Magerl W, Disque-Kaiser U, Martin E, Reuss S & Boehmer G (2004). Contribution of Ca2+-Activated K+ Channels to Hyperpolarizing After-Potentials and Discharge Pattern in Rat Supraoptic Neurones. *J Neuroendocrinol* **16,** 577–588.

Greffrath W, Martin E, Reuss S & Boehmer G (1998). Components of after-hyperpolarization in magnocellular neurones of the rat supraoptic nucleus in vitro. *J Physiol* **513,** 493–506.

Harris GW (1951). Neural Control of the Pituitary Gland.—I. *Br Med J* **2,** 559–564.

Haselton JR & Vari RC (1998). Neuronal cell bodies in paraventricular nucleus affect renal hemodynamics and excretion via the renal nerves. *Am J Physiol-Regul Integr Comp Physiol* **275,** R1334–R1342.

Hatton GI & Li Z –H. (1999). Chapter 2.1.2 Neurophysiology of magnocellular neuroendocrine cells: Recent advances. *Prog Brain Res* **119,** 77–99.

Hatton GI & Wang Y-F (2008). Neural mechanisms underlying the milk ejection burst and reflex. In *Progress in brain research*, ed. Landgraf IDN and R, Advances in vasopressin and oxytocin — From genes to behaviour to disease, pp. 155–166. Elsevier.

Heesch CM (1999). Reflexes that control cardiovascular function. *Adv Physiol Educ* **277,** S234.

Herbison AE (1994). Immunocytochemical Evidence for Oestrogen Receptors within GABA Neurones Located in the Perinuclear Zone of the Supraoptic Nucleus and GABAA Receptor β2/β3 Subunits on Supraoptic Oxytocin Neurones. *J Neuroendocrinol* **6,** 5–11.

Herculano-Houzel S & Lent R (2005). Isotropic Fractionator: A Simple, Rapid Method for the Quantification of Total Cell and Neuron Numbers in the Brain. *J Neurosci* **25,** 2518–2521.

Herget U, Gutierrez-Triana JA, Salazar Thula O, Knerr B & Ryu S (2017). Single-cell reconstruction of oxytocinergic neurons reveals separate hypophysiotropic and encephalotropic subtypes in larval zebrafish. *eNeuro*; DOI: 10.1523/ENEURO.0278-16.2016.

Higuchi T, Honda K, Fukuoka T, Negoro H & Wakabayashi K (1985). Release of oxytocin during suckling and parturition in the rat. *J Endocrinol* **105,** 339–346.

Higuchi T, Honda K, Takano S & Negoro H (1988). Reduced oxytocin response to osmotic stimulus and immobilization stress in lactating rats. *J Endocrinol* **116,** 225–230.

Hodgkin AL & Huxley AF (1952). A quantitative description of membrane current and its application to conduction and excitation in nerve. *J Physiol* **117,** 500–544.

Hsu HK & Peng MT (1978). Hypothalamic Neuron Number of Old Female Rats. *Gerontology* **24,** 434–440.

Huang W, Lee SL, Arnason SS & Sjoquist M (1996). Dehydration natriuresis in male rats is mediated by oxytocin. *Am J Physiol-Regul Integr Comp Physiol* **270,** R427–R433.

Huang W, Lee SL & Sjoquist M (1995). Natriuretic role of endogenous oxytocin in male rats infused with hypertonic NaCl. *Am J Physiol-Regul Integr Comp Physiol* **268,** R634–R640.

Hume C, Sabatier N & Menzies J (2017). High-Sugar, but Not High-Fat, Food Activates Supraoptic Nucleus Neurons in the Male Rat. *Endocrinology* **158,** 2200–2211.

Izhikevich EM (2004). Which Model to Use for Cortical Spiking Neurons? *IEEE Trans Neural Netw* **15,** 1063–1070.

Jackson MB, Konnerth A & Augustine GJ (1991). Action potential broadening and frequency-dependent facilitation of calcium signals in pituitary nerve terminals. *Proc Natl Acad Sci* **88,** 380–384.

Järvelä K, Koskinen M & Kööbi T (2003). Effects of hypertonic saline (7.5%) on extracellular fluid volumes in healthy volunteers. *Anaesthesia* **58,** 878–881.

Jebbink M, Jansen J, Masclee A & Lamers C (1990). Lack of effect of the specific cholecystokinin receptor antagonist loxiglumide on cholecystokinin clearance from plasma in man. *Br J Clin Pharmacol* **29,** 770–773.

Kamm O, Aldrich TB, Grote IW, Rowe LW & Bugbee EP (1928). The active principles of the posterior lobe of the pituitary gland. 1 i. the demonstration of the presence of two active principles. ii. the separation of the two principles and their concentration in the form of potent solid preparations. *J Am Chem Soc* **50,** 573–601.

Katoh A, Shoguchi K, Matsuoka H, Yoshimura M, Ohkubo J-I, Matsuura T, Maruyama T, Ishikura T, Aritomi T, Fujihara H, Hashimoto H, Suzuki H, Murphy D & Ueta Y (2014). Fluorescent Visualisation of the Hypothalamic Oxytocin Neurones Activated by Cholecystokinin-8 in Rats Expressing c-fos-Enhanced Green Fluorescent Protein and Oxytocin-Monomeric Red Fluorescent Protein 1 Fusion Transgenes. *J Neuroendocrinol* **26,** 341–347.

Katz B & Miledi R (1970). Further study of the role of calcium in synaptic transmission. *J Physiol* **207,** 789–801.

Kim CK, Adhikari A & Deisseroth K (2017). Integration of optogenetics with complementary methodologies in systems neuroscience. *Nat Rev Neurosci* **18,** 222–235.

Kirkpatrick K & Bourque CW (1996). Activity dependence and functional role of the apamin-sensitive K+ current in rat supraoptic neurones in vitro. *J Physiol* **494,** 389–398.

Knobloch HS & Grinevich V (2014). Evolution of oxytocin pathways in the brain of vertebrates. *Front Behav Neurosci*; DOI: 10.3389/fnbeh.2014.00031.

Knott TK, Marrero HG, Custer EE & Lemos JR (2008). Endogenous ATP potentiates only vasopressin secretion from neurohypophysial terminals. *J Cell Physiol* **217,** 155–161.

Knott TK, Marrero HG, Fenton RA, Custer EE, Dobson JG & Lemos JR (2007). Endogenous adenosine inhibits CNS terminal Ca2+ currents and exocytosis. *J Cell Physiol* **210,** 309–314.

Koetsier T (2001). On the prehistory of programmable machines: musical automata, looms, calculators. *Mech Mach Theory* **36,** 589–603.

Kosmak GW (1918). The use and abuse of pituitary extract. *J Am Med Assoc* **71,** 1117–1120.

Lang T, Wacker I, Steyer J, Kaether C, Wunderlich I, Soldati T, Gerdes H-H & Almers W (1997). Ca2+-Triggered Peptide Secretion in Single Cells Imaged with Green Fluorescent Protein and Evanescent-Wave Microscopy. *Neuron* **18,** 857–863.

Lapicque L (1907). Recherches quantitatives sur l'excitation electrique des nerfs traitee comme une polarization. *J Physiol Pathol Gen* **9,** 620–635.

Lee MR, Scheidweiler KB, Diao XX, Akhlaghi F, Cummins A, Huestis MA, Leggio L & Averbeck BB (2018). Oxytocin by intranasal and intravenous routes reaches the cerebrospinal fluid in rhesus macaques: determination using a novel oxytocin assay. *Mol Psychiatry* **23,** 115–122.

Lemos JR, Ortiz-Miranda SI, Cuadra AE, Velázquez-Marrero C, Custer EE, Dad T & Dayanithi G (2012). Modulation/physiology of calcium channel sub-types in neurosecretory terminals. *Cell Calcium* **51,** 284–292.

Leng G (2018*a*). *The Heart of the Brain: The hypothalamus and its hormones*. MIT Press.

Leng G (2018*b*). The endocrinology of the brain. *Endocr Connect* **7,** R275–R285.

Leng G, Bicknell RJ, Brown D, Bowden C, Chapman C & Russell JA (1994). Stimulus-Induced Depletion of Pro-Enkephalins, Oxytocin and Vasopressin and Pro-Enkephalin Interaction with Posterior Pituitary Hormone Release in vitro. *Neuroendocrinology* **60,** 559–566.

Leng G, Brown CH, Bull PM, Brown D, Scullion S, Currie J, Blackburn-Munro RE, Feng J, Onaka T, Verbalis JG, Russell JA & Ludwig M (2001). Responses of magnocellular neurons to osmotic stimulation involves coactivation of excitatory and inhibitory input: an experimental and theoretical analysis. *J Neurosci* **21,** 6967–6977.

Leng G, Brown CH & Russell JA (1999). Physiological pathways regulating the activity of magnocellular neurosecretory cells. *Prog Neurobiol* **57,** 625–655.

Leng G & Brown D (1997). The origins and significance of pulsatility in hormone secretion from the pituitary. *J Neuroendocrinol* **9,** 493–513.

Leng G, Dyball RE & Way SA (1992). Naloxone potentiates the release of oxytocin induced by systemic administration of cholecystokinin without enhancing the electrical activity of supraoptic oxytocin neurones. *Exp Brain Res* **88,** 321–325.

Leng G, Dye S & Bicknell RJ (1997). Kappa-opioid restraint of oxytocin secretion: plasticity through pregnancy. *Neuroendocrinology* **66,** 378–383.

Leng G & Ludwig M (2008). Neurotransmitters and peptides: whispered secrets and public announcements. *J Physiol* **586,** 5625–5632.

Leng G & MacGregor DJ (2008). Mathematical Modelling in Neuroendocrinology. *J Neuroendocrinol* **20,** 713–718.

Leng G, Onaka T, Caquineau C, Sabatier N, Tobin VA & Takayanagi Y (2008). Oxytocin and appetite. *Prog Brain Res* **170,** 137–151.

Leng G, Pineda R, Sabatier N & Ludwig M (2015). The posterior pituitary: from Geoffrey Harris to our present understanding. *J Endocrinol*JOE-15-0087.

Leng G & Sabatier N (2014). Electrophysiology of Magnocellular Neurons in Vivo. In *Neurophysiology of Neuroendocrine Neurons*, pp. 1–28. John Wiley & Sons, Ltd.

Leng G & Sabatier N (2016). Measuring Oxytocin and Vasopressin: Bioassays, Immunoassays and Random Numbers. *J Neuroendocrinol*; DOI: 10.1111/jne.12413.

Leng G & Sabatier N (2017). Oxytocin – The sweet hormone? *Trends Endocrinol Metab* **28,** 365–376.

Leng G, Way S & Dyball REJ (1991). Identification of oxytoxin cells in the rat supraoptic nucleus by their response to cholecystokinin injection. *Neurosci Lett* **122,** 159–162.

Leng T, Leng G & MacGregor DJ (2017). Spike patterning in oxytocin neurons: Capturing physiological behaviour with Hodgkin-Huxley and integrate-and-fire models. *PLOS ONE* **12,** e0180368.

Levitan IB & Kaczmarek LK (2015). *The neuron: cell and molecular biology*. Oxford University Press, USA.

Li C, Tripathi PK & Armstrong WE (2007). Differences in spike train variability in rat vasopressin and oxytocin neurons and their relationship to synaptic activity. *J Physiol* **581,** 221–240.

Li Z & Hatton GI (1997). Reduced outward K+ conductances generate depolarizing after-potentials in rat supraoptic nucleus neurones. *J Physiol* **505,** 95–106.

Luckman SM, Hamamura M, Antonijevic I, Dye S & Leng G (1993). Involvement of cholecystokinin receptor types in pathways controlling oxytocin secretion. *Br J Pharmacol* **110,** 378–384.

Ludwig M (1998). Dendritic release of vasopressin and oxytocin. *J Neuroendocrinol* **10,** 881–895.

Ludwig M & Leng G (2006). Dendritic peptide release and peptide-dependent behaviours. *Nat Rev Neurosci* **7,** 126–136.

Ludwig M, Sabatier N, Bull PM, Landgraf R, Dayanithi G & Leng G (2002). Intracellular calcium stores regulate activity-dependent neuropeptide release from dendrites. *Nature* **418,** 85–89.

MacGregor DJ & Leng G (2012). Phasic Firing in Vasopressin Cells: Understanding Its Functional Significance through Computational Models. *PLoS Comput Biol* **8,** e1002740.

MacGregor DJ & Leng G (2013). Spike triggered hormone secretion in vasopressin cells; a model investigation of mechanism and heterogeneous population function. *PLoS Comput Biol* **9,** e1003187.

MacGregor DJ, Williams CKI & Leng G (2009). A new method of spike modelling and interval analysis. *J Neurosci Methods* **176,** 45–56.

Maícas-Royo J, Brown CH, Leng G & MacGregor DJ (2016). Oxytocin Neurones: Intrinsic Mechanisms Governing the Regularity of Spiking Activity. *J Neuroendocrinol* **28,** n/a-n/a.

Maícas-Royo J, Leng G & MacGregor DJ (2018). A Predictive, Quantitative Model of Spiking Activity and Stimulus-Secretion Coupling in Oxytocin Neurons. *Endocrinology* **159,** 1433–1452.

Mansvelder HD & Kits KS (2000). Calcium channels and the release of large dense core vesicles from neuroendocrine cells: spatial organization and functional coupling. *Prog Neurobiol* **62,** 427–441.

Marrero HG & Lemos JR (2003). Loose-patch clamp currents from the hypothalamo-neurohypophysial system of the rat. *Pflüg Arch* **446,** 702–713.

Matsukawa T & Miyamoto T (2010). Angiotensin II-stimulated secretion of arginine vasopressin is inhibited by atrial natriuretic peptide in humans. *Am J Physiol-Regul Integr Comp Physiol* **300,** R624–R629.

Mazzoni MC, Borgstrom P, Arfors K-E & Intaglietta M (1988). Dynamic fluid redistribution in hyperosmotic resuscitation of hypovolemic hemorrhage. *Am J Physiol-Heart Circ Physiol* **255,** H629–H637.

McCann MJ, Verbalis JG & Stricker EM (1989). LiCl and CCK inhibit gastric emptying and feeding and stimulate OT secretion in rats. *Am J Physiol* **256,** R463–R468.

McCartney S (1999). *ENIAC: The triumphs and tragedies of the world's first computer*. Walker & Company.

McKinley MJ, Mathai ML, McAllen RM, McClear RC, Miselis RR, Pennington GL, Vivas L, Wade JD & Oldfield BJ (2004). Vasopressin Secretion: Osmotic and Hormonal Regulation by the Lamina Terminalis. *J Neuroendocrinol* **16,** 340–347.

McKinley MJ, McAllen RM, Davern PJ, Giles ME, Penschow J, Sunn N, Uschakov A & Oldfield B (2003). *The sensory circumventricular organs of the mammalian brain: subfornical organ, OVLT and area postrema*. Springer Science & Business Media.

McNally JM, Custer EE, Ortiz-Miranda S, Woodbury DJ, Kraner SD, Salzberg BM & Lemos JR (2014). Functional ryanodine receptors in the membranes of neurohypophysial secretory granules. *J Gen Physiol* **143,** 693–702.

Mens WBJ, Witter A & Van Wimersma Greidanus TB (1983). Penetration of neurohypophyseal hormones from plasma into cerebrospinal fluid (CSF): Half-times of disappearance of these neuropeptides from CSF. *Brain Res* **262,** 143–149.

Morton GJ, Meek TH & Schwartz MW (2014). Neurobiology of food intake in health and disease. *Nat Rev Neurosci* **15,** 367–378.

Muschol M & Salzberg BM (2000). Dependence of Transient and Residual Calcium Dynamics on Action-Potential Patterning during Neuropeptide Secretion. *J Neurosci* **20,** 6773–6780.

de Navarrete MF (1837). *Expediciones al Maluco, viage de Magallanes y de Elcano*. Imprenta Nacional. Available at: https://books.google.es/books?id=-FnUAAAAMAAJ.

Neher E (2012). Introduction: Regulated exocytosis. *Cell Calcium* **52,** 196–198.

Nordmann JJ & Morris JF (1984). Method for quantitating the molecular content of a subcellular organelle: hormone and neurophysin content of newly formed and aged neurosecretory granules. *Proc Natl Acad Sci* **81,** 180–184.

Nowycky MC, Seward EP & Chernevskaya NI (1998). Excitation–secretion coupling in mammalian neurohypophysial nerve terminals. *Cell Mol Neurobiol* **18,** 65–80.

Nudge-it (n.d.). Nudge-it. Available at: https://www.nudge-it.eu/ [Accessed October 9, 2018].

Oliet SH & Bourque CW (1992). Properties of supraoptic magnocellular neurones isolated from the adult rat. *J Physiol* **455,** 291–306.

Oliver G & Schäfer EA (1895). On the Physiological Action of Extracts of Pituitary Body and certain other Glandular Organs. *J Physiol* **18,** 277–279.

Olszewski PK, Klockars A & Levine AS (2016). Oxytocin: A Conditional Anorexigen whose Effects on Appetite Depend on the Physiological, Behavioural and Social Contexts. *J Neuroendocrinol*; DOI: 10.1111/jne.12376.

Onaka T, Luckman SM, Antonijevic I, Palmer JR & Leng G (1995). Involvement of the noradrenergic afferents from the nucleus tractus solitarii to the supraoptic nucleus in oxytocin release after peripheral cholecystokinin octapeptide in the rat. *Neuroscience* **66,** 403–412.

Ott I & Scott JC (1910). The action of infundibulin upon the mammary secretion. *Proc Soc Exp Biol Med* **8,** 48–49.

Paiva L, Sabatier N, Leng G & Ludwig M (2017). Effect of Melanotan-II on Brain Fos Immunoreactivity and Oxytocin Neuronal Activity and Secretion in Rats. *J Neuroendocrinol*; DOI: 10.1111/jne.12454.

Panda S, Kumar NM & Sarkar CK (2009). Transistor count optimization of conventional CMOS full adder amp; optimization of power and delay of new implementation of 18 transistor full adder by dual threshold node design with submicron channel length. In *2009 4th International Conference on Computers and Devices for Communication (CODEC)*, pp. 1–4.

Perlmutter LS, Tweedle CD & Hatton GI (1984). Neuronal/glial plasticity in the supraoptic dendritic zone: Dendritic bundling and double synapse formation at parturition. *Neuroscience* **13,** 769–779.

Phillips IM (1987). Functions of Angiotensin in the Central Nervous System. *Annu Rev Physiol* **49,** 413–433.

Pigafetta A (1986). *Primer viaje alrededor del globo*. Orbis, Barcelona.

Pittman JQ, Kombian SB, Mouginot D, Chen X & van Eerdenberg FJCM (1999). Electrophysiological studies of neurohypophysial neurons and peptides. *Prog Brain Res* **119,** 311–320.

Prager-Khoutorsky M & Bourque CW (2015). Mechanical Basis of Osmosensory Transduction in Magnocellular Neurosecretory Neurones of the Rat Supraoptic Nucleus. *J Neuroendocrinol* **27,** 507–515.

Randle JCR, Mazurek M, Kneifel D, Dufresne J & Renaud LP (1986). α1-Adrenergic receptor activation releases vasopressin and oxytocin from perfused rat hypothalamic explants. *Neurosci Lett* **65,** 219–223.

Rasmussen MS, Simonsen JA, Sandgaard NCF, Høilund-Carlsen PF & Bie P (2003). Mechanisms of acute natriuresis in normal humans on low sodium diet. *J Physiol* **546,** 591–603.

Rasmussen MS, Simonsen JA, Sandgaard NCF, Høilund-Carlsen PF & Bie P (2004). Effects of oxytocin in normal man during low and high sodium diets. *Acta Physiol Scand* **181,** 247–257.

Renaud LP, Tang M, McCann MJ, Stricker EM & Verbalis JG (1987). Cholecystokinin and gastric distension activate oxytocinergic cells in rat hypothalamus. *Am J Physiol* **253,** R661-665.

Rhodes CH, Morriell JI & Pfaff DW (1981). Immunohistochemical analysis of magnocellular elements in rat hypothalamus: Distribution and numbers of cells containing neurophysin, oxytocin, and vasopressin. *J Comp Neurol* **198,** 45–64.

Richard D & Bourque CW (1995). Synaptic control of rat supraoptic neurones during osmotic stimulation of the organum vasculosum lamina terminalis in vitro. *J Physiol* **489,** 567–577.

Richard P, Moos F, Dayanithi G, Gouzènes L & Sabatier N (1997). Rhythmic activities of hypothalamic magnocellular neurons: Autocontrol mechanisms. *Biol Cell* **89,** 555–560.

Rinaman L, Hoffman GE, Dohanics J, Le W-W, Stricker EM & Verbalis JG (1995). Cholecystokinin activates catecholaminergic neurons in the caudal medulla that innervate the paraventricular nucleus of the hypothalamus in rats. *J Comp Neurol* **360,** 246–256.

Ringrose CAD (1962). The Obstetrical Use of Ergot: A Violation of the Doctrine "Primum Non Nocere." *Can Med Assoc J* **87,** 712–714.

Roper P, Callaway J, Shevchenko T, Teruyama R & Armstrong W (2003). AHP's, HAP's and DAP's: How Potassium Currents Regulate the Excitability of Rat Supraoptic Neurones. *J Comput Neurosci* **15,** 367–389.

Rossoni E, Feng J, Tirozzi B, Brown D, Leng G & Moos F (2008). Emergent Synchronous Bursting of Oxytocin Neuronal Network. *PLOS Comput Biol* **4,** e1000123.

Russell JA & Leng G (1998). Sex, parturition and motherhood without oxytocin? *J Endocrinol* **157,** 343–359.

Sabatier N, Brown CH, Ludwig M & Leng G (2004). Phasic spike patterning in rat supraoptic neurones in vivo and in vitro. *J Physiol* **558,** 161–180.

Sabatier N, Leng G & Menzies J (2013). Oxytocin, Feeding, and Satiety. *Front Endocrinol*; DOI: 10.3389/fendo.2013.00035.

Sah P (1996). Ca2+-activated K+ currents in neurones: types, physiological roles and modulation. *Trends Neurosci* **19,** 150–154.

Sannino S, Chini B & Grinevich V (2017). Lifespan oxytocin signaling: Maturation, flexibility, and stability in newborn, adolescent, and aged brain. *Dev Neurobiol* **77,** 158–168.

Schadt JC & Ludbrook J (1991). Hemodynamic and neurohumoral responses to acute hypovolemia in conscious mammals. *Am J Physiol-Heart Circ Physiol* **260,** H305–H318.

Schiff PL (2006). Ergot and Its Alkaloids. *Am J Pharm Educ*. Available at: https://www.ncbi.nlm.nih.gov/pmc/articles/PMC1637017/ [Accessed September 3, 2018].

Seward EP, Chernevskaya NI & Nowycky MC (1995). Exocytosis in peptidergic nerve terminals exhibits two calcium- sensitive phases during pulsatile calcium entry. *J Neurosci* **15,** 3390–3399.

Share L (1988). Role of vasopressin in cardiovascular regulation. *Physiol Rev* **68,** 1248–1284.

Sharpey-Schafer EA & Mackenzie K (1911). The action of animal extracts on milk secretion. *Proc R Soc Lond B* **84,** 16–22.

Sheng H-P & Huggins RA (1979). A review of body composition studies with emphasis on total body water and fat. *Am J Clin Nutr* **32,** 630–647.

Shioda S, Nakajo S, Hirabayashi T, Nakayama H, Nakaya K, Matsuda K & Nakai Y (1997). Neuronal nicotinic acetylcholine receptor in the hypothalamus: morphological diversity and neuroendocrine regulations. *Mol Brain Res* **49,** 45–54.

Sidel VW & Solomon AK (1957). Entrance of Water into Human Red Cells Under an Osmotic Pressure Gradient. *J Gen Physiol* **41,** 243–257.

Smith BN & Armstrong WE (1993). Histamine enhances the depolarizing afterpotential of immunohistochemically identified vasopressin neurons in the rat supraoptic nucleus via H1-receptor activation. *Neuroscience* **53,** 855–864.

Smith DW & Day TA (1995). Hypovolaemic and osmotic stimuli induce distinct patterns of c-Fos expression in the rat subfornical organ. *Brain Res* **698,** 232–236.

Smith DW & Day TA (2003). Catecholamine and oxytocin cells respond to hypovolaemia as well as hypotension. *Neuroreport* **14,** 1493–1495.

Smith TC (1892). The use of ergot in the second stage of labor. *Am J Obstet Dis Women Child 1869-1919* **26,** 895.

Sokol HW & Valtin H (1967). Evidence for the Synthesis of Oxytocin and Vasopressin in Separate Neurons. *Nature* **214,** 314–316.

Stamatakis AM, Schachter MJ, Gulati S, Zitelli KT, Malanowski S, Tajik A, Fritz C, Trulson M & Otte SL (2018). Simultaneous Optogenetics and Cellular Resolution Calcium Imaging During Active Behavior Using a Miniaturized Microscope. *Front Neurosci*; DOI: 10.3389/fnins.2018.00496.

Stern JE & Armstrong WE (1996). Changes in the Electrical Properties of Supraoptic Nucleus Oxytocin and Vasopressin Neurons during Lactation. *J Neurosci* **16,** 4861–4871.

Stricker EM, Hosutt JA & Verbalis JG (1987). Neurohypophyseal secretion in hypovolemic rats: inverse relation to sodium appetite. *Am J Physiol-Regul Integr Comp Physiol* **252,** R889–R896.

Stricker EM & Verbalis JG (1986). Interaction of osmotic and volume stimuli in regulation of neurohypophyseal secretion in rats. *Am J Physiol-Regul Integr Comp Physiol* **250,** R267–R275.

Takekawa T, Isomura Y & Fukai T (2010). Accurate spike sorting for multi-unit recordings. *Eur J Neurosci* **31,** 263–272.

Tansey EM (2006). Henry Dale and the discovery of acetylcholine. *C R Biol* **329,** 419–425.

Teruyama R & Armstrong WE (2005). Enhancement of calcium-dependent afterpotentials in oxytocin neurons of the rat supraoptic nucleus during lactation. *J Physiol* **566,** 505–518.

Teruyama R & Armstrong WE (2007). Calcium-dependent fast depolarizing afterpotentials in vasopressin neurons in the rat supraoptic nucleus. *J Neurophysiol* **98,** 2612–2621.

Tobin VA, Douglas AJ, Leng G & Ludwig M (2011). The Involvement of Voltage-Operated Calcium Channels in Somato-Dendritic Oxytocin Release. *PLOS ONE* **6,** e25366.

Velázquez-Marrero CM, Marrero HG & Lemos JR (2010). Voltage-dependent κ-opioid modulation of action potential waveform-elicited calcium currents in neurohypophysial terminals. *J Cell Physiol* **225,** 223–232.

Velmurugan S, Brunton PJ, Leng G & Russell JA (2010). Circulating secretin activates supraoptic nucleus oxytocin and vasopressin neurons via noradrenergic pathways in the rat. *Endocrinology* **151,** 2681–2688.

Velmurugan S, Russell JA & Leng G (2013). Systemic leptin increases the electrical activity of supraoptic nucleus oxytocin neurones in virgin and late pregnant rats. *J Neuroendocrinol* **25,** 383–390.

Verbalis JG (2007). How Does the Brain Sense Osmolality? *J Am Soc Nephrol* **18,** 3056–3059.

Verbalis JG, Baldwin EF & Robinson AG (1986). Osmotic regulation of plasma vasopressin and oxytocin after sustained hyponatremia. *Am J Physiol* **250,** R444-451.

Verbalis JG & Dohanics J (1991). Vasopressin and oxytocin secretion in chronically hyposmolar rats. *Am J Physiol* **261,** R1028-1038.

Verbalis JG, Mangione MP & Stricker EM (1991). Oxytocin produces natriuresis in rats at physiological plasma concentrations. *Endocrinology* **128,** 1317–1322.

du Vigneaud V, Ressler C, Swan JM, Roberts CW & Katsoyannis PG (1954). The Synthesis of Oxytocin1. *J Am Chem Soc* **76,** 3115–3121.

Vygotsky LS (1980). *Mind in society: The development of higher psychological processes*. Harvard university press.

Wakerley JB & Lincoln DW (1973). The milk-ejection reflex of the rat: a 20- to 40-fold acceleration in the firing of paraventricular neurones during oxytocin release. *J Endocrinol* **57,** 477–493.

Wakerley JB, Poulain DA & Brown D (1978). Comparison of firing patterns in oxytocin- and vasopressin-releasing neurones during progressive dehydration. *Brain Res* **148,** 425–440.

Wang L, Ennis M, Szabó G & Armstrong WE (2015). Characteristics of GABAergic and cholinergic neurons in perinuclear zone of mouse supraoptic nucleus. *J Neurophysiol* **113,** 754–767.

Weitzman RE, Glatz TH & Fisher DA (1978). The effect of hemorrhage and hypertonic saline upon plasma oxytocin and arginine vasopressin in conscious dogs. *Endocrinology* **103,** 2154–2160.

Windle RJ, Forsling ML, Smith CP & Balment RJ (1993). Patterns of neurohypophysial hormone release during dehydration in the rat. *J Endocrinol* **137,** 311–319.

Xu Y, Jia Y, Ge M, Lu L, Yang L & Zhan X (2018). Effects of ion channel blocks on electrical activity of stochastic Hodgkin–Huxley neural network under electromagnetic induction. *Neurocomputing* **283,** 196–204.

Yamaguchi K & Hama H (2011). Changes in vasopressin release and autonomic function induced by manipulating forebrain GABAergic signaling under euvolemia and hypovolemia in conscious rats. *Endocr J* **58,** 559–573.

Yang CR, Senatorov VV & Renaud LP (1994). Organum vasculosum lamina terminalis-evoked postsynaptic responses in rat supraoptic neurones in vitro. *J Physiol* **477,** 59–74.

Yao Y, Deng H, Ma C, Yi M & Ma J (2017). Impact of Bounded Noise and Rewiring on the Formation and Instability of Spiral Waves in a Small-World Network of Hodgkin-Huxley Neurons. *PLOS ONE* **12,** e0171273.

Yoshimura M & Ueta Y (2018). Advanced genetic and viral methods for labelling and manipulation of oxytocin and vasopressin neurones in rats. *Cell Tissue Res*; DOI: 10.1007/s00441-018-2932-9.

Zimmerman CA, Leib DE & Knight ZA (2017). Neural circuits underlying thirst and fluid homeostasis. *Nat Rev Neurosci* **18,** 459.